2017 Friends of the Pleistocene Guidebook

Northern Owens Valley

7 – 9 October 2017

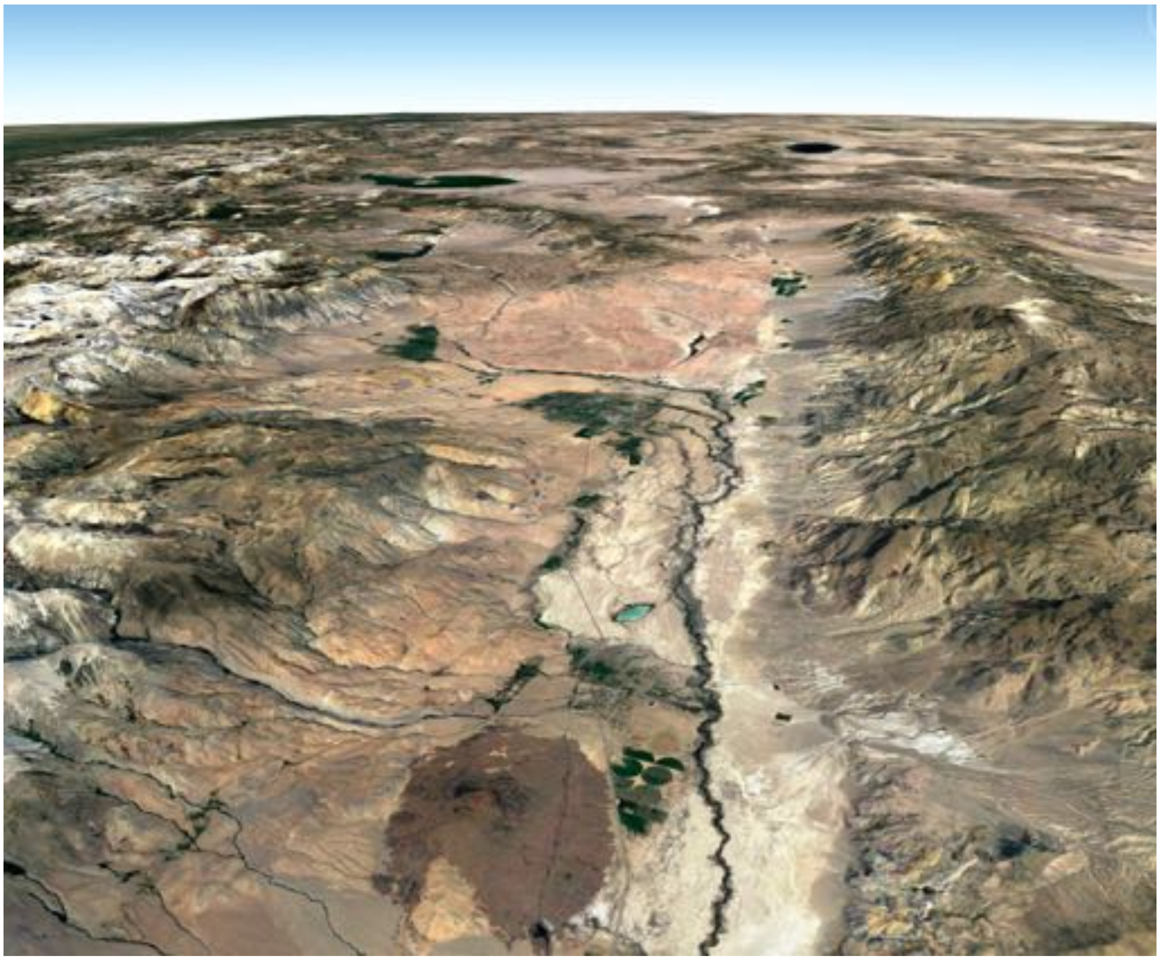

Trip Leaders

Fred M. Phillips, Drew Levy, Paul Hancock

Dedicated to the memories of Alfred Knopf, Elliot Blackwelder, Paul Bateman, and Clem Nelson

“we stand on the shoulders of giants…”

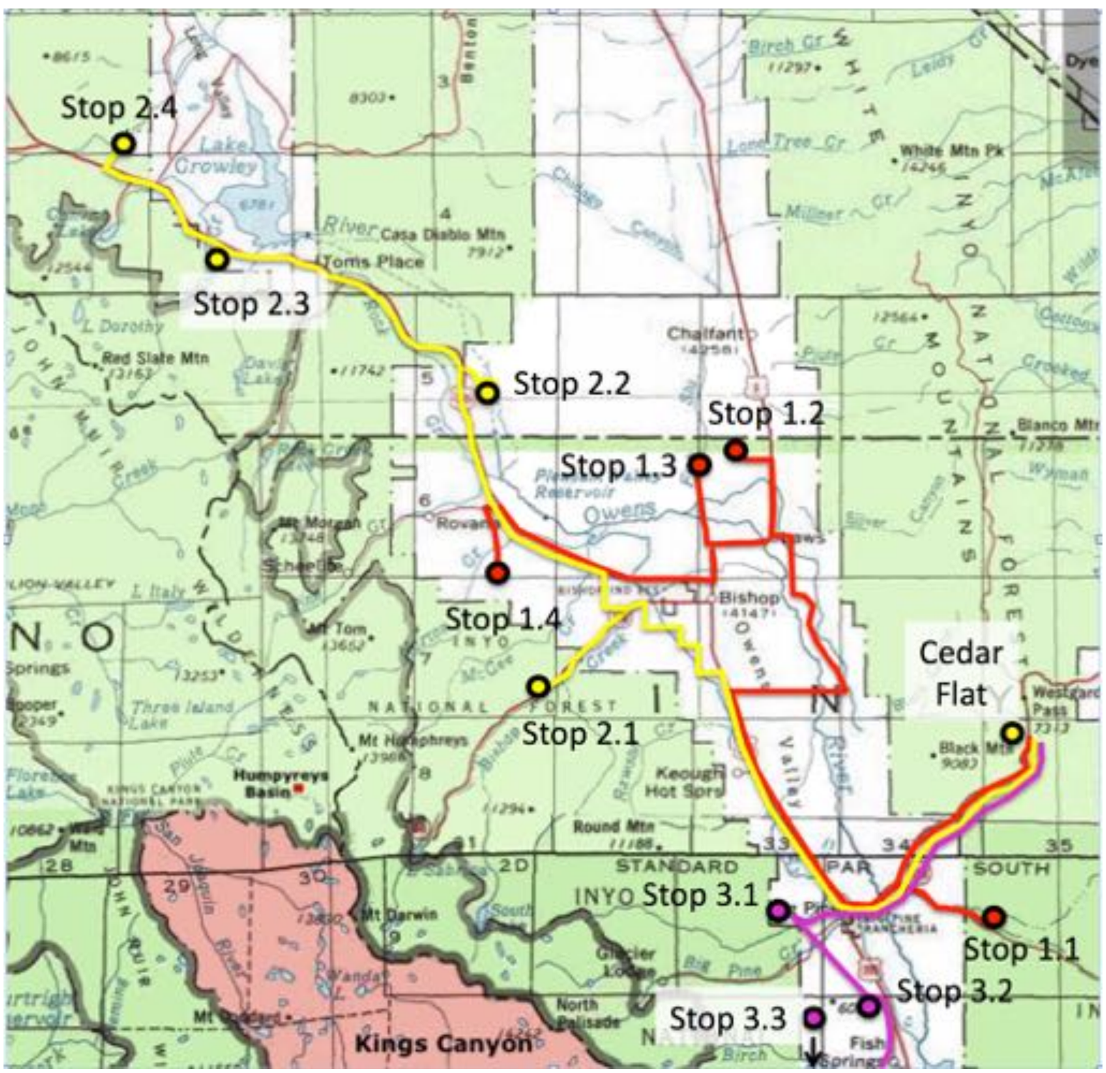

Errata: This version of the 2017 road log has been slightly modified from that distributed at the field trip on October 6, 2017. A figure to illustrate regional tectonics has been added on p. 8. The mileage between Stops 2.1 and 2.2 (and hence also subsequent stops that day) was in error; this has been corrected. A figure missing from Phillips and Jayko (starting on p. 42) has been added back in. Because of these changes the page numbers and table of contents have also changed.

Table of Contents

Description and Logistics

Locality: The Owens Valley is a deep trough between the Sierra Nevada on the west and the White/Inyo Mountains on the east. The valley is tectonically very active, with most of the dislocation being accommodated on transtensional systems of faults. The climate fluctuations of the Pleistocene left a major imprint on the area, including impressive moraines at canyon mouths and evidence of extensive pluvial lakes.

Scope: The 2017 trip will examine mountain-front faulting along both the White Mountains and Sierra Nevada and the valley-center Owens Valley fault. We will visit early Pleistocene lacustrine exposures in the Waucoba embayment, see new evidence for mid-to-late Pleistocene lakes in Long Valley, and inspect dated moraines at Bishop Creek and in Long Valley. The area is the source of the widely distributed Bishop Tuff and we will visit the source area in Long Valley and extensive exposures of the ignimbrite sheet, as well as other minor volcanic centers.

The last time there was a Pacific Cell FOP in the northern Owens Valley was in 1971!

The **headquarters** for the 2017 Pacific FOP will be the USFS Cedar Flat campground The campground has pit toilets (which we will supplement with porta-potties), but no running water. It is 12 miles east of the small town of Big Pine down a winding mountain road, so come prepared with water, ice and all necessary supplies. It is at 2250 m (7400 feet), so expect nights to be cool, possibly below freezing. Hopefully we will have glorious fall weather for the field trips, but if a cold front comes through it is not impossible we could be snowed on, and if there is a heat wave it could be up in the 90's. In other words, be prepared for anything.

Vehicles: The routes for Days 1 and 2 should be passable for passenger cars with reasonable clearance (not low-slung sports cars!). That for Day 3 will involve dirt roads with some projecting boulders and several ~2 foot-deep stream crossings, so high clearance vehicles are required. Plan on car pooling on Day 3 with somebody who has a high-clearance vehicle if you do not!

In general, parking a large number of vehicles and walking back and forth from them to the actual stop sites are the number-one waste of time on FOP trips, so please make every attempt to car pool if you are in a vehicle that has only one or two people in it.

Directions: The 2017 Pacific Cell FoP will be headquartered at the USFS Cedar Flat Group Campsite in Inyo National Forest. To reach Cedar Flat, drive either north or south on U.S. 395 to reach Big Pine, in the northern Owens Valley. Drive to the north end of Big Pine. Turn right on California State Highway 168. This intersection is easy to spot because it is marked by both a Giant Sequoia tree and a giant American flag. Drive 12.5

miles east on 168 (in 2.2 miles you reach the intersection with the Death Valley/Saline Valley Road; continue straight on 168, do not turn off toward Death Valley). The road proceeds up a narrow and twisty canyon before emerging onto the broad expanse of Cedar Flat. In 12.5 miles from the US 395 intersection you will see the sign for the Cedar Flat Group Camp with the turnoff on the north side of 168. The coordinates of this intersection are 37.27674 N and -118.1512 E. Driving ~0.3 mile north on a gravel road you encounter three group camp sites: Camp Nelson, Camp Noren, and Camp Ferguson. All three sites have been reserved for the FOP. When you arrive, please check in at the FOP headquarters to receive your guidebook and T-shirt.
Note that the Cedar Flat facility does not have running water. Vault toilets and port-a-potties will be provided. The nearest point for resupply is Big Pine, 12 miles to the west. Make sure you have adequate water, food, gasoline, and other supplies for the trip before you leave Big Pine. You are completely responsible for your own provisions while on the trip.

Regulations and Safety

Inyo National Forest is currently under fire restrictions, so no open fires *except in specifically constructed structures at the Cedar Flat Group Camps*.

We do not have any permits for digging or sample collection, so *do not excavate anything (except maybe a poop hole) and do not collect rocks, soil, etc.*

Bring at least a gallon of water per person per day (remember that no water is provided at Cedar Flat CG).

Never drive off the recognized road or across vegetation.

We will have to turn across traffic, or into high-speed traffic, numerous times on this trip. Other drivers are not expecting a slow-moving caravan. EXERCISE EXTREME AWARENESS AND CAUTION WHEN GETTING ONTO OR OFF OF HIGH-SPEED HIGHWAYS.

On the daily trips don't drive by yourself. Carpool with somebody else to avoid slow stops, congestion, and pollution.

Day 3 will require high-clearance vehicles.

Road Log

Day 1

Cedar Flat to Horton Creek: Sedimentary Records of Climate and Tectonics from 3 to 0.5 Ma, and Active Faulting, in the Northern Owens Valley

The field trip will depart from Cedar Flat Group Camp at 8:00 AM, Saturday, October 7.

Summary: The northern Owens Valley is a region of dramatic topography and active volcanism. These characteristics stem from its role as a locus of transtensional strain associated with the transform plate boundary on the west coast of North America. Approximately two-thirds of the total strain between the stable North American craton and the east side of the San Andreas Fault is accomplished in the 100 km between Piper Peak, on the east side of Fish Lake Valley, and Wheeler Crest, on the west side of Owens Valley. Unfortunately, neither the history of strain accumulation nor the mechanisms by which faults accommodate the strain are currently very well understood. On the first day of the 2017 Friends of the Pleistocene Field Trip we will examine sedimentary deposits (lacustrine, fluvial, and alluvial fan) in the Waucoba embayment and along the front of the White Mountains between Black Canyon and Piute Canyon that contain a record of the opening of the Owens Valley during the Plio-Pleistocene. We will also see fault scarps and faulted mountain fronts that contain clues to the geometry and kinematics of the faults that are largely responsible for the accumulation of tectonic strain across the region.

Prior to ~12 Ma the region was apparently a low-relief upland of moderate elevation (perhaps ~2.5 km) that stretched from the central Sierra Nevada to central Nevada (Phillips, 2008; Jayko, 2009; Henry et al., 2012). Both thermochronology (Stockli et al., 2003; Lee et al., 2009) and $^{40}Ar/^{39}Ar$ dating of regional-scale volcanic eruptions (Phillips et al., 2011) indicate that the Owens Valley area was extended during two pulses that began at 11.8 and 3.4 Ma. During the Miocene pulse the extension was oriented east-west, whereas by the time of the Pliocene pulse the extension vector had shifted to northwest-southeast (Jones et al., 2004; McQuarrie and Wernicke, 2005). The resumption of active extension in the late Pliocene thus reactivated normal faults that had originally developed during the Miocene, but the shift in the direction of extension produced both a reorganization in the displacements and interrelation of the existing faults and the development of new faults. Some questions that arise from this overview are: how much of the topographic development of the Owens Valley can be attributed to events in the Miocene and how much to the renewal of tectonic activity in the Plio-Pleistocene? how is transtension accommodated on faults that developed as simple dip-slip structures? what is the relation between valley-bounding structures and the uplift of the mountain blocks that comprise their footwalls?

We will first examine a thick section of interbedded lacustrine and deltaic deposits, capped with alluvial fan gravels, in the Waucoba embayment and along the face of the southern White Mountains. These deposits constitute a continuous sedimentary record that dates between approximately 3 and 2 Ma, with younger inset deposits along the White Mountain front that are as young as the eruption of the Bishop Tuff at 767 ka (Chamberlain et al., 2014). They contain a record of paleoclimate during this period and sediment lithology gives clues to the tectonic history. They also provide what is virtually our only regional archive of aquatic fossils for the Pliocene and early Pleistocene. These deposits are found at the base of the White Mountains and in some places extend half-way up the range front. In the Waucoba embayent they are consistently tilted toward the west, but further north do not appear to be tilted. They raise questions: why are the deposit bases so close to the elevation of the present-day Owens Valley floor? What is responsible for the tilting? What explains the very clear limits on the geographical distribution of the deposits up and down the White Mountain front? What processes created the accommodation space for deposition of these thick lacustrine sequences?

We will next view the White Mountain Fault Zone (WMFZ), the Fish Slough fault, and the Round Valley fault (RVF), which is a portion of the Sierra Nevada Frontal Fault (SNFF). One notable characteristic of these faults is that the sense of displacement shifts along strike. For example, the WMFZ at its south end appears to be a simple dip-slip normal fault, but then becomes a dextral-oblique fault, then separates into parallel normal and dextral strike-slip faults, then the strike-slip fault disappears, leaving only normal faulting along the northern portion of the area that we will view. This is all accomplished without any significant change in the fault strike. What fault geometries can explain this variation in fault behavior? If we see parallel low-to-moderate angle normal and nearly vertical strike-slip faults, which one is the "real fault"? How do changes in fault geometry relate to active tectonics of the mountain front? And, in a more regional context, what are the structures along which the opening of the Owens Valley and the down-drop of its floor have been accomplished?

The Owens Valley constitutes one of the most dramatic landscapes in North America. For us, as Quaternary geologists and geomorphologists, the overriding question it presents is "How can we explain the formation of this landscape?" What tectonic forcings are responsible, how long did it take, what were the rates, and most fundamentally, what are the structures that are responsible for its formation? These are the questions that we will address on this Friends of the Pleistocene Field Trip.

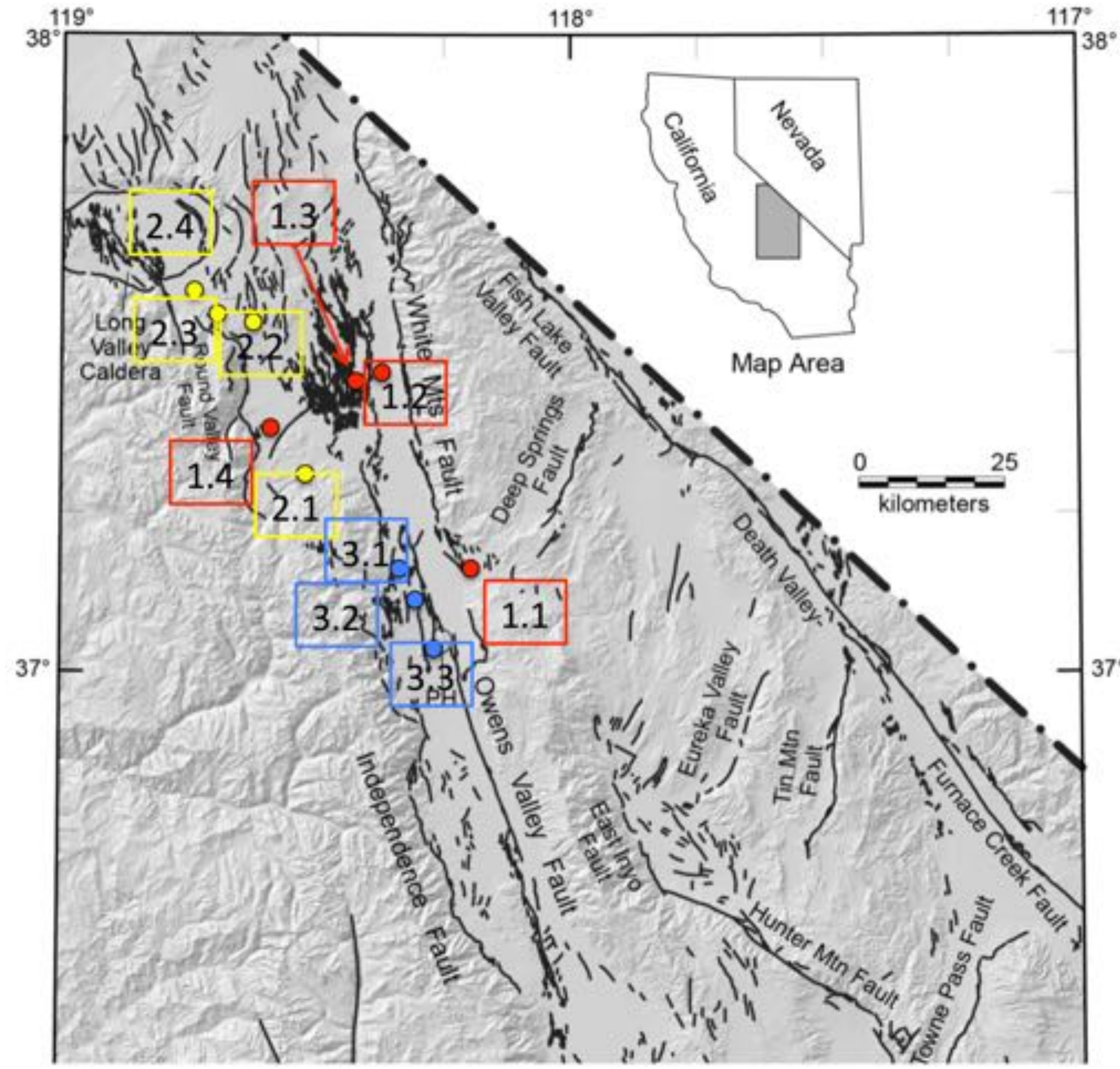

Figure 1. Active faults and topography of the northern Owens Valley and surrounding region. FOP 2017 stops are shown by colored dots. Figure modified from Stevens et al. (2013).

Mileage **Description**

0.0 Start point is the intersection of the exit road from the Cedar Flats Group Campground to state highway 168, the Westgard Pass road. Set your odometer as you reach the intersection, and turn right (west).

2.1 The route starts in alluvial Quaternary deposits of Cedar Flats. At about 1.5 miles the road begins to descend into Paleozoic sedimentary rocks of the White Mountain block. Down this canyon these are almost entirely lower Cambrian Campito Formation. The lithology is mostly quartzitic sandstone and shale. At this point the road passes from the shale-dominated Montenegro Member, dominated by shale, into the Andrews Mountain Member, dominated by massive quartzitic sandstone, and as it does so the canyon becomes a narrow, deep gorge, nicknamed "The Narrows". The geology of this canyon is given on the Blanco Mountain and Waucoba Mountain Geological Quadrangle Maps (Nelson, 1966b; Nelson, 1966a). The road becomes one-lane, so please drive carefully and show courtesy to uphill drivers, who have the right of way.

The Narrows and the rocks of the overlying lower Cambrian Poleta Formation are a famous site for Cambrian fossils, in particular archaeocyathids and trilobites, and the area is an officially protected U.S. Forest Service geological area of interest. Some years ago the California highway department wanted to reroute Highway 168 to avoid The Narrows, but was thwarted because of the damage to the fossils that would have resulted. More information on the fossils can be found at http://inyo2.coffeecup.com/westgard/westgardpass.html.

4.3 On the right (N) side of the road is a small stand of trees and a concrete trough. A steady flow of cool water is piped into the trough from a spring about 50 m up the canyon wall, known as Batchelder Spring. The spring was named for a Mr. Batchelder who first constructed the road over Westgard Pass in the 19th Century and who maintained a toll station here. The tollhouse was still standing when I (FMP) visited the site in the 1960's. The concrete trough served to water the teams of horses and mules that pulled the wagons over the pass.

4.8 At this point the outcrops on the left (S) side of the road are still lower Cambrian metasediments, but on the north side, Plio-Pleistocene debris-flow deposits belonging the basin fill of the Waucoba embayment onlap the Paleozoic bedrock as a buttress unconformity.

7.4 For the past 2.6 miles the canyon has been walled by relatively undeformed debris-flow deposits, but at this point the road crosses a fault that forms the eastern boundary of the Waucoba Embayment, strictly defined. It is part of a series of en echelon structure that extend 7 km to the southeast and 4 km to the northwest from this point. The faults have previously been regarded as simple, valley-down normal faults (Nelson, 1966b; Jager, 2002), but the nature of displacement is enigmatic and will be discussed at Stop 1.1.

7.7 At this point Highway 168 crosses the arroyo in the canyon bottom. Note a tributary canyon on the north side about 100 m ahead. This stream channel has been tectonically deflected from a drainage about 500 m to the north, and flows parallel to the fault. Note also that part of the flow from the Westgard Pass canyon (that we have been following) is deflected across Highway 168 and flows southwest down the same drainage that the highway follows.

10.3 Intersection with the Big Pine/Death Valley Road. Turn left (S). As we drive southward there are good views to the east of the white lacustrine beds of the Waucoba embayment.

11.2 The green grove to the east of the road is Uhlmeyer Spring. It discharges from the fault that forms the western boundary of the Waucoba Embayment and is actively depositing elemental sulfur.

11.7 An inselberg of Cretaceous granodiorite protrudes through the Waucoba beds on the east side of the road.

13.0 Good exposures of lacustrine Waucoba beds on the north side of the road. Note the very uniform westward dip of 6°.

14.1 Turn-around point; make a U-turn here. Follow directions of flaggers. WATCH FOR ONCOMING TRAFFIC WHEN TURNING. Park on both sides of the road. PARK FAR ENOUGH OFF THE PAVEMENT THAT TRAFFIC CAN GO BY IN BOTH DIRECTIONS. Stop 1.1 is about 100 yards to the north of the road, on an unpaved road.

Stop 1.1 Waucoba beds and tectonics of the Waucoba embayment (De Masi), Tectonics of the Waucoba embayment (Phillips/Kirby).

The Waucoba Lake Beds of Owens Valley, California

Conni De Masi[1], Alan Deino[2] and Gary Scott[2]

[1]Graduated MS Student, California State University Long Beach; Now in Campbell, California

[2]Berkeley Geochronology Center, Berkeley, California

connidemasi@gmail.com

The Pliocene-Pleistocene Waucoba Lake Beds, are 7 km east of Big Pine, Owens Valley, California. Owens Valley is an intra-continental transtensional basin in the western Basin and Range geomorphic province. The development of the Waucoba lake basin reflects tectonic changes of the surrounding landscape while simultaneously recording the climate evolution of the Sierra Nevada and White-Inyo Mountains, making the basin an ideal study for paleorelief transformation of the western Basin and Range. The lake beds record a major environmental shift from saline-alkaline water to fresher water while other lake systems in the region underwent desiccation. Tuff layers within the exposed lacustrine section range in age from ~2.6 to 2.0 Ma ($^{40}Ar/^{39}Ar$), with the transition from saline to fresh water facies around ~2.5 Ma. The change in paleo-environment is contemporaneous with a co-seismically deformed layer, a ~1.5 m thick seismite with an age of ~2.5 Ma. The stratigraphic interval containing the seismic bed is of reversed polarity, attributed to the early part of the Matuyama magnetochron. Contrasting environmental differences of the Waucoba Lake Beds to other coexisting lake systems suggests that tectonic activity is the driving force of environmental changes in ancient Lake Waucoba, rather than regional changes in climate. This unique set of lake beds and overlying sediments record uplift of the Sierra Nevada and the White-Inyo Mountains, as well as subsidence of Owens Valley.

The Waucoba Name

The Waucoba Lake Beds (Fig. 1) were named by the pioneering USGS geologist Charles D. Walcott, who surveyed Owens Valley between 1889-1900. The Big Pine Paiute named this particular landscape and Walcott used their names in his reconnaissance. Pronunciations amongst the Paiute varied from the Lone Pine tribe in southern Owens Valley, to the Bishop tribe in northern Owens Valley (with the Big Pine tribe in the middle). The Big Pine Paiute word for a big pine tree is Wakopa, hence the name Wakopa (Waucoba) Mountain comes from the mountain with lots of big pine trees. Wakopi is the Big Pine Paiute word for Owens River so Walcott, thinking that it may have been a source for the ancient lake, called the lake beds Waucobi (Walcott, 1897). It is to be noted that the Paiute was mostly a spoken language with few

Figure 1. Photograph of Waucoba Lake Beds looking east toward the White Mountains. Notice cliff forming layer

written words until the 1940s, so spellings at the time are unknown. Walcott went on to use the Paiute name for Waucoba Springs and Waucoba Canyon most likely because it was located near Waucoba Mountain. Nelson (1966) used Waucobi Lake Beds; however, the formal USGS name is Waucoba Lake Beds (WLB) and the formal landmarks are Waucoba Spring and Waucoba Mountain.

Geologic Setting

The dramatic badland morphology and white layering of the WLB are visible from U.S. Highway 395 (Fig. 1). The lacustrine sequence (>115 m thick) is composed principally of weakly consolidated mudstones and siltstones, cut by younger normal faults (Nelson, 1966). The WLB are within the Big Pine Graben, situated between the White Mountains [NE], Inyo Mountains [SE], and Owens Valley [W]. The Southern Sierra Nevada Frontal fault and Independence fault bound the Big Pine Graben to the west, and the oblique-dextral White Mountain faults to the east (Gillespie, 1991). These faults mark the lateral extent of Owens Valley. The Graben is separated down the axis of the valley by the Owens Valley fault and is divided into two micro-blocks by the northeast-southwest trending Deep Springs fault. Waucoba exposures can be found east of the Owens Valley fault and north of the Deep Springs fault along the White-Inyo Mountains (Fig. 2). The WLB cover about 16 km^2 and are overlain by Quaternary older alluvium (Nelson, 1966).

Nelson (1966) suggested that the WLB were Quaternary and noted that some portions were tuffaceous. Hay (1966) used K/Ar and placed the lake beds at 2.3 Ma. Sarna-Wojcicki et al. (2005) correlated several tephra beds and several locations in the WLB. At the Ryser tuff mine location, Sarna-Wojcicki et al. (2005) identified tuffs of Emigrant Pass (2.06-1.96 Ma) and tuffs of Blind Spring Valley (2.219-2.135 Ma) in a 5-m-thick section. Jordan at al. (2015, 2016) correlated tephra beds in WLB that confirmed previous work by Sarna-Wojcicki et al. (2005) along with tuffs of The Badlands (2.89-2.22 Ma). These data indicate that the WLB are late Neogene-early Quaternary.

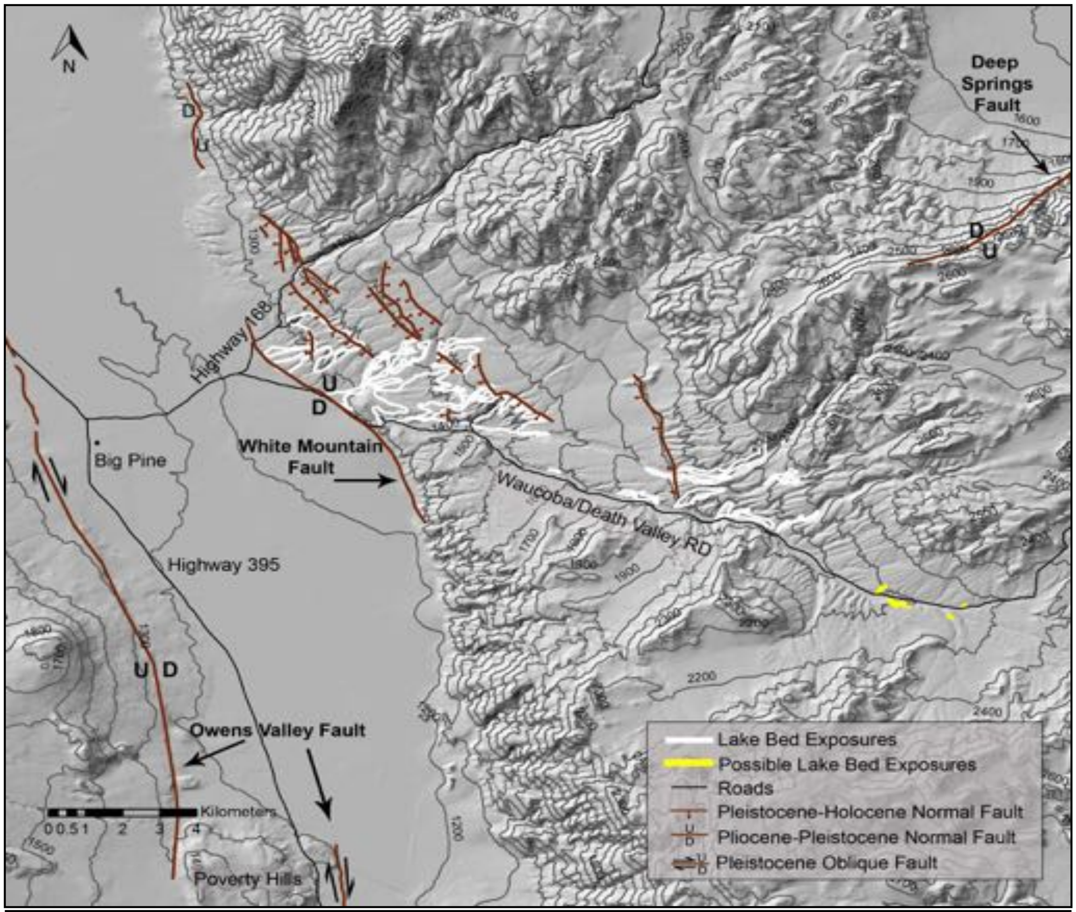

Figure 2. Shaded relief map of Waucobi Lake Beds with major faults. (De Masi, 2013)

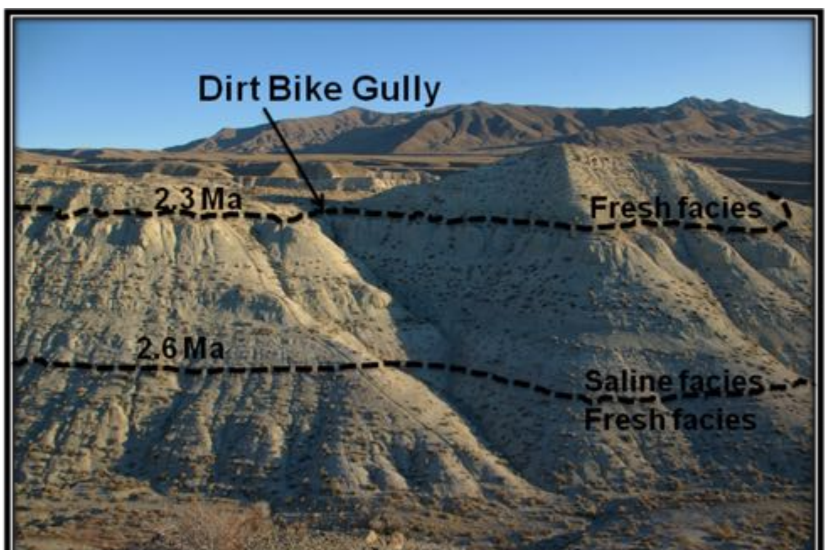

Figure 3. Waucoba Lake Beds exposed in Duchess canyon. Ages of tuffs at facies transition are in black dashed lines.

We studied two stratigraphic sequences of WLB. The first is a 25-m-thick sequence found at the Ryser tuff mine where Crooked Road Canyon enters Owens Valley. The second sequence is 90-m-thick lake bed found in Duchess canyon about 3 km east of the Ryser mine. The maximum thickness of the lake basin is still unknown. In this study, we collected tuff samples for radiometric dating, and measured paleomagnetism on bulk sediment samples and combined the newly acquired data with the mineralogy data of De Masi (2013).

Chronology and Regional Climate

Radiometric dates ($^{40}Ar/^{39}Ar$ on sanidine) in the WLB span ~2.6 to 2.0 Ma. An $^{40}Ar/^{39}Ar$ age of ~1.2 Ma was determined for a tephra bed in the overlying older fanglomerate of Nelson (1966). Claystones in the interval ~2.6–2.5 Ma (Fig. 3) are comprised mostly of phillipsite and evaporite deposits (De Masi, 2013, Hay, 1966). Phillipsite, a zeolite mineral that forms in alkaline water, and the presence of evaporites implies a shallow intermittently closed lake (Hay, 1966), suggesting the lake had higher salinity as well as higher alkalinity before ~2.5 Ma. Montmorillonite in the interval ~2.5–2.3 Ma indicate a transition from alkaline-lower moisture conditions to more fresh water conditions. Montmorillonite is increasingly abundant in tuffs dated <~2.3 Ma. Between 2.3 to 2.0 Ma the mineralogy of the lake beds continue to shift to montmorillonite, suggesting fresher, possibly deeper water (Fig. 4).

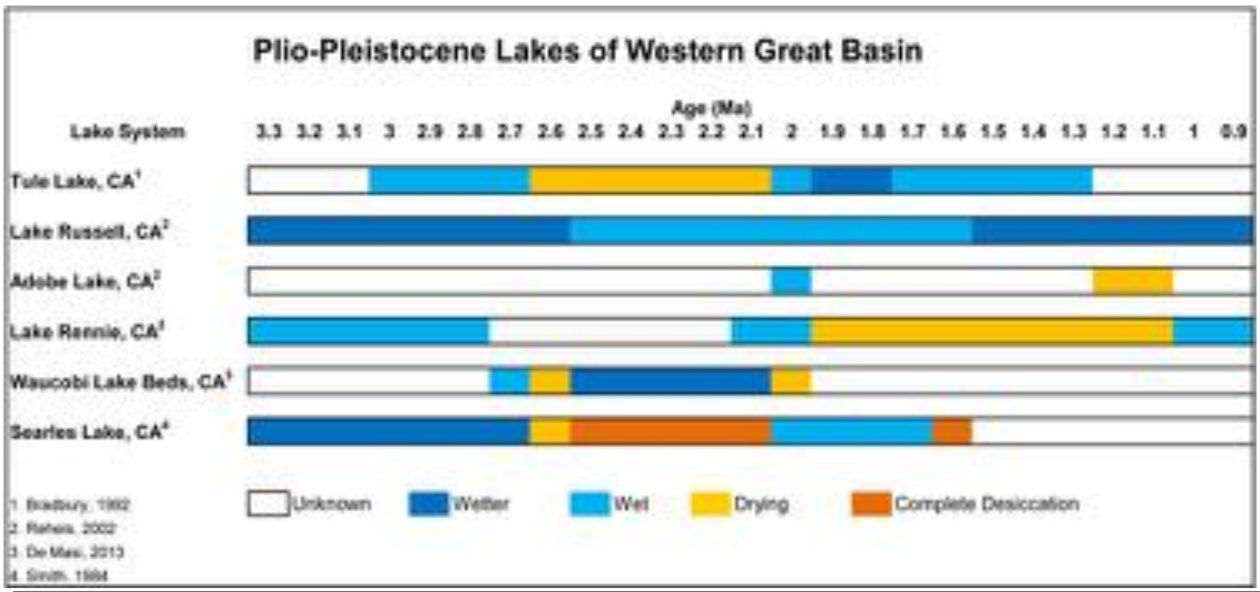

Figure 4. Environments of Plio-Pleistocene lakes in the Western Great Basin. (De Masi, 2013)

The transition from phillipsite to montmorillonite after ~2.5 Ma indicates an environmental change different from other regional lakes (Fig. 4). Prior to 2.6 Ma, the regional lake systems all contain fresh water and then experience drying by 2.5 Ma (Bradbury, 1992, De Masi, 2013, Phillips, 2008, Reheis et al., 2002, Smith, 1984). The sedimentation rate in the Waucoba basin at Duchess canyon reflects this change. After 2.5 Ma the sediment accumulation rate drastically increases, accompanied by a shift in clay mineralogy from phillipsite to montmorillonite. This is followed by periods of relatively slow clastic accumulation in an open, fresh water lake environment. After ~2.2 Ma, the Waucoba Lake Beds record the onset of drying of the lake and by 2.0 Ma the lake returns to a closed alkaline-saline basin. By this time, the other lake systems contained abundant water (De Masi, 2013). The differences in hydrology of Waucoba and the other lake systems (Fig. 4) represent regional topographic changes occurring east of the White-Inyo Mountains, to the Sierra Nevada during the late Pliocene and early Pleistocene.

Tectonics and Regional Hydrology

The Waucoba basin hosted planar deposition during the interval of ~2.6-2.0 Ma, though the lake beds are currently tilted ~4-12 degrees. Our preliminary findings suggest there is no significant evidence of tilting during deposition of the lakebeds, such as distinct fanning, implying uplift of the White-Inyo Mountains. Instead, lakebeds pinch out to the east while thicken west, suggesting basin growth and alteration. Fanglomerate material overlying the Waucoba Lake Beds, and lack of it mixed within the lacustrine sediment prior to ~2.0 Ma, indicate that fans accumulated after lake formation. Dated ash from the fanglomerate directly overlying the uppermost lake beds has a $^{40}Ar/^{39}Ar$ age of ~1.2 Ma, suggesting that rapid uplift in the White-Inyo Mountains did not occur until cessation of the ancient lake near the end of the Early Pleistocene.

Several lake systems in the Western Great Basin may have been hydrologically connected during the Pliocene and Pleistocene (Phillips et al., 2008; Reheis et al., 2002). Eastern Sierra Nevada lakes surrounding the Owens Valley region were possibly linked

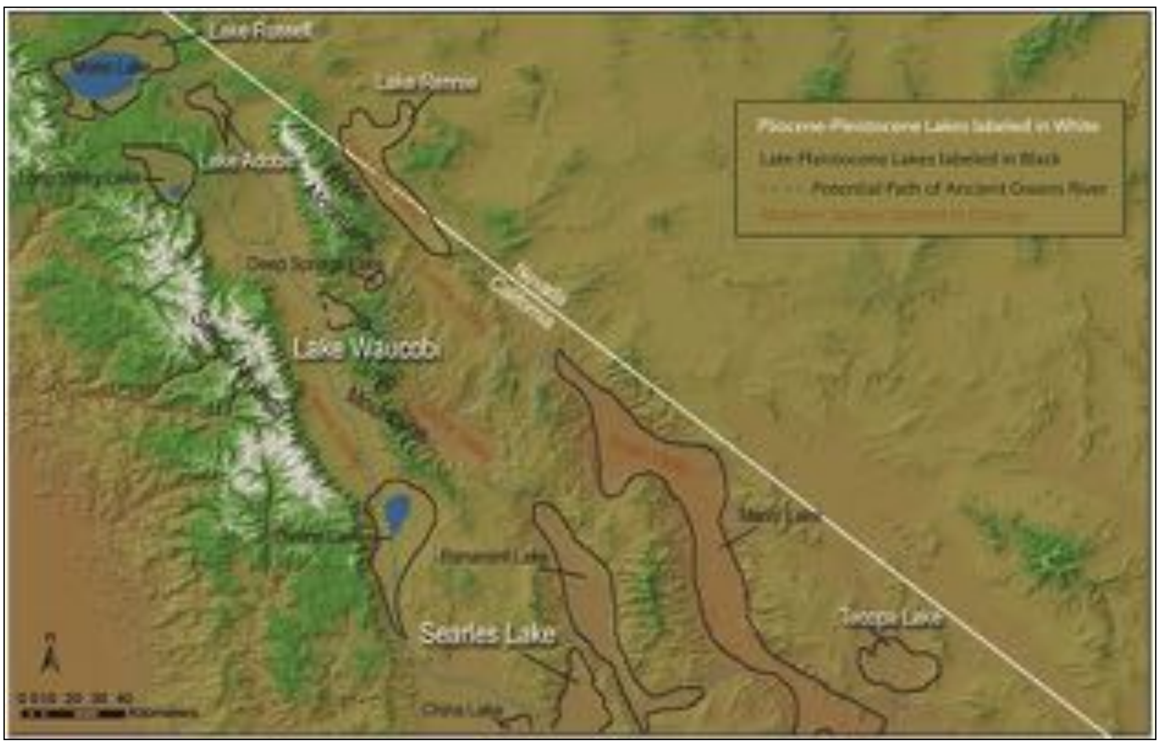

Figure 5. Map of paleo-Owens River with regional lake systems (De Masi, 2013).

through the paleo-Owens River, including Waucoba and Searles lakes (Fig. 5). Re-routing of the paleo-Owens River could feed one lake while depriving others. The ancient Owens River was probably a major source of water input for paleo-Lake Waucoba. Phillips et al. (2008) postulated that one possible path of the Owens River flowed south through the Waucoba Embayment and eastward into Saline Valley. Interference-patterned wave ripples preserved in carbonate sediment underlying ~2.5-2.3 Ma tuffs could be evidence of directional flow within the Waucoba lakebeds (Bachman, 1974 and De Masi, 2013), however evidence of lacustrine deposits of this age are lacking in Eureka Valley.

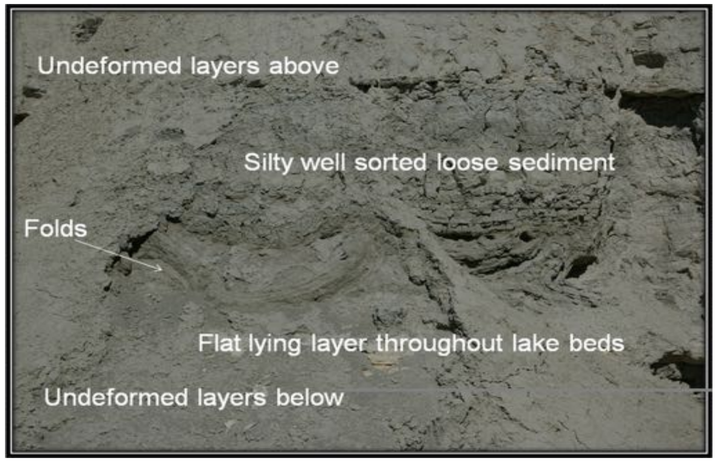

Figure 6. Seismite, co-seismically deformed sediments in Duchess canyon. (De Masi, 2013)

Our observations indicate several co-seismically deformed beds within the Waucoba basin on centimeter and meter scales. A 1.5 m package of deformed sediments in Duchess canyon is constrained by Ar/Ar dating to have occurred between 2.5-2.4 Ma. The deformation that caused the disturbed layer (Fig. 6) occurred during the period of increasing moisture in paleo-Lake Waucoba, while desiccation was occurring in several other local basins (Fig. 5). It is possible that an outlet of the Owens River went east through the embayment and through a gap in the proto-White-Inyo Mountains prior to this time period as indicated by changes in wave direction (Bachman, 1974). The deformed layers could represent a tectonic or volcanic event that affected the topography, creating a landslide or scarp, closing the water pathway. The elimination of that outlet would have deprived lakes to the south from river input, while accounting for the fresh water of ancient Lake Waucoba. Coincidentally, the lake starts to desiccate at the time Owens Valley fault becomes active, ~2 Ma. We infer that the formation and deformation of the Waucoba basin record changes in regional tectonics and paleorelief; from crustal extension and subsidence, to translation and uplift of the western Basin and Range during the Pliocene-Pleistocene boundary associated with western dip-slip along the White Mountain Fault Zone, northeastern slip along Deep Springs fault, and oblique slip along the Owens Valley fault.

Acknowledgements

This is an ongoing study based off work from De Masi's 2013 M.S. thesis at California State University Long Beach. Jeffrey Knott from California State University Fullerton assisted with Ar/Ar sample collecting, Chris Castillo from Stanford University performed the seismic survey, and Elmira Wan, Scott Starratt, Laura Walkup and Leslie Jordan of the U.S. Geological Survey assisted with Tephrochronology. Yvonne Katzenstein provided us with gracious hospitality.

References

Bachman, S., 1974, Depositional and structural history of the Waucobi Lake Bed Deposits, Owens Valley, CA [M.S. thesis]: Los Angeles, University of California.
Bradbury, J.P., 1992, Late Cenozoic lacustrine and climatic environments at Tule Lake, northern Great Basin, USA: Climate Dynamics, v. 6, p. 275-285.
De Masi, Conni, 2013, Ancient sedimentary fill of the Waucobi Lake Beds as an archive of Owens Valley, California tectonics and climate [M.S. thesis]: Long Beach, California State University.
Gillespie, A.R., 1991, Quaternary subsidence of Owens Valley, California, *in* Proceedings of the White Mountain Research Station symposium: p. 356-382.
Hay, R.L., 1966, Zeolites and zeolitic reactions in sedimentary rocks: Geological Society of America Special Paper 85, 130 pp.
Jordan, L.M., Wan, E., De Masi, C., Knott, J.R., Starratt, S.W., Walkup, L.C., 2015, Initial geochronologic framework, stratigraphic correlations, and paleoenvironmental interpretation of the Waucoba Lake Beds, Inyo County California- A multidisciplinary spot check using tephrochronostratigraphy, 40Ar/39Ar dating and micropaleontology: Geological Society of America Abstracts with Programs, v. 47, n. 7, p. 755.
Jordan, L. M., Wan, E., Starratt, S.W., Deino, A.L., Walkup, L.C., Knott, J.R., and De Masi, C., 2016, Using tephrochronology, $^{40}Ar/^{39}Ar$, ostracods, and diatoms to date and reconstruct the environment of an early Pleistocene time-slice of Waucoba Lake, Inyo County, California, USA: Geological Society of America Abstracts with Programs, v. 48, n. 7,
Nelson, C.A., 1966, Geologic map of the Waucoba Mountain Quadrangle, Inyo County, California: U.S. Geological Survey Geologic Quadrangle Map GQ-528, 1:62,500.
Phillips, F.M., 2008, Geological and hydrological history of the paleo–Owens River drainage since the late Miocene, *in* Reheis, M.C., Hershler, R., and Miller, D.M., eds., Late Cenozoic Drainage History of the Southwestern Great Basin and Lower Colorado River Region: Geologic and Biotic Perspectives: Geological Society of America Special Paper 439, p. 115–150.
Prisson, Louis V., and Schuchert, Charles, 1915, A text-book of geology: For use in universities, colleges, schools of science, etc. And for the general reader: London, John Wiley and Sons p.443, 594-599.
Reheis, M.C., Sarna-Wojcicki, A.M., Reynolds, R.L., Repenning, C.A., and Mifflin, M., 2002, Pliocene to middle Pleistocene lakes in the western Great Basin: Ages and connections, *in* Hershler, R., Madsen, D.B., and Currey, D.R., eds., Great Basin Aquatic Systems History: Smithsonian Contributions to the Earth Sciences, v. 33, Washington, D.C., Smithsonian Institution Press, p. 53–108.
Sarna-Wojcicki, A.M., and 10 others, 2005, Tephra layers of Blind Spring Valley and related upper Pliocene and Pleistocene tephra layers, California, Nevada, and Utah: Isotopic ages, correlation, and magnetostratigraphy: U.S. Geological Survey Professional Paper 1701, 63 pp.
Smith, G.I., 1984. Paleohydraulic regimes in the southwestern Great Basin, 0–3.2 my ago, compared with other long records of "global" climate: Quaternary Research, v. 22, p. 1–17.
Taylor, R.L., 1963, Cenozoic volcanism, block faulting, and erosion in the northern White Mountains, Nevada [M.S. thesis]: Berkeley, University of California, p. 95.

Stop 1.1: An outrageous hypothesis to explain faulting in the Waucoba embayment

Fred M. Phillips and Eric Kirby

Earth & Environmental Science Department, New Mexico Tech, Socorro NM 87801

Forward

Ninety-one years ago William Morris Davis, in his paper entitled *On the Value of Outrageous Hypotheses* stated “For inasmuch as the great advances of physics in recent years and as the great advances in geology in the past have all been made by outraging in one way or another a body of preconceived opinions, we may be pretty sure that the advances yet to be made in geology will at first be regarded as outrages upon the accumulated convictions of to-day, which we are too prone to regard as geologically sacred.” To keep the spirit of W.M. Davis alive, we are going to propose an outrageous hypothesis to explain the anomalous nature of faulting in the Waucoba embayment.

Fig. 1. William Morris Davis ponders outrageous hypotheses in 1890.

Introduction and Geologic Setting

The Waucoba embayment (frequently also spelled “Waucobi”) forms the boundary between the White and Inyo Mountains on the west side of the ranges. To the north and south the delineation between the alluvial fans on the eastern flank of the Owens Valley and the mountain front is provided by distinct normal faults that separate steep, relatively uplifted mountain blocks formed of sedimentary or plutonic bedrock from alluvium-filled valley floors. In contrast, at the embayment the normal faulting is weak and discontinuous and east of the faults is a gradually sloping (~7°) surface draped with lacustrine and alluvial sediments. These sediments pinch out against the face of the White/Inyo Mountains as the topography begins to rise more steeply. Toward the eastern edge of the sedimentary fill are a series of rather enigmatic faults. These form a discontinuous, en echelon array, stepping westward as one goes north. These are shown in Fig. 2 in red. Fig. 2 also shows a portion of the bedrock geology from Nelson (1966). In the bedrock to the east of the embayment the major active faults are the Deep Springs fault and faults related to it. Offset of the Wyman Formation/Reed Formation contact (outlined in blue in Fig. 2) and the Deep Springs Formation (all Proterozoic) appear to indicate a total of ~2 km of sinistral shear. This sense of motion is plausible, inasmuch as the hanging wall of the Deep Springs fault on the southwest side of Deep Springs Valley curves around to intersect the fault plane at an oblique angle. Progressively larger

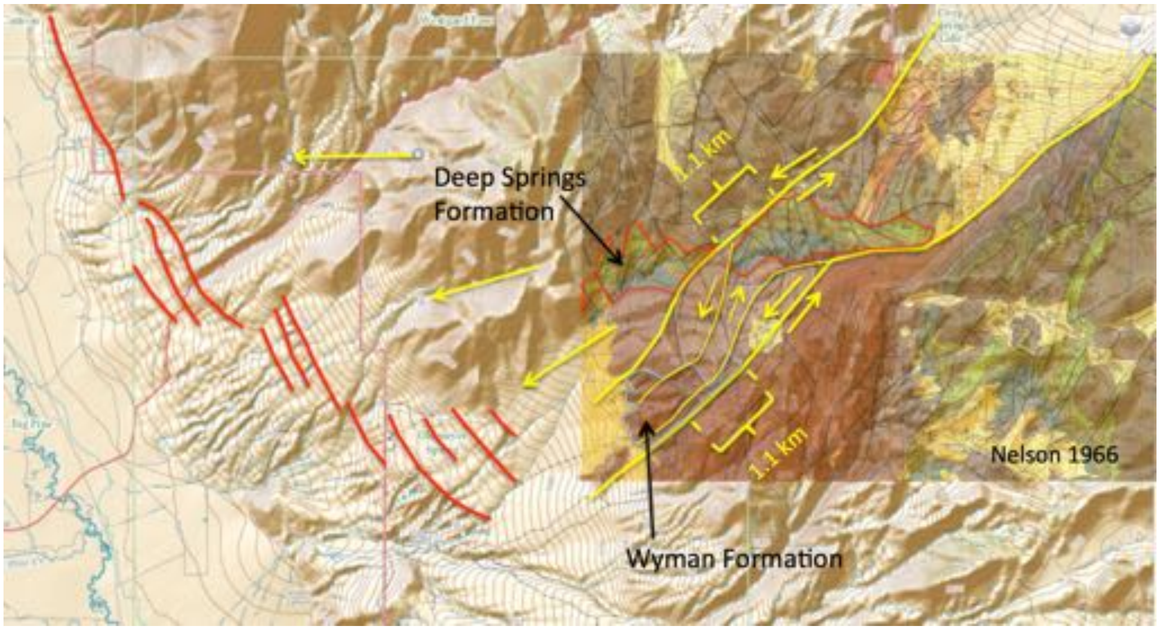

Figure 2. Overview of the Waucoba embayment, with faults in the embayment shown in red and other faults in yellow. Geologic map by Nelson (1966) is overlain on the north-eastern part of the topographic map. Yellow arrows show inferred directions of tectonic displacement.

displacement toward the middle of the fault would produce sinistral shear as the fault opened.

The Waucoba embayment faults were initially mentioned by Walcott (1897), who stated he was going to publish a paper on them, but never did. This holds the distinction of being the first of many unpublished research projects in the Waucoba embayment. The Waucoba embayment faults were described in some detail by Taylor (1933). They were mapped at large scale by Nelson (1966) and in much finer detail by Bachman (1974); Bachman (1978). The definitive work on the tectonics of the embayment is the M.S. thesis by Jager (2002). All of the previous works were in substantial agreement with the following summary by Jager: "In the Waucobi Embayment, the faults occur in a left-stepping *en echelon* pattern, striking NNW-SSE. Displacements on the fan surfaces are predominantly normal: very little strike-slip or oblique motion is recorded geomorphically. The orientation and displacement on these faults indicate that slip is not transferred from the OVF to the FCF through the DSF."

In the face of this consensus of prior research, we propose an outrageous alternative: that displacements on the en echelon NNW-SSE faults are predominantly reverse faulting and that they exhibit geomorphic evidence for a component of sinistral slip. We base this proposal on four observations: 1) anomalous drainage patterns, 2) apparent displacement of stream channels, 3) apparent reverse faulting in bedrock faults, and 4) anomalous fault morphology.

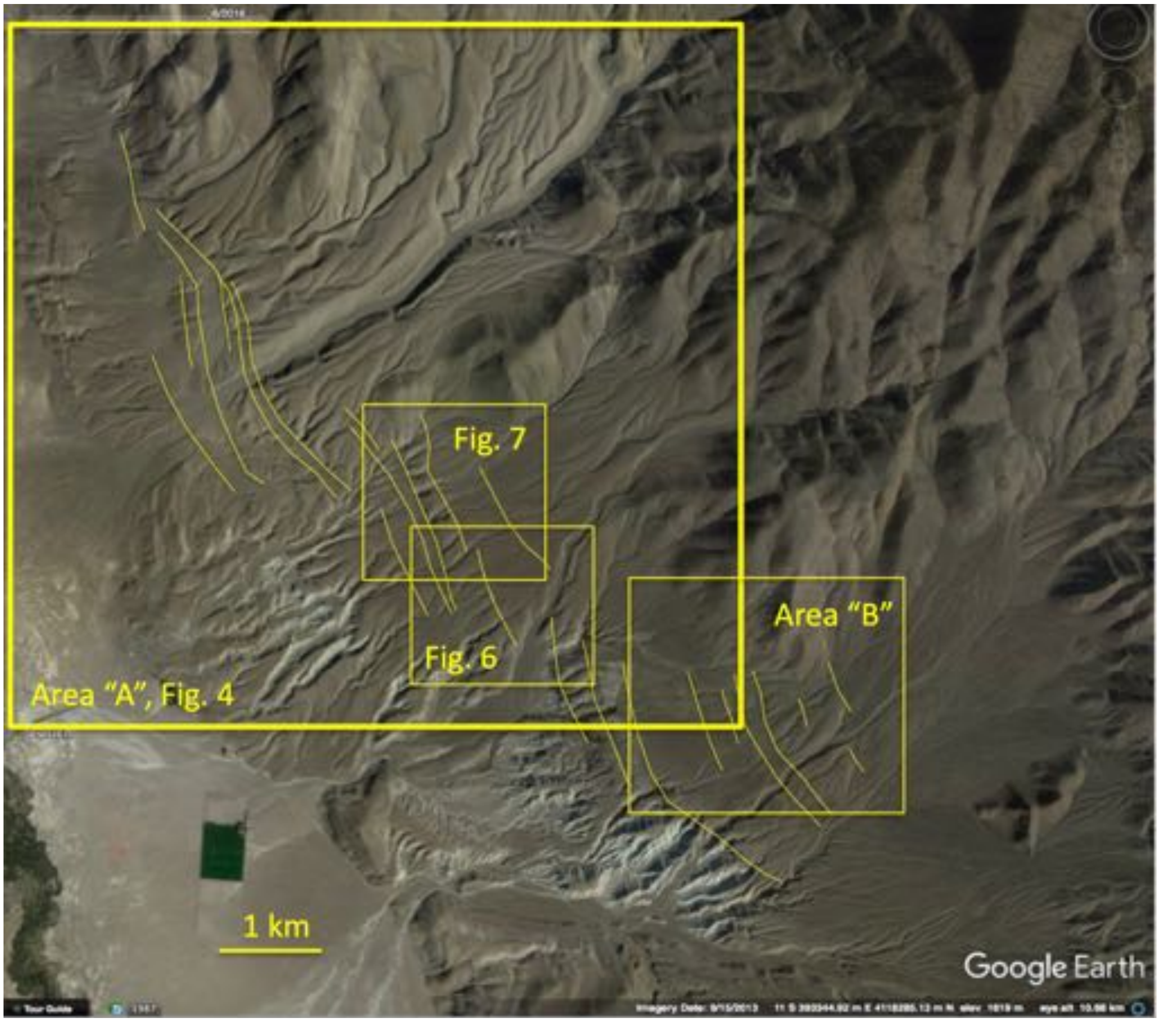

Figure 4. Overview of faulting in the Waucoba embayment. Stream deflection studies were conducted in areas A and B.

Anomalous Drainage Patterns

Streams flowing across strike-slip faults often exhibit anomalous steps at the fault, with the direction of stepping presumably indicating the sense of displacement. Fig. 4 is an overview of the Waucoba embayment with the locations of the faults in question shown in yellow. We mapped out the course of 43 drainages crossing the fault in areas A and B. Channels were numbered sequentially by category from north to south. They were divided into five categories. "Normal" (N) streams that flowed directly downslope and did not exhibit any unusual deflections. "Right Stepping" (RS) drainages deflected to the right when viewed downhill. "Right Distributory" (RS) drainages split, with part flowing straight down hill, but with another channel splitting off and deflecting along the course of the fault in a right-hand sense. "Left Stepping" (LS) and "Left Distributory" (LD) are analogous to RS and RD, but to the left. Fig. 5 shows the classification for "Area A" in Fig. 4.

Figure 5. Drainage classification for "Area A" in Fig. 4. The legend in the upper right shows the totals for the drainage classification in Area A and Area B.

The legend in Fig. 5 shows the totals for all the drainage classifications in both Areas A and B (graphic for Area B is not shown). Lumping the deflections into only right, normal, and left, the totals are 2 right deflections, 25 normal, and 16 left. Were there no strike-slip component of movement on the faults, one would expect that most drainages would be normal, with a much smaller and approximately equal number of right and left deflections. The strong predominance of left deflections suggests that there is ongoing sinistral movement on the faults.

Apparent Displacement of Stream Channels

The suggestion of sinistral motion is reinforced by a more detailed reconstruction of an area near the middle of the embayment, shown in Fig. 6. Here drainages that cross the fault show anomalous behavior, including terminating at the fault and sinistral deflection along the fault. The southernmost drainage highlighted in Fig. 6A is particularly interesting. It is deeply incised, which is unusual at this location, but it terminates at the fault without any headwater drainage. In Fig. 6B the same area is shown with 250 m of sinistral displacement restored. The headless drainage now connects to a significant and deeply incised headwater drainage. All but one of the original drainages are now continuous. The hypothesized reconstruction is matched to drainage in the center of the figure; those to the south show a slight mismatch in a dextral sense and those to the north a similar mismatch in a sinistral sense, suggesting that displacement may decrease from north to south.

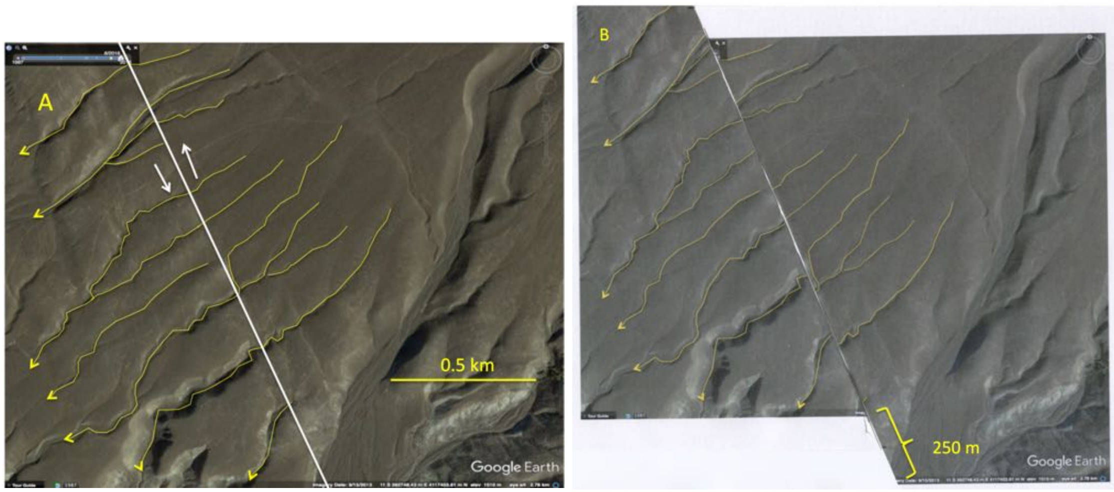

Figure 6. Possible reconstruction of apparently sinistrally displaced drainages in the central Waucoba embayment. The location is shown in Fig. 4.

Apparent Reverse Faulting in Bedrock

Nelson (1966) mapped a fault extending through the Campito and Deep Springs Formations north of Soldier Canyon. The outcrop of these bedrock units forms the northeastern side of the Waucoba embayment, with the fault centered close to 37.20 N and -118.18 E. This fault shows apparent reverse displacement (Fig. 7). The displacement extends into overlying Quaternary colluvium, indicating that it is ongoing. The total amount of displacement does not appear to be large and the feature is probably a reactivated Paleozoic fault. But it does support the hypothesis of a local compressive stress regime.

Anomalous Fault Morphology

The surficial expression of the faults in the Waucoba embayment exhibits a characteristic morphology that is not shared by any other normal faults in the Owens Valley area, so far as we know. Normal faults appear as a single step, or a series of steps, with the treads of the steps, of course, on the downthrown side. Evidence of downfaulted displacement is common. In contrast, the faults of the Waucoba embayment typically appear to as an aligned series of flat-topped ridges, or horst-like figures (Fig. 8C). Jager (2002) refers to them as consisting “predominantly of many narrow grabens” but this description is equivalent, just emphasizing the lows instead of the highs. Although major faults in the Owens Valley, such as portions of the Owens Valley fault or the White

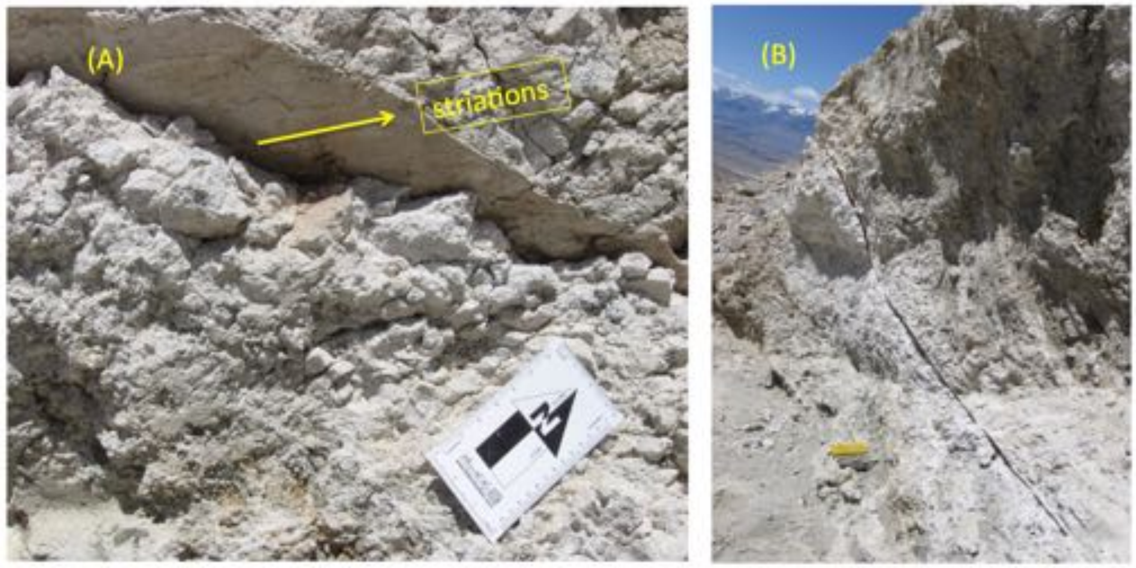

Figure 7. Fault on the east side of the Waucoba embayment that shows apparent reverse displacement. (A) Close up showing slickensides and striations. (B) View along strike looking west.

Mountain Fault Zone between Black Canyon and Laws sometimes exhibit graben structures parallel to the major fault, continuous lines of horst such as are shown in Fig. 7C, and extending laterally over large distances are not found elsewhere. Jager (2002) also notes that the “subsurface geometry of most faults was not observable in the field” and this concurs with our observations. Like Jager, we have observed a number of small-displacement faults in the lake sediments, dipping both east and west. However, these do not appear to explain the down-stepping of the embayment sediments to the west.

What appear to be more pervasive and more significant are anticlinal structures that underlie the horst-like features. We have outlined one of these in Fig. 8C. We have observed similar features in numerous locations. Rarely, if ever, are the lacustrine sediment beds simply terminated at the edges of the horst as would be expected for normal fault displacement. These suggest that the anticlinal features are actually compressional features, specifically, fault-bend folds (Fig. 8A, 8B). We hypothesize that the underlying faults are west-directed thrusts representing the westward termination of the fault blocks moving sinistrally on the Deep Springs fault. As shown in Fig. 2, the direction of displacement, if parallel to the faults, is slightly oblique to the Waucoba embayment fault array, which would also produce a small component of sinistral displacement in Waucoba. The rheology of the Waucoba embayment is ideal for producing fault-bend folds, with a fairly thin layer (~100 m) of very soft lacustrine sediment draped over comparatively rigid basement rock.

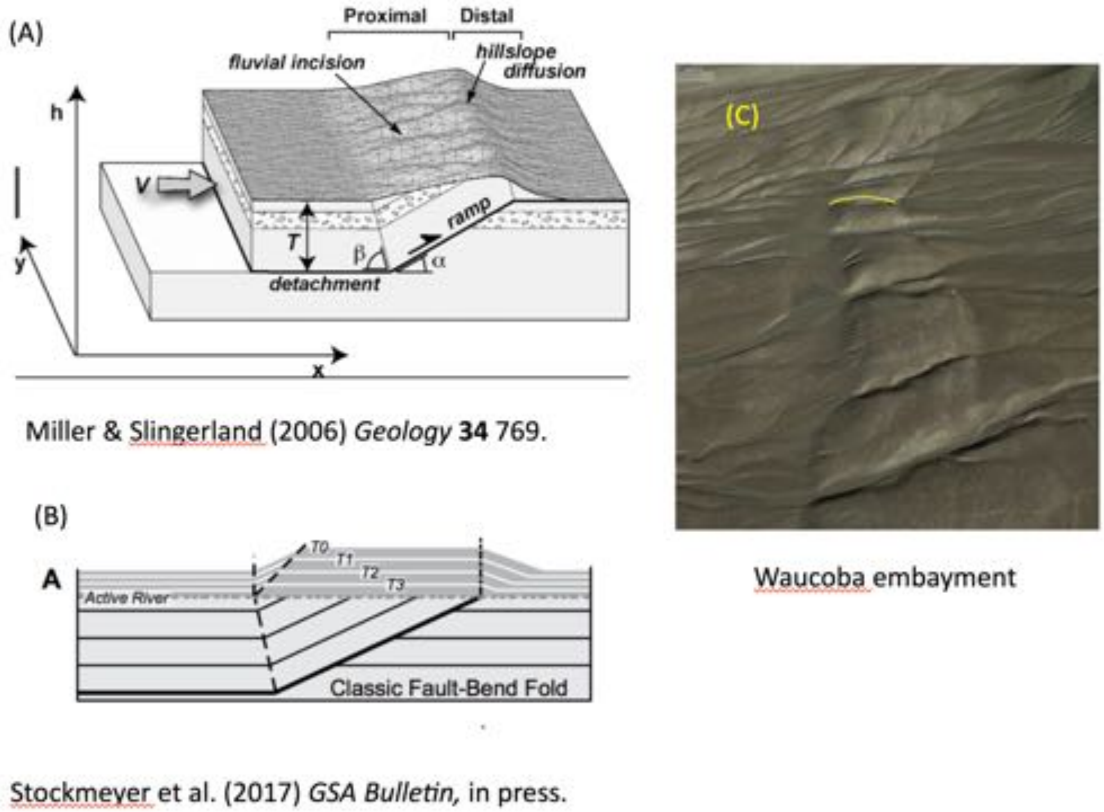

Figure 8. (A) Geometry of a fault-bend fold without sedimentary cover, from Miller and Slingerland (2006). (B) Cross section of a fault-bend fold covered by relatively thin plastic flexible sediment, from Stockmeyer et al. (2017). (C) Google Earth image, looking northwest, of a structure we interpret as a likely fault-bend fold. Yellow highlights anticlinal deformation of a light-colored lacustrine bed (compare with panel B). The location of the image is shown in Fig. 4; it is the prominent dissected feature oriented diagonally across the box in Fig. 4. Note that the inferred vergence of the feature in (C) is opposite to those in (A) and (B).

Implications

We hypothesize that the anomalous faults observed on the east side of the Waucoba embayment are a combination of thrust fault-bend folds and minor sinistral strike-slip faults, and that these constitute the western edge of the hanging wall of the Deep Springs fault. We note that the Waucoba embayment directly faces the Big Pine accommodation zone. To the south, active faulting is focused on the Sierra Nevada frontal fault, on the west side of the valley, whereas to the north it is on the White Mountain fault zone, on the east side. The accommodation zone itself is the narrowest point in the entire Owens Valley, indicating that net extension is restrained at its center. This restraint may have propagated into minor compression at the western edge of the Deep Springs fault hanging wall.

We further hypothesize that this compression may have been an important factor in the formation of the Waucoba embayment. If the Inyo/White Mountain block has to a minor extent overridden the area on its western margin, this would tend to suppress isostatic rebound in response to the downfaulting of the Owens Valley floor. Formation of the Waucoba embayment may thus be tied to the initiation of faulting in Deep Springs Valley.

References

Bachman S. B. (1974) Depositional and structural history of the Waucobi Lake bed deposits, Owens Valley, California: M.S. Thesis, University of California at Los Angeles, 129 pp.

Bachman S. B. (1978) Pliocene - Pleistocene break-up of the Sierra Nevada - White - Inyo Mountain block and the formation of the Owens Valley: *Geology* **6** 461-463.

Davis W. M. (1926) The value of outrageous geological hypotheses: *Science* **63** 463-468.

Jager J. M. (2002) Patterns of Quaternary deformation in the Waucobi embayment, Owens Valley, California: M.S. thesis, University of California, Santa Barbara, 53 pp.

Miller S. R. and Slingerland R. L. (2006) Topographic advection on fault-bend folds: Inheritance of valley positions and the formation of wind gaps: *Geology* **34**(9) 769-772.

Nelson C. A. (1966) Geologic map of the Waucoba Mountain Quadrangle, Inyo County, California: U.S. Geological Survey Map GQ-0528, U.S. Geological Survey Map GQ-0528, Scale 1:62,500.

Stockmeyer J. M., Shaw J. H., Brown N. D., Rhodes E. J., Richardson P. W., Wang M., Lavin L. C., and Guan S. (2017) Active thrust sheet deformation over multiple rupture cycles: A quantitative basis for relating terrace folds to fault slip rates: *Geological Society of America Bulletin*.

Taylor G. F. (1933) Quaternary fault structure of the Bishop region, east-central California: unpublished Ph.D. dissertation, California Instutite of Technology, Pasadena, 161 pp.

Walcott C. D. (1897) The post-Pleistocene elevation of the Inyo Range and the lake beds of Waucobi embayment, Inyo County, California: *Journal of Geology* **5** 340-348.

Road Log

14.1 Resume driving westward on the Big Pine/Death Valley Road. The direction provides a good perspective on the Sierra Nevada to the west. The small town of Big Pine is directly across the valley. The prominent basaltic volcano south of Big Pine is Crater Mountain, whose height is in large part due to its situation on top of a granite horst. Depending on the light you may be able to make out the streak near its base created by movement on the Owens Valley fault. We will visit this site on Stop 3.2.

The Sierra Nevada behind Crater Mountain was formed as a result of normal displacement on a single strand of the Sierra Nevada Frontal Fault. Toward the north this splits into numerous strands. North of Big Pine the Sierra front is no longer defined by a single normal fault, or any normal fault, for that matter. Instead the range front is warped downward into the Owens Valley in a structure that Bateman (1965) named the Coyote Warp. The narrowest width of the entire Owens Valley, 7 km, is between the southern end of the Coyote Warp, named Warren Bench, and the Waucoba embayment. We will visit Warren Bench on Stop 3.1.

17.9 Rejoin State Highway 168 and turn left (W). Watch for traffic in both directions.

18.3 Zurich. Highway 168 crosses the abandoned roadbed of the narrow gauge Carson & Colorado Railroad, constructed in 1882. At this point a station house named 'Zurich' was constructed and a small community grew up around it. The rail line, later acquired by the Southern Pacific, was abandoned in 1960.

18.7 Cross the Owens River.

20.2 Junction with Highway 395. Turn right (N), watching for traffic coming from the left. The Giant Sequoia just to the south of the intersection, one of very few on the west side of the Sierra Nevada, is named the Roosevelt Tree. It was planted on July 23, 1913 in honor of U.S. president Teddy Roosevelt. It is accompanied by a giant U.S. flag, flown in memory of U.S. armed services veterans.

As you drive north on 395, look east across the Owens Valley. The prominent canyon in the White Mountain front is Black Canyon and the large peak to its south is Black Mountain. Note the diminutive size of the alluvial fan at the canyon mouth, in spite of Black Canyon being one of the largest drainages on the west side of the White Mountains. To the north of Black Canyon you should be able to distinguish light colored alluvial deposits plastered on the mountain face, up to about two-thirds of the height of the mountain face. This is the Alluvium of Black Canyon, named by Bateman (1965). This deposit contains a record of sedimentation, environment, and tectonics from about 3 to 2 Ma. It will be one of the topics presented at our next stop.

To the west you get good views of the Coyote Warp. You will be able to contrast the geomorphic character of this mountain front with the much more precipitous and linear Sierra front at Round Valley, the last stop on today's trip.

22.4 0.8 km to the east is Klondike Lake. This shallow lake is dammed by the scarp of a northeast-trending down-to-the-northwest fault. This fault is part of the poorly understood transfer of displacement from the northern end of the Owens Valley fault to the White Mountain fault zone, whose scarps are visible at the base of the White Mountains across the Owens Valley. Beyond Klondike Lake are visible the white 'dishes' of the Owens Valley Radioastronomy Observatory, operated by Cal Tech.

32.4 Warm Spring Road. Turn right (E). Road proceeds east across the probably late Pleistocene alluvial plain of the Owens Valley floor.

36.2 The road drops to a lower terrace, probably the Holocene floodplain.

36.7 Cross Owens River. The Alluvium of Black Canyon and related Quaternary alluvial deposits lie straight ahead, and does the White Mountain Fault Zone (WMFZ) (see Figure 2). Keep an eye on these for the next few miles. Note the height of the Alluvium on the face of the ridge to the right (the one immediately north of the mouth of Black Canyon). These extend up to 1900 m, compared to a ridge-top elevation of 2400 m. The depth to bedrock (which is effectively the plane of the White Mountain fault) under our feet is about 3.5 km.

37.0 Intersection with the Eastside Road. Turn left (N).

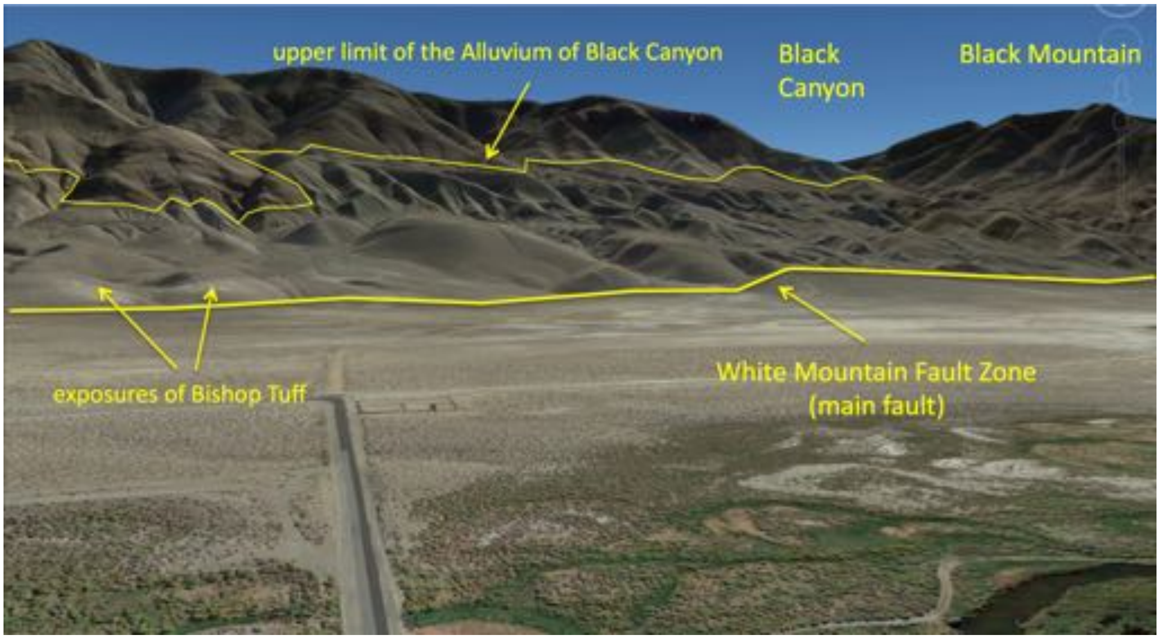

Figure 2. View eastward from the Owens River toward the face of the White Mountains.

37.1 Note, at the base of the mountain to the east, shutter ridges along the WMFZ. Light-colored patches on the shutter ridges are outcrops of the Bishop Tuff (767 ka). These are not contained in the Alluvium of Black Canyon, but rather the younger (middle Pleistocene) Alluvium of Gunter Creek (Kirby et al., 2006).

38.0 For the next 1 ½ mile we drive past the large alluvial fan of Poleta Canyon to the east. The lower half of the fan is composed of the Alluvium of Gunter Creek and the upper half of the Alluvium of Black Canyon. The fan is extensively faulted, with numerous shutter ridges. Most of the displacement appears to be dextral strike slip. Tephras dating to ~3 Ma are exposed in the upper portion (Lueddecke et al., 1998) and 767 ka Bishop Tuff outcrops are visible from the road in the lower part (Kirby et al., 2006), thus vertical displacement in the fan cannot be large. The depth to basement below the road we are on is ~ 2 km and shallows northward. The Bishop Tuff is found in the subsurface at ~200 m depth (Bateman, 1965), thus the vertical displacement rate on the main fault (at the base of the exposed fan deposits) is about 0.3 mm/yr. Kirby et al. (2006) calculated a dextral displacement rate of 0.7 to 0.8 mm/yr at this location.

39.6 The road begins to bend gradually to the west.

40.2 The green oasis to the west is the White Mountain Research Station, run by the University of California. Many famous geologists have used the facility or been based there, notably Clem Nelson and Angela Jayko.

40.4 Poleta-Laws Road. Turn right (N).

42.0 Continue to observe WMFZ to the east. Just ahead the nature of the faulting changes significantly. Between the Waucoba embayment and Black Canyon the WMFZ appears to be a simple dip-slip structure, although it may be accommodating dextral-oblique slip with a large vertical component. North of Black Canyon this changes to a more complex fault zone with numerous strands between the westernmost expression of the fault and the Paleozoic bedrock of the White Mountains. As described above, these seem to principally strike-slip structures. Most of the vertical component is at the westernmost, range-bounding fault. North of Silver Canyon this changes to a regime in which slip partitioning is much more explicit. Dextral strike-slip motion is accommodated on a very high-angle fault that cuts across the alluvial fans well west of the mountain front. This fault seems to have very little vertical component of slip. The vertical component is accommodated on the faults that form the contact between the alluvial fill and the Paleozoic bedrock. These faults are relatively shallow (60° to 30°) and motion appears to be entirely dip slip. At Stop 1.2 we will examine the question: which of these faults is the one along which regional-scale displacement is happening?

43.3 Intersection with Laws Road. Turn left (W).

43.9 Laws Railroad Museum to the left. Laws was the station on the narrow gauge Carson & Colorado Railroad (later the Southern Pacific) that served Bishop. Trains ran here from 1883 to 1960. The author rode on the last steam train to leave Laws, in 1958. In addition to Engine 9 that pulled that train, the site contains an extensive museum of railroad artifacts and rolling stock and numerous historical buildings and mementos of frontier life in the Owens Valley. It is well worth a visit.

44.2 Junction with U.S. Highway 6. Turn right (N) and WATCH FOR ONCOMING TRAFFIC!

44.7 The pinkish mesas to the west are part of the Volcanic Tableland, formed from welded Bishop tuff. We will discuss the emplacement of the Bishop Tuff outflow sheet at Stop 1.2.

48.3 Junction with Rudolf Road. Turn left (W). WATCH FOR ONCOMING TRAFFIC!

49.0 Turn right (N) at unmarked road junction.

49.1 Turn left (W) at entrance road to Bishop Tuff open-pit mine. You will drive into the excavated area, make a complete circle, and exit by means of a small road trending northeast. Follow flagger instructions carefully.

49.3 **Stop 1.2** Exit your vehicle and walk ~50 m southeast to a vantage point overlooking the face of the White Mountains. This is the lunch stop, so remember to BRING YOUR LUNCH!

Stop 1.2: Emplacement of the Bishop Tuff (Hildreth), Age and significance of the Alluvium of Black Canyon (Jayko/Phillips), Tectonic significance of the Alluvium of Black Canyon (Phillips/Jayko), Chalfant Valley earthquake of 1986 (Phillips), Kinematics and tectonic geomorphology of the White Mountain fault zone (Kirby/Knott).

Stop 1.2: Bishop Tuff at the Chalfant Valley Pumice Quarry

Wes Hildreth and Judy Fierstein

US Geological Survey

(This passage is quoted from Hildreth and Fierstein, 2017, p. 36-38, with minor editing to make it consistent with this guidebook)

Excavations here provide fine exposures of plinian pumice-fall deposits and distal nonwelded ignimbrite. The fall deposits, here 5.4 m thick (fig. 1), were subdivided by Wilson and Hildreth (1997) into nine units (F1–F9), most of which are identifiable at all exposures west of the White Mountains. The underlying paleosol and F1–F5 are beneath the floor of the quarry. Layer-by-layer deposition was from an eruption plume estimated to have increased in height from 18 to 45 km and to have lasted 5–6 days, most of the material having been blown eastward as ashfall. Little fine ash is present in the fall deposits here, 42 km southeast of the opening vent site, owing to winnowing in the eruption plume. Vertical changes in pumice-clast size reflect to a first order the power of the eruption. The sparser, smaller and denser, lithic fragments are equivalent aerodynamically to co-deposited pumice. Unlike the flow deposits, the only opportunity for lithics to be incorporated in the fallout was at the vent. Scrutiny of the lithic assemblage in the fall deposits has thus been used to identify the initial vent site in the south-central part of the caldera and to recognize changing vent sites later in the eruptive sequence (Hildreth and Mahood, 1986). Recognition of the first appearance of rhyolite lithics just below the F8–F9 contact, for example, signals vent migration eastward into the Glass Mountain pyroclastic fan. The first appearance and subsequently increasing proportion of rhyolite in the lithic suite provided key stratigraphic markers for both fall and flow deposits (Wilson and Hildreth, 1997).

Crystal content of the fall deposits increases upward, although this is not generally true of the co-deposited pumices. This reflects the expectation and inference that, with increasing column height, the mean sizes of all clast types increases, and, for F6–F9, the range in fall velocities represented by deposition at this particular distance and azimuth from the vent coincided with that of the mode (0.5–2 mm) of the phenocryst population. Low-angle cross-bedding in some of the fall deposits is interpreted as induced by strong swirling winds during deposition of the falling pyroclasts (Wilson and Hildreth, 1998), as promoted by atmospheric inflow toward buoyant thermal updrafts above concurrent pyroclastic flows.

No break is recognized in the F1–F8 sequence. The fine-ash-bearing layer a few centimeters thick at the F8–F9 contact may represent the only hour-long pause in the eruption. By comparing accumulation rates of historic eruptions with thickness and lithic-dispersal characteristics comparable to each of the Bishop fall units, we estimated that the F1–F8 sequence took ~90 hours and F9 an additional ~26 hours (Wilson and Hildreth, 1997, tables 3, 4; Hildreth and Wilson, 2007).

The ignimbrite is manifestly ill-sorted, with grain sizes ranging from dust to blocks, reflecting transport in concentrated pyroclastic flows that provided little opportunity for mixing with air or consequent winnowing of fine and low-density components. Pumice clasts can be rafted buoyantly to far greater distances than their size equivalents in the fallout. The concentrated deposits also retain sufficient heat that thermal oxidation is common and welding is typical of thicker, more proximal, sections. The ignimbrite here was deposited in a series of pulses that produced meter-scale layering commonly defined by trains of pumice clasts. Accumulation was seldom slow enough to allow formation of clear flow-unit boundaries nor continuous enough to produce homogeneous material. In contrast to the fall deposits, stratification cannot be traced for more than tens to hundreds of meters around the quarry. Correlation of ignimbrite between different exposures was done by defining multi-flow packages that share distinguishable populations of pumice and lithics (Wilson and Hildreth, 1997; Hildreth and Wilson, 2007).

A distal flow of package Ig1Eb, only 1–2 m thick, is intercalated here in F8 (fig. 2). Like the fall layers below, it contains no rhyolite lithics, no pyroxene-bearing pumice, and no crystal-rich pumice. All three of these components are present in F9, however, and in package Ig2Ea, which here overlies part of F9. North of here, Ig1Eb thickens into a wedge of similar material >80 m thick, much of which is densely welded. West of here, Ig2Ea forms the lower part of the Volcanic Tableland and crops out along the Chalk Bluff escarpment for ~10 km (as far as Stop 15).

Elsewhere, F9 is as thick as 207 cm (4 times as thick as here) and is thought to have erupted synchronously with all the radial sectors of Ig2. Since Ig1E was entirely coeval with F1–F8 and Ig2 with F9, then the entire eruption took less than six days. The importance of the chronostratigraphic framework is threefold (Wilson and Hildreth, 1997, 2003; Hildreth and Wilson, 2007; Chamberlain and others, 2015). (1) Because much of the Bishop Tuff underwent devitrification and vapor-phase crystallization, many phenocrysts are exsolved, oxidized, or otherwise altered. Understanding of the emplacement sequence allows sampling of pumice from fresh glassy parts of every package.

(2) Proportions of pumice clasts of different characteristics or composition can be estimated by clast counts of each eruptive subunit, permitting assessment of the time-volume-compositional progress of the eruption. (3) Understanding the opening and migration of successive vents around the caldera and the changing proportions of different compositions that erupted from each vent segment provides evidence important for attempting to reconstruct the distribution of magma in the pre-eruptive reservoir and to model dynamic processes of magma withdrawal.

Figure 1. Bishop Tuff plinian fall deposit at Chalfant Valley pumice quarry (Stop 13). Subdivision into nine fall units (F1–F9) is widely recognizable east and southeast of the caldera (Wilson and Hildreth, 1997). Thickness of F6–F9 part of section continuously exposed in quarry is ~3.5 m. F8 and F9 are separated by a few centimeters of white fines-bearing ash that accumulated during a short break in plinian deposition; see also figure 28. Where excavated to base of F1 (inset), complete fall section here is 5.4 m, ~42 km southeast of the initial vent site. Fall deposit is overlain by several meters of nonwelded ignimbrite package Ig2Ea, in which faint stratification reflects episodic deposition as a series of pulses. Spade work and photo for inset by C.J.N. Wilson, master excavator.

Figure 2. Thin distal bilobate flow unit of Ig1Eb synchronous with deposition of fall unit F8, at Chalfant Valley pumice quarry (Stop 13). Accumulation rates of fall deposits in comparably powerful historic eruptions inform an estimate of three hours for deposition of F8 (Wilson and Hildreth, 1997). As ignimbrite flowed ~42 km from the vent area, many pumice clasts were buoyantly rafted, leading to preferential accumulation of low-density pumice at distal edges of flow units, as represented by the pumice rubble at margins of the Ig1Eb flow lobes intercalated here. Darker F9 is 65 cm thick and overlies a 3–5 cm layer of white ash that represents the only time break (~1 hour?) recognized in accumulation of Plinian falls F1 through F9. Streaky to weakly cross-bedded aspect of F8 and F9 is attributed to penecontemporaneous mobilization of falling pyroclasts by swirling winds associated with concurrent pyroclastic flows (called hybrid fall deposits by Wilson and Hildreth, 1998). Note the pumice-poor ~20-cm fine-grained basal layer of Ig2Ea above F9.

References

Chamberlain, K.J., Wilson, C.J.N., Wallace, P.J., and Millet, M.-A., 2015, Micro-analytical perspectives on the Bishop Tuff and its magma chamber: Journal of Petrology, v. 56, p. 605–640

Hildreth, W., and Mahood, G.A., 1986, Ring-fracture eruption of the Bishop Tuff: Geological Society of America Bulletin, v. 97, p. 396–403.
Hildreth, W., and Fierstein, J. (2017) Geologic field-trip guide to Long Valley Caldera, California: USGS Scientific Investigations Report 2016-5022-Y, 119 p.
Hildreth, W., and Wilson, C.J.N., 2007, Compositional zoning of the Bishop Tuff: Journal of Petrology, v. 48, p. 951–999.
Wilson, C.J.N., and Hildreth, W., 1997, The Bishop Tuff—New insights from eruptive stratigraphy: Journal of Geology, v. 105, p. 407–439.
Wilson, C.J.N., and Hildreth, W., 1998, Hybrid fall deposits in the Bishop Tuff, California—A novel pyroclastic depositional mechanism: Geology, v. 26, p. 7–10.
Wilson, C.J.N., and Hildreth, W., 2003, Assembling an ignimbrite—Mechanical and thermal building blocks in the Bishop Tuff, California: Journal of Geology, v. 111, p. 653–670.

Neogene deformation in Owens Valley reactivates a major shear zone of probable Laramide age

John M. Bartley[1], Allen F. Glazner[2], Andrew R. C. Kylander-Clark[3], Drew S. Coleman[2], Ryan E. Frazer[2]
[1]Department of Geology and Geophysics, University of Utah, Salt Lake City, Utah 84112; john.bartley@utah.edu
[2]Department of Geological Sciences, University of North Carolina, Chapel Hill, North Carolina 27599
[3]Department of Earth Sciences, University of California Santa Barbara, Santa Barbara, California 93106

Introduction

Geomorphic, seismologic, paleoseismologic, and geodetic studies indicate that late Cenozoic deformation across Owens Valley is characterized by right-lateral transtension. However, the valley also straddles the boundary between the Mesozoic subduction-related Sierra Nevada batholith, and its back-arc region which is characterized by isolated plutons emplaced into variably deformed and metamorphosed sedimentary and volcanic rocks. The eastern margin of the Sierra Nevada batholith has been a locus of folding, thrusting, and lateral shear since Triassic initiation of the subduction-related magmatism that formed the batholith (e.g., Dunne, 1986; Schweickert and Lahren, 1993; Stevens and Greene, 2000; Bartley et al., 2007, 2012). Bedrock geologic relations across Owens Valley thus reflect overprinting of multiple tectonic regimes.

Offset geologic markers

Right-lateral shear across the valley was long believed to have begun in Plio-Pleistocene time (e.g., Monastero et al., 2002) and early attempts to correlate Jurassic intrusive rocks across the valley concluded that net lateral displacement does not exceed ~5 km (Moore and Hopson, 1961; Ross, 1962). This view began to change when Stevens and Stone (2002) correlated a distinctive submarine channel facies in Devonian rocks in the Mt. Morrison pendant to similar rocks at the foot of the Inyo Mountains near Tinemaha Reservoir. The correlation led Stevens and Stone to infer ~65 km of dextral offset between the Sierra Nevada and White/Inyo Mountains that they interpreted to be older than 225 Ma, i.e., pre-middle Triassic.

Subsequent work has identified other markers that indicate a similar magnitude of dextral offset, but require the offset to be much younger (Fig. 1). Kylander-Clark et al. (2005) reported identical 83.5 Ma U-Pb zircon dates from closely similar porphyritic granite dikes in the Coso Range (Duffield et al., 1980) and in the Sierra Nevada (Golden Bear dike; Moore, 1963, 1981). Correlation of the dikes implies 65 ± 5 km of dextral offset between the Sierra Nevada and the Coso Range since 83.5 Ma.

Kylander-Clark et al. (2005) noted that the dikes in both ranges were intruded into ~102 Ma leucogranite, the Cactus Flat leucogranite in the Coso Range (Whitmarsh, 2002) and the Bullfrog-Independence pluton in the Sierra Nevada (Saleeby et al., 1990; Kylander-Clark et al., 2005; Frazer et al., 2016). The leucogranite plutons are too large to provide a precise estimate of offset but their correlation is important owing to its uniqueness. The Cactus Flat leucogranite is the only known 102 Ma pluton on the eastern side of Owens Valley and, although ~102 Ma plutons are widespread in the Sierra Nevada, the Bullfrog-Independence pluton is the only one exposed at the eastern Sierran range front.

If there is 65 km of post-83.5 Ma right-lateral offset across Owens Valley, then the ~148 Ma Independence dike swarm (IDS)—the marker that Moore and Hopson (1961) interpreted to preclude large offset—also must be offset. Bartley et al. (2007) distinguished within the IDS a central zone, 5 to 20 km wide, of abundant and compositionally diverse dikes (Fig. 1) which is surrounded by a halo of much sparser and almost exclusively mafic dikes. Like the Golden Bear-Coso dikes and 102 Ma leucogranites, the IDS central zone steps dextrally across Owens Valley but, because the IDS intersects the valley at a low angle (~20°), the offset estimate carries a large uncertainty (see Bartley et al., 2007, for further discussion). However, restoration of 65 km as indicated by the Golden Bear-Coso dike correlation brings segments of the IDS central zone into close alignment (Fig. 1).

Correlation of the Golden Bear and Coso dikes recently has been challenged. Pluhar et al. (2008, 2009) reported that a single paleomagnetic site in the Golden Bear dike records normal magnetic polarity whereas sites in the Coso dikes record mixed polarities. Pluhar et al. argued that this casts doubt on correlation of the dikes. Polon et al. (2016) contrasted the small swarm of dikes mapped in the Coso Range with the single thick Golden Bear dike exposed at the Sierran range front. They argued that this favors correlation of the Coso dikes with a swarm of 83 Ma porphyritic granite dikes in the Sierra Nevada near Cottonwood Lakes, implying a dextral offset of only ~25 km.

We regard the Golden Bear-Coso dike correlation as still the most probable for several reasons. The dikes were emplaced near the end of the Cretaceous Normal Superchron (~84-83 Ma; Ogg et al., 2016). The duration of dike intrusion is unknown and could have lasted through the magnetic field reversal; even if dike intrusion per se did not continue through the field reversal, magnetic remanence acquisition by the dikes might have occurred over such a duration. Thus the paleomagnetic data raise interesting questions about the timing and duration of dike intrusion and magnetic remanence acquisition, but they do not exclude the correlation. The number of dikes and their individual thicknesses actually vary in both ranges (Kylander-Clark et al., 2005), but exposures closest to the valley in both ranges consist of a single 20 m thick dike. Probably most conclusively, the inference of large right-lateral displacement does not depend uniquely on the Golden Bear-Coso dike correlation. The dike correlation is important because it provides the narrowest bounds on the magnitude and the timing of offset, but three independent geologic markers also indicate right-lateral offset of a similar magnitude.

Timing

Among the questions posed by large lateral offset across Owens Valley are its timing and its tectonic setting and significance. Estimates of the recent displacement rate imply that 5 - 10 km of the total displacement accumulated since initiation of the modern tectonic regime in the late Pliocene. Bartley et al. (2007) argued that continuity of the Garlock fault across the southern projection of Owens Valley suggests that the remainder of the 65 km displacement probably accumulated prior to initiation of the Garlock fault at ~15 Ma (Monastero et al., 1997). Therefore, 50 - 60 km of right-lateral displacement across Owens Valley probably occurred between 83.5 and 15 Ma.

Observed deformation

Structures responsible for the large pre-late Miocene offset are largely concealed by valley fill, but local exposures provide indications of the nature of the deformation. The closest approach of bedrock exposures on either side of the shear zone is in the Little Lake area at the southern end of Owens Valley (Fig. 1; Bartley et al., 2007). At Little Lake, the Owens Valley shear zone places Jurassic granodioritic orthogneiss in the Sierra Nevada that lacks Independence dikes against unfoliated, compositionally diverse plutonic rocks in the Coso Range that are cut by numerous Independence dikes. Along the western edge of the Coso Range, the IDS is dismembered by numerous greenschist-facies phyllonite zones. Rock fabrics in the shear zones indicated right-lateral transpressive shear. This ductile deformation is overprinted by a broad zone of brittle shattering that probably reflects neotectonic reactivation of the tectonic boundary.

The ductile shear zones exposed at Little Lake probably belong to a regionally extensive system of late Cretaceous ductile shear zones. Vines (1999) inferred dextral transpressive shear across the Santa Rita shear zone at the western base of the Inyo Mountains, and Sullivan and Law (2003) and Sullivan (2003) reported similar kinematics from the White Mountain shear zone. Geochronology from those shear zones indicates that both formed in the late Cretaceous (~70-80 Ma). Bartley et al. (2007) thus proposed that these three areas are local exposures of a crustal-scale structure that accommodated most of the 65 km of displacement across Owens Valley.

Because intracontinental strike-slip faults rarely have slip rates that exceed a few mm/yr, 50-60 km of offset probably required 20-30 Ma to accumulate. This implies that the early dextral shear across Owens Valley probably persisted across the K-Pg boundary into the Paleogene and corresponds in time to the Laramide orogeny in the continental interior.

The Laramide-aged Owens Valley shear system lies outside of the main Sierran arc and movement across it postdates the end of major Sierran magmatism at ~84 Ma (Stern and others, 1981; Chen and Moore, 1982). The shear zone therefore is not part of the Sierra Crest shear zone of Tikoff and de Saint Blanquat (1997) which was localized within the active arc (Tikoff and Teyssier, 1992). However, the Owens Valley shear zone probably represents a continuation of the same kinematic regime. The Sierra Crest shear zone is interpreted to reflect partitioning of the lateral component of dextral-oblique subduction away from the plate boundary (e.g., Jarrard, 1986). Oblique subduction continued along the western margin of North America for tens of millions of years after magmatism ceased in the Sierran arc (e.g., Doubrovine and Tarduno, 2008). Accommodation of the lateral component of relative plate motion therefore may have shifted from within the arc to the eastern margin of the batholith when lithospheric strength within the batholith increased after igneous activity ceased.

Relationship to modern tectonic regime

Although modern tectonic deformation in Owens Valley includes a large component of right-lateral shear, the substantial majority of right-lateral displacement recorded by bedrock offsets appears to reflect Laramide transpression rather than Neogene transtension. Late Cenozoic deformation in and around Owens Valley thus appears to represent reactivation of a crustal-scale shear zone that formed in the late Cretaceous between the Sierra Nevada batholith and its wallrocks.

Acknowledgments

We thank Pete Lippert for technical review of this paper. The work reviewed here was supported by the Geothermal Program Office of the China Lake Naval Air Warfare Center through contract N68936-01-C-0090 to DSC and AFG, and by NSF grants EAR-9814787 to JMB, EAR-9526803 and EAR-9814789 to AFG, and EAR-9814788 to DSC.

References

Bartley, J.M., Glazner, A. F., Coleman, D. S., Kylander-Clark, A.R.C., and Friedrich, A.M., 2007, Large Laramide dextral offset across Owens Valley, California, and its possible relation to tectonic unroofing of the southern Sierra Nevada, *in* Till, A. B., Roeske, S. M., Foster, D. A. and Sample, J. C., eds., Exhumation Processes Along Major Continental Strike-slip Fault Systems: Geological Society of America Special Paper 434, p. 129-148.

Bartley, J. M., Glazner, A. F., and Mahan, K. H., 2012, Formation of pluton roofs, floors, and walls by crack opening at Split Mountain, Sierra Nevada, California: Geosphere, v. 8, no. 5, p. 1086-1103, doi: 10.1130/GES00722.1

Chen, J. H., and Moore, J. G., 1982, Uranium-lead isotopic ages from the Sierra Nevada batholith, California: Journal of Geophysical Research, v. 87, p. 4761-4784.

Doubrovine, P. V., and Tarduno, J. A., 2008, A revised kinematic model for the relative motion between Pacific oceanic plates and North America since the

Late Cretaceous: Journal of Geophysical Research, v. 113, p. 2156-2202. doi: 10.1029/2008JB005585
Duffield, W. A., Bacon, C. R., and Dalrymple, G. B., 1980, Late Cenozoic volcanism, geochronology, and structure of the Coso Range, Inyo County, California: Journal of Geophysical Research, v. 85, p. 2381-2404.
Dunne, G., 1986, Mesozoic evolution of the southern Inyo mountains, Darwin plateau, and Argus and Slate ranges, in Dunne, G., ed., Mesozoic and Cenozoic structural evolution of selected areas, east-central California: Los Angeles, Geological Society of America, Cordilleran Section Meeting, Guidebook and volume Trips 2 and 14, p. 3-21.
Frazer, R.E., Gaynor, S., and Coleman, D.S., 2016, Implications of a 102 Ma Alabama Hills granite for dextral offset in Owens Valley, CA, and the organization of Sierran magmatism: Geological Society of America Abstracts with Programs, v. 48, No. 4. doi: 10.1130/abs/2016CD-274718
Jarrard, R. D., 1986, Terrane motion by strike-slip faulting of forearc slivers: Geology, v. 14, p. 780-783.doi: 10.1130/0091-7613(1986)14<780:TMBSFO>2.0.CO;2
Kylander-Clark, A.R.C., Coleman, D.S., Glazner, A.F., and Bartley, J.M., 2005, Evidence for 65 km of dextral slip across Owens Valley, California, since 83 Ma: Geological Society of America Bulletin, v. 117, no. 7, p. 962–968.
Monastero, F. C., Sabin, A. E., and Walker, J. D., 1997, Evidence for post-early Miocene initiation of movement on the Garlock fault from offset of the Cudahy Camp Formation, east-central California: Geology, v. 25, p. 247-250.
Monastero, F. C., Walker, J. D., Katzenstein, A. M., and Sabin, A. E., 2002, Neogene evolution of the Indian Wells Valley, east-central California, *in* Glazner, A. F., Walker, J. D., and Bartley, J. M., eds., Geologic evolution of the Mojave Desert and southwestern Basin and Range: Boulder, CO, Geological Society of America Memoir, v. 195, p. 199-228.
Moore, J. G., 1963, Geology of the Mount Pinchot Quadrangle, southern Sierra Nevada, California: U. S. Geological Survey Bulletin, v. 1130, p. 152 pp.
Moore, J. G., 1981, Geologic map of the Mount Whitney quadrangle, Inyo and Tulare Counties, California: U.S. Geological Survey Map GQ-1012, scale 1:62,500.
Moore, J. G., and Hopson, C. A., 1961, The Independence dike swarm in eastern California: American Journal of Science, v. 259, p. 241-259.
Ogg, J. G., Ogg, G., and Gradstein, F. M., 2016, A concise geologic time scale: Elsevier, 240 p.
Pluhar, C. J, Ngo My, M., Larsen, M. T., and Carlson, C. W., 2009, Testing correlation of the Golden Bear and Coso dikes in eastern California; implications for dike emplacement and tectonic reconstruction since 83 Ma: Geological Society of America Abstracts with Programs, v. 41, No. 7, p, 137.
Polon, C. K., Pluhar, C. J., Gledhill, T. A., Trayler, R., Crowley, J., Ward, P., Schmitz, M., Ngo My, M., Larsen, M. T., and Carlson, C. W., 2016, 65 km of dextral slip across Owens Valley since 83 Ma; Possible, but unnecessary: Geological Society of America Abstracts with Programs, v. 48, No. 7, abstract no. 347-32.

Ross, D. C., 1962, Correlation of granitic plutons across faulted Owens Valley, California; Article 145: U.S. Geological Survey Professional Paper, v. 450-D, p. D86-D88.
Saleeby, J. B., Kistler, R. W., Longiaru, S., Moore, J. G., and Nokleberg, W. J., 1990, Middle Cretaceous silicic metavolcanic rocks in the Kings Canyon area, central Sierra Nevada, California: Geological Society of America Memoir, v. 174, p. 251-270.
Schweickert, R. A., and Lahren, M. M., 1993, Tectonics of the east-central Sierra Nevada; Saddlebag Lake and northern Ritter Range pendants, *in* Lahren, Trexler, J. H., Jr., and Spinosa, C., eds., Crustal Evolution of the Great Basin and Sierra Nevada: University of Nevada. Reno, Nevada, United States.
Stern, T. W., Bateman, P. C., Morgan, B. A., Newell, M. F., and Peck, D. L., 1981, Isotopic U-Pb ages of zircons from the granitoids of the central Sierra Nevada: U. S. Geological Survey Professional Paper, v. 1071, p. 17.
Stevens, C. H., and Greene, D. C., 2000, Geology of Paleozoic rocks in eastern Sierra Nevada roof pendants: Geological Society of America Field Guide 2, p. 237-254.
Stevens, C. H., and Stone, P., 2002, Correlation of Permian and Triassic deformation in the western Great Basin and eastern Sierra Nevada: Evidence from the northern Inyo Mountains near Tinemaha Reservoir, east-central California: Geological Society of America Bulletin, v. 114, no. 10, p. 1210-1221.
Sullivan, W. A., 2003, Geometry, kinematics, and age of the northern half of the White Mountain shear zone, eastern California and Nevada [unpublished M.S. thesis]: Blacksburg, Virginia, Virginia Polytechnic Institute and State University, 45 p.
Sullivan, W. A., and Law, R. D., 2003, Geometry, kinematics, and age of the northern half of the White Mountain shear zone: Extending the range and duration of dextral transpression along the western margin of North America: Geological Society of America Abstracts with Programs, v. 35, no. 6, p. 114.
Tikoff, B. and de Saint Blanquat. M.. 1997, Transpressional shearing and strike-slip partitioning in the Late Cretaceous Sierra Nevada magmatic arc, California: Tectonics, v. 16, no, 3, p. 442-459.
Tikoff, B., and Teyssier, C., 1992, Crustal-scale, en echelon "P-shear" tensional bridges; a possible solution to the batholithic room problem: Geology, v. 20, no. 10, p. 927-930.
Vines, J. A., 1999, Emplacement of the Santa Rita Flat pluton and kinematic analysis of cross-cutting shear zones, eastern California [unpublished M.S. Thesis]: Blacksburg, Virginia, Virginia Polytechnic Institute and State University, 89 p.
Whitmarsh, R. W., 1998, Geologic map of the Coso Range: Geological Society of America Online Map Series, DOI 10.1130/1998-whitmarsh-coso.

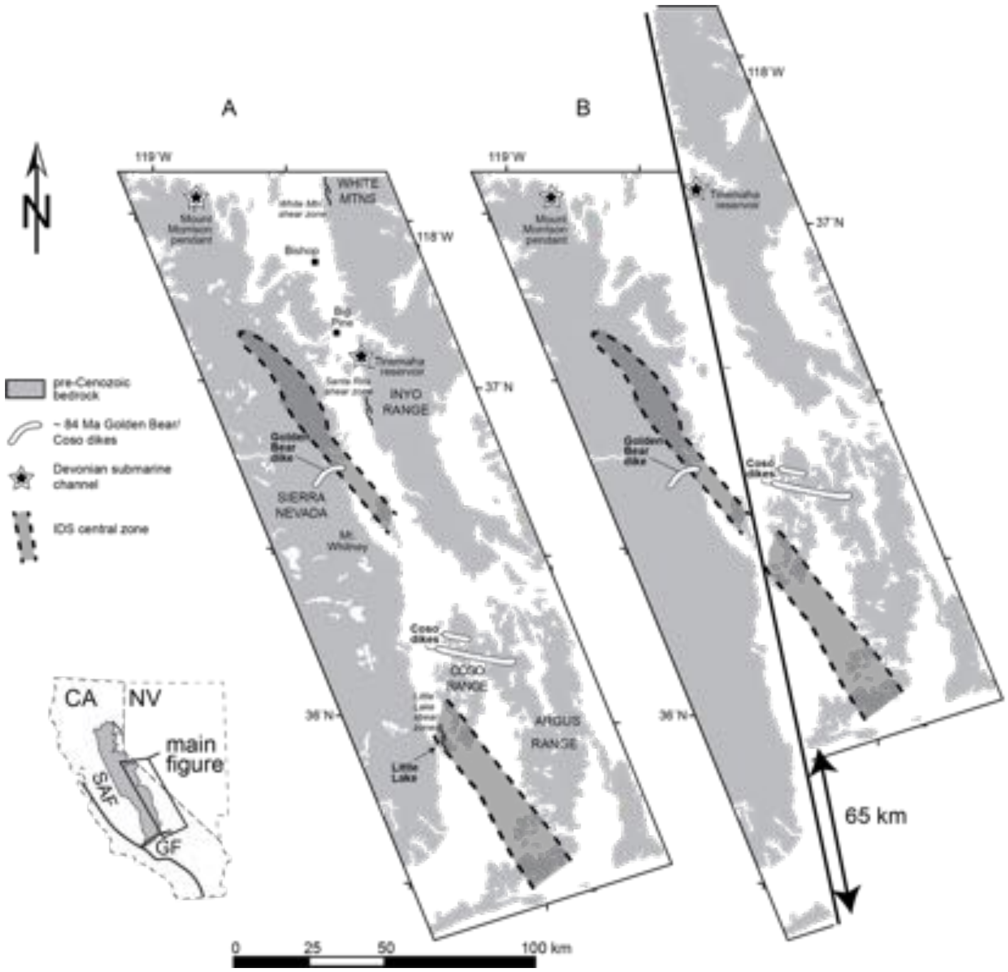

Figure 1: A--Present-day locations of offset bedrock markers in the eastern Sierra Nevada and ranges to the east. Also shown are exposures of dextral transpressive shear zones of known or inferred late Cretaceous-Paleogene age. B—Relative locations of the markers after removal of 65 km of post-83.5 Ma right-lateral displacement across Owens Valley. Simplified from figures in Bartley et al. (2007).

Stop 1.2: Tectonic Significance of the Alluvium of Black Canyon, Owens Valley, California

Fred M. Phillips and Angela Jayko

New Mexico Institute of Mining & Technology and U.S. Geological Survey

Introduction

The Alluvium of Black Canyon is a package of latest Pliocene and early Pleistocene sediment that is found along the lower elevations of the White Mountains from Black Canyon northward to Piute Canyon. The deposits were mentioned in passing by Walcott (1897). They were originally mapped by Knopf (1918) as "Older alluvial cones of the Inyo Range". He noted debris-flow units containing tephra beds, but did not notice the lacustrine beds. The unit was described in some detail by Taylor (1933), who photographed some of the tephras that we and other investigators have dated. He correctly inferred that the setting of the lacustrine beds "suggests strongly at once that rather extensive faulting has occurred along the range front since its deposition" (p. 23). He suggested the name "Zurich formation" for these units extending from the Waucoba embayment northward to Coldwater Canyon, but this name has not generally been adopted. The unit was mapped and named "Alluvium of Black Canyon" (ABC) by Bateman (1965) and this name is generally used. Kirby et al. (2006) subdivided Bateman's unit by separating out the 'Alluvium of Gunter Creek', which does contain the Bishop ash and is thus substantially younger than their 'Alluvium of Black Canyon'.

The ABC consists largely of coarse debris-flow deposits interbedded with a range of lacustrine lithologies. The lacustrine materials include fine-grained marls that are in some cases laminated, silty to sandy deltaic beds, tufas both as isolated heads and encrusting layers and beachrock cement, and thick packages of cross-bedded beach shingle. The lacustrine deposits are characterized by high-energy beach facies near the eastern extent of the ABC (i.e., close to the bedrock of the White Mountains), deltaic deposits in the middle of the belt of 'alluvium', and fine-grained marls at the western edge, suggesting increasing depth of deposition to the west. In most places the sediment package laps onto the White Mountains sedimentary bedrock as a buttress unconformity. In a few places faulted contacts were observed. The number of faulted contacts increases to the north, but most basal contacts are still depositional unconformities. In many places the ABC progrades up tributary canyons, forming dendritic canyon fills that are clearly depositional (see Bateman, 1965). The lacustrine and debris-flow deposits are interbedded with prominent rhyolitic tephras. Bateman (1965), like most previous investigators, correlated these with the Bishop Tuff, but subsequent work has shown that they substantially predate the Long Valley eruption (Lueddecke et al., 1998; Sarna-Wojcicki et al., 2005; Kirby et al., 2006). The total thickness of the ABC exceeds 300 m. It extends up to 1900 m elevation on the White Mountain front, which constitutes 60% of the total range relief at this location (Fig. 1).

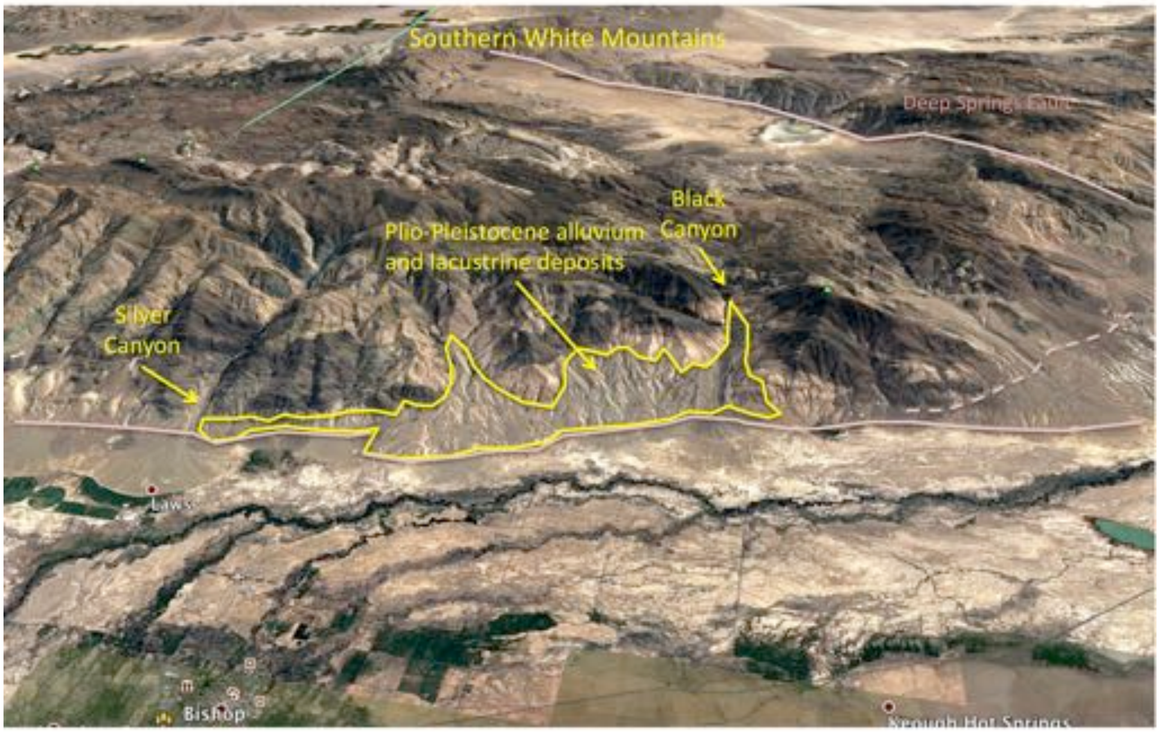

Figure 1. Overview of the southern White Mountains, looking east. The Alluvium of Black Canyon and associated Alluvium of Gunter Creek are outlined in yellow (south of Silver Canyon only). The nearer purple line is the White Mountain fault (WMF). Note the height of the top of the ABC relative to the mountain crest and the narrowing of the deposit to the north.

Chronology for the aggradation of the ABC has been provided by tephra dates measured by Lueddecke et al. (1998), Kirby et al. (2006), and our work. These range from 2.82±0.02 Ma for the Tephra of Black Canyon to the 2.0 Ma Huckleberry Ridge tephra (M. Reheis, personal communication). Our four Ar/Ar ages fall between these, in correct stratigraphic order.

The greatest thicknesses of the ABC are found along the courses of present-day canyons draining the White Mountains and the thinnest portions are over bedrock ridges projecting from the range. This gives the strong impression that the bedrock topography of the range preceded the deposition of the formation. This impression is confirmed by a bedrock narrows in Black Canyon at 37.2906 and -118.2425 (Fig. 2). Fluvial incision has cut through what was formerly a bedrock ridge projecting transversely into Black Canyon from the north. The ancient southward ridge slope is preserved on the south side of the cut, but it is buried in ABC. At this locality the 2.82±0.2 Ma Black Canyon tephra (Lueddecke et al., 1998) is interbedded in the debris-flow alluvium about 80 m above the current channel. The ancient canyon base is not exposed because it was deeper than the

Figure 2. Google Earth perspective overview of the mouth of Black Canyon, looking west. The bedrock channel cut through superposed drainage development is in the center. The Pliocene channel was to the right (south) of the current one. The inset photo shows the bedrock cut from upstream, with the buried Pliocene channel to the right (south).

present channel incision. The relationships at this site clearly indicate that Black Canyon was deeper than its modern depth prior to 2.8 Ma. The canyon relatively rapidly backfilled between >2.8 Ma and 2.0 Ma. Sometime after 2.0 Ma aggradation ceased and the ABC was reincised to nearly its Pliocene depth.

The ABC Paradox

A large amount of evidence indicates that the Owens Valley was extended in two pulses: the first starting at ca. 11.8 Ma and the second at ca. 3.4 Ma (Stockli et al., 2003; Jones et al., 2004; Lee et al., 2009; Phillips et al., 2011). Most of the range exhumation and canyon incision that predates 2.8 Ma must have taken place between 11.8 and 3.4 Ma. One would expect that the second pulse of extension would result in rapid relative downdrop of the Owens Valley floor and resultant incision of the White Mountain canyons. Instead, the opposite happened. The floor of the Owens Valley aggraded and the canyons backfilled, starting at roughly 3 Ma. This continued until the White Mountains were buried in approximately 600 m of alluvium and lacustrine sediment.   At ca. 2 Ma the process reversed and subsequently the valley floor has cut down to nearly its late Pliocene elevation relative to the mountain crest. We term this reduction of down faulting and consequent aggradation during an evident period of rapid extension the "ABC paradox".

One obvious potential explanation for the ABC paradox is that the Owens Valley was dammed at ~3 Ma. However, there is no satisfactory feature, such as a trans-valley volcano or an exceptionally massive landslide, to provide the necessary sill. Also, one would expect that damming of the valley would produce lacustrine fills on both sides of the valley, but there are no deposits corresponding to the ABC on the western side of the valley. What then produced the aggradation?

The Role of Deep Springs Valley

We hypothesize that the ABC paradox is linked to the initiation of faulting on the Deep Springs Valley fault (DSVF). The relation of the DSVF is shown in Fig. 1. The DSVF opened with maximum displacement toward the northwest, indicating that it likely happened during the Plio-Pleistocene episode of transtension rather than the Miocene period of east-west extension (Stockli, 1998). Maximum extension across the valley now totals ~6 km. Alluvial fill in Deep Springs Valley is shallow, only about 800 m (Wilson, 1975), probably indicating a shallowly dipping fault plane (Lee et al., 2001). The southern White Mountains block is effectively the hanging wall of the fault. We illustrate a conceptual geometry of the DSVF and WMF in Fig. 3.

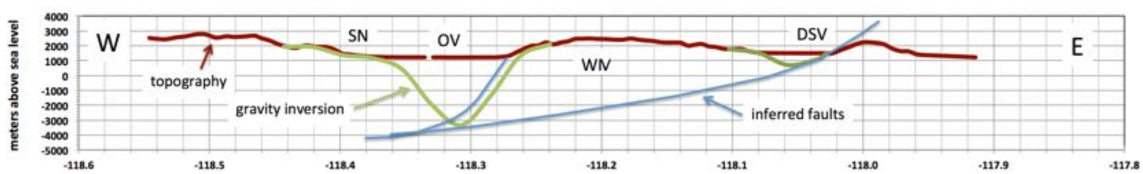

Figure 3. Speculative E-W cross section from Deep Springs Valley (DSV) to the Sierra Nevada (SN). WM = White Mountains, OV = Owens Valley. The green line is the alluvium/bedrock contact, from gravity inversion by Saltus and Jachens (1995). The left blue line is the White Mountain fault. X-axis labels are longitude. No vertical exaggeration.

Initiation of extension on the DSVF would have two important effects on the relation of the elevation of the Owens Valley floor to the White Mountain block. The first is that the White Mountain block would subside during translocation on the sloping fault plane whereas the floor of the Owens Valley, on the west side of the WMF, would not change. This subsidence of the White Mountains would decrease with time if the fault is listric, as portrayed. The second effect is that when displacement formerly focused on the WMF is distributed between the two faults the rate of separation on the WMF will decrease, resulting in a decrease in the rate of creation of accommodation space in both the horizontal and vertical dimensions. This would increase the relative rate of aggradation of the valley floor. However, as the valley floor grew wider, the rate of creation of accommodation space by vertical displacement of the valley floor would grow.

A Simple Model of Relative Aggradation

We have formulated an extremely parsimonious model to simulate the processes described above. It is given by the equation:

$$z_{valley\ floor\ rel\ White\ Mtn} = \sum_{i}^{0}\left(z_{vfo} + \Delta v_{wmfi}\left(\frac{\Delta z}{\Delta x}\right)_{wmf} - \Delta v_{dsfi}\left(\frac{\Delta z}{\Delta x}\right)_{dsf}\right)\frac{S}{L(t)_i}\Delta t_i$$

z_{vfo} = initial elevation of valley floor

Δv_{wmfi} = horizontal displacement rate across White Mtn fault at step i
= 2.75 km/Ma from 3.7 to 3.0 Ma
= 1.5 km/Ma from 3.0 Ma to present

Δv_{dsfi} = horizontal displacement rate across Deep Springs fault at step i
= 0 km/Ma from 3.7 to 3.0 Ma
= 2 km/Ma from 3.0 Ma to present

$(\Delta z/\Delta x)_{wmf}$ = gradient of White Mountain fault plane
= 1.0

$(\Delta z/\Delta x)_{dsf}$ = gradient of Deep Springs fault plane
varies linearly from 0.2 at 3.0 Ma to 0.1 at present

S = sediment delivery rate
= 6.8 km^3 (km valley length N-S)$^{-1}$ Ma^{-1}

$L(t)_i$ = valley width as a function of time
= $L_o + \Delta v_{wmfi}\Delta t$
L_o = initial valley width at 3.7 Ma

Δt = time step
= 0.1 Ma

This equation describes the balance between the creation of accommodation space and the rate of sediment delivery (sediment delivery is assumed to remain constant). Here the first term inside the parenthesis describes the initial elevation of the valley floor, the second one the vertical effect of sliding the White Mountain block down the DSVF plane, the third one the reduction in displacement rate on the WMF due to partitioning between the two faults, and the denominator the increase in Owens Valley width with time due to horizontal displacement on the WMF.

The model results are shown in Fig. 4. The sedimentation rate (sediment delivery divided by valley width times vertical displacement rate of valley floor) decreases with time as the valley widens, but is influenced strongly by the decrease in horizontal displacement at 3 Ma. This causes the elevation of the valley floor to increase and the

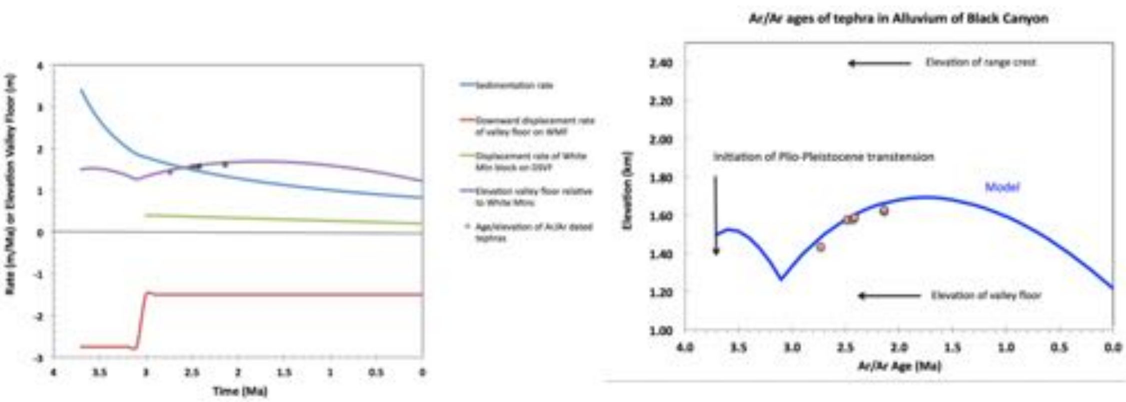

Figure 4. Left panel: change in model terms with time as a result of the initiation of faulting on the DSVF at 3 Ma. Right panel: blow-up of the purple curve (valley floor elevation) and comparison with Ar/Ar-dated tephra elevations in the ABC.

elevation of the White Mountains to decrease, leading to relative aggradation. The pattern of aggradation predicted by the model matches well the measured variation of elevation of the Ar/Ar-dated tephras with time. We note that, although an explanation of lacustrine conditions is provided by subsidence of the White Mountain block on the DSVF, some stable threshold to the south is still required and this may have been provided by the Big Pine accommodation zone.

Implications

The model we test is both simplistic and speculative, but does show a promising match of predicted and measured valley-floor elevations. This result has implications for several phenomena:

1) We note that the chronology of tephras in the Waucoba embayment is strikingly similar to that of the ABC (De Masi, this volume). This hypothesis explains that similarity by linking both to the opening of the DSVF.

2) The Owens Valley is notably narrower along the southern White Mountain front than it is further north (~8 km versus ~25 km). This may to a considerable degree be attributed to a slower rate of displacement across the southern WMF because of partitioning of about half that rate to the DSVF starting at ~3 Ma.

3) North of Bishop the Owens Valley is a full graben with normal faulting on both sides. South if it it is a half graben with faulting only on the east side. This may be attributed to the slower rate of strain to the south because part of the strain is partitioned onto the DSVF.

4) The width and maximum height of the ABC decreases to the north (Fig. 1). This may be attributed to the increase in distance from the DSVF to the north. This would result in less net slip and hence a lower rate of downward displacement of the White Mountain block.

In summary, the modeling and evidence we review above suggests that consideration of the Deep Springs Valley fault and the White Mountain fault as a linked system can explain many aspects of Owens Valley neotectonics.

References

Bateman P. C. (1965) Geology and tungsten mineralization of the Bishop District, California: U.S. Geological Survey Professional Paper 470, Professional Paper 470, 208 p. pp.

Jones C. H., Farmer G. L., and Unruh J. (2004) Tectonics of Pliocene removal of lithosphere of the Sierra Nevada, California: *Geological Society of America Bulletin* **116** 1408-1422.

Kirby E., Burbank D. W., Reheis M., and Phillips F. M. (2006) Temporal variations in slip rate of the White Mountain Fault Zone, eastern California: *Earth and Planetary Science Letters* **248** 168-185.

Knopf A. (1918) A geologic reconnaissance of the Inyo Range and the eastern slope of the Sierra Nevada, California, with a section on the stratigraphy of the Inyo Range by Edwin Kirk: U. S. Geological Survey Professional Paper 110, 130 pp.

Lee J., Rubin C. M., and Calvert A. (2001) Quaternary faulting history along the Deep Springs fault, California: *Geological Society of America Bulletin* **113** 855-869.

Lee J., Stockli D. F., Owen L. A., Finkel R. C., and Kislitsyn R. (2009) Exhumation of the Inyo Mountains, California: Implications for the timing of extension along the western boundary of the Basin and Range Province and distribution of dextral fault slip rates across the eastern California shear zone: *Tectonics* **28** TC1001, doi:10.1029/2008TC002295.

Lueddecke S. B., Pinter N., and Gans P. (1998) Plio-Pleistocene ash falls, sedimentation, and range-front faulting along the White-Inyo Mountains, California: *Journal of Geology* **106** 511-522.

Phillips F. M., McIntosh W. C., and Dunbar N. W. (2011) The chronology of late Cenozoic volcanic eruptions on relict surfaces in the south-central Sierra Nevada, California: *Geological Society of America Bulletin* **123** 890-910.

Saltus R. W. and Jachens R. C. (1995) Gravity and basin-depth maps of the Basin and Range Province, western United States: U.S. Geological Survey, Geophysical Investigation Map GP-1012, Scale??

Sarna-Wojcicki A. M., Reheis M. C., Pringle M. S., Fleck R. J., Burbank D. W., Meyer C. E., Slate J. L., Wan E., Budahn J. R., Troxel B. W., and Walker J. P. (2005) Tephra layers of Blind Spring Valley and related Upper Pliocene and Pleistocene tephra layers, California, Nevada, and Utah: Isotopic ages, correlation, and magnetostratigraphy: U.S. Geological Survey, Professional Paper 1701, 63 pp.

Stockli D. F. (1998) Late Miocene transition from east-west extension to right-lateral transtension in the western Basin and Range province, White Mountains, California-Nevada: *Geological Society of America Abstracts with Programs* **30** 74.

Stockli D. F., Dumitru T. A., McWilliams M. O., and Farley K. A. (2003) Cenozoic tectonic evolution of the White Mountains, California and Nevada: *Geological Society of America Bulletin* **115** 788-816.

Taylor G. F. (1933) Quaternary fault structure of the Bishop region, east-central California: Ph.D. dissertation, California Institute of Technology, Pasadena, 161 pp.

Walcott C. D. (1897) The post-Pleistocene elevation of the Inyo Range and the lake beds of Waucobi embayment, Inyo County, California: *Journal of Geology* **5** 340-348.

Wilson D. V. (1975) Geophysical investigation of the subsurface structure of Deep Springs Valley, California: M.S. Thesis, University of California at Los Angeles, 65 pp.

Stop 1.2: Alluvium of Black Canyon and Implications of the 1986 Chalfant Valley Earthquake for Slip Partitioning on the White Mountain Fault Zone

Fred M. Phillips
New Mexico Institute of Mining & Technology

Introduction

South of the Big Pine accommodation zone the transtensional strain across the Owens Valley is carried principally on two structures: the Owens Valley fault (dextral strike slip) and the Sierra Nevada frontal fault (normal, down to the east). North of the accommodation zone for about 20 km it is carried on just the White Mountain fault zone, which is dextral oblique (Fig. 1). Further north the Round Valley fault appears on the west side of the valley. It is normal in its southern extent, but dextral oblique toward the north end (Phillips and Majkowski, 2011).

North of Silver Canyon the character of the White Mountain fault changes from a fairly complex pattern of dextral-oblique slip on numerous strands to a simpler configuration in which the dip-slip component of strain is localized on a series of faults at the base of the range and somewhat above it, and the strike-slip component on a simple linear fault running across the proximal alluvial fans about 1 km west of the mountain front (Fig. 2). This pattern continues for 25 km north of Silver Canyon, up to Milner Canyon. At this point the surface trace of the strike-slip fault disappears. The configuration of the mountain-front faults also changes at the same position. Between Straight Canyon and Milner Canyon the trace of the normal faults increasingly loops over ridge crests higher up the mountain front, indicating a steadily decreasing fault dip. North of Milner Canyon the dips average about 40°. There is no indication of oblique slip, nor of strike-slip displacement at the range front.

This type of fault behavior is common in the transtensional portion (Oldow, 2003) of the Eastern California shear zone. Partitioning of strain between the Owens Valley fault and the Sierra Nevada frontal fault south of the Big Pine accommodation zone is but one of many examples. This type of fault behavior raises two important questions. The first is "which is the 'real fault'?" (see Fig. 3). This question has previously explicitly been raised by Henry et al. (2007), without a conclusive answer. The normal faults at the range base are clearly dipping west and the strike-slip fault west of them is clearly nearly vertical. It is geometrically impossible for these two faults to cross each other and move independently. As is illustrated in Fig. 3, either the strike-slip fault must terminate against the dip-slip one, in which case the inclined fault plane must become oblique slip, or the inclined plane must terminate against the vertical one, in which case the portion of the vertical one below the intersection must become oblique.

The second question involves the transfer of strain at the point at which the fault transitions from partitioned dip and strike slip to just dip slip. Either the northward component of strain has to be absorbed in distributed deformation such as a fold belt, or it has to be transferred northward on a fault that is not apparent. In this case there is no indication of a fold belt in front of the range near Milner Canyon, nor is there any indication of a continuing northwestward fault. To the best of my knowledge, no prior investigators have mapped a fault trending away from Milner Canyon to the north or northwest. I have examined the terrain on the ground and aerial photos and Google Earth

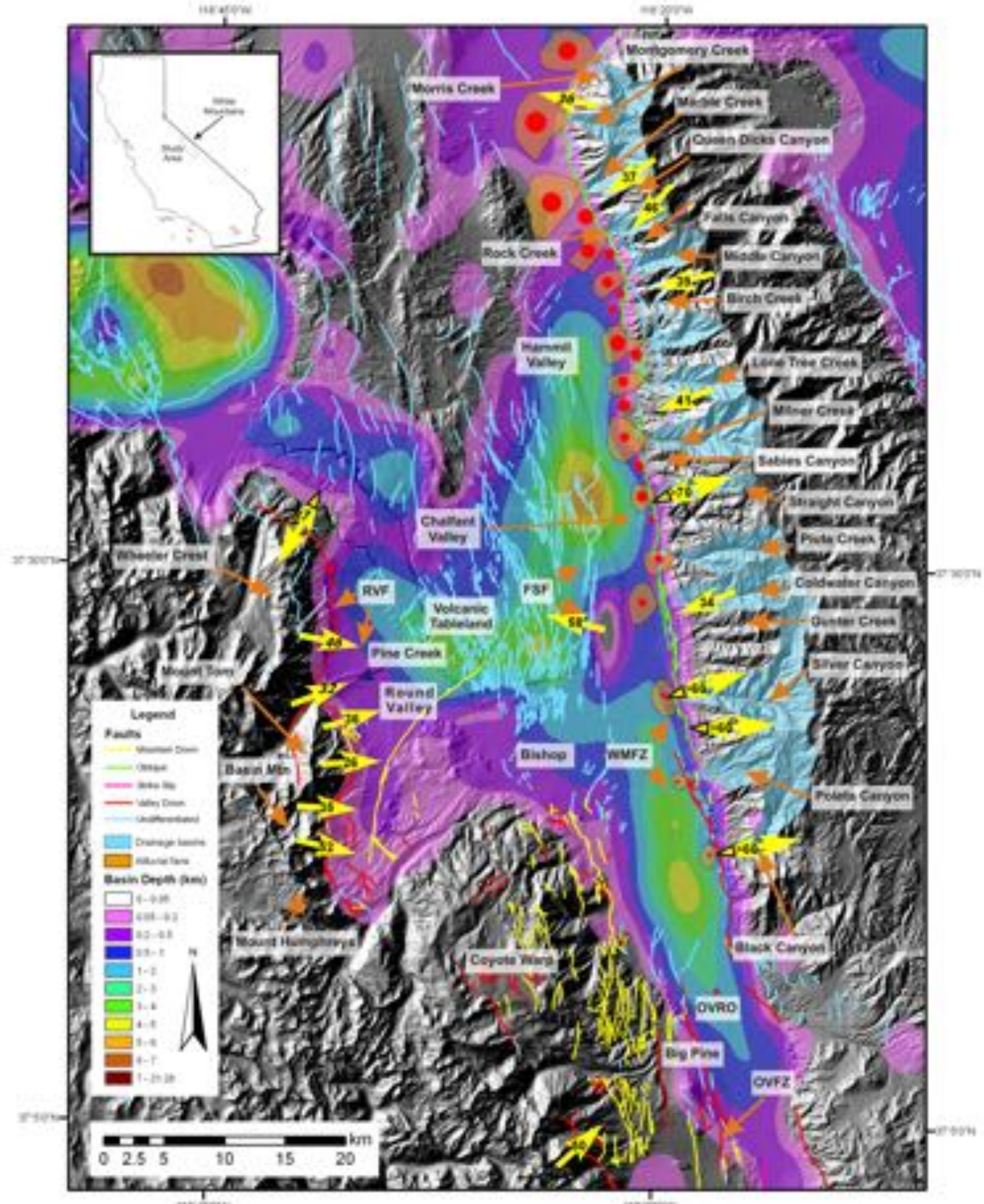

Figure 1. Topography, basin depth, and faults of the northern Owens Valley. Faults are from the USGS Quaternary Fault Database. Stike-slip faults are in green, normal (valley-down) and oblique-slip faults in red, and mountain-down normal faults in yellow. Basin

depth is from gravity inversion by Saltus and Jachens (1995). Yellow arrows are measured fault dips at outcrop. Figure reproduced from Phillips and Majkowski (2011).

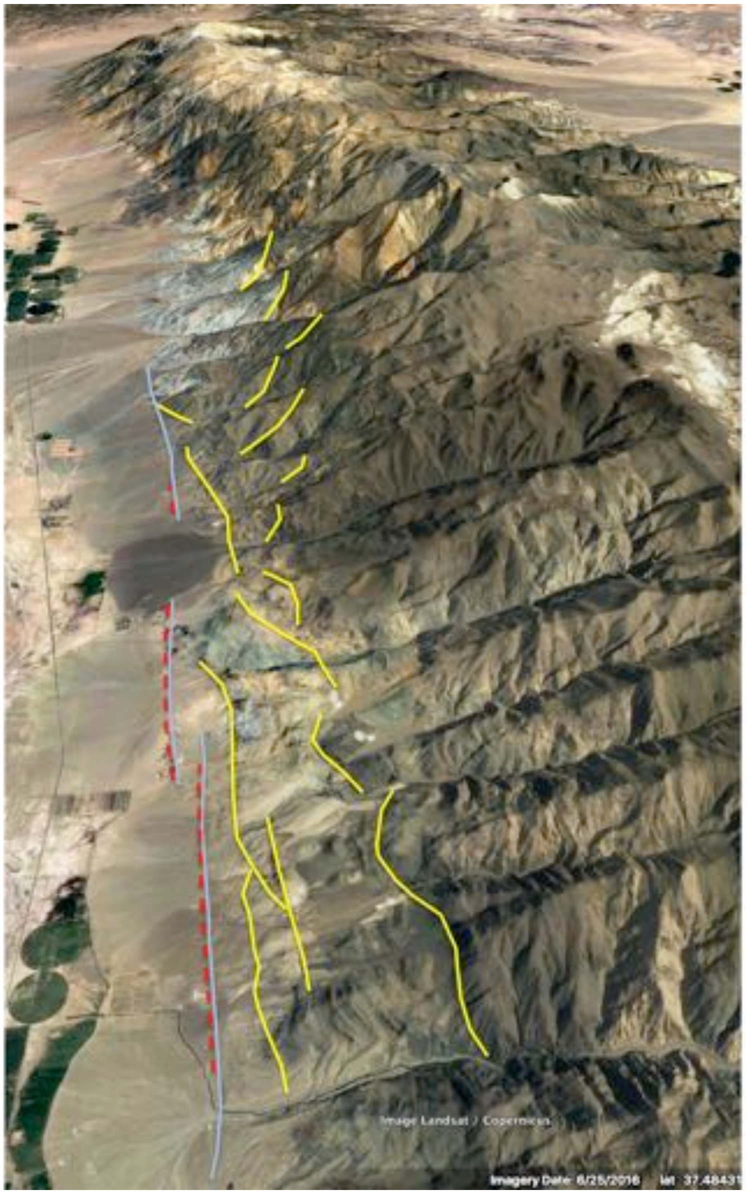

Figure 2. Overview of the eastern side of the northern White Mountains. Normal faults are shown in yellow and strike-slip ones in blue. Red dashed line indicates locations where dextral strike-slip surface rupture was observed between the second and third events of the 1986 Chalfant Valley earthquake sequence by Lienkaemper et al. (1987) and dePolo and Ramelli (1987).

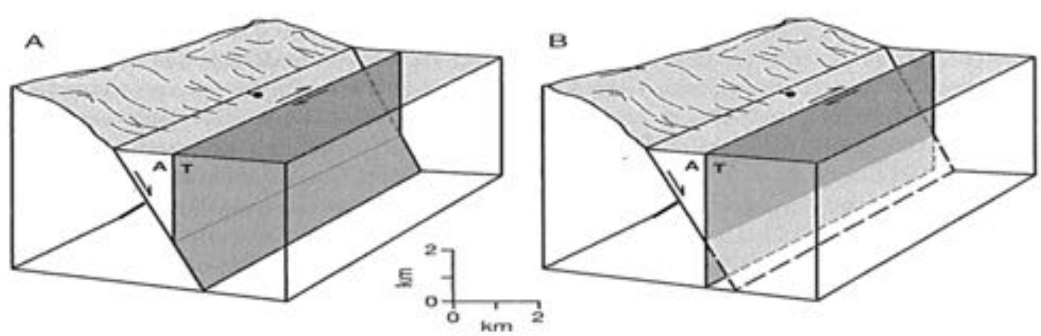

Figure 3. Possible alternative configurations of the White Mountain fault zone and similar slip-partitioned transtensional faults elsewhere. A. The inclined normal fault (oblique where shaded) is the dominant fault. B. The near-vertical strike-slip fault is the normal fault. The dashed portion of the inclined fault is presumed not to exist, or to not be active. Figure modified from Henry et al. (2007).

imagery and have not detected any traces of such a fault.

Insights from Geophysical Data

Both of the questions raised above involve subsurface features and thus subsurface geophysics may prove helpful. In particular, data on subsurface structure from gravity data yield insights. Fig. 1 contains color shading to help visualize depth-to-basement values based on inversion of gravity data by Saltus and Jachens (1995). This figure shows that the White Mountains are fronted to the west by a fairly deep (6 to 3 km) sedimentary basin along its entire length from Black Canyon in the south to Lone Tree Canyon in the north. The exception to this is a 10-km stretch from Silver Canyon to Piute Creek where basin depths are less than 0.5 km. The southern edge of this bedrock block underlying the valley floor corresponds to the area where the WMFZ transitions from oblique slip to partitioned dip/strike slip and the northern boundary to where strike slip begins to die out. The changes in fault configuration in outcrop thus appear to correspond to differences in mechanics involved in obliquely translocating a bedrock block down the face of the range versus those involved in the formation of deep sedimentary basin.

The WMFZ offers an unusual opportunity for subsurface visualization because it was the site of three large earthquakes in 1986, collectively known as the 'Chalfant Valley sequence'. These have been analyzed in detail by Smith and Priestley (2000). The initial event, at 14:29 on July 20, 1986 was magnitude 5.7. It was not on the White Mountain fault, but rather was a deep event on a subsidiary fault striking southwest, but it apparently triggered the main event 24 hours later. The main event was magnitude 6.4 and at 10.8 km depth under Chalfant Valley and was nearly entirely dextral strike slip. The third event was 10 days after the second at 8.8 km and magnitude 5.8. It was southeast of the first two, approximately opposite Gunter Canyon, closer to the mountain front, and was dextral oblique. All of these were followed by extensive series of aftershocks. Due to concern about magmatic inflation at nearby Long Valley the area was blanketed with a dense seismic network, permitting accurate location of even small aftershocks. These events have more recently been relocated by Waldhauser and Schaff (2008) using cross-correlation and double-difference methods, permitting accurate visualization of subsurface fault geometries.

The ability to visualize the fault planes permits a test of the two hypotheses for fault geometry presented in Fig. 3 by Henry et al. (2007). If Panel A is correct, we should see aftershock hypocenters concentrated in a planar zone dipping westward and to the west of the WMFZ. If Panel B is the correct geometry the hypocenters should be in a vertical plane directly below the WMFZ. Fig. 4 shows aftershocks projected onto a cross section located at the mouth of Piute Canyon, which is near the north end of the bedrock block. The cross section is oriented 261°, which is perpendicular to the strike of the WMFZ, and should thus be directly down dip. Aftershock hypocenters for 0.6 km (0.005°) on either side of the cross section are projected onto it. The red arrow is the surface fault dip I inferred from field measurements. Brown lines are my inferred fault geometries. The yellow dot is the displacement vector of the main (second) event, projected from the hypocenter.

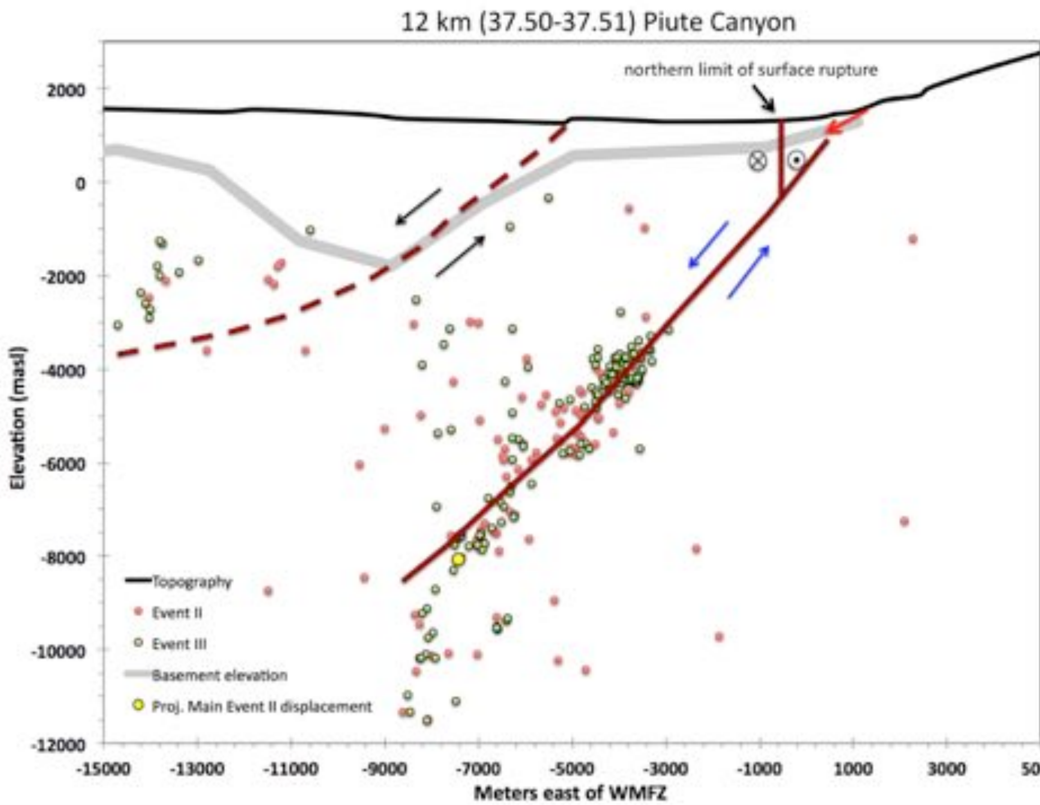

Figure 4. Cross section located at the mouth of Piute Creek, looking north. Hypocenters are from the catalog of Waldhauser and Schaff (2008). Grey line is basement depth from gravity inversion by Saltus and Jachens (1995). Red arrow is dip of fault at outcrop based on my observations. Brown lines are my interpretations of fault geometry. The dashed fault is the Fish Slough fault.

The distribution of hypocenters provides unequivocal support for the geometry in Panel A of Fig. 3. The line (or plane, if visualized in three dimensions) projected upward from the hypocenters follows the surface trace of the mountain-front normal faults; it bears no resemblance to the distribution that would projected downward from the trace of the strike-slip fault. The smoking gun is provided by the dextral surface ruptures produced by Event II in 1986. The focal-plane solution for Event II was almost pure strike slip and the surface ruptures were dextral strike slip, yet the hypocenters clearly follow the projection of the normal mountain-front faults. The geometry of Panel A is fully consistent with all the observations.

Fig. 5 shows a similar cross section further north, at the mouth of Milner Creek, near the center of the deep Chalfant-Hammil basin. Here the outcrop of the WMFZ is entirely dip slip. The basin configuration is clearly imaged by the gravity data, with the hanging wall rollover on the right half of the figure. Here the plane of the strike-slip fault is imaged by the aftershocks to be 12 km to the west of the active normal fault, which is high in the range front. Cross sections in between Piute and Milner Canyons show the strike-slip plane trending steadily westward. The strike-slip aftershocks terminate upward at the inferred base of the low-angle fault plane on which the rollover is warping. Cross sections from further north where the strike-slip plane is more centered beneath the rollover also show the same pattern.

Fig. 5, and other cross sections referenced but not shown here, provide the answer to the second question. The strike-slip component of displacement is not terminated between Piute and Milner Canyons, but continues toward the northwest on a buried extension of the portion of the WMFZ that dominates the Silver-Piute segment. The complicated system of faults is probably best visualized as an interaction of the Fish Slough Fault and the segment of the WMFZ south of Piute Creek. The Fish Slough fault is low-angle at depth (see article for next stop) and carries much of the westward component of strain where the White Mountains are bounded by the bedrock block to the west. To the north the bedrock block does not terminate in an abrupt face bounded by a strike-slip connecting fault, but rather the bedrock/fill contact gradually leans back to shallower angles. It appears that the additional dip-slip motion follows this contact (i.e., it is an expression of a fault) and is transferred to the WMFZ. As it does so, the high-angle strike slip fault diverges from the range front beneath the sedimentary basin created by the low-angle dip-slip fault. The lack of any evidence of surficial strike-slip displacement parallel to this fault indicates that the low-angle fault plane serves to largely isolate the hanging wall of the low-angle fault from the underlying dextral displacement.

Conclusions

The northern portion of the WMFZ exhibits features typical of range-front faults in transtensional strain regimes. These include slip partitioned onto normal range-base faults and strike-slip faults outboard of the range front and portions of the fault system transitioning along strike from partitioned oblique slip to simple dip slip. These features raise questions regarding the subsurface geometries that permit these surface patterns of displacement. The northern WMFZ presents an unusual opportunity to answer the questions due to the combination of aftershocks from a well-monitored earthquake that

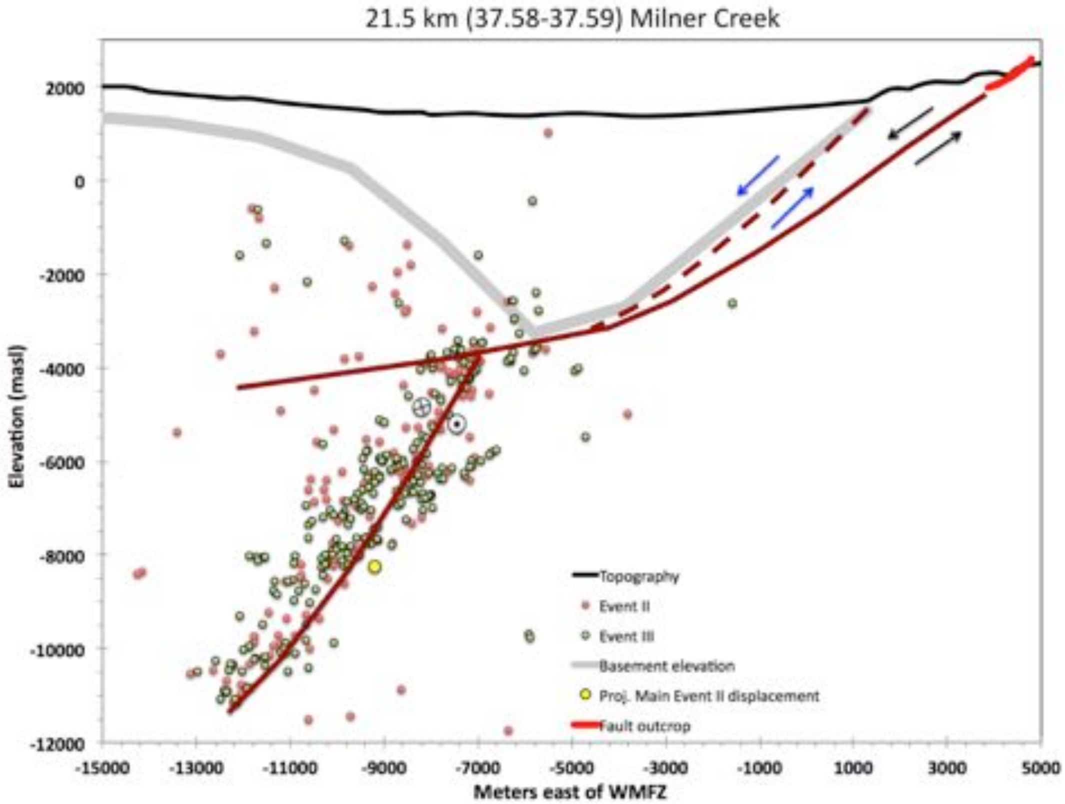

Figure 5. Cross section located at the mouth of Milner Creek, looking north. Hypocenters are from the catalog of Waldhauser and Schaff (2008). Grey line is basement depth from gravity inversion by Saltus and Jachens (1995). Red arrow is dip of fault at outcrop based on my observations. Brown lines are my interpretations of fault geometry.

allows fault geometry to be imaged, gravity inversions that provide further information on subsurface fault geometry, and surface data on fault dips.

These data fairly unequivocally indicate that the 'dominant' range-front fault is the one that manifests as an inclined dip-slip plane. The near-vertical strike-slip fault soles into the inclined one, creating an oblique-slip fault below the intersection. They also demonstrate that the strike-slip motion does not actually disappear northward, nor is it absorbed in distributed deformation. Rather, the strike-slip component of the fault diverges westward beneath the sedimentary basin in front of the range. The strike-slip motion is evidently terminated at the low-angle fault plane that forms the base of the basin. In other words, west of the intersection with the strike-slip fault the low-angle fault absorbs not only the dip-slip component of motion originating from the range front, but also the northwest-directed horizontal motion on the high-angle strike-slip fault.

I propose that these geometries are typical of other slip-partitioned faults in the Eastern California Shear Zone, and in other transtensional regimes worldwide. In fact, the conclusion that the inclined structure is the dominant one is virtually a necessity in active transtensional strain regimes. Significant transtensional displacement requires significant horizontal strain and this cannot be accommodated on vertical faults that are oriented oblique to the regional strain vector.

The finding that high-angle strike-slip faults can terminate at low-angle ones without transferring the strain through to the surface is less expected, but seems plausible. If it is correct it can provide an answer to the question of continuity of strain in many areas where high and low angle faults interact.

References

dePolo C. M. and Ramelli A. R. (1987) Preliminary report on surface fractures along the White Mountains fault zone associated with the July 1986 Chalfant Valley earthquake sequence: *Seismological Society of America Bulletin* **77** 290-296.

Henry C. D., Faulds J. E., and dePolo C. M. (2007) Geometry and timing of strike-slip and normal faults in the northern Walker Lane, northwestern Nevada and northeastern California: Strain partitioning or sequentila extensional and strike-slip deformation?, In *Exhumation Associated with Continental Strike-Slip Fault Systems* (A. B. Till, S. M. Roeske, S. M. Sample, and D. A. Foster; eds.), Geological Society of America, Special Paper 434, Boulder, Colorado, pp. 59-79.

Lienkaemper J. J., Pezzopane S. K., Clark M. M., and Rymer M. J. (1987) Fault fractures formed in association with the 1986 Chalfant Valley, California, earthquake sequence - Preliminary report: *Bulletin Seismological Society of America* **77** 297-305.

Oldow J. S. (2003) Active transtensional boundary zone between the western Great Basin and Sierra Nevada block, western U.S. cordillera: *Geology* **31** 1033-1036.

Phillips F. M. and Majkowski L. (2011) The role of low-angle normal faulting in active tectonics of the northern Owens Valley, California: *Lithosphere* **3**(1) 22-36.

Saltus R. W. and Jachens R. C. (1995) Gravity and basin-depth maps of the Basin and Range Province, western United States: U.S. Geological Survey, Geophysical Investigation Map GP-1012, Scale??

Smith K. D. and Priestley K. F. (2000) Faulting in the 1986 Chalfant, California, sequence; local tectonics and earthquake source parameters: *Bulletin of the Seismological Society of America* **90** 813-831.

Waldhauser F. and Schaff D. P. (2008) Large-scale relocation of two decades of northern California seismicity using cross-correlation and double-difference methods: *Journal of Geophysical Research* **113** B08311, doi:10.1029/2007JB005479. .

Stop 1.2: Tectonic geomorphology of the White/Inyo Mountains, CA

Aaron J. Katona, *Department of Geological Sciences, California State University, Fullerton*
Now at California Regional Water Quality Control Board, San Luis Obispo, CA
Jeffrey R. Knott, *Department of Geological Sciences, California State University, Fullerton*

Abstract

Tectonic geomorphic indices (mountain front sinuosity, valley floor width to height ratio, basin elongation ratio, basin area, fan area, basin relief, stream concavity index, range crest/piedmont profile, and range front strike) measured along the western White/Inyo Mountains using Google Earth show uplift rates increase northward and define White Mountains fault zone (WMfz) sections at intermediate- and long-term scales. The tectonic and geomorphic changes where the WMfz meets the Owens Valley fault zone may be related to the Deep Springs fault (DSf), which we hypothesize extends below the Waucoba Lake Beds and is an important component of Owens Valley tectonics. Geomorphic indices reinforce previous work that indicated that tectonics is the primary control on fluvial system development with lithology exerting greater control as tectonic activity lessens.

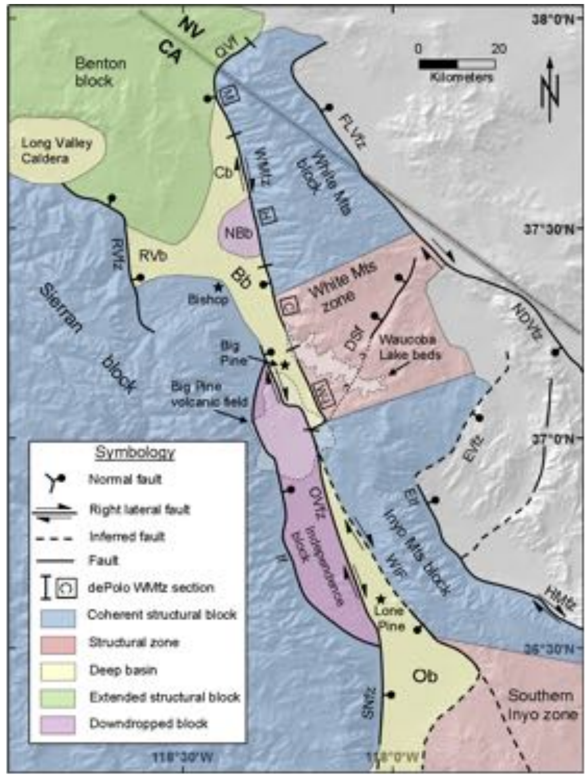

Figure 1 - Map of the White/Inyo Mountains and Owens Valley area. The map shows primary structural blocks: North Bishop block (NBb), the Big Pine volcanic field, the Waucoba Lake beds, major faults and sections of the White Mountain fault zone (from dePolo, 1989): Montgomery (M), Hammil (H), Central (C), Waucoba-Inyo (W-I). Major faults and fault zones shown are the Deep Springs fault (DSf), East Inyo fault (EIf), Eureka Valley fault zone (EVfz), Fish Lake Valley fault zone (FLVfz), Hunter Mountain fault zone (HMfz), Independence fault (If), Northern Death Valley fault zone (NDVfz), Owens Valley fault zone (OVfz), Queen Valley fault (QVf), Round Valley fault zone (RVfz), Sierra Nevada frontal fault zone (SNfz), West Inyo fault (WIf), and White Mountains fault zone (WMfz). Basins: Bishop (Bb), Chalfant (Cb), Owens (Ob), and Round Valley (RVb) (modified from Stevens et al., 2013).

Introduction

Observation of tectonic geomorphology along the western White Mountains and Inyo Mountains (White/Inyo Mountains), and the adjacent Owens Valley, goes as far back as 1911 when Arthur C. Trowbridge hypothesized the morphological differences of the alluvial deposits were a result of tectonic uplift. A number of subsequent geomorphic studies have measured a variety of tectonic geomorphic indices with the general conclusions that the White/Inyo Mountains mountain front is active, segmented with higher uplift rates to the north (dePolo, 1989; Leece, 1991; Whipple and Trayler, 1996; dePolo and Anderson, 2000; Bryant, 2000; Phillips and Majkowski, 2011). These studies commonly used a limited number of tectonic geomorphic indices because, as stated by dePolo and Anderson (2000), manually producing these indices is time consuming. Digitally compiling indices using digital elevation models in a Geographic Information System-based (Arc-GIS) program is possible; however, the learning curve is steep.

In this study, tectonic geomorphic indices were measured using Google Earth. Google Earth has built-in tools that can quickly calculate position, distance, elevation, gradient, and surface area. We compiled multiple indices along the White/Inyo Mountains western piedmont in a relatively short time and use these data to discuss the tectonic geomorphology of the range.

Background

Stevens et al. (2013) divided the White/Inyo Mountains into two coherent structural blocks separated by two uplifted, highly faulted structural zones (Fig. 1). Two smaller down-dropped blocks, and two deep basins border the western flank of the structural components of the White/Inyo Mountains. Normal and right-lateral fault zones separate the different structures. Many of these fault zones have undergone changes in slip type and rate since the Pliocene (e.g. Stockli et al., 2003; Lee et al., 2009; Phillips and Majkowski, 2011; Stevens et al., 2013). The White Mountains fault zone (WMfz), West Inyo fault (WIf) and Owens Valley fault zone (OVfz) are the three largest fault zones bordering the western White/Inyo Mountains. Slip along the WMfz and WIf is normal-oblique whereas the OVfz is predominantly strike-slip.

Geomorphically, dePolo (1989) and dePolo and Anderson (2000) divided the WMfz into five late Pleistocene-Holocene fault sections. Bryant (2000) reclassified these sections into (from north to south) the Montgomery, Hammil, Waucoba, and Waucoba-Inyo sections. Two significant Neogene-Quaternary deposits in the study are the Waucoba Lake beds, which are uplifted onto the WMfz footwall, and the Big Pine volcanic field, which are a series of basic cinder cones and flows in Owens Valley.

Geomorphic analyses of the White Mountains western piedmont was done by several researchers (dePolo, 1989; Leece, 1991; Whipple and Trayler, 1996; dePolo and Anderson, 2000; Phillips and Majkowski, 2011). Among these analyses, Leece (1991) measured alluvial fan area and basin area and concluded that basin lithology controlled alluvial fan size along the White Mountains. In contrast, Whipple and Trayler (1996), using the same parameters, determined that the primary control on White Mountain alluvial fan area was tectonic subsidence. Phillips and Majkowski (2011) used fault dip and alluvial fan/basin area ratio to designate relative changes in basin subsidence and mountain uplift. They concluded that the northern White Mountains was the locus of rapid uplift, but also recognized that other geomorphic indices (i.e., mountain front sinuosity) were not consistent with the fan/basin area ratio fault segmentation.

Methods

The White Mountains' northern boundary is at Montgomery Pass where Highway 6 exits Queen Valley to the east. The divide between the White Mountains and Inyo Mountains is Westgard Pass and Highway 168. The southern limit of the Inyo Mountains is Highway 190. Geologically, the study area is bound to the north and south by Pliocene-Pleistocene volcanic rocks that mark a lithologic and morphologic change from steep mountains to flatter uplands (Jennings, 1958; Strand, 1967).

Google Earth satellite imagery with the visible terrain layer enabled was used as the base map for all measurements. All linear and area measurements were taken using one or a combination of Google Earth tools: Ruler, Add Path, and/or Add Polygon. California geologic maps (1:250,000) as Google Earth overlays provided a reference for lithology (Jennings, 1958; Strand, 1967). The USGS Quaternary fault and fold database was a reference for faults.

The efficacy and accuracy of Google Earth were confirmed by first replicating tectonic geomorphic indices measured using traditional methods (Bull and McFadden, 1977; Knott, 1998; Phillips and Majkowski, 2011; Figueroa and Knott, 2010). Once verified, the methods were then applied to the White/Inyo Mountains.

Twenty-four canyons in the White Mountains and thirty-three canyons in the Inyo Mountains with a minimum length of 1 km were examined for a number of geomorphic parameters. Indices measured at basins were: valley floor width to valley height ratio, basin elongation, basin area and alluvial fan size, basin relief ratio and stream concavity index. Linear indices measured across the entire range were: mountain front sinuosity, range crest and mountain front/piedmont intersection profiles and range front strike. Fault dip data were from Phillips and Majkowski (2011).

Summary of Results

Several tectonic geomorphic indices are summarized on Figures 2 & 3.

- The geomorphology shows that the northern White Mountains are the classified as active to slightly active using the Bull and McFadden (1977) classification scheme. The northern White Mountains have low mountain front sinuosity values (Fig. 2) and the range and mountain front are at higher elevations. The valley-floor width-to-height ratio is generally low (more active) as well (Fig. 2). Basin elongation is also greatest to the north.
- The indices show a distinct difference between the White Mountain, which are bound by the dominantly normal slip WMfz and the Inyo Mountains, which are bound by the dominantly strike slip OVfz.
- The segments, or sections, of the WMfz proposed by dePolo (1989) and Bryant (2000) were based mainly on faulting that cuts the alluvial fan piedmont and, therefore, are likely indicators of short-term fault sections. Tectonic geomorphic indices are more likely reflective of intermediate- (e.g., mountain front sinuosity) and long-term (e.g., range crest elevation) fault sections.
    - Using mountain front sinuosity as a key, we infer that the Montgomery/Hammil boundary is at Birch Creek. This is supported by steps in the range crest and mountain front profiles (Fig. 3).
    - The Hammil section is defined by higher mountain front sinuosity from Birch Creek to Sacramento Canyon where an abrupt eastward shift in range front strike occurs along with a decrease in basin elongation. The Hammil section also corresponds with shallowing of the hanging-wall basin (North Bishop basin of Stevens et al., 2013).
    - The Central and Inyo-Waucoba sections are not as well defined using intermediate-indices. DePolo's (1989) proposed Central/Inyo-Waucoba boundary north of Westgard Pass is at a point where mountain front sinuosity is consistently higher to the south. The range crest profile shows that the Central and Inyo-Waucoba sections are a region of lower uplift along the WMfz (Fig. 3).
    - The southern termination of the WMfz is associated with increased mountain front sinuosity as faulting transitions from normal (WMfz) to strike slip (OVfz) southward.
- It's uncertain that the higher mountain front sinuosity along the Hammil section reflects a less active mountain front or lower uplift rate. The shallower basin fill is attributed to a large landslide block in the subsurface (Hollet et al., 1991), which may impact morphology. Similarly, the variation in morphology along the Central section may be attributed to slip partitioning to faults within the range rather than along the range front and landsliding (Crowder and Sheridan, 1972).
- Lee et al. (2009) proposed that the intersection of the Queen Valley fault (QVf) and the WMfz is a small, incipient pull-apart basin. Phillips and Majkowski (2011) were perplexed

by the significant increase in basin/fan area ratios near the Queen Valley and Owens Valley intersection (Fig. 2) that may signify decreasing tectonic activity. Another hypothesis is that the uplift rate does not change, but rather the larger basin and fan (Figs. 1 & 2) may form as a result fault segmentation (e.g., Leeder and Jackson, 1993). Similarly, the larger drainage basins associated with the Waucoba embayment may be related to fault section terminations as well.

- The westward tilt of the Waucoba Lake Beds is somewhat problematic. Simply put, the lake beds should tilt east due to footwall uplift along the WMfz. Geomorphically, the Waucoba Lake Beds are coincident with lower net mountain range uplift (Fig. 3) and a change from dominantly normal faulting to dominantly strike-slip faulting. We speculate that the Waucoba Lake Beds may be related to the Deep Springs fault (DSf), which, if continued to the southwest during the Pliocene, would project along the east side of the Waucoba Lake Beds. The projected DSf would enter Owens Valley where the WMfz meets the OVfz and the Pleistocene Big Pine volcanic field erupted (Fig.1). Dilek and Robinson (2004) hypothesized that the eruptions of Big Pine volcanic field used a plumbing system provided by the intersection of the DSf and OVfz.

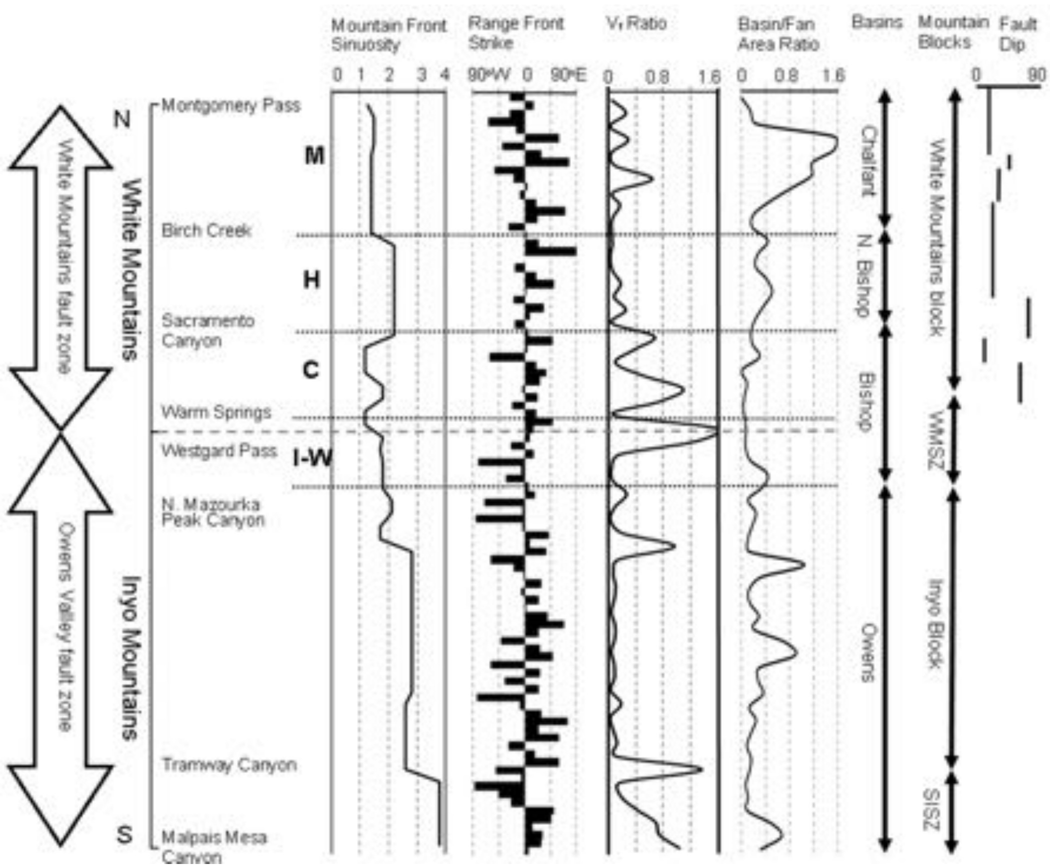

Figure 2 - Plots of mountain front sinuosity range front strike, valley floor width to height ratios, and fan/basin area ratios from north (top) to south along the White/Inyo Mountains. The WMfz sections Montgomery (M), Hammil (H), Central (C), Inyo-Waucoba (I-W) are adjusted from dePolo (1989) to reflect

revised sections based on this study. Basin and Mountain blocks are from Stevens et al. (2013). The fault dip data are from Phillips and Majkowski (2011).

- A hypothetical history is: About 3.5-3 Ma, the west-side-down normal slip on the DSf initiated in the southwest transferring slip from the OVfz to the FLVfz. This formed the accommodation space in the Owens Valley for the Waucoba Lake Beds to form. By 2 Ma, the DSf slip had progressed NE forming what would become Deep Springs Valley and Deep Springs Valley ridge. At the same time, west-side-up slip on the East Inyo fault began uplifting the northern Inyo Mountains (Lee et al., 2009) and uplifting and tilting the Waucoba Lake Beds. Later deposition of alluvial fan deposits (ca. 1.2 Ma) obscured the southwestern DSf in the Waucoba embayment and eruptions in the Big Pine volcanic field began.

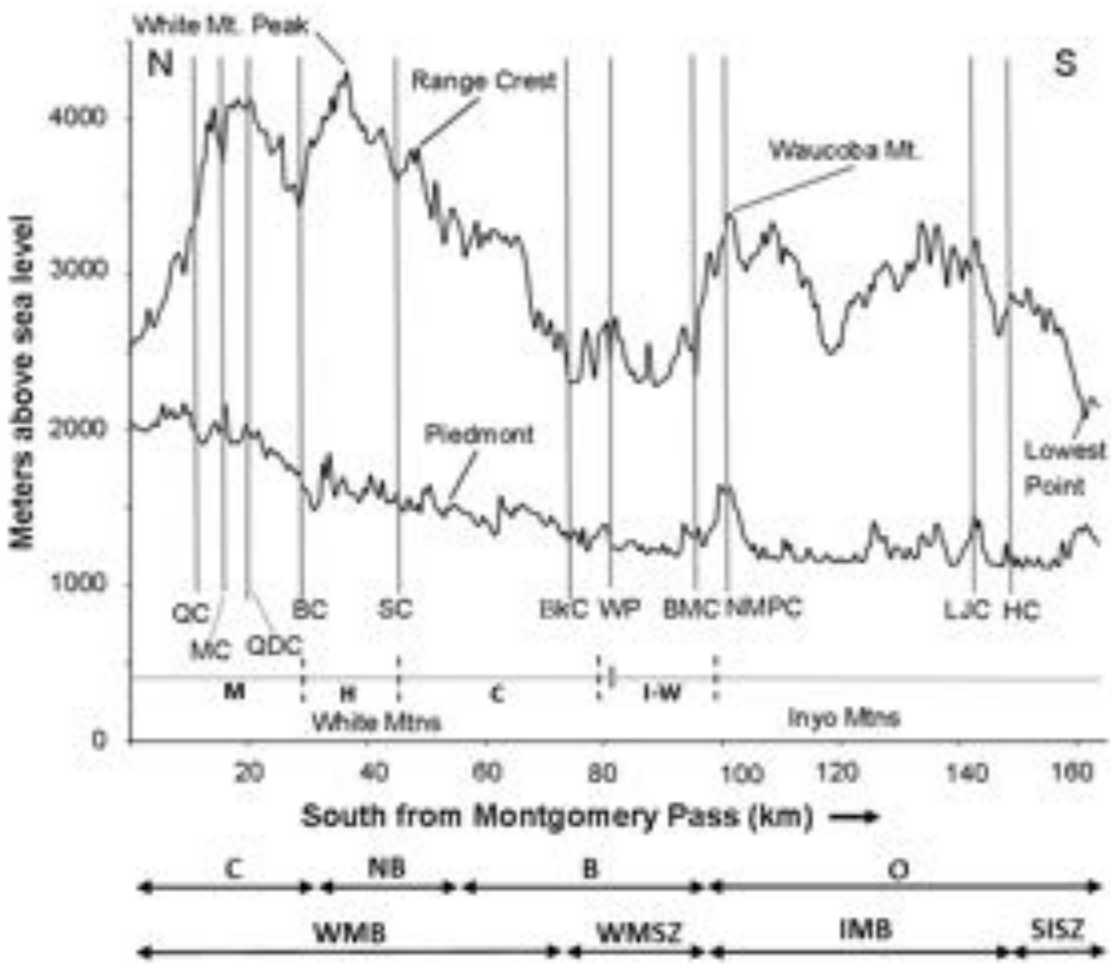

Figure 3 - Range crest and piedmont profiles of the White/Inyo Mountains. Arrows indicate extent of basins and structural blocks from Stevens et al., 2013: Chalfant basin (C), North Bishop basin (NB), Bishop basin (B), Owens basin (O), White Mountains Block (WMB), White Mountains Structural Zone (WMSZ), Inyo Mountains Block (IMB), Southern Inyo Structural Zone (SISZ). Drainages are labeled from north to south: Queen Canyon (QC), Montgomery Creek (MC), Queen Dicks Canyon (QDC), Birch Creek (BC), Sacramento Canyon (SC), Black Canyon (Buck), Westgard Pass (WP), Blake Mine Canyon (BMC), North Mazourka Peak Canyon (NMPC), Long John

Canyon (LJC), Haystack Canyon (HC). Vertical dashed lines indicate revised WMfz section boundaries. Section names are identified by bold letters between boundary lines: Montgomery (M), Hammil (H), Central (C), Inyo-Waucoba (I-W).

- Structure and lithology do influence geomorphic indices and expression can be significant. For example, Mazourka Canyon is a large basin (72.5 km^2) whose trend is parallel to the range front. Mazourka Canyon is incised parallel to the strike of Paleozoic beds which provides the structural control on the orientation of the stream channel and producing a high valley-floor with to height ratio (Fig. 2).
- A comparison of canyon geology and morphology reveals that generally, similar ratio values are calculated for canyons along the same section of tectonic activity with similar lithology. We found that where there were significant lithology changes in a basin that valley-floor width to height ratio changes as well and nick points were discernible in normalized stream profiles; however, these variations rarely were the sole reason for significant outliers in the geomorphic indices. Based on these data, we speculate that valley floor width to height ratios are primarily controlled by tectonic activity with lithology is a strong secondary influence, which is similar to the conclusion reached by Whipple and Trayler (1996).

Acknowledgements

Support for this study was provided by the Jonathan O. Davis Scholarship from the Desert Research Institute (to Katona) and a California State University Fullerton Junior/Senior Grant (to Knott).

References

Bryant, W.A., 2000b, Fault number 47c, White Mountains fault zone, central section, in Quaternary fault and fold database of the United States: U.S. Geological Survey website, http://earthquakes.usgs.gov/hazards/qfaults (accessed September 2016)

Bull, W.B., McFadden, L.D., 1977, Tectonic geomorphology north and south of the Garlock fault, California. In: Doehring, D.O. (Ed.), Geomorphology in arid regions, Publications in Geomorphology, State University of New York at Binghamton, p. 115–138.

Crowder, D.F. and Sheridan, M.F., 1972, Geologic map of the White Mountain Peak quadrangle, California: U.S. Geological Survey Geologic Quadrangle Map GQ-1012, scale 1:62,500.

dePolo, C.M., 1989, A reconnaissance technique for estimating the slip rate of normal-slip faults in the Great Basin, and application to faults in Nevada, U.S.A.: Reno, University of Nevada, unpublished Ph.D. dissertation, 199 p.

dePolo, C.M., 1989, A reconnaissance technique for estimating the slip rate of normal-slip faults in the Great Basin, and application to faults in Nevada, U.S.A.: Reno, University of Nevada, unpublished Ph.D. dissertation, 199 p.

Dilek, Y. and Robinson, P.T., 2004, Petrogenesis of Quaternary potassic volcanism (Big Pine Volcanic Field) along the Owens Valley fault zone in the Eastern California Shear Zone: American Geophysical Union, Fall Meeting, San Francisco, California, Abstracts, V12B-1435, p. 83.

Figueroa, A.M., Knott, J.R., 2010, Tectonic geomorphology of the southern Sierra Nevada Mountains (California): Evidence for uplift and basin formation: Geomorphology, 123, p. 34-45.

Hollett, K.J., Danskin, W.R., McCaffrey, W.H., and Walti, C.L., 1989, Geology and water resources Owens Valley, California: U.S. Geological Survey Paper 2370-B, 77 p.

Leece, S.A., 1991, Influence of Lithology on Alluvial Fan Morphometry, White and Inyo Mountains, California and Nevada: Journal of the Arizona-Nevada Academy of Science, v. 23, no. 2, p. 91.

Leeder, M.R. and Jackson, J.A., 1993, The interaction between normal faulting and drainage in active extensional basins, with examples from the western United States and central Greece: Basin Research, v. 5, p. 79-102.

Jennings, C.W., compiler, 1958, Geologic map of California Death Valley sheet: Department of Natural Resources, scale 1:250,000.

Lee, J., Garwood, J., Stockli, D.F., and Gosse, J., 2009, Quaternary faulting in Queen Valley, California-Nevada: Implications for kinematics of fault-slip transfer in the eastern California shear zone– Walker Lane belt: GSA Bulletin, v. 121, no. 3/4, p. 599-614.

Lee, J., Stockli, D.F., Owen, L.A., Finkel, R.C., and Kislitsyn, R., 2009, Exhumation of the Inyo Mountains, California: Implications for the timing of extension along the western boundary of the Basin and Range Province and distribution of dextral fault slip rates across the eastern California shear zone: Tectonics, v. 28, 20 p.

Menges, C. M., 1990, Late Quaternary fault scarps, mountain -front landforms, and Pliocene-Quaternary segmentation on the range-bounding fault zone, Sangre de Cristo, Mountains, New Mexico, in Krinitzsky, E. L., and Slemmons, D. B., Neotectonics in earthquake evaluation: Boulder, Colorado, Geological Society of America Reviews in Engineering Geology, v. 8, p. 131-156.

Stevens, C.H., Stone, P., and Blakely, and R.J., 2013, Structural Evolution of the East Sierra Valley System (Owens Valley and Vicinity), California: A Geologic and Geophysical Synthesis: Geosciences, v. 3, p. 176-215.

Knott, J.R., 1998, Tectonic geomorphology of the western Black Mountains and Death Valley Fault Zone, Central Death Valley, California [Ph.D. Thesis]: University of California, Riverside, 407 p.

Phillips, F.M. and Majkowski, L., 2011, The role of low-angle normal faulting in active tectonics of the northern Owens Valley, California: Lithosphere, v. 3, no. 1, p. 22-36.

Stockli, D.F., Dumitru, T.A. McWilliams, M.O., Farley, K.A., 2003, Cenozoic tectonic evolution of the White Mountains, California and Nevada: GSA Bulletin v. 115, no. 7, p. 788-816.

Strand, R.G., compiler, 1967, Geologic map of California Mariposa sheet: Department of Conservation, scale 1:250,000.

Trowbridge, A.C., 1911, The terrestrial deposits of Owens Valley, California, v. 19, no. 8, p. 706-747.

Wells, S. G., Bullard, T. F., Menges, C. M., Drake, P. G., Karas, P. A., Kelson, K. I., Ritter, J. B. and Wesling, J. R., 1988., Regional variations in tectonic geomorphology along a segmented convergent plate boundary, Pacific coast of Costa Rica: Geomorphology, v. 1, no. 3, p. 239–265.

Whipple, K.X., and Trayler, C.R., 1996, Tectonic control of fan size: The importance of spatially variable subsidence rates: Basin Research, v. 8, p. 351-366.

Road Log

49.4 Turn right (S) on ‘Mill Road’ (unmarked).

49.5 Turn left (E) on Rudolf Road (unmarked).

50.4 Highway 6. Turn right (S) WATCHING FOR HIGH SPEED ONCOMING TRAFFIC.

54.6 Cross Owens River.

56.3 The prominent valley in the Volcanic Tableland to the north contains Fish Slough. It is formed by gap between the footwall and hanging wall of a major low-angle fault.

56.4 Five Bridges Road. Turn right (N)

58.1 Cross Owens River.

59.3 Note breached relay ramps to the northeast, on the exposed dip slope of the Fish Slough fault.

61.6 Turn around, as directed by flaggers, and park well off of the Fish Slough Road.

[*Alternative route:* To avoid treading on BLM land, drive 5 miles north on the Fish Slough Road. Turn around on turn circle on east side of road, next to fence. Drive 1.25 miles back south and park. This alternative adds 10 miles to road log below.]

Stop 1.3 Fish Slough. Fish Slough as a refugia for endangered aquatic species (Sada). Tectonic significance of the Fish Slough fault (Phillips).

Stop 1.3: Ancient Inter-Basin Connectivity and Changing Environments Influence Life in Owens Basin Wetlands

Donald W. Sada, Desert Research Institute, Reno, NV
Steven N. Bacon, Desert Research Institute, Reno, NV

Introduction

Ecology is the study of relationships between the environment and the abundance and distribution of species, and biogeography examines the distribution of ecosystems and species in geographic space. The distribution of a species is attributed to its ability to disperse then survive and reproduce. Some species are vagile (e.g., species that can fly) and easily move across the landscape to occupy a large area. The vagility of others is weak and they move across the landscape only when there is suitable habitat connecting ancestral and new habitats. Habitat use by widely distributed species is generally broad, and narrow for species with limited distribution. Owens Basin wetlands are occupied by many wide spread species, and 11 known plants and weakly vagile animals that are endemic to the basin (Table 1). This summary focuses on the ancestral affinities of Owens Basin fish and springsnails due to knowledge gained from recent systematic and molecular studies (e.g., Echelle 2008, Hershler and Liu 2008).

Early Great Basin and Mojave Desert surveys documented distinct fishes and mollusks in rivers, streams, lakes, and springs (e.g., Cope 1883, Gilbert 1893, Pilsbry 1899). More recent studies have described more than 150 aquatic invertebrates and vertebrates that are endemic to the region (e.g., Shepard 1992, Hershler 1989, 1998; Schmude 1999, Polhemus and Polhemus 2002, Sada and Vinyard 2002). Within this region, the Death Valley System is distinguished by the presence of more than 60 endemic fishes, mollusks, mammals, aquatic insects, and crustaceans (see Sada 1990, 2000; Skinner and Pavlik 1994, Sada et al. 1995, U.S. Fish and Wildlife Service 1998, Baldinger et al. 2002, Hershler et al. 2013). Ancestral affinities of these aquatic species have been the focus of studies due to their reliance on aquatic connectivity for dispersal. Hubbs and Miller (1948) first recognized similarities between Great Basin fishes and species in surrounding drainages. They hypothesized that fish invaded the region during Pleistocene connections, then genetically diverged following isolation that occurred as the climate warmed and dried, and basins became isolated and endorheic. The basic construct of their isolation model

Table 1. Types of occupied habitat and the rare and endemic aquatic and terrestrial animals and plants that occupy Owens Basin wetlands. Wongs springsnail and the Grated Tryonia are not endemic to the Owens Basin. Wongs springsnail also occurs in Fish Lake, Deep Springs, and Huntoon Valleys, and Teels Marsh, and the Tryonia occurs in many thermal springs in the western US. * denotes crenobiontic taxa. The ancestral origin of P. aardlahi has not been studied and is uncertain, but most likely similar to other Death Valley Systems *Pyrgulopsis* sp..

Common Name	**Scientific Name**	**Habitat**	**Ancestral Affinities**
Owens pupfish	*Cyprinodon radiosus*	Low gradient river, springs	Northeastern Mexico
Owens tui chub	*Siphateles bicolor snyderi*	Low gradient river	Lahontan basin
Owens speckled dace	*Rhinichthys osculus ssp.*	Low gradient river, springs	Lahontan basin
Owens sucker	*Catostomus fumeiventris*	Low gradient river	Lahontan basin
Owens checker mallow	*Sidalcea covillei*	Mesic alkali meadow	
Inyo County mariposa lily	*Calochortus excavatus*	Mesic alkali meadow	
Fish Slough milk-vetch	*Astragalus lentiginosus var. piscinensis*	Mesic alkali meadow	Western North America
Owens vole	*Microtus californicus vallicola*	Mesic alkali meadow	Western California
Fish Slough springsnail*	*Pyrgulopsis perturbata*	Thermal springs	Northeastern Mexico
Aardhals springsnail*	*Pyrgulopsis aardlhali*	Springs	Northeastern Mexico ?
Owens Valley springsnail*	*Pyrgulopsis owensensis*	Springs	Northeastern Mexico
Wongs springsnail*	*Pyrgulopsis wongi*	Springs	Northeastern Mexico
Grated Tryonia*	*Tryonia porrecta*	Thermal springs	Western US and Hawaii

has been validated, but more recent studies find that many colonizations occurred during the late Miocene or Pliocene (e.g., Billman et al. 2010, Smith et al. 2002, Echelle, 2008, Hershler and Liu 2008). Advances in molecular analyses for systematic and biogeographic studies is rapidly increasing knowledge about ancestral affinities and divergence times for related taxa. In spite of these advances, a greater clarity is needed to understand the interacting influences of climate, geology, mountain building, and environmental conditions on the dispersal and persistence of taxa.

Owens Basin Wetlands

The Owens Basin is known for its dramatic mountain scenery, but a variety of wetlands can be found with closer examination. Although water diversion, livestock use, and recreation have altered much of the basin, wetlands persist along streams and the Owens River, and at springs (U.S. Fish and Wildlife Service 1998). It appears that wetlands have always been scarce. Some accounts from early expeditions refer to luxuriance of the area and abundant water (e.g., Davidson 1859), while in 1864 W.H. Brewer reported there were 'great meadows' adjacent to the Owens River and streams flowing from the Sierra Nevada, but estimated these meadows comprised less than 10 percent of the valley and 'the rest is desert' (in Farquar 1974, page 535). Most Owens Basin wetlands support cattails (*Typha* sp.), reeds (*Scirpus* sp.), or rushes (Family Juncaceae) All of the endemic plants occupy mesic-alkali meadows, as well as the Owens vole (*Microtus californicus vallicola*) that also occupies meadows bordering streams and the river (Table 1). All of these species are closely related to taxa in other portions of California and the southwestern US.

Modern Aquatic Species

The modern Owens Basin fish fauna includes four species that are endemic to the basin (Table 1.) These species historically occupied all valley floor habitats were water is warmest and current velocity low (Moyle 2002). The Owens pupfish (*Cyprinodon radiosus*) occurred only in the Owens Valley where it was abundant in marshlands bordering the river (e.g., Snyder 1917), while the Owens sucker (*Catostomus fumeiventris*), speckled dace (*Rhinichthys osculus* spp.), and tui chub (*Siphateles bicolor snyderi*) occupied swifter habitats in the river and low gradient tributary streams from Owens Lake to Long Valley. Speckled dace is the only modern species occupying the east fork pluvial Owens River, where it inhabits persistent springs (Sada et al. 1993). The distribution and abundance of all native fish has declined from competition and predation by sports fish, genetic introgression with closely related species, and water management (U.S. Fish and Wildlife Service 1998). The sucker, speckled dace and tui chub are most closely related to taxa in the Lahontan Basin (Miller 1973, Smith et al. 2002). Reheis et al. (2002) reported early Pleistocene connections between pluvial Lake Russell (modern Mono Lake) and the Walker River basin that provided an avenue for invasion of Lahontan Basin fish into the Owens, Mono Basin was historically fishless.

The Owens pupfish is the most divergent pupfish in the Death Valley System, and its ancestral form invaded the Owens Basin from northeastern Mexico during the late Miocene to early Pliocene (Echelle 2008).

Owens Basin springsnails (Family Hydrobiidae) include species endemic to the Death Valley System, endemic to the Great Basin (occupying several endorheic basins), and the grated tryonia (*Tryonia porrecta*) that occupies many thermal springs in the western US (Hershler …., (Hershler and Liu 2008, Table 1). Widespread springsnails may be dispersal by birds, and not solely through interbasin connections (Hershler …..). Ancestral affinities of these taxa are unclear. Similar to findings of Echelle (2008), Hershler and Liu (2008) found that ancestral forms to springsnails that are endemic to the Death Valley System occupy northeastern Mexico and they colonized the modern Owens Basin during the late Miocene or early Pliocene.

Fish and Gastropod Fossil Records

Jayko et al. (2014) found late Pleistocene chub (genus *Sipahteles*) and sucker (genus *Catostomus*) fossils from pluvial Lake Gale (modern Panamint Valley). As mentioned above for extant Owens Basin species, both taxa are closely related to Lahontan Basin fishes. Miller and Smith (1981) reported Pliocene *Chasmistes* fossils in the modern Mono Basin. This genus is 'the best known genus of American freshwater fishes' and it occurs in Pleistocene to Miocene deposits in Utah, Idaho, Wyoming, Oregon, California, and Nevada. Mono Basin fossils represent the southwestern extent of this genus, and modern *Chasmistes* are known from the Klamath Basin (southern Oregon) (*C. brevirostis*), Utah Lake, Utah (*C. liorus*), Pyramid Lake, Nevada (*C. cujus*), and the Snake River in Idaho (*C. muriei*). The status of modern species has declined from historical conditions. *C. muriei* is believed extinct, and all other species are Federally listed as endangered due to the effects of water diversion and non-native species.

The Owens Basin is known for its dramatic scenery, and trout are its most distinguished aquatic life. Scenery can be attributed to the natural processes of mountain building, volcanism, and glaciation, but all of its modern trout (Family Salmonidae) come from elsewhere. Brook and brown trout are introduced from the northeastern US and Europe, respectively, rainbows are a hatchery creation that combine salmon and redband trout from northern California, whereas golden trout are native to western Sierra Nevada drainages (Moyle 2002). The only Owens Basin native salmonids are whitefish (genus *Prosopium*) and trout (genus *Oncorhynchus*), which have only been identified in Owens Lake sediment core OL-92 at depths of 286.81 m and 287.29 m (~695 ka) and 296.23 m (!730 ka) (Firby et al. 1997). Both of these taxa occur in the Lahontan Basin, and may have invaded through the early Pleistocene connection between Lahontan and Owens Basins of Reheis et al. (2002). Why these salmonids did not persist in the Owens Basin aftern ~700 ka, where introduced trout flourish today, is unknown? One plausible explanation for the salmonids apparent middle Pleistocene extinction is associated with environmental impacts associated with volcanism.

The collapse of the Long Valley Caldera and eruption of the Bishop Tuff occurred at 767 ka, which was followed by sustained eruptions of rhyolitic lavas and tuffs between

~750 and 640 ka (Bailey et al. 1976, Hildreth and Fierstein 2016). The tephra associated with the Bishop ash bed in core OL-92 occurs at depths between 309.2 and 298.6 m (Sarna-Wojcicki et al. 1997). An additional ~10 cm-thick tephra occurs at a depth of ~296 m (Smith 1997), which is within ~10 cm of the depth where salmonids were last observed in the core. At the time of the eruption, the hydrologic system of the basin was apparently effected by relatively warm and dry regional hydroclimatic variability related to the middle of an interglacial period corresponding to marine oxygen-isotope stage 19 (~761 - 790 ka). Evidence from core OL-92 demonstrates that Owens Lake began to shallow from both filling with the large volume of ash that was deposited in the basin and reduced stream discharge to the lake from climate change (Sarna-Wojcicki et al. 1997). Given the age of sediments in core OL-092 that contain salmonid fossils, it is likely that the initial and subsequent volcanic eruptions of the Long Valley Caldera combined with reduced perennial streamflow in the basin created environmental and hydrological conditions in the Owens Basin that could not be survived by salmonids. It is doubtful that modern Owens Basin fishes were not also affected by impacts of the Long Valley Caldera volcanism, but these particular fish apparently survived due to their greater tolerance of relatively high water temperatures and harsh water chemistry.

References

Bailey, R.A. G.B. Dalrymple, and M.A. Lanphere. 1976. Volcanism, structure, and geochronology of Long Valley Caldera, Mono County, California. Journal of Geophysical Research 81:725-744.

Baldinger, A.J., W.D. Shepard, and D.L. Threloff. 2000. Two new species of *Hyalella* (Crustacea: Amphipoda: Hyalellidae) from Death Valley National Park, California, U.S.A. Proceedings of the Biological Society of Washington 113:443-457.

Billman, E.J., J.B. Lee, D.O. Young, M.D. McKell, R.P. Evans, and D.K. Shiozawa. 2011. Phylogenetic divergence in desert fish: Differentiation of speckled dace within the Bonneville, Lahontan, and upper Snake River Basins. Western North American Naturalist 70:39-47.

Cope, E.D. 1883. On the fishes of the recent and Pliocene lakes of the Great Basin, of the Idaho Pliocene lake. Proceedings of the Academy of Natural Sciences of Philadelphia, 1883:134-167.

Davidson, J.W. 1859. Report of the results of an expedition to Owens Lake and River, with the topographical features of the country, climate, soil, timber, water, and also habits, arms, and means of subsistence, of the Indian Tribe seen from the march. July and August, 1859. Pages 14-31. *In*, P.J. Wilke and H.W. Lawton (eds.). The expedition of Capt. J.W. Davidson from Fort Tejon to Owens Valley in 1859. Ballena Press Publications in Archaeology, Ethnology, and History No. 8.

Echelle, E.E. 2008. The western North American pupfish clade (Cyprinodontidae: *Cyprinodon*): Mitochondrial DNA divergence and drainage history. Pages 27- 38. *In*, M.C. Reheis, R. Hershler, and D.M. Miller (eds.). Late Cenozoic Drainage History of the Southwestern Great Basin and Lower Colorado River System: Geologic and Biotic Perspectives. U.S. Geological Survey of America Special Paper 439.

Farquar, F.P. (ed.). 1974. Up and down California in 1860-1864. The Journal of William H. Brewer, Professor of Agriculture in Sheffield Scientific School form 1864-1903. University of California Press. Berkeley.

Firby, J.R., S.E. Sharpe, J.F. Whelan, G.R. Smith, and W.G. Spaulding. 1997. Paleobiotic and isotopic analysis of mollusks, fish, and plants from core OL-92: Indicators for an open or closed system. Pages 121 – 126. *In*, G.I. Smith and J.L. Bischoff (eds.). An 800,000-Year Paleoclimate Record from Core OL-92, Owens Lake, Southeast California. Geological Society of America Special Paper 317.

Gilbert, C.H. 1893. Report on the fishes of the Death Valley Expedition, collected in southern California and Nevada in 1891, with descriptions of new species. North American Fauna, Number 7:229-234.

Hall, E.R. 1981. The Mammals of North America. John Wiley and Sons, New York.

Hershler, R. 2001. Systematics of the North and Central American aquatic snail genus *Tryonia* (Rissooidea: Hydrobiidae). Smithsonian Contributions to Zoology 612.

Hershler, R. 1998. A systematic review of the hydrobiid snails (Gastropoda: Rissooidea) of the Great Basin, Western United States. Part I. Genus *Pyrgulopsis*. The Veliger 41:1-132.

Hershler, R. 1999. A systematic review of the hydrobiid snails (Gastropoda: Rissooidea) of the Great Basin, western United States. Part II. Genera *Colligyrus, Eremopygrus, Fluminicola, Prinstinicola*, and *Tryonia*. The Veliger 42:306-337.

Hershler, R. 1989. Springsnails (Gastropoda: Hydrobiidae) of Owens and Amargosa River (exclusive of Ash Meadows) drainages, Death Valley System, California-Nevada. Proceedings of the Biological Society of Washington 102:176-248.

Hershler, R. and H-P. Liu. 2008. Ancient vicariance and recent dispersal of springsnails (Hydrobiidae: *Pyrgulopsis*) in the Death Valley system, California and Nevada. Pages 91 - 101. *In*, M.C. Reheis, R. Hershler, and D.M. Miller (eds.). Late Cenozoic Drainage History of the Southwestern Great Basin and Lower Colorado River System: Geologic and Biotic Perspectives. U.S. Geological Survey of America Special Paper 439.

Hershler, R., H-P, Liu, and C. Bradford. 2013. Systematics of a widely distributed western North American springsnail, *Pyrgulopsis micrococcus* (Caenogastropoda, Hydrobiidae), with descriptions of three new congeners. *Zookeys*,330: 27-52.

Hershler, R., D.B. Madsen, and D. Currey (eds.). Great Basin Aquatic Systems History. Smithsonian Contributions to the Earth Sciences No. 33.

Hildreth, W. and J. Fierstein. 2016. Long Valley Caldera lake and reincision of Owens River gorge. U.S. Geological Survey, Scientific Investigations Report 2016-5120.

Hubbs, C.L. and R.R. Miller. 1972. Diagnosis of new cyprinid fishes of isolated waters in the Great Basin of western North America. Transactions of the San Diego Society of Natural History 17:101-106.

Hubbs, C.L. and R.R. Miller. 1948. The zoological evidence: Correlation between fish distribution and hydrographic history in the desert basins of the western United States. Pages 17-166. *In*, The Great Basin, with Emphasis on Glacial and Postglacial Times. University of Utah Bulletin 38, No. 20.

Jayco, A.S. R.M. Forester, and G.R. Smith. 2014. *Siphateles* (*Gila*) sp. and *Catostomus* sp. from Pleistocene OIS-6 Lake Gale, Panamint Valley, Owens River system, California. American Geophysical Union Fall Meeting, 2014, Abstract #PP23C-1407.

Knott, J.R.., M.N. Machette, R.E. Klinger, A.M. Sarna-Wojcicki, J.C. Liddicoat, J.C. Tinsley III, B.T. David, and V.M. Ebbs. Reconstructing late Pliocene to middle Pleistocene Death Valley lakes and river systems as a test of pupfish (Cyprinodontidae) dispersal hypotheses. Pages 1- 26. *In*, M.C. Reheis, R. Hershler, and D.M. Miller (eds.). Late Cenozoic Drainage History of the Southwestern Great Basin and Lower Colorado River System: Geologic and Biotic Perspectives. U.S. Geological Survey of America Special Paper 439.

Miller, R.R. 1973. Two new fishes, *Gila bicolor snyderi* and *Catostomus fumeiventris*, from the Owens River basin, California. Occasional Papers of the University of Michigan Museum of Zoology 667:1-19.

Miller, R.R. and G.R. Smith. 1981. Distribution and evolution of *Chasmistes* (Pisces:Catostomidae) in western North America. Occasional Papers of the Museum of Zoology, University of Michigan Number 696.

Moyle, P.B. 2002. Inland Fishes of California. University of California Press. Berkeley.

Phillips, F.M. 2008. Geological and hydrological history of the paleo-Owens River drainage since the late Miocene. Pages 115- 150. *In*, M.C. Reheis, R. Hershler, and D.M. Miller (eds.). Late Cenozoic Drainage History of the Southwestern Great Basin and Lower Colorado River System: Geologic and Biotic Perspectives. U.S. Geological Survey of America Special Paper 439.

Pilsbry, H.A. 1899. Catalogue of the Aminicolidae of the western United States. Nautilus 12:142-143.

Polhemus, D.A. and J.T. Polhemus. 2002. Basin and Ranges: The biogeography of aquatic true bugs (Insecta: Hemiptera) in the Great Basin. Pages 235-254. *In,* R. Hershler, D.B. Madsen, and D. Currey (eds.). Great Basin Aquatic Systems History. Smithsonian Contributions to the Earth Sciences No. 33.

Reheis, M.C., R. Hershler, and D.M. Miller (eds.). Late Cenozoic Drainage History of the Southwestern Great Basin and Lower Colorado River System: Geologic and Biotic Perspectives. U.S. Geological Survey of America Special Paper 439.

Sada, D.W. 2000. Native fishes. Pages 246-264. *In*, G. Smith (ed.). Sierra East: Edge of the Great Basin. A Natural History. University of California Press. Berkeley.

Sada, D.W. 1990. Recovery Plan for the Endangered and Threatened Species of Ash Meadows, Nevada. U.S. Fish and Wildlife Service, Portland, OR.

Sada, D.W. and G.L. Vinyard. 2002. Anthropogenic changes in historical biogeography of Great Basin aquatic biota. Pages 277-293. *In,* R. Hershler, D.B. Madsen, and D. Currey (eds.). Great Basin Aquatic Systems History. Smithsonian Contributions to the Earth Sciences No. 33.

Sada, D.W., H.B. Britten, and P.F. Brussard. 1995. Desert aquatic ecosystems and the genetic and morphological diversity of Death Valley system speckled dace (*Rhinichthys osculus*). American Fisheries Society Symposium 17:350-359.

Sarna-Wojcicki, A.M., C.E. Meyer, and E. Wan. 1997. Age and correlation of tephra layers, position of the Matuyama-Brunhes chron boundary, and effects of Bishop ash eruption on Owens Lake, as determined from drill hole OL-92, southeast California. Pages 79–90. *In*, Smith, G.I. and J.L. Bischoff (eds.), An 800,000-year Paleoclimatic Record from Core OL-92, Owens Lake, Southeast California. Geological Society of America Special Paper 317.

Schmude, K. L. 1999. Riffle beetles in the genus *Stenelmis* (Coleoptera: Elmidae) from warm springs in southern Nevada: New species, new status, and a key. Entomological News 110:1-12.

Schönhuth, S. D. K. Shiozawa, T.E. Dowling, and R.L. Mayden. 2012. Molecular systematics of western North American cyprinids (Cyprinoformes: Cyprinidae). Zootaxa 3586:281-303.

Shepard, W.D. 1992. Riffle beetles (Coleoptera: Elmidae) of Death Valley National Monument, California. Great Basin Naturalist 52:378-381.

Skinner, W.M. and B.M. Pavlik (eds.). 1994. Inventory of rare and endangered vascular plants of California. Fifth Edition. California Native Plant Society Special Publication No. 1.

Smith, G.I. 1997. Stratigraphy, lithologies, and sedimentary structures of Owens Lake core OL-92. Pages 9–23. *In*, Smith, G.I. and J.L. Bischoff (eds.), An 800,000-year Paleoclimatic Record from Core OL-92, Owens Lake, Southeast California. Geological Society of America Special Paper 317, pp.

Smith, G.R., T.E. Dowling, K.W. Gobalet, T. Lugaski, D.K. Shiozawa, and R.P. Evans. 2002. Pages 175-234. *In,* R. Hershler, D.B. Madsen, and D. Currey (eds.). Great Basin Aquatic Systems History. Smithsonian Contributions to the Earth Sciences No. 33.

Snyder, J.O. 1917. An account of some fishes from Owens River, California. Proceedings of the U.S. National Museum 54:201-205.

Steward, J.H. 1933. Ethnology of the Owens Valley Paiute. University of California Publications in American Archaeology and Ethnology 33.

U.S. Fish and Wildlife Service. 1998. Owens Basin Wetland and Aquatic Species Recovery Plan, Inyo and Mono Counties, California. U.S. Fish and Wildlife Service, Portland, OR.

Stop 1.3: Role of the Fish Slough fault in neotectonics of the Owens Valley

Fred M. Phillips
New Mexico Institute of Mining & Technology

The erosionally resistant surface of the welded Bishop Tuff ignimbrite sheet provides a superb record of fault displacements since the eruption of the tuff at 767 ka. By far the most prominent of these is the Fish Slough fault (FSF), named for the wetland at the base of the scarp. The Fish Slough fault is a north-south oriented normal fault that is down to the west. The measured dip of the fault plane at outcrop is 58° (Phillips and Majkowski, 2011).

The FSF is a major structure in the context of the neotectonics of the Owens Valley. Vertical separation between the tuff on the top of the scarp and the valley fill to the west averages about 80 m and total separation is clearly larger than this. The heave can only be estimated because the edge of the hanging wall is covered by sediment, but is probably no more than 300 or 400 m. This yields a horizontal (E-W) extension rate of about 0.5 mm/yr since 767 ka. However, imaging of the depth to basement using gravity inversion (Saltus and Jachens, 1995), shown in Fig. 4 of my article for Stop 1.2 on the White Mountain fault zone (WMFZ), shows 3 km of vertical separation and 4 km of heave. The timing for the initiation of this extension is uncertain, but likely was close to 11 Ma (Phillips and Majkowski, 2011). If the rate of extension has remained constant at 0.5 mm/kyr, 8 Ma would be required for the observed displacement. In any case, 4 km is a significant fraction of the apparent total extension across this portion of the valley, which is about 15 km.

The FSF is anomalous in that it is the only fault with significant displacement that is found in the central portion of the Owens Valley. The other faults with significant displacement are at the bases of the bounding mountain ranges. What is the explanation for this anomalous position, and what is the role of the fault in the opening of the Owens Valley?

The position of the FSF is readily explained by the depth-to-basement map shown in Fig. 1 of the White Mtn fault zone paper in this volume referenced above. The FSF bounds the western edge of a block of shallow bedrock that extends from Silver Canyon in the south to Piute Canyon in the north, about 10 km. I hypothesize that during the early stages of extensional faulting during the Miocene the range-front faults initiated opposite the current south and north basin depocenters: near Black Canyon and near Sabies Canyon. These incipient faults propagated north and south, but evidently did not succeed in linking. This left a gap between their tips that is now represented by the buried bedrock block. This evidently caused the FSF to initiate on the western side of the block. At some point the gap between the south and north faults was bridged by a new fault, but it formed at a much higher angle, probably because the FSF was already absorbing most of the horizontal strain at that time. Since then the “new” mountain-front fault has undergone about 2 km of both horizontal and vertical displacement. In terms of total displacement the relatively unimpressive FSF is thus considerably more significant than the much-studied WMFZ opposite it.

As for the WMFZ discussed in the previous paper, the 1986 Chalfant Valley earthquake sequence (Smith and Priestley, 2000) aftershocks provide subsurface imaging that helps elucidate the subsurface portion of the FSF and its relation to the Round Valley fault (RVF) to the west. Some seismicity was recorded in the vicinity of the FSF following the 1984 Round Valley earthquake event (Priestley et al., 1988), but it was minor (further west there was a large amount of seismicity). There was no seismicity nearby after Event I of the Chalfant sequence, but about 3.5 hours following the Main Event (Event II) there was a magnitude 4.5 event at 2.5 km depth on the FSF (I refer to this as the ‘Great Fish Slough Event of 1986’). Following this were hundreds of aftershocks in the vicinity of the FSF, shown in Fig. 1.

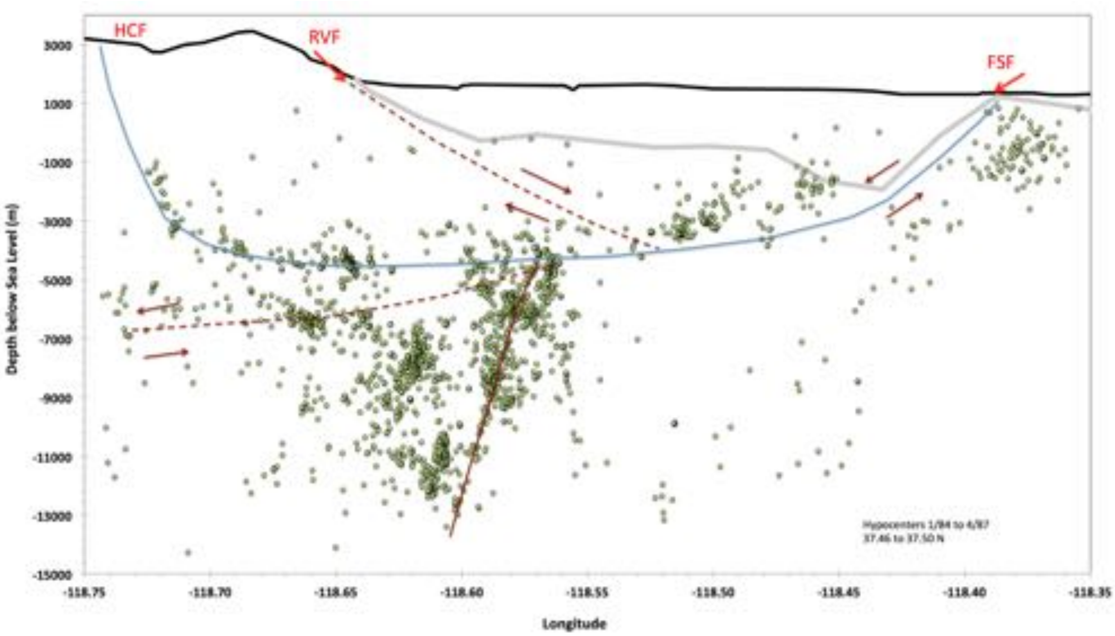

Figure 1. Cross section of the Owens Valley, looking north, from the Fish Slough Fault (FSF) on the east to the Hilton Creek Fault (HCF) on the west. The cross section is oriented east-west along 36.58°±0.02°. Dots are hypocenters from the 1984 Round Valley earthquake and the 1986 event on the FSF that was apparently triggered by the 1986 Chalfant Valley main event. They are not differentiated. Grey lines are depth to basement from Saltus and Jachens (1995) and red arrows are my measurements of fault dip at outcrop. Other lines are interpreted faults. RVF is the Round Valley fault. The high ridge to the west of the RVF is Wheeler Crest.

The gravity data clearly show the position of the FSF in the subsurface and image the hanging wall rollover. The aftershocks following the 1986 FSF event are concentrated in the shallow foot wall below the fault outcrop and in the hanging wall block above the deeper portions of the fault. The hypocenters to the west of this point are very largely those following the 1984 Round Valley event. That event was magnitude 6 and was left-lateral strike slip on a fault striking 30° (Priestley et al., 1988). This is the very high-angle fault indicated above -118.60° latitude in Fig. 1. This event triggered activity on a listric fault to the west, which if projected to the surface, intersects the surface trace of the southern end of the Hilton Creek fault.

I have interpreted the Hilton Creek and Fish Slough faults as opposite ends of a large detachment fault. In accordance with the conclusions in the White Mountain fault zone article, I have interpreted the strike-slip displacement as terminating at the detachment. The Round Valley fault showed no activity during these events, but I have interpreted its configuration based on extrapolation of the surface and gravity data. The low-angle fault extending to the west below the detachment is quite speculative. It is included because the size and position of the hanging-wall block between the RVF and FSF indicates at least 10 km of extension and this can be achieved only if there is a detachment that extends to deeper levels of the crust.

My interpretations indicate that the FSF is a major contributor to net extension across the northern Owens Valley. The hypocenter data support the conceptual model that it is the surface expression of a regional detachment fault at about 6 km depth, and that it is linked to the Round Valley and Hilton Creek faults.

References

Phillips F. M. and Majkowski L. (2011) The role of low-angle normal faulting in active tectonics of the northern Owens Valley, California: *Lithosphere* **3**(1) 22-36.

Priestley K. F., Smith K. D., and Cockerham R. S. (1988) The 1984 Round Valley, California Earthquake Sequence: *Geophysical Journal* **95**(2) 215-235.

Saltus R. W. and Jachens R. C. (1995) Gravity and basin-depth maps of the Basin and Range Province, western United States: U.S. Geological Survey, Geophysical Investigation Map GP-1012, Scale??

Smith K. D. and Priestley K. F. (2000) Faulting in the 1986 Chalfant, California, sequence; local tectonics and earthquake source parameters: *Bulletin of the Seismological Society of America* **90** 813-831.

Road Log

Resume driving back south on the Fish Slough Road.

64.1 Junction Chalk Bluff Road. Turn left (E) on paved road toward Five Bridges.

66.6 Highway 6. Turn right (S) WATCHING FOR HIGH-SPEED ONCOMING TRAFFIC.

67.9 “The Y” junction with U.S. 395. Turn right (W) on the cutoff road behind the gas station.

68.1 Merge onto westbound traffic on 395.

70.9 The prominent red cinder cone to the southwest is Red Hill, dated to 3.38±0.02 Ma by Phillips et al. (2011) using Ar/Ar.

71.2 The shooting range for the Bishop gun club is to the right. At this location on October 1 1871 three convicts who had escaped from the Nevada State Prison, and who had killed several people in a gunfight in Long Valley to the north, were apprehended. After a two-hour trial, two of them were hanged on the spot. The outcome of the trial was not much in doubt, since the scaffold was being constructed as the trial was being conducted.

72.2 Highway 395 traverses the intermediate-level terrace of the Owens River. This terrace and its significance will be discussed at Stop 1.4.

73.1 Note the basalt plug to the right (N) of 395. It was Ar/Ar dated to 11.79±0.06 Ma, indicating long-term stability of the landscape at this location.

77.3 Move into left lane in anticipation of making a left turn ahead.

77.8 Junction with Pine Creek Road. Turn left (W) WATCHING CAREFULLY FOR ONCOMING HIGH-SPEED TRAFFIC.

78.5 Directly ahead and slightly to the south are the moraines of Pine Creek. These are among the largest in the eastern Sierra Nevada. Bateman (1965) differentiated them into four age groups: Younger Tioga, Older Tioga, Tahoe, and Older Tahoe. The moraines surrounding Rovana, the small community located where Pine Creek exits the moraines, are probably older than the classic Tahoe (MIS 6). Soil development on the Pine Creek moraines has been analyzed by Berry (1994) and Bach and Elliott-Fisk (1996). Where the moraines cross the Round Valley fault, just below where they abut the bedrock of Mt. Tom and Wheeler Crest, are prominent scarps, showing about 14 m of vertical offset (Berry, 1997). The fault dip indicated by the displaced moraines is about 30° (Phillips and Majkowski, 2011). The longitudinal moraine profile shows distinct convex upward curvature, probably due to rollover of the hanging wall of the Round Valley fault, on which they are situated, as the fault is approached (Phillips and Majkowski, 2011), supporting a listric geometry for the fault.

79.6 Junction with Round Valley Road. Turn left (S).

81.7 Junction with Horton Creek Campground access road. Turn right (S).

82.5 Horton Creek Campground entrance. Follow the small loop road to the right and reverse course. Park on the road shoulder, well out of traffic. Walk to the west side of the road. Stop 1.4.

[*Alternative Route:* To avoid BLM land, drive 0.5 miles north and park.]

Stop 1.4: Tectonics of the Round Valley fault (Levy), Tectonic deformation of the Owens River terraces and Volcanic Tableland (Pinter), Tectonic synthesis across the Owens Valley (Phillips).

Stop 1.4: Tectonics of the Sierra Nevada frontal fault zone

Drew Levy
University of California at Los Angeles

Owens Valley is an ideal location for studying strain partitioning in a transtensional rift system. In southern and central Owens Valley, strain is partitioned between the north-trending, extensional Sierra Nevada frontal fault zone along the western rift shoulder and the right-slip Owens Valley fault bisecting the rift. In northern Owens Valley, located between the town of Big Pine and the Long Valley Caldera, strain partitioning is less clearly defined as the Owens Valley fault terminates, and the valley and rift shoulders take on a new geometry: the valley becomes ~30 km wide, compared to an average of 17 km in central and southern Owens Valley. At the transition between central and northern Owens Valley, the Coyote Warp interrupts the Sierra Nevada frontal fault zone for ~15 km between the towns of Big Pine and Bishop, CA. The role of the Coyote Warp, a N-NE plugging anticlinal Pliocene erosional surface, in partitioning transtensional deformation across northern Owens Valley remains unclear. On a regional scale, this area is considered the northern segment of the eastern California shear zone, a north-trending corridor of right-slip shear, which transitions to the Walker Lane belt through the right-stepping Mina Deflection (Dokka and Travis, 1990, Lee et al. 2009). Furthermore, how right-slip motion is distributed between the White Mountains fault zone, the Sierra Nevada frontal fault zone, and the Round Valley fault remains unsettled.

Existing tectonic models to explain the transfer of right-slip motion from the Owens Valley fault to multiple fault zones to the north have come in varying forms. Kirby et al. (2006) and Lee et al. (2009) suggest a dextral fault-slip component is transferred northeastward from the Owens Valley fault to the White Mountains fault zone. More recently, other workers showed dextral shear is transferred northward through the Volcanic Tableland and Adobe Valley via a series of en echelon normal faults and releasing bends (Nagorsen-Rinke et al., 2013; Warren, 2014; DeLano, 2015). These studies collectively exhibit a transfer of dextral slip to the Mina Deflection via two of the three major fault zones in the northern Owens Valley: White Mountains fault zone and Volcanic Tableland-Adobe Valley (Fig.1). Alternatively, right-slip motion could be transferred between the Owens Valley fault to the Sierra Nevada frontal fault zone and the Long Valley Caldera to the north.

The segment of the Sierra Nevada frontal fault zone located south of Big Pine is defined as series of east-dipping normal faults along the base of the Sierra Nevada escarpment (Fig. 1 and 2). Normal faults in central Owens Valley are steeply dipping between 60º and 80ºE in the Lone Pine area (Stone et al., 2000), as well as along the Inyo Mountain front to the east (Fig. 2). Strain within this portion of Owens Valley is partitioned between the range-bounding normal faults and the right-slip Owens Valley fault. A study of late Quaternary slip rates along the Sierra Nevada frontal fault zone directly west of Lone Pine yielded dip slip rates of 0.2-0.3 mm/yr (Le et al., 2006). These rates are comparable with other slip rates throughout the Basin

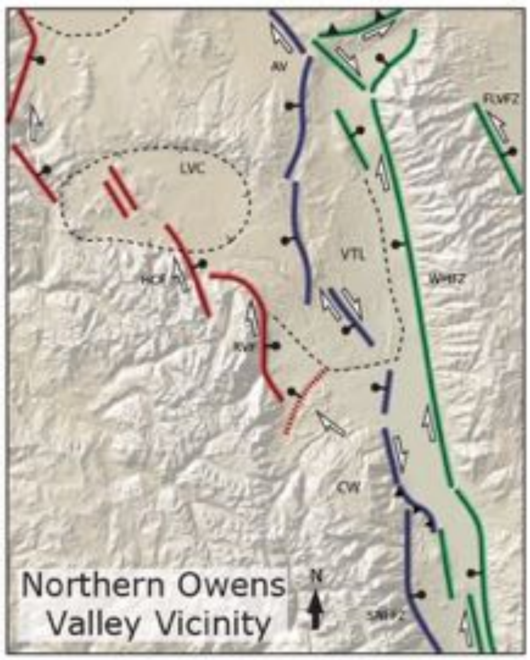

Figure 1: Sketch map of fault zones in northern Owens Valley and proposed models for the northward transfer of right-lateral slip to faults north of the Owens Valley fault. Kirby et al. (2006) and Lee et al. (2009) favor a model where dextral shear is transferred northeastward to the White Mountains fault zone (WMFZ) (green faults) from the northward termination of the Owens Valley fault near Bishop. More recent models proposed by Nagorsen-Rinke et al. (2013), Warren (2014, MS thesis), and DeLano (2015, MS thesis) suggest that dextral shear is transferred northward through the Volcanic Tableland and Adobe Hills, in addition to transfer to the White Mountains fault zone, as was previously illustrated (blue faults). Alternatively, it is possible that a component of dextral fault-slip is transferred to the Sierra Nevada frontal fault zone (SNFFZ) and into the Long Valley Caldera (LVC) (red faults), in addition to the White Mountains fault zone and Volcanic Tableland-Adobe Hills (Levy et al., 2016 AGU Abstract). AV = Adobe Valley. RVF = Round Valley fault. HCF = Hilton Creek fault. CW = Coyote Warp.

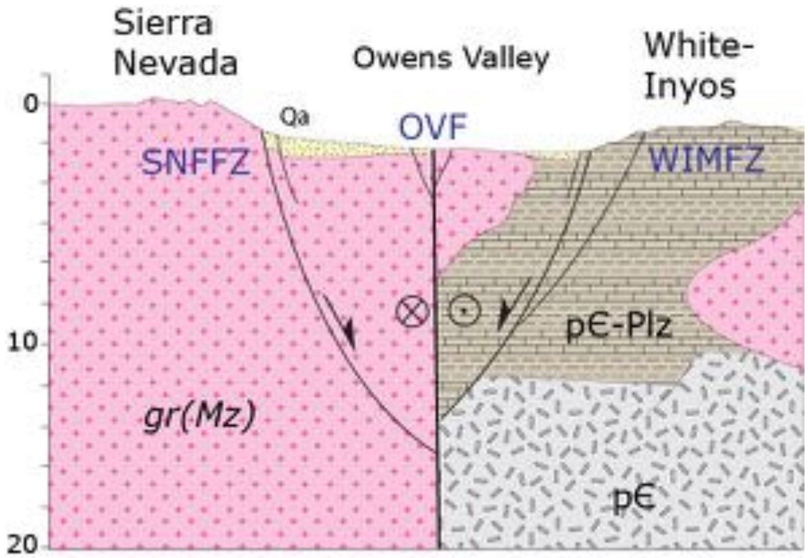

Figure 2: Schematic E-W cross section across central Owens Valley near the town of Lone Pine. High-angle normal faults along the Sierra Nevada frontal fault zone (SNFFZ) and the White-Inyo Mountains fault zone (WIMFZ) accommodate E-W extension, while dextral shear is accommodated on the strike-slip OVF. (Figure modified from Haproff and Yin, 2014 AGU abstract).

and Range Province. A similar study by Zehfuss (2001) focused on the Fish Springs fault, a subsidiary fault of the Sierra Nevada frontal fault zone located ~10 km south of Big Pine, determined a similar slip rate of 0.24 mm/yr. In both studies, normal faults within the Sierra Nevada frontal fault zone of central Owens Valley have strictly normal sense kinematics, coeval with right slip motion accommodated along the Owens Valley fault to the east.

The Wheeler Crest is a prominent escarpment that dominates the skyline directly west of Bishop, north of Coyote Warp. Peaks along the Wheeler Crest rise continuously for ~2500 m from the valley floor. The Round Valley fault, a subsidiary fault of the Sierra Nevada frontal fault zone, is located at the base of the escarpment. Fault scarps can be observed cutting fan surfaces at multiple locations along the trace of the fault. Berry (1997) reports normal-sense displacements and slip-rate estimates of 0.5-1.0 mm/yr. Whereas the majority of such scarps appear a result of normal-slip motion, three locations show evidence of right-slip motion. The slip rates of Berry (1997) are significantly less than those determined to the south, which could be explained by a southward shift in strain partitioning and fault geometries. Much like the southern segment of the Sierra Nevada frontal fault zone in southern Owens Valley, the range-front normal faults in northern Owens Valley are low-angle between 26-52ºE along the Round Valley fault, and between 36-70ºW along the White Mountains fault zone (Phillips and Majkowski, 2011). Models of possible configurations of low-angle normal faults are illustrated by Phillips and Majkowski (2011) determined from fault plane measurements and earthquake hypocenter relocation (Fig. 3).

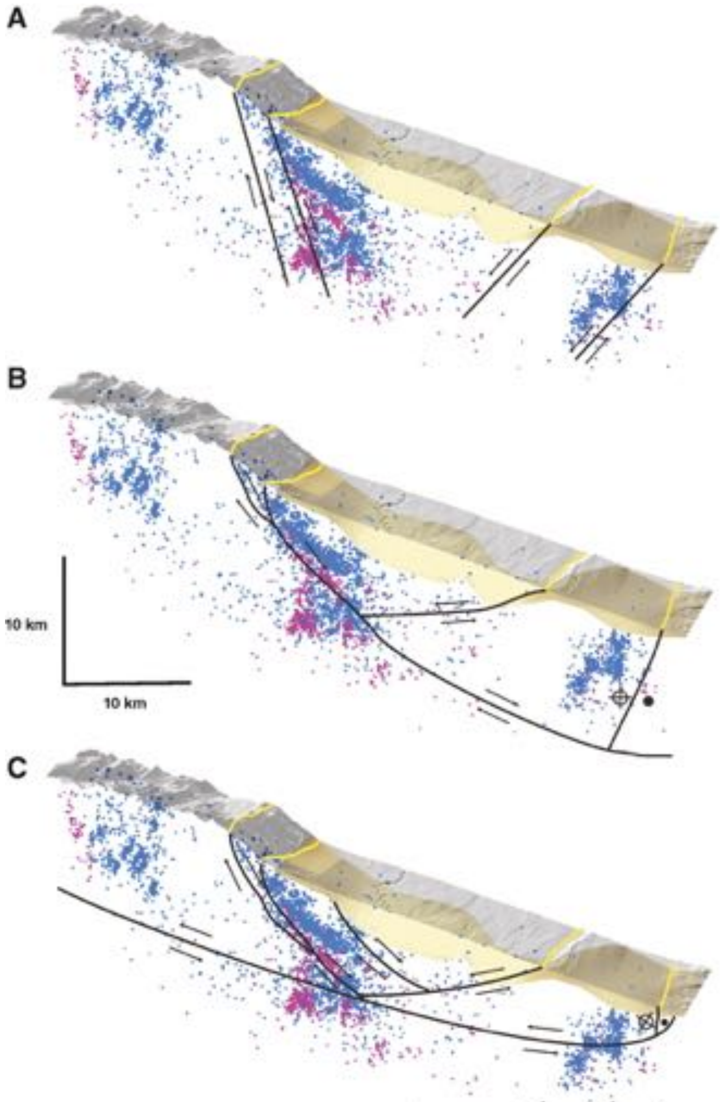

Figure 3: East-trending cross-sections along the latitude of the Wheeler Crest (~37.45°N) showing possible fault configurations based on fault dip and earthquake hypocenter relocations (Phillips and Majkowski, 2011). Sections B and C are favorable over the high-angle normal fault configuration of section A. See Phillips and Majkowski (2011) for additional details.

Whether master detachment faults in Owens Valley dip to the east or west remains unresolved, but a study of structural controls on magmatism in Owens Valley by Haproff and Yin (2014) suggests that the master detachment fault in northern Owens Valley dips to the west. In this work, the authors suggest volcanic centers in Owens Valley are located above the maximum zone of lithospheric thinning accommodated by slip along a master detachment fault. In southern Owens Valley, Coso volcanic field is located along the east side of the valley, which correlates with an east-dipping detachment fault of the Sierra Nevada frontal fault zone. While there is no detachment in central Owens Valley, the Owens Valley fault acts as a conduit for magma to reach the surface and erupt at Big Pine Volcanic field. In the northern Owens Valley, the White Mountains fault zone dips to the west and volcanism associated with Long Valley Caldera and Mono-Inyo craters is distributed along the west side of the valley. This model agrees with the geometry of Fig. 3c, which defines the Round Valley fault as an low-angle antithetic fault in the hanging wall of the west-dipping White Mountains fault zone. At some point along the Sierra Nevada frontal fault zone, the dip of the fault transitions from steep to shallow. This transition likely occurs in the vicinity of the Coyote Warp.

As discussed later in this guide, the causes of faulting and folding within the Coyote Warp is not well understood (Bateman, 1965; Pinter, 1995; Pinter and Keller, 1995). Gaining a better understanding of the development of the Coyote Warp is important in determining the connection between the Sierra Nevada frontal fault zone to the south and north of Bishop. In particular, we want to understand if and to what extent dextral fault-slip is transferred from the Owens Valley fault to the Sierra Nevada frontal fault zone.

Several geomorphic features along the range front directly west of Bishop that may hold the key to understanding the transfer of right-slip motion in Owens Valley. These include incised fans, fault scarps, and offset basement rock outcrops, alluvial fans, and moraines (Fig. 4). The rupture history and slip rates of faults directly west of Bishop remain unconstrained. Offset features to the south and north of the Bishop Creek drainage appear to be a result of oblique fault motion. This includes the basement outcrop directly south of Bishop that is right-laterally displaced from the hillside (Fig. 4b), as well as an alluvial fan along the Wheeler Crest, the Rock Creek moraine, and a set of channels just northwest of Rock Creek, which are all obliquely offset (Fig. 4a; Phillips and Majkowski, 2011). Geomorphic features including scarps and a NE-SW trending fault located within the drainage are obscured by Quaternary sediments. Future field-based research is needed to elucidate the role and significance of these features.

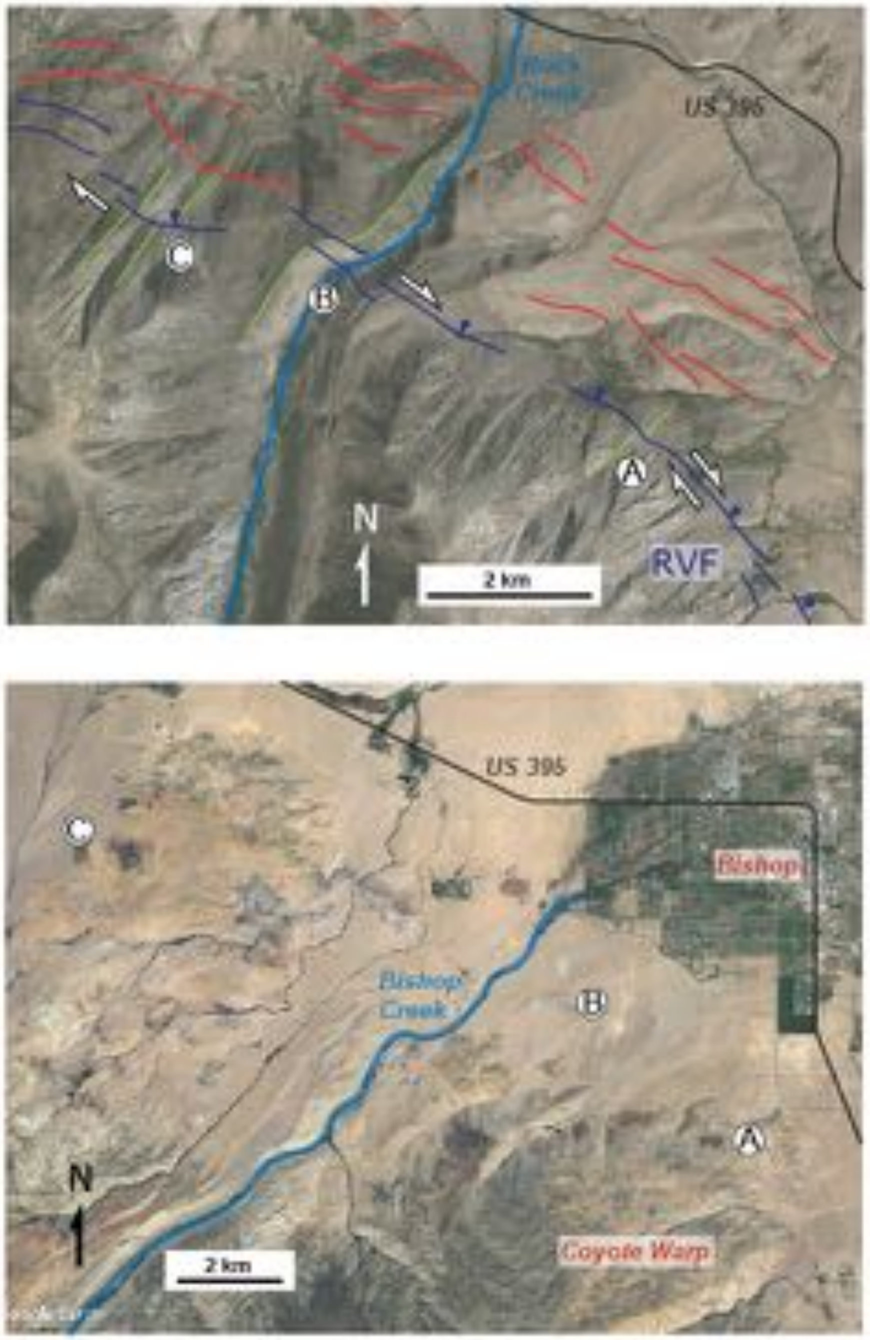

Figure 4: (a) Fault map of right-laterally displace features along the Round Valley normal fault. A = alluvial fan. B = Rock Creek moraine. C = channels along the hillside NW of Rock Creek. (b) Location map of offset features within the Bishop Creek drainage. A = basement outcrop offset dextrally from hillside along a mountain-down normal fault. B = fault scarps bounding incised alluvial fans. C = NE-SE trending normal fault bounding the NW edge of the Tungsten Hills. Base images from Google Earth.

References

Bateman, P.C., 1965, Geology and tungsten mineralization of the Bishop district, California: U.S. Geological Survey Professional Paper 470, 208 p.

Beanland, S., and Clark, M.M., 1994, The Owens Valley Fault Zone, Eastern California, and Surface Faulting Associated with the 1872 Earthquake: U.S. Geological Survey QE75.B9 U.S. Geological Survey bulletin 1982, 1–29 p.

Berry, M.E., 1997, Geomorphic analysis of late Quaternary faulting on Hilton Creek, Round Valley and Coyote Warp faults, east-central Sierra Nevada, California, USA: Geomorphology, v. 20, p. 177-195.

DeLano, K.M., 2015, Geologic Mapping in the Black Mountain area, northern Eastern California shear zone: Testing a kinematic and geometric fault slip transfer model [M.S. Thesis]: Central Washington University, 83 p.

Dokka, R.K., and Travis, C.J., 1990, Role of the Eastern California Shear Zone in Accommodating Pacific-North American Plate Motion: Geophysical Research Letters, v. 17, p. 1323-1326.

Foy, A.T., Frankel, K.L., Lifton, Z.M., Johnson, C.W., Caffee, M.W., 2012, Distributed extensional deformation in a zone of right-lateral shear: Implications for geodetic versus geologic rates of deformation in the eastern California shear zone-Walker Lane: Tectonics, v. 31, TC4008, doi:10.1029/2011tc002930.

Haproff, P.J., Yin, A., 2014, Structural controls on the spatial distribution and geochemical composition of volcanism in a continental rift zone; an example from Owens Valley, eastern California, Abstract V51B-4738 presented at 2014 Fall Meeting, AGU, San Francisco, CA, 15-19 Dec.

Kirby, E., Burbank, D.W., Reheis, M., and Phillips, F., 2006, Temporal variations in slip rate of the White Mountain fault zone, eastern California: Earth and Planetary Science Letters, v. 248, p. 153–170.

Le, K., Lee, J., Owen, L.A., and Finkel, R., 2007, Late Quaternary slip rates along the Sierra Nevada frontal fault zone, California: Slip partitioning across the western margin of the Eastern California Shear Zone–Basin and Range Province: Geological Society of America Bulletin, v. 119, p. 240-256.

Lee, J., Stockli, D.F., Owen, L.A., Finkel, R.C., Kislitsyn, R., 2009, Exhumation of the Inyo Mountains, California: Implications for the timing of extension along the western boundary of the Basin and Range Province and distribution of dextral fault slip rates across the eastern California shear zone: Tectonics, v. 28, TC1001.

Levy, D.A., Haproff, P.J., Yin, A., 2016, Reexamining Owens Valley: Partitioning of Discrete and Distributed Deformation, Structural Controls on Magmatism, and

Seismic Potential within an Active Rift Zone, Eastern California, Abstract T13A-2670 presented at 2016 Fall Meeting, AGU, San Francisco, CA, 11-15 Dec.

Nagorsen-Rinke, S., Lee, J., and Calvert, A., 2013, Pliocene sinistral slip across the Adobe Hills, eastern California–western Nevada: Kinematics of fault slip transfer across the Mina deflection: Geosphere, v. 9, no. 1, p. 37–53.

Phillips, F. M., and Majkowski, L., 2011, The role of low-angle normal faulting in active tectonics of the northern Owens Valley, California, Lithosphere, v. 3, p. 22–36.

Pinter, N., 1995, Faulting on the volcanic tableland, Owens Valley, California: The Journal of Geology, p. 73–83.

Pinter, N., and Keller, E.A., 1995 Geomorphological analysis of geotectonic deformation, northern Owens Valley, California: Geologische Rundschau, v. 84, p. 200-212.

Reheis, M.C., and Dixon, T.H., 1996, Kinematics of the eastern California shear zone: Evidence for slip transfer from the Owens and Saline Valley fault zones to Fish Lake Valley fault zone: Geology, v. 24, p. 339–342.

Wakabayashi, J., and Sawyer, T.L., 2001, Stream Incision, Tectonics, Uplift, and Evolution of Topography of the Sierra Nevada, California: The Journal of Geology, v.109, no. 5, p. 539–562.

Warren, R.M., 2014, Testing Kinematic Fault-Slip Models in the Eastern California Shear Zone-Walker Lane Belt: Field Studies in the Southwester Mina deflection, California-Nevada [M.S. Thesis]: Central Washington University, 63 p.

Zehfuss, P.H., Bierman, P.R., Gillespie, A.R., Burke, R.M., and Caffee, M.W., 2001, Slip rates on the Fish Springs fault, Owens Valley, California, deduced from cosmogenic ^{10}Be and ^{26}Al and soil development on fan surfaces: Geological Society of America Bulletin, v. 113, p. 241–255.

Tectonic deformation of surfaces in the Owens Valley

Nicholas Pinter, Dept. of Earth and Planetary Sciences, UC Davis

Looking north, we get a broad view of the Volcanic Tableland and the full sweep of the northernmost Owens Valley. The Volcanic Tableland is the brittle surface of the Bishop Tuff, which was erupted from Long Valley Caldera 0.757±0.004 Ma (Lueddecke et al., 1998). An estimated 500 km^3 of tephra was erupted during the main Bishop Tuff, caldera-forming event. Bishop ash now covers an area of 1100 km^2, with traces found in Quaternary deposits across North America. In the northernmost Owens Valley, the Bishop Tuff consists of a basal airfall ash overlain by a welded tuff, the surface of which forms the Volcanic Tableland.

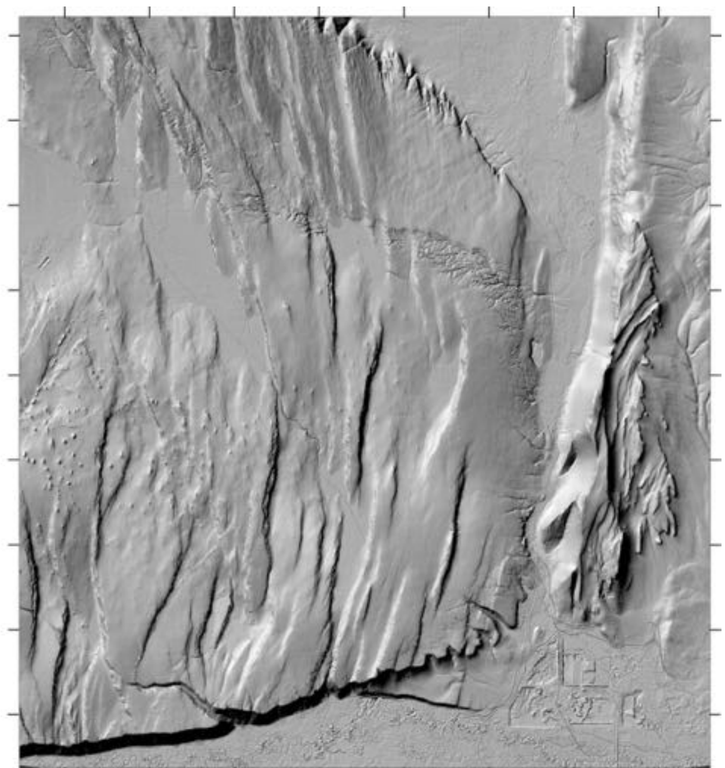

Fig. 1. Shaded relief image from LiDAR showing the southwestern corner of the Volcanic Tableland. (After Ferrill et al, 2016; with permission of the first author)

The Tableland surface (Fig. 1) exhibits a number of features of volcanic, geomorphic, and structural interest. These features include fumarole mounds related to cooling and outgassing shortly after tuff emplacement (left center of Fig. 1), paleo-channels across the Tableland surface, and at least 226 fault scarps ranging in height from a few meters up to 140 m tall (Pinter, 1995).

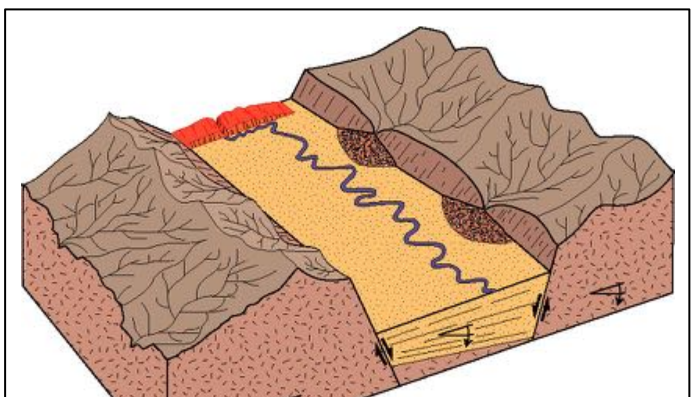

Fig. 2. Since ~3 Ma, the northern Owens Valley has undergone block faulting and tilting as shown. (After Fig. 6C, Lueddecke et al., 1998)

The Volcanic Tableland has acted as a geomorphic timeline, recording tectonic deformation of the northern Owens Valley during the past ~757,000 years. Particular attention has been paid to the spectacular array of fault scarps, with studies looking at the faults as proxies for petroleum systems in rift basins (e.g., Ravnas and Steel, 1998), as evidence of regional tectonic kinematics (e.g., Reheis and Dixon, 1996), and to illustrate fundamental fault scaling relationships (Dawers et al., 1993). The faults trend N10-20°W and are dominantly normal, recording an average of 290 m of cross-valley extension (Pinter, 1995). Some of the Tableland faults are arranged in left-stepping, en echelon groups, which has been interpreted as a secondary component of right-lateral shear through the system.

The durable welded tuff that forms the modern-day Tableland surface preserves cumulative deformation that fully spans the Late Pleistocene. Lueddecke et al. (1998) developed a model and age control for development of the Owens Valley since the Pliocene, with regional tectonic processes during the Late Pleistocene dominated by: (1) westward tilting of the Sierra Nevada block to the west, (2) eastward tilting of the White-Inyo Mountain block to the east, and (3) range-front faulting and down-dropping and eastward tilting of the Owens Valley itself (Fig. 2). Regional tectonic translation associated with the Eastern California Shear Zone has been superimposed upon these large-scale vertical deformation (e.g., McClusky et al., 2001).

Down-to-the-east tilting of the Owens Valley block was suggested by Pakiser et al. (1964) based on geophysical surveys that showed that the bedrock floor of the valley, deeply mantled by sedimentary fill, dips 11.0-13.7° eastward. On-going tilting is also suggested, at least circumstantially, by the location of the Owens River, which hugs the eastern wall of the valley along much of its length, consistent with active half-graben deformation. Indeed, the Owens River cuts east as soon as it leaves the confinement of the Owens Gorge, which locks the river into place across the Tableland. Atop the Tableland itself, the network of paleochannels suggest on-going tilting during the past ~757 kyrs. These incised channels date to early in the history of the Tableland and are now inactive, with their thalwegs offset both up and down across a number of faults (Pinter and Keller, 1995; Ferrill et al., 2016). Geometrical analysis of the paleochannel network shows that they have a mean orientation close to the modern surface of the Tableland, but systematically offset 8-10° in azimuth to the east. The initial drainage pattern was locked in after the eruption– i.e., downhill at the time these streams began incising into the Bishop Tuff – but the Tableland has subsequently tilted to the east. Additional evidence of eastward tectonic tilt is found along the Owens Valley-White Mts. range front, where dated Pliocene fanglomerates (2.82 Ma; Lueddecke et al., 1998) are back-tilted into the range by 4.9° relative to modern fan deposits. Similarly, the active alluvial fans are systematically asymmetrical, showing significant and on-going eastward tilting (Pinter and Keller, 1995).

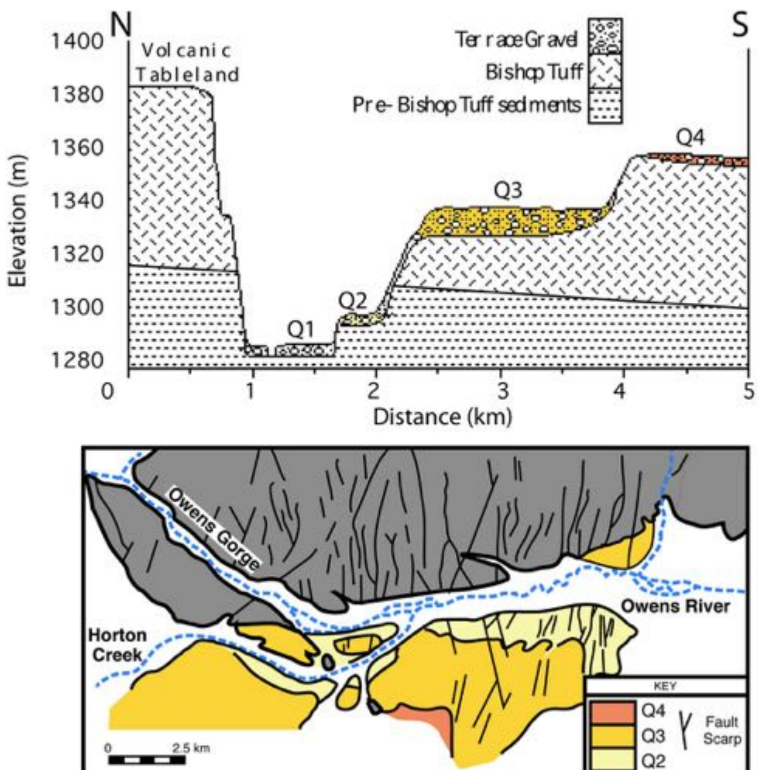

Fig. 3. Terraces of the Owens River at the southern margin of the Volcanic Tableland. (After figures in Pinter et al., 1994 and Pinter and Keller, 1995)

Lastly, some of the clearest evidence of continued tectonic tilting, including age control on rates, comes from fluvial terraces of the Owens River at the southern margin of the Tableland (Fig. 3). These terraces are located along the east-west reach of the river, ~perpendicular to the axis of the valley. The three uplifted terrace levels (Q2-Q4) have been dated and correlated with the last three major glacial periods of the eastern Sierra Nevada: the Tioga, Tahoe, and pre-Tahoe glacial phases (Pinter et al., 1994). The Owens River terraces converge sharply, dropping from >65 m above the modern floodplain in the Owens Gorge area to zero, converging at the outlet to Fish Slough. Thus, eastward tilting of the Owens Valley over the past ~160 kyrs is consistent with the pattern and general rates of tilt (3.5-6.1°/Ma; Pinter and Keller, 1995) dating back to ~3 Ma (Lueddecke et al., 1998).

Eastward tectonic tilting of the Owens Valley and White-Inyo Mountains since the late Pliocene creates a geometrical challenge, a space problem that is difficult to reconcile with simple block-model dynamics. In short, down-to-the-east, half-graben tilting of the Owens Valley is difficult to juxtapose against a west-tilting Sierra Nevada block just to the west (e.g., Unruh, 1991). Pinter (1995) suggested that the tectonic hinge between the northern Owens Valley and the Sierra Nevada block runs through the westernmost Volcanic Tableland and is the north-northeasterly extension of the Coyote Warp. The Coyote Warp (Bateman, 1965) is a broad bedrock planation surface, of inferred Pliocene age, running through the diffuse Sierran range front west of Bishop. The eastern flank of the Warp dips 11° to the east, and the crest of the warp is cut by a system of normal faults. Pinter (1995) interpreted the normal faulting across the Volcanic Tableland and on the Coyote Warp as the structural expression of tectonic hinging between the Sierra Nevada and this portion of the Owens Valley. In this model (Fig. 4), extensional faulting represents brittle fracture due to flexure of the crust. Measured extension across the Volcanic Tableland (at least 290 m over the past ~757 kyrs) is consistent with the rates of westward tilting of the Sierra Nevada and eastward tilting of the Owens Valley measured here. Such tectonic hinges, or accommodation zones, have been observed elsewhere in the Basin and Range where the vergence of half-graben deformation switches. This model also may help to explain the prevalence of normal strain in the northern Owens Valley despite regional shear driven by the Eastern California Shear Zone. A flexural driving mechanism is also consistent with ground deformation observed during the 1986 Chalfant Valley earthquake (Smith and Priestley, 2000), which had an epicenter located on the eastern Tableland. With a magnitude of $M_w6.2$, the Chalfant earthquake cannot be representative of events that produce the Tableland fault scarps. Pinter (1995) calculated the total seismic energy recorded by faults cutting the Volcanic Tableland and estimated at least ~250 M7.2 earthquake over the past 757 kyrs, yielding a ballpark recurrence interval of not more than 3000 years for large scarp-forming earthquakes on the Tableland. This ballpark estimate is generally corroborated by the number of fault scarps and their size (single- to multi-event scarps) that cut the late Pleistocene terraces of the Owens River (see Fig. 3 and full discussion in Pinter, 1995).

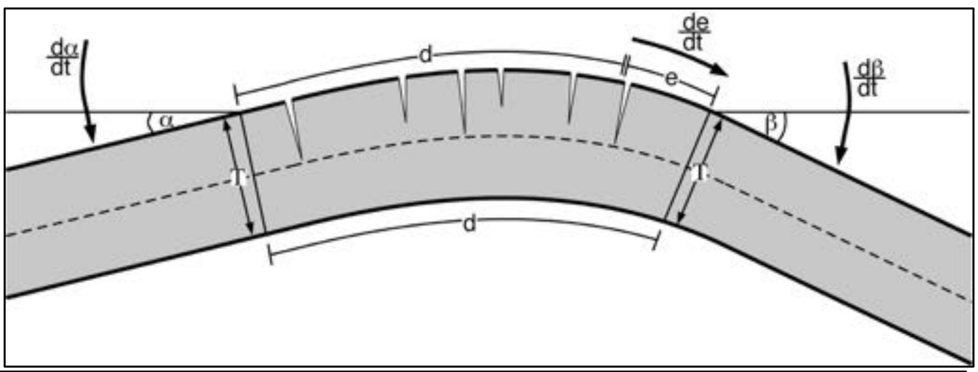

Fig. 4. Pinter (1995) interpreted distributed normal faulting in the northern Owens Valley as flexural extension. This flexure was interpreted as the accommodation zone between the west-tilting Sierra Nevada and the east-tilting Owens Valley.

References Cited

Dawers, N.H., M.H. Anders, and C.H. Scholz, 1993. Growth of normal faults: Displacement-length scale. Geology, 21: 1107-1110.

Bateman, P.C., 1965. Geology and Tungsten Mineralization of the Bishop District, California. U.S. Geological Survey Professional Paper, 470.

Ferrill, D.A., A.P. Morris, R.N. McGinnis, K.J. Smart, M.J. Watson-Morris, and S.S. Wigginton, 2016. Observations on normal-fault scarp morphology and fault system evolution of the Bishop Tuff in the Volcanic Tableland, Owens Valley, California, U.S.A. Lithosphere, 8: 238–253.

Lueddecke, S.B., N. Pinter, and P. Gans, 1998. Plio-Pleistocene ash falls, sedimentation, and range-front faulting along the White-Inyo Mountains front, California. Journal of Geology, 106: 511-522.

McClusky, S.C., S.C. Bjornstad, B.H. Hager, et al., 2001. Present day kinematics of the Eastern California Shear Zone from a geodetically constrained block model. Geophysical Research Letters, 28: 3369-3372.

Pakiser, L. C.; Kane, M. F.; and Jackson, W. H., 1964. Structural geology and volcanism of Owens Valley region, California—A geophysical study: U.S. Geol. Survey Professional Paper 43.

Pinter, N., 1995. Faulting on the Volcanic Tableland, California. Journal of Geology, 103: 73-83.

Pinter, N., and E.A. Keller, 1995. Geomorphic analysis of neotectonic deformation, northern Owens Valley, California. Geologische Rundschau, 84: 200-212.

Pinter, N., E.A. Keller, and R.B. West, 1994. Relative dating of terraces of the Owens River, northern Owens Valley, California and correlation with moraines of the Sierra Nevada. Quaternary Research, 42: 266-276.

Ravnas, R., and R.J. Steel, 1998. Architecture of marine rift-basin successions. AAPG Bulletin-American Association of Petroleum Geologists, 82: 110-146.

Reheis, M.C., and T.H. Dixon, 1996. Kinematics of the Eastern California shear zone: Evidence for slip transfer from Owens and Saline Valley fault zones to Fish Lake Valley fault zone. Geology, 24: 339-342.

Smith, K.D., and K.F. Priestley, 2000. Faulting in the 1986 Chalfant, California, sequence: Local tectonics and earthquake source parameters. Bulletin of the Seismological Society of America, 90: 813-831 .

Unruh, J.R., 1991. The uplift of the Sierra Nevada and implications for late Cenozoic epeirogeny in the western Cordillera. Geological Society of America Bulletin, 103: 1395-1404

Stop 1.4: The Round Valley fault

Fred M. Phillips
New Mexico Institute of Mining & Technology

Introduction

The Owens Valley is clearly a tectonically produced feature and its structural characteristics have largely been a matter of consensus for the past 140 years. It is bounded on the west side by the Sierra Nevada frontal fault (SNFF) and on the east by the White Mountains fault zone (WMFZ) and the Inyo Mountains fault zone (Fig. 1). These are normal faults, with the exception of the the WMFZ, which exhibits oblique slip. The Owens Valley fault zone (OVFZ) runs down the center of most of the valley and is predominantly a right-lateral strike-slip fault. The earliest investigators (Gilbert, 1883; Gilbert, 1884; Le Conte, 1901; Lee, 1906; Knopf, 1918) considered the Owens Valley to be a graben, by which they meant a crustal block that has been lowered (in a relative sense) along high-angle normal faults that bound mountain ranges on either side (i.e., horsts). Although the realization that the OVFZ is a strike-slip fault has somewhat complicated this model (Beanland and Clark, 1994), high-angle normal block faulting has continued to be accepted as the mechanism for the formation of the Owens Valley as a topographic feature (Matthes, 1937; Pakiser et al., 1964; Bateman, 1965; Bateman and Wahrhaftig, 1966; Hollett et al., 1991; Berry, 1997; Lueddecke et al., 1998; Le et al., 2007).

Two factors, in particular, motivate a reexamination of the mechanics of faulting in the northern Owens Valley. The first is structural. The Owens Valley is a relatively shallow graben. Only small portions of the basin exceed 3 km of basin fill. A large proportion, especially of the southern Owens Valley, contains <1.5 km of fill (Saltus and Jachens, 1995). Given an average topographic difference of 2.7 km between the crest of the Sierra Nevada and the valley floor, this indicates typical total vertical displacement of about 4 km. This is surprisingly shallow if the Owens Valley has been the locus of strong east-west extension (~1.5 mm yr^{-1}) over the past 3.5 Ma. If the bounding faults dip at 60º, 8 to 10 km of vertical displacement would be produced. This discrepancy between observed and calculated displacement can, of course, be reconciled by calling on temporal variations in strain rate or orientation, but it nevertheless raises the question of whether other structural configurations might produce better agreement between observed and inferred vertical displacement.

Round Valley fault overview

The Round Valley fault (RVF) is an excellent location for reevaluation of fault geometry. The fault trace is very well exposed on the face of the Sierra Nevada, and in the Owens Valley to the east the erosion-resistant surface of the Bishop tuff provides an excellent marker for deformation of the past 767 ka. Fig. 1 provides a high-altitude overview of the fault from the east. The fault position is shown based mainly on mapping by Bateman (1965), supplemented by my own mapping. The fault dips are based on taking x-y-z positions on the fault outcrops that spanned a range of elevation, using GPS, then rotating them perpendicular to the fault strike to obtain the actual dip. Two features are notable. The first is that the fault does not form a relatively linear scarp at the base of the range, as is typically shown in textbooks. Instead, it appears as a

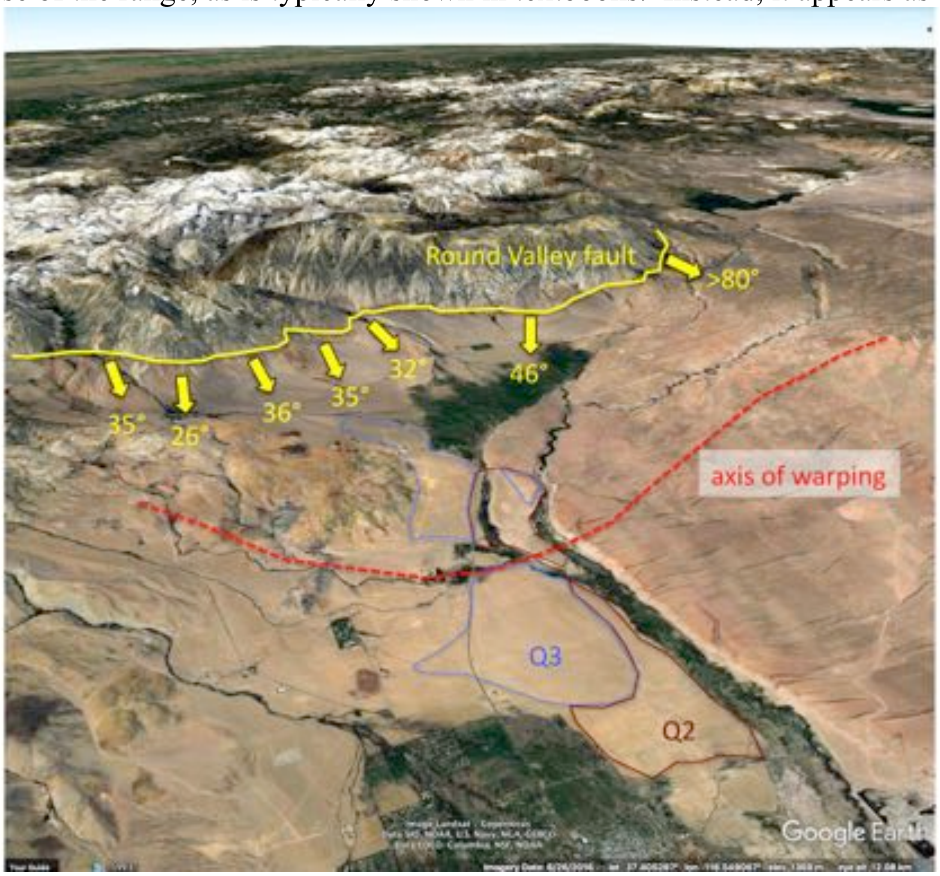

Figure 1. Google Earth overview of the Round Valley fault and Owens Valley from the east. Yellow arrows are locations where the fault dip was measured, from Phillips and Majkowski (2011). The red line delineates the axis of warping, as described by Pinter in this guidebook. Warping is down to the west to the west of the line and down to the east to the east of the line. Q2 and Q3 designate the Owens River terraces.

sinuous line about one-third of the way up the face of the Sierra Nevada. The reason for this is apparent from the dips in Figure 1. The fault dip is so low that its outcrop runs up the face of the mountain, particularly along ridges.

This low dip is confirmed by depth-to-basement values from the gravity inversion by Saltus and Jachens (1995). These are shown in map view in Fig. 1 of my write-up on the White Mountain fault zone for Stop 1.2 of this guide, and are also shown in cross section in Fig. 1 of the write-up for the Fish Slough fault for Stop 1.3. These confirm that the alluvial basin under Round Valley is shallow, with maximum depths of about 3 km. The slope of the gravity-determined sediment/basement interface (i.e., the fault) in the cross section is very similar to that directly measured on the outcrop.

Stranded hanging-wall block

The RVF fault plane is evidently listric. This is indicated by direct field measurements, which tend to show steeper dips as outcrop elevation is increased. It is also indicated by a feature found along the fault that is shown in Fig. 2. It is located on the face of Mt. Tom 3.5 km south of Pine Creek, which is on the left right side of Fig. 2. This feature is surrounded by the colluvial/alluvial wedge that forms the hanging wall of the RVF, but it is composed of badly shattered bedrock. It is a wedge of the bedrock that originally formed the hanging wall that was left stranded between the main RVF and a subsidiary strand to the east. This block is cut transversely by three

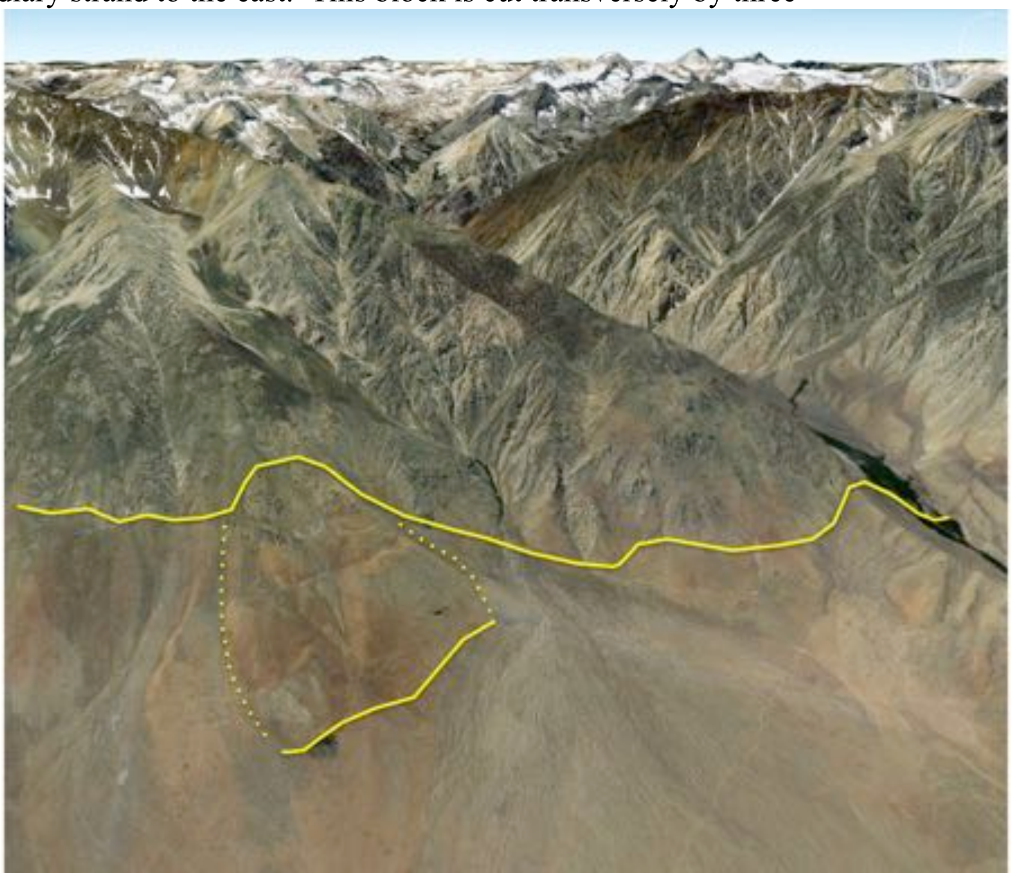

Figure 2. Stranded block of bedrock hanging wall on the face of Mt. Tom. The fault is shown in yellow and the subsidiary strand that isolated the block is shown below it. The block is cut by three prominent antithetic (mountain-down) faults. The northern (right) end of the RVF is not shown so that the fault scarp cutting the left lateral moraine of Pine Creek can be seen clearly.

antithetic (mountain-down) scarps. These scarps are very steep and prominent and are clearly very active (Fig. 3). Bateman (1965) found them so anomalous that he included a photo of them in his professional paper and discussed them at some length. He called them sackung, which are small faults produced by gravitational slumping of the tops of bedrock prominences that lack sufficient lateral support. Due to their midslope position and very limited lateral extent these are quite unlikely to be sackung. Instead they are most probably a result of geometric adjustment of a vertically extensive rock block traveling down a curved surface.

Figure 3. Large antithetic fault scarp on stranded bedrock block on the face of Mt. Tom. This is the middle scarp shown in Fig. 3. Photo is looking south, the summit of Mt. Tom is to the right. Jeffrey pines are about 10 m tall.

Owens Valley warping related to the RVF

Numerous features in the vicinity of Round Valley, which forms the hanging wall of the RVF, show deformation indicative of subsurface fault geometry. The late Pleistocene moraines of Pine Creek show significant back-curvature as they approach the RVF. This is illustrated in Phillips and Majkowski (2011) and not reproduced here. Fig. 4 is a Google Earth overview of the eastern edge of the northern portion of Round Valley and the Volcanic Tableland to the east. Highway 395 runs northward through the center of the photo. To the east of 395 the surface of the Tableland slopes gently to the south, but is relatively flat in E-W profile. As one moves westward past the trace of 395 the surface begins to curve down to the west and this curvature is quite pronounced where it rolls under the alluvium of Round Valley. The cross section shown by Fig. 1 in the paper on the Fish Slough fault, for Stop 1.3, cuts across the very northern end of Round Valley.

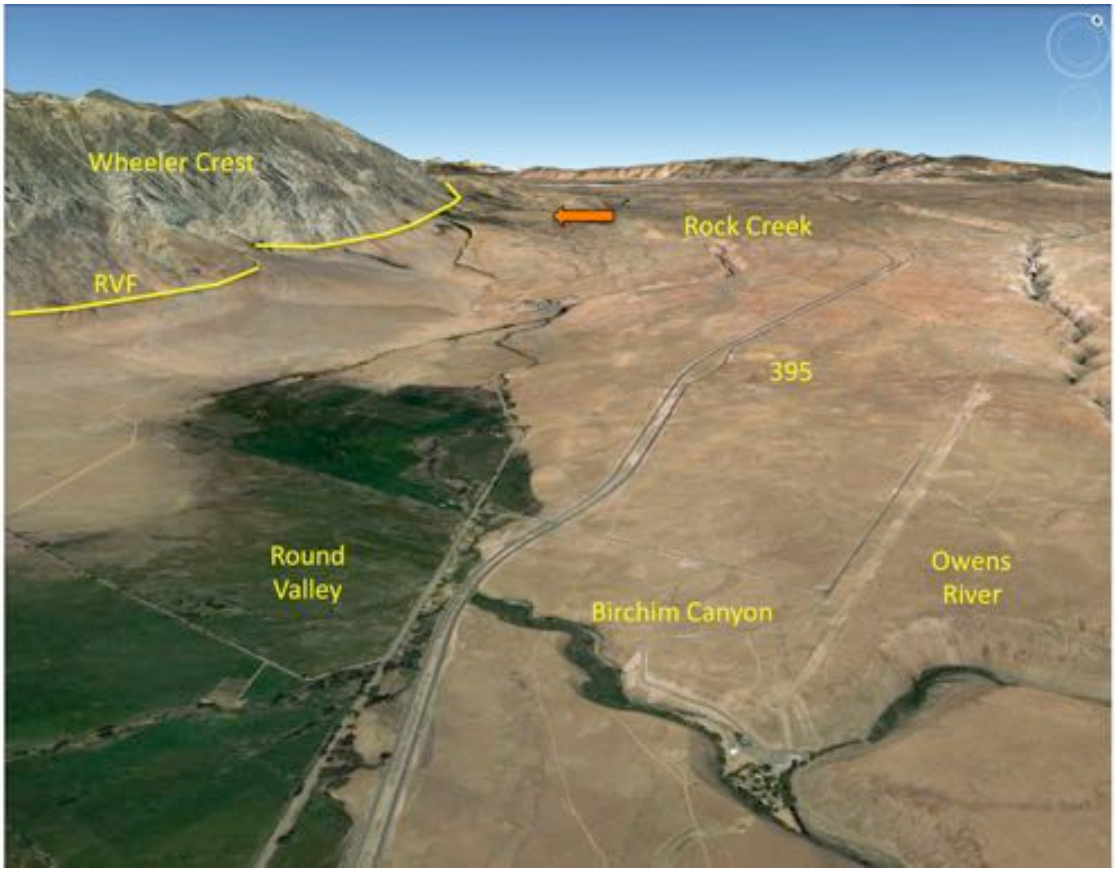

Figure 4. Google Earth overview of the northern end of Round Valley and the Volcanic Tableland (surface of the Bishop Tuff) to the east. View is looking northwest. Orange arrow indicates where rollover of the hanging wall of the RVF becomes negligible.

According to the gravity inversion, depth to bedrock here is only about 1.5 km, due to the shallow dip of the fault. The inversion indicates that the buried bedrock of the original hanging wall also rolls over at the same position. Fig . 4 shows that rollover decreases to the north and is no longer visible north of the orange arrow. This is because the dip of the fault steadily increases to the north. North of the arrow the RVF also begins to show evidence of dextral strike-slip displacement (Phillips and Majkowski, 2011) as it curves northwest and becomes more parallel to the regional strain vector, illustrating that even though most of the Sierra Nevada frontal fault system is simple dip slip, it is still a component of a regionally transtensive strain regime.

The development of rollover as a geologically dynamic process is most dramatically illustrated by Birchim Canyon. Birchim Canyon is the outlet of Pine Creek from Round Valley. The lowest point around the rim of Round Valley is along the course of Horton Creek, below and slightly to the east of this stop, at 1370 m elevation. In contrast the surface of the Volcanic Tableland just west of the Owens River Gorge at Birchim Canyon is 1400 m. Clearly Pine Creek is an antecedent stream. Not too long subsequent to the eruption of the Bishop tuff the topographic gradient from Round Valley to the Owens River at Birchim Canyon was downhill all the way. As displacement on the RVF proceeded, the Bishop tuff rolled over into the fault, creating the accommodation space for the Round Valley sedimentary fill, thus raising the level of the original channel of the Owens River above that of the surface of Round Valley. However, Pine Creek was able to keep pace with the relative increase of elevation of the tuff created by the warping and maintained its course through the growing topographic barrier.

The development of pronounced rollover such as this is most easily attributed to the geometric effects of hanging-wall displacement over the curved surface of a listric fault (Hamblin, 1965). Observations on the fault outcrop and gravity-inferred depth profiles (Fig. 1, Fish Slough fault paper) support a curved fault plane. However, elastic effects during faulting can also contribute to rollover (Grasemann et al., 2005; Resor and Pollard, 2012).

Pinter and Keller (1995) and Pinter, this stop, have shown convincingly that the Volcanic Tableland forms a broad arch, warped down to both the west and east. The axis of this arch is shown in Fig. 1. This axis is surprisingly far to the west (total valley width here is ~30 km, the axis is ~10 km west of the RVF). The Owens River terraces, 5 km east of this stop, are tilting *east* at about 5°/Ma. This tilting increases to the east until the Bishop tuff rolls under the alluvial fans coming off of the White Mountains in a fashion very similar to that seen at Round Valley in Fig. 4.

As noted by Pinter, this guidebook: "eastward tectonic tilting of the Owens Valley and White-Inyo Mountains since the late Pliocene creates a geometrical challenge, a space problem that is difficult to reconcile with simple block-model dynamics". This assessment is entirely valid for "simple block-model dynamics", however, the observed tilting is completely consistent with listric detachment models. Fig. 1 in the Fish Slough write-up shows that the inferred intersection of the RVF and the FSF in the subsurface directly underlies the axis of warping. Geometric accommodation to the fault surface of opposite curvature will produce warping down to the west to the west of the intersection and down to the east to the east of it.

Conclusions

The tectonics of the Owens Valley have traditionally been regard as horst-and-graben produced by simple high-angle block-faulting dynamics. However, field evidence gathered on the RVF indicates that it is a moderate-to-low-angle fault (25° to 35° in its central portion, steeper toward both tips) and that fault dip increases with increasing elevation. Gravity data and earthquake hypocenter location data support the idea that it is also curved in the subsurface and that it is the outcrop of a low-angle detachment at 6-8 km depth under the Owens Valley that links to similar faults on the east side of the valley. This model is supported by deformation data from the Owens Valley hanging-wall block that show pronounced rollover approaching the RVF and a general arching of the valley floor whose axis corresponds to the intersection of the east-dipping and west-dipping fault planes.

References

Bateman P. C. (1965) Geology and tungsten mineralization of the Bishop District, California: U.S. Geological Survey Professional Paper 470, Professional Paper 470, 208 p. pp.

Bateman P. C. and Wahrhaftig C. (1966) Geology of the Sierra Nevada, Vol. Bulletin 190, In *Geology of northern California* (E. H. Bailey; ed.), California Division of Mines and Geology, Sacramento, pp. 107-172.

Beanland S. and Clark M. L. (1994) The Owens Valley fault zone, eastern California, and surface faulting associated with the 1872 earthquake: U.S. Geological Survey, Bulletin 1982.

Berry M. E. (1997) Geomorphic analysis of late Quaternary faulting on Hilton Creek, Round Valley and Coyote warp faults, east-central Sierra Nevada, California, USA: *Geomorphology* **20** 177-195.

Gilbert G. K. (1883) Whitney's climatic changes: *Science* **1** 194-195.

Gilbert G. K. (1884) A theory of the earthquakes of the Great Basin, with a practical application: *American Journal of Science* **27, 3^d^ Series** 49-53.

Grasemann B., Martel S., and Passchier C. (2005) Reverse and normal drag along a fault: *Journal of Structural Geology* **27**(6) 999-1010.

Hamblin W. K. (1965) Origin of "reverse drag" on the downthrown side of normal faults: *Geologic Society of America Bulletin* **76** 1145-1164.

Hollett K. J., Danskin W. R., McCaffrey W. F., and Walti C. L. (1991) Geology and water resources of Owens Valley, California, *in* Hydrology and soil-plant relations in Owens Valley, California: U.S. Geological Survey, U.S.G.S. Water-Supply Paper, Water-Supply Paper 2370B, p. 1-77.

Knopf A. (1918) A geologic reconnaissance of the Inyo Range and the eastern slope of the Sierra Nevada, California, with a section on the stratigraphy of the Inyo Range by Edwin Kirk: U. S. Geological Survey Professional Paper 110, 130 pp.

Le Conte J. (1901) *Elements of Geology*(4th Ed.): D. Appleton and Company,New York, 670 pp.

Le K., Lee J., Owen L. A., and Finkel R. (2007) Late Quaternary slip rates along the Sierra Nevada frontal fault zone, California: Slip partitioning across the western margin of the Eastern California Shear Zone - Basin and Range Province: *Geological Society of America Bulletin* **119**(1) 240-256.

Lee W. T. (1906) Geology and water resources of the Owens Valley, California: U. S. Geologic Survey Water Supply Paper 181, 28p.

Lueddecke S. B., Pinter N., and Gans P. (1998) Plio-Pleistocene ash falls, sedimentation, and range-front faulting along the White-Inyo Mountains, California: *Journal of Geology* **106** 511-522.

Matthes F. E. (1937) The geologic history of Mount Whitney: *Sierra Club Bulletin* **22** 1-18.

Pakiser L. C., Kane M. F., and Jackson W. H. (1964) Structural geology and volcanism of Owens Valley region, California - A geophysical study: U.S. Geological Survey, Professional Paper 438.

Phillips F. M. and Majkowski L. (2011) The role of low-angle normal faulting in active tectonics of the northern Owens Valley, California: *Lithosphere* **3**(1) 22-36.

Pinter N. and Keller E. A. (1995) Geomorphological analysis of neotectonic deformation, northern Owens Valley, California: *Geologische Rundschau* **84**(1) 200-212.

Resor P. G. and Pollard D. D. (2012) Reverse drag revisited: Why footwall deformation may be the key to inferring listric fault geometry: *Journal of Structural Geology* **41**(0) 98-109.

Saltus R. W. and Jachens R. C. (1995) Gravity and basin-depth maps of the Basin and Range Province, western United States: U.S. Geological Survey, Geophysical Investigation Map GP-1012.

Day 2

Cedar Flat to Convict Creek: Chronology of Glacial Advances in the Sierra Nevada and History of the Long Valley Lake and Owens River Gorge

The field trip will depart from Cedar Flat Group Camp at 8:00 AM, Sunday, October 8.

Summary: The Sierra Nevada constitutes a continuous high-elevation topographic barrier across the west coast of North America from latitude 35° to 41°. Storm tracks are predominantly from the Pacific Ocean on the west toward the east, thus the topographic barrier forces large amounts of orographic precipitation to fall on the range. Under current climate, snow is not retained over the summer on even the summit of Mount Whitney (the highest point in the range), but under the significantly colder and wetter climate of glacial periods the glacial equilibrium-line altitude dropped by as much as 3,000 m (Plummer, 2002). This produced glaciers many kilometers long that in some cases advanced onto the desert floor of the Owens Valley.

The evidence for major glacial advances was noted by the earliest geological workers in the region (King, 1878; Russell, 1889; Turner, 1900; Knopf, 1918). Quoting Phillips (2017): "…but the classical systematic delineation of the glacial sequence was the work of Blackwelder (1931) on the east side and Matthes (1929); (1930) on the west side. Because the moraines on the east side are generally much larger and easier to distinguish than those on the west, and are also vegetated principally by low-standing sagebrush whereas the west-slope ones are typically covered by pine forest that renders them difficult to visualize, the terminology of Blackwelder (1931) has generally been adopted for the entire range. Blackwelder (1931) divided the glacial deposits into four stages. Starting with the oldest, they are the McGee, the Sherwin, the Tahoe and the Tioga."

In Blackwelder's time the ages of these glacial advances could only be crudely estimated. Since his time we have seen two major improvements in understanding Quaternary glaciations: the development of numerous methods to quantitatively date moraines and associated geological features, and a greatly enhanced understanding of global glacial-interglacial history through the analysis of marine cores that provide continuous sedimentary records spanning the entire Quaternary.

The area covered by this Friends of the Pleistocene field trip contains innumerable sites that have been affected by Quaternary glaciation of the Sierra Nevada. In fact, one earlier field trip in the same area, the 1979 trip to the Mono Recesses, focused entirely on glacial features (we hope, though, to not rival the casualty list of that legendary expedition!). On today's expedition we will visit two sites that have been the focus of study because of the excellent preservation of an uncommonly large number of moraines at both sites: Bishop Creek and Convict Creek. The moraines we will visit at Bishop

Creek are mainly assigned to the Tahoe glaciation and those at Convict Creek mainly to the Tioga one. At both sites we will review results from modern dating methods (principally cosmogenic-nuclide surface-exposure dating) that constrain the timing of moraine formation. Then we will examine the implications of these ages: do the periods of glacial advance correspond to the recognized global glacial maxima? how do they correlate to local paleoclimatic events such as the highstand of Lake Lahontan? what can we infer regarding the climate controls on these events?

Another paleohydrologic feature of great interest is the lake that formerly occupied the crater left by the cataclysmic eruption of the Bishop Tuff at 767 ka. At some point this lake overflowed and carved the Owens River Gorge through the Volcanic Tableland. The timing and significance of these events has been poorly understood until recently. Wes Hildreth will discuss new data that bring the Long Valley into sharper focus. We will examine the cause of the breaching of the sill of the Long Valley lake and its relation to glacial/interglacial cycles and tectonic forcings.

Mileage **Description**

0.0 Start point is the intersection of the exit road from the Cedar Flats Group Campground to state highway 168, the Westgard Pass road. Set your odometer as you reach the intersection, and turn right (west). Our route follows that of Day 1 down to the Big Pine/Death Valley Road intersection. Remember to give way to uphill traffic on the one-lane road through The Narrows.

10.3 Big Pine/Death Valley Road intersection. Continue straight ahead (W) toward Big Pine.

12.5 Highway 395. Turn right (N) WATCHING FOR TRAFFIC FROM THE LEFT. Continue north on 395.

21.5 Collins Road. Turn left (W) WATCHING FOR ONCOMING HIGH-SPEED TRAFFIC. On the right (N) in 0.4 mile we will pass a prominent mountain-down normal fault scarp. This style of faulting is typical of the Coyote Warp, the rugged mountain mass to the west. If you look south you can see a similar, but much larger, mountain-down scarp at the base of the Coyote Warp.

22.2 Gerkin Road. Turn right. You have a good view of the mountain-down scarp to the east immediately after the turn.

22.8 The mound of granitic hills at 11 o'clock is the northeast corner of the Coyote Warp. Both the east and north faces of the Warp are characterized by slope-parallel mountain-down normal faulting and here these trends intersect, resulting in complex deformation. Levy (write-up for Stop 1.4) has identified this faulted block as showing dextral displacement from the northeast corner of the Coyote Warp.

24.5 Directly east, on the opposite side of U.S. 395, is the scarp of yet another mountain-down normal fault.

24.8 Sunland Drive. Turn left (W). Here we begin a series of turns on small country roads that will ultimately bring us to West Line Street on the west side of Bishop. The turns are rather tedious, but they avoid bringing the caravan through the heavy traffic and stoplights of Bishop, and this route provides good views of the north face of the Coyote Warp. The relatively flat ridge crests in the western portion of the north face of the Coyote Warp are capped by 11.75 Ma basalt flows (Phillips et al., 2011). These extensive sheets of basalt were presumably erupted onto a relatively flat surface, but are now tilted ~16° to the north, as a result of the warping of the Coyote Plateau.

26.7 Sunland Reservation Road. Turn left (W). This is named "Reservation Road" because it was the location of the original Paiute Indian Reservation for the Bishop Band of Paiutes. The Paiutes owned the water rights on their small reservation. In the 1930's the City of Los Angeles traded them a much larger and more fertile tract of land due west of Bishop for this small parcel, but Los Angeles retained the water rights appertaining to the new reservation. After 0.5 mile Sunland Reservation Road bends north.

27.8 Schober Lane. Turn left (W).

28.3 Barlow Lane. Turn right (N).

28.4 Underwood Lane. Turn left (W).

28.9 Orinda Lane. Go straight (W). In 0.5 mile the road curves gradually to the north and becomes Reata Road.

30.5 West Line Street. Turn left (W). WATCH FOR ONCOMING TRAFFIC.

31.0 Red Hill Road. Keep to the left on West Line Street. Behind the intersection is the small basaltic cinder cone and flow named Red Hill. It is part of a pulse of high-potassium basaltic volcanism at 3.40±0.06 Ma that probably marked the Pliocene resumption of active extensional tectonics in the region (Phillips et al., 2011).

32.8 To the right (W) of Line Street where it curves is a small basaltic neck, presumably the throat of a basalt cinder cone. It is part of the same pulse of basaltic volcanism at 11.75 Ma that produced the extensive flows on the Coyote Warp. The volcanic neck is bounded by columns of partially re-fused quartz monzanite. Knopf (1918) and Bateman (1965) have described in detail the mineralogical transformations accompanying partial assimilation of the quartz monzanite into the basalt. We are now approaching the Tahoe-age moraines of Bishop Creek, to the south of the Bishop Creek Road that we are now on.

36.2 The road curves and enters a roadcut giving a spectacular cross-section of the terminal Tahoe moraine. The prominent cemented layer in the soil on the Tahoe moraine is largely due to silcrete rather than calcrete development, although the B-horizons soils on these moraines do show both carbonate and silica accumulation. The silcrete formation may be due to at least in part to the relatively frequent deposition of silicic tephras on the land surface from local volcanic sources. Tephra layers were found in several soil pits on the moraines (Bach, 1995).

36.8 The road now enters a valley formed by the lateral and terminal moraines of the Tahoe-age glacier that flowed down Bishop Creek.

37.6 Old Forest Service Entrance Station for the Bishop Creek Recreation Area. Turn right (W), WATCHING FOR ONCOMING TRAFFIC. Park as directed.

Stop 2.1: Tectonics of the northern Coyote Warp, Glacial geology and chronology of Bishop Creek (Phillips).

Stop 2.1: The Bishop Creek terminal moraine complex

Fred M. Phillips
New Mexico Institute of Mining & Technology

Introduction

Along the eastern escarpment of the central Sierra Nevada the mouths of virtually all large canyons are distinguished by impressive sets of glacial moraines. These constitute a record of major climatic events in the region and have been the subject of numerous geological investigations over the past 100 years. Multiple glaciations of the eastern Sierra Nevada were first recognized by Russell (1889) . Knopf (1918) subsequently mapped glacial deposits of two ages in the Owens Valley region. The classic classification of glacial deposits in the region was laid out by Blackwelder (1931). He proposed four glacial stages (from oldest to youngest): McGee, Sherwin, Tahoe, and Tioga. The McGee glaciation is probably Pliocene and will not be discussed in this study. The type Sherwin deposits are known to date to ~800 ka due to their stratigraphic relationship (Sharp, 1968) with the well-dated Bishop Tuff (Izett and Obradovich, 1991; Sarna-Wojcicki et al., 2000). Some glacial deposits in this area may correlate with the McGee glaciation (Bateman, 1965), but if so, we have no methods that are able to confirm this correlation. This field guide will therefore focus on evaluating the significance of Blackwelder's Tahoe and Tioga designations in this study area.

Blackwelder did not propose a quantitative chronology for his glacial sequence because numerical dating of geological materials was in its infancy when he published his study, but he did tentatively correlate the Tioga glaciation with the midcontinental Wisconsin glaciation, the Tahoe with the Iowan (now early Wisconsin) and the Sherwin with the now-abandoned Kansan. Subsequently, Sharp and Birman (1963) proposed two additions: the Tenaya (between the Tioga and Tahoe) and the Mono Basin (between the Tahoe and Sherwin). Burke and Birkeland (1979), however, argued that these new subdivisions were not actually distinguishable from the original classification of (Blackwelder, 1931), based on the semiquantitative relative-weathering parameters that were then the principal criteria. Birman (1964) further proposed three additional

Holocene advances: the Hilgard (mid-Holocene), the Recess Peak (late Holocene), and the Matthes (Little Ice Age). Clark and Gillespie (1997) however, have demonstrated that the Hilgard and Recess Peak constitute only one advance, and that the timing of that advance was shortly after retreat of the Tioga glaciers. The glacial stratigraphy of the eastern Sierra Nevada has been reviewed and critically evaluated by (Warhaftig and Birman, 1965; Porter et al., 1983; Fullerton, 1986; Gillespie et al., 1999; Osborn and Bevis, 2001; Clark et al., 2003).

Bishop Creek has the largest drainage basin on the eastern slope of the southern Sierra Nevada. Most of the streams drain directly eastward into the Owens River, but Bishop Creek has been forced into a northeasterly course by the Coyote plateau to the east (Plate 1, Fig. 1) and hence collects runoff from a 35 km interval of the Sierra Nevada crest. As a result of this large collection area, the Pleistocene glaciers at Bishop Creek descended to an elevation of 1500 m, among the lowest in the eastern Sierra Nevada. At this elevation, an arid Great Basin climate prevails (150 mm annual precipitation at the nearby Bishop airport, compared to 440 mm at South Lake, about half the distance to the range crest). The Tahoe terminal moraine complex has been isolated from glacial advances during the last glacial maximum (Tioga glaciation) by an avulsion of the glacier course through the Tahoe right lateral moraine. The combination of dry climate and diversion of Tioga ice has resulted in an unusually complete and uneroded sequence of Tahoe glacial deposits. The comparatively great length of the Bishop Creek glacier has also provided a large area from which to select samples to document the chronology of the maximum and retreat of the Tioga glaciation. This combination of unusually abundant and well-preserved glacial landforms motivated us to focus a cosmogenic surface-exposure dating study on the Bishop Creek drainage. Fig. 1 gives a map of the Bishop Creek terminal moraine complex.

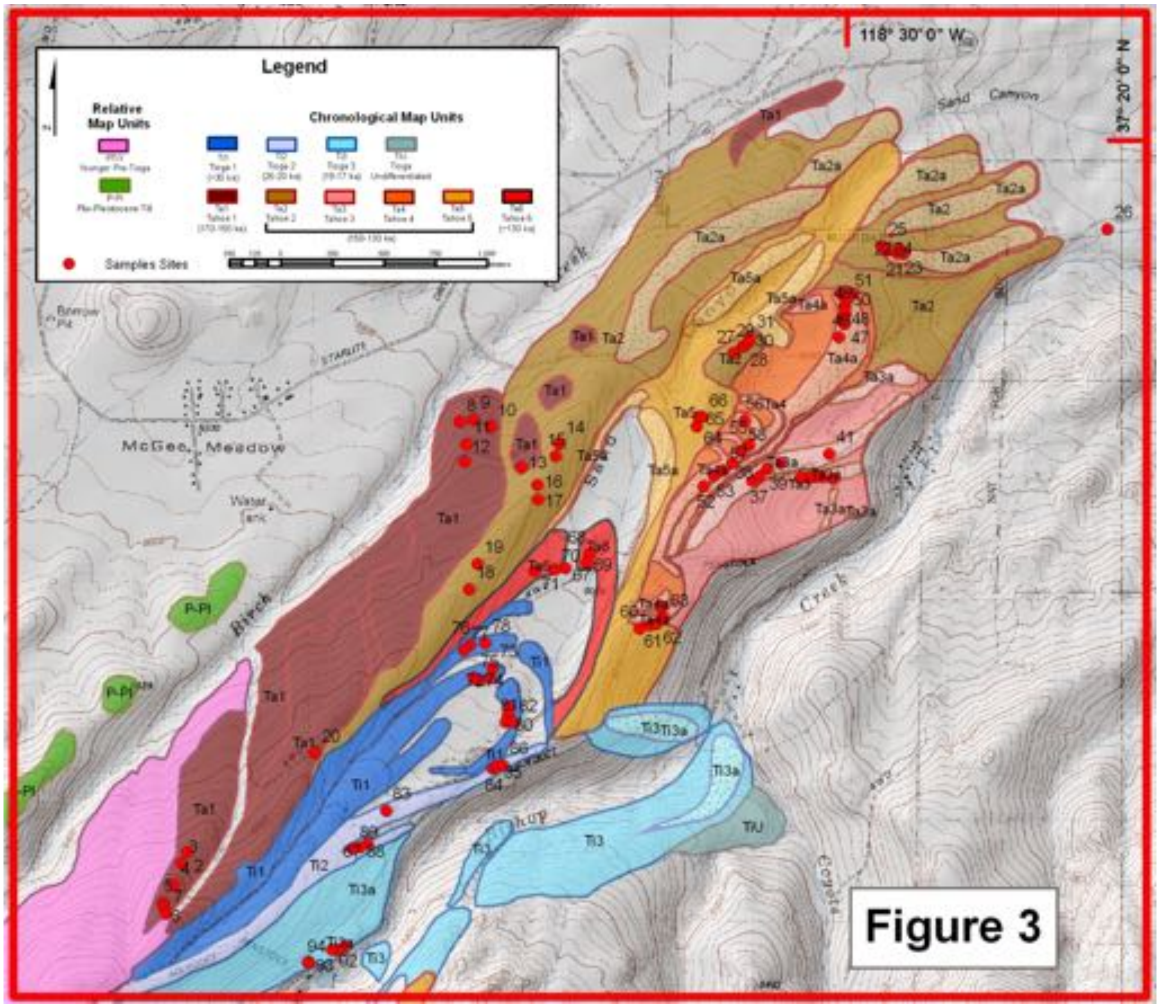

Figure 1. Geological map of the terminal moraine complex at Bishop Creek, from Phillips et al (2009). Brown, tan, and pink are various features of the Tahoe moraines. The Tioga 1 moraines are in dark blue, the Tioga 2 in blue-grey, and the Tioga 3 in light blue.

The terminal moraine complex is composed mostly of landforms assigned to the Tahoe glaciation. Notably, the valley below Stop 2.1 (to the northeast) contains the outermost (and only preserved) recessional moraine of the Tahoe advance(s), depicted in red on the map. Inboard of it are a nested sequence of small and much fresher moraines, mapped as Tioga. However, clearly subsequent to the deposition of these, the Tioga moraines mapped in blue-grey and light blue do not extend down the valley formed by the Tahoe terminal complex, but cut transverse to it, with the youngest deposited on the bottom of a deep canyon cut through the right lateral Tahoe moraine. Thus between early Tioga time and late Tioga time the Bishop Creek glacier avulsed thorough its right lateral and established a new course.

This map does not illustrate a series of Tioga recessional moraines further up the valley of Bishop Creek. Above these, where the South and Middle Forks of Bishop Creek flow together, is the final Tioga moraine, which we termed the Tioga 4 (Fig. 2). These moraines are 7.5 km upstream from the terminal complex where we are. About 12 km above these are a large number of diminutive moraines that were named the 'Recess Peak advance' by Birman (1964).

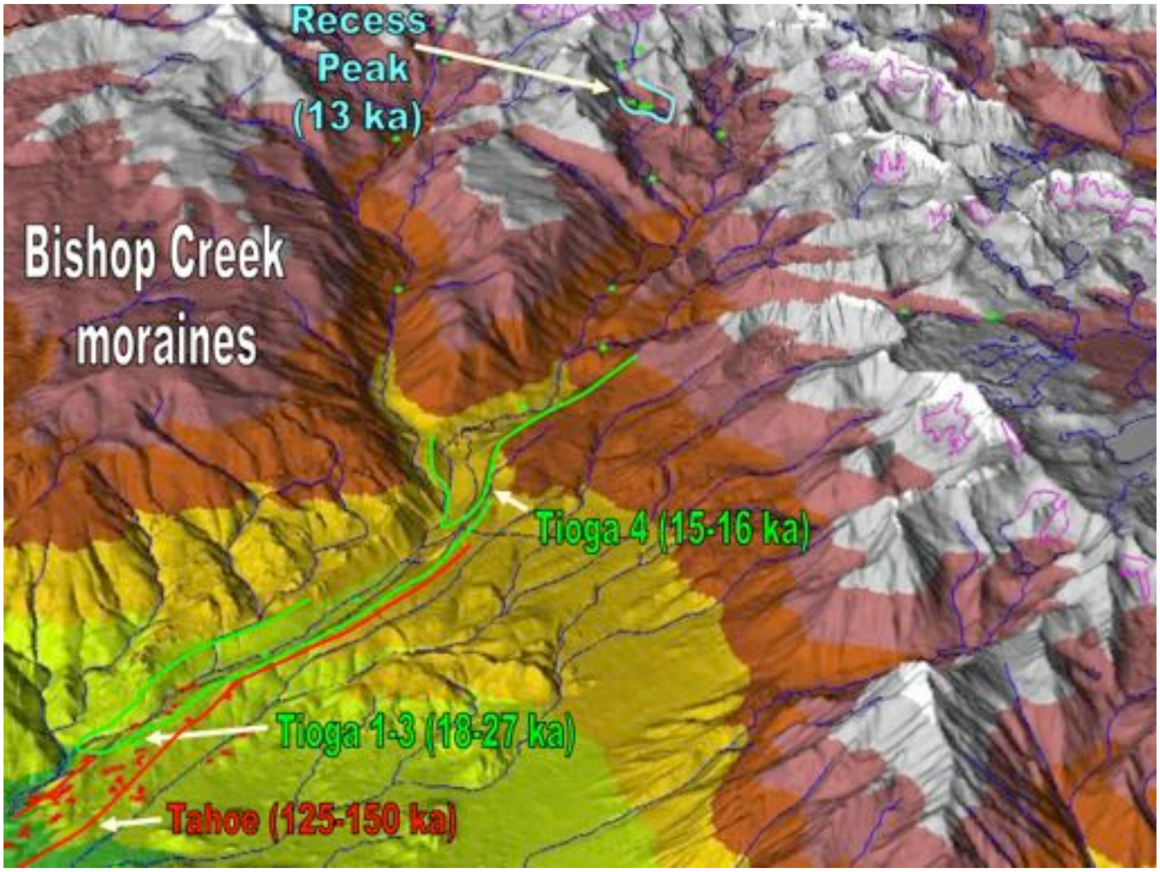

Figure 2. Shaded relief map showing locations of the various mapped glacial deposits of Bishop Creek. The location of the Recess Peak moraines is merely indicative; there are many other Recess Peak moraines mapped that are not shown. Stop 2.1 is located approximately at the tip of the arrow to the left of "Tioga 1-3'.

Cosmogenic dating of the Bishop Creek complex

This stop write-up is largely based on the cosmogenic dating study of Phillips et al. (2009), supplemented by the glacial modeling study of Plummer and Phillips (2003) and the subsequent reviews by Phillips (2016) and Phillips (2017). These studies sought to answer several questions based on prior studies of Sierra Nevada glaciation and on observations at Bishop Creek:

- The 'Tahoe' moraines are complex, with multiple crests giving evidence of multiple advances, while the 'Tioga' ones are much simpler. Are these the result of just two discrete glacial episodes (i.e., corresponding to marine isotope stages), or do they reflect multiple episodes spanning a long time range?

- When did the Tioga glacier avulse through the Tahoe right-lateral moraine and what caused the event?
- Blackwelder (1931) asserted that in general the Tahoe moraines were much more voluminous than the Tioga ones and that this reflected a longer glacial episode. The moraines at Bishop Creek do indeed show this pattern. Do they support Blackwelder's inference?
- Bateman (1965) inferred that the moraine at the confluence of the South and Middle Forks of Bishop Creek represented a late readvance of the Tioga glacier and Clark (1976) and Clark and Clark (1995) inferred that retreat from this position was rapid. Does the chronology from Bishop Creek support this?

The results from ^{36}Cl exposure dating are shown in Fig. 3. Note that these are calculated using the old production calibration of Phillips et al. (2001). Selected samples have been recalculated using the current production rate of Marrero et al. (2016) and will be discussed below.

Ages from the Tahoe moraines fall in the range from 170 to 60 ka. We consider that most of this downward scatter is due to 'late' (i.e., after moraine deposition) erosion of boulders out of the till matrix (Zreda et al., 1994) and that the oldest ages are to be preferred. On the Tahoe terminal complex the oldest ages are found on the upper left lateral moraine and are about 170 ka. This section of moraine is very bouldery and resistant to erosion. Morphologically, the youngest moraine has to be the recessional in the valley floor below Stop 2.1; this moraine would have been obliterated by being overridden if downstream moraines had been deposited subsequent to them. The recessional yields maximum ages of ~130 ka. Thus the entire Tahoe terminal complex was created during Marine Isotope Stage 6 (MIS 6). Moraines of the terminal area and outboard of the right lateral consistently give young ages (100 to 60 ka). We attribute this to the large proportion of sand and low proportion of boulders in these areas (probably due to reworking of outwash) making them susceptible to erosion, and due to inducement of erosion caused by subsequent undercutting by Bishop Creek.

The oldest Tioga moraines are the terminal loops in the valley bottom inboard of the final Tahoe recessional. Although these ages scatter widely, the oldest group between 27 and 24 ka. These are assigned to the Tioga 1, an advance during the early stages of MIS 2. They appear to be effectively a group of recessional moraines and Phillips et al. (2009) linked this behavior to the creation of the right-lateral avulsion down the present course

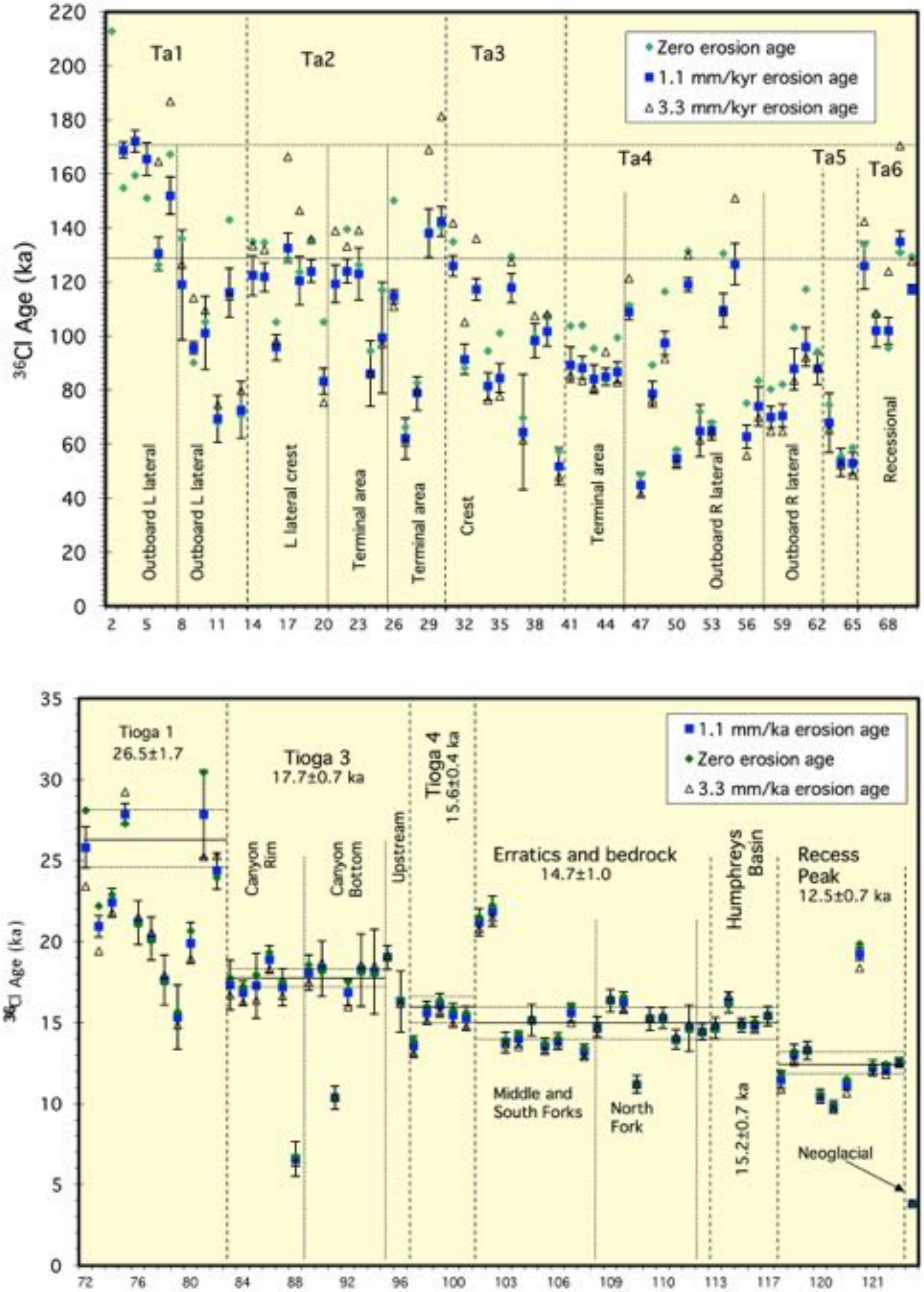

Figure 3. Results from ^{36}Cl surface exposure dating of Bishop Creek glacial features, from Phillips et al. (2009). Note that ages are based on the old calibration of Phillips et al. (2001). Upper panel is Tahoe ages and lower one Tioga ones. Numbers on x-axis are sample designations from Phillips et al. (2009).

of Bishop Creek. The Tioga 3 moraines on the canyon rim, clearly subsequent to the avulsion event, date to 19.2±0.8 ka, using the new calibration of Marrero et al. (2016) (Phillips, 2017). Thus the avulsion event took place between ~27 ka and ~19 ka, probably much closer to 27 ka. Following the avulsion event the glacier snout was confined within the narrow walls of the canyon of Bishop Creek, without space to deposit much moraine, and thus most of the glacial sediment load was evidently flushed onto the Bishop Creek outwash fan. The most extensive moraines in the canyon bottom give essentially identical ages (~19 ka) and are thus also Tioga 3.

The recalibrated ages for the readvance moraine at the confluence of the South and Middle Forks cluster tightly at 16.1±0.3 ka (Phillips, 2017). Samples upstream of this (erratics and polished bedrock, since there are no significant moraines) give essentially identical ages all the way to the crest of the range. Additonally, the morphology of the Tioga 4 moraine (Bateman, 1965) and the 3 ka gap between the Tioga 3 and 4 events support the idea that the Tioga 4 was a significant readvance and that retreat from the Tioga 4 maximum position was rapid and complete.

Paleoclimatic significance of the Bishop Creek moraines

The ages for the Tahoe complex clearly indicate that it took place during MIS 6. Additional refinement of the climatic significance is probably premature until the ages are recalculated using current production rates, and in any case are limited by the wide dispersion of the ages. The lack of any dated features in the terminal area between ~130 ka and 26 ka demonstrates that Bishop Creek glaciers did not reach their maximum extent during Stages 5, 4, or 3 (i.e., the local glacial maxima coincided with the global glacial maxima). This does not preclude significant advances during these other stages.

The Bishop Creek Tioga chronology is secure enough to compare with regional and global records from the same period. In Fig. 4 the glacial positions, expressed in terms of Equilibrium Line Altitude (ELA; m) from Bishop Creek and other nearby drainages, is compared to the percent left-coiling *Neogloboquadrina pachyderma* from core 893A in the Santa Barbara Basin, from Hendy et al. (2002) but plotted on the revised time scale of Kennett et al. (2008). The percentage of sinistral *N. pachyderma* increases as surface sea water grows colder. The two records show a close correspondence, indicating that temperature reduction played a major role in forcing Sierra Nevada glaciation. The initiation of glaciation was during early MIS 2, a time when glaciers and ice sheets were growing worldwide, forced principally by decreased summer insolation at high latitude in the Northern Hemisphere. The Sierra Nevada glaciers begin to shrink at a time (~18 ka) when many mountain glaciers worldwide did the same, apparently driven by the reversal toward increased northern insolation (i.e., the Milankovich cycle).

The Tioga 4 readvance happened at a time of increasing insolation and was also too rapid to be explained by the Milankovich mechanism. The most notable correlation is that the Tioga 4 glaciers readvanced at the very early stages of the Heinrich 1 event

(H1) in the North Atlantic, but the Sierra glaciers began to retreat about half way through

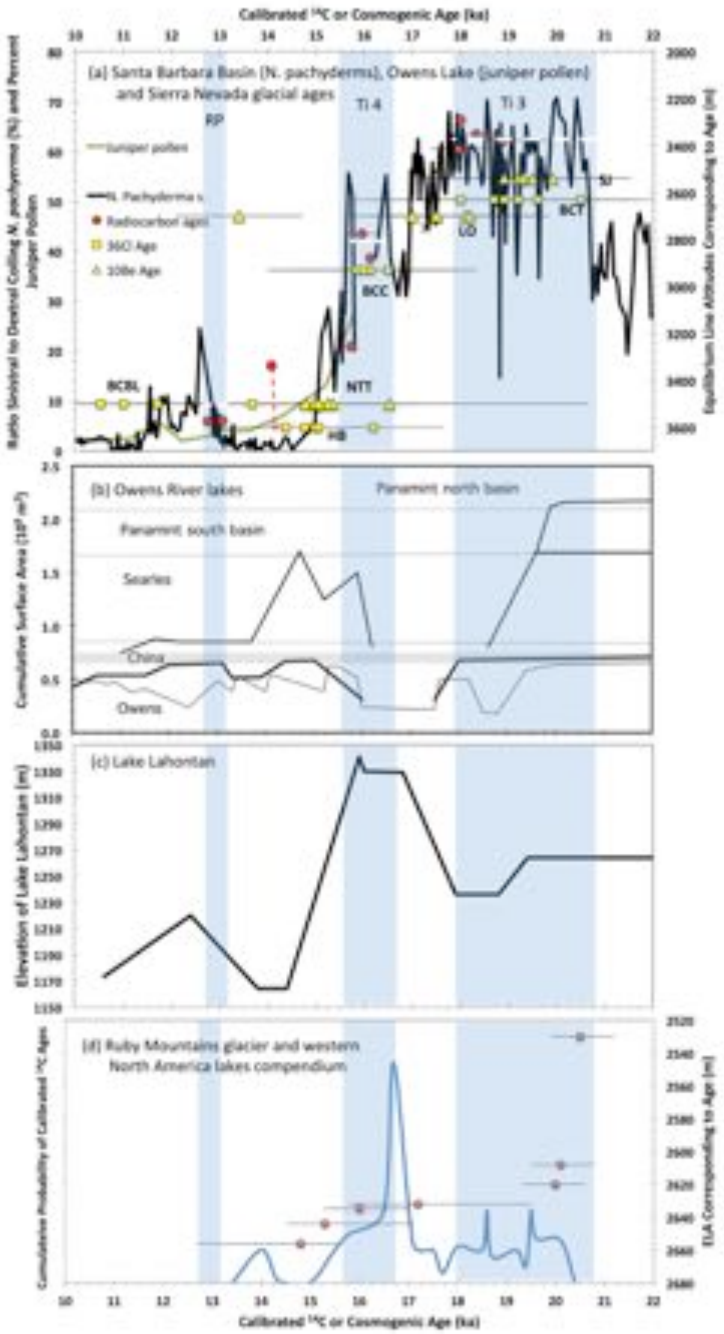

Figure 4. (a) Comparison of central Sierra Nevada ELA positions with time series of sinistral *Neogloboquadrina pachyderma* from core 893A, Santa Barbara Basin. (b) Reconstructed levels of lakes in the paleo-Owens River system. (c) Reconstruction of Lake Lahontan elevation history, from Reheis et al. (2014). (e) Records of lakes and

glaciers in the northeastern Great Basin. Figure from Phillips (2017); see this for further information on methods and sources.

the H1 event, thus there was no simple one-to-one correspondence with H1. As discussed by Phillips (2017), the most notable aspect of this part of H1 was the development of very extensive ice cover over the North Atlantic. Simulations by climate models (Chiang and Bitz, 2005; Chiang et al., 2014) have supported the idea of a teleconnection between North Atlantic sea ice and influxes of cold, moist air from the eastern Pacific over western North America at the latitude of the Sierra Nevada.

Notably, as shown in Fig. 4(c), the highstand of Lake Lahontan was correlative with the Tioga 4 maximum. This supports the idea that the same forcing mechanism (possibly, extensive North Atlantic sea ice) may have produced the events in both settings. The fact that Sierra Nevada glaciers were more extensive during the Ti3 but Lake Lahontan during Ti4 likely indicates that climate was cold during both intervals, but colder at 20-18 ka and less cold but wetter at ~16 ka. This is consistent with global climatic trends.

Conclusions

Results from the Bishop Creek study are adequate to give at least tentative answers to the questions raised above. First, although the Tahoe terminal complex is exceptionally complex, it apparently all dates from MIS 6 and indicates multiple advances and retreats during that period. There is no evidence in the terminal area to support advances between the end of MIS 6 and the beginning of MIS 2.

The glacier advanced through the right lateral Tahoe moraine at about 25 ka, early in the Tioga 1 advance. There is no evidence that would indicate damming of the terminal area to produce an overflowing lake, thus mass failure, perhaps by groundwater sapping, appears more likely.

The volume of Tahoe moraine at Bishop Creek is much greater than that of Tioga, but the principal reason is that after the avulsion event the Tioga glacier emptied into a narrow canyon where moraines could not be stabilized. Thus, although the relative volumes support Blackwelder's hypothesis, the actual mechanics do not support his hypothesis of longer deposition time during the Tahoe.

The ^{36}Cl ages do indeed support Clark and Clark's hypothesis of rapid Tioga 4 retreat. As described above, the Tioga 4 advance may be linked with extensive sea ice during the early stages of H1. The rapid retreat may also be linked with evidence that the episode of extensive sea ice ended rapidly, apparently mainly due to ending of the flow of meltwater to produce a light, easily frozen cap over the North Atlantic.

References

Bateman P. C. (1965) Geology and tungsten mineralization of the Bishop District, California: U.S. Geological Survey Professional Paper 470, Professional Paper 470, 208 p. pp.

Birman J. H. (1964) Glacial geology across the crest of the Sierra Nevada: Geological Society of America Special Paper 75, Boulder, Colorado, 80 pp.

Blackwelder E. (1931) Pleistocene glaciation in the Sierra Nevada and Basin ranges: *Bulletin of the Geological Society of America* **42** 865-922.

Burke R. M. and Birkeland P. W. (1979) Re-evaluation of multiparameter relative dating techniques and their application to the glacial sequence along the eastern escarpment of the Sierra Nevada, California: *Quaternary Research* **11** 21-51.

Chiang J. C. H. and Bitz C. M. (2005) Influence of high latitude ice cover on the marine Intertropical Convergence Zone: *Climate Dynamics* **25**(5) 477-496.

Chiang J. C. H., Lee S.-Y., Putnam A. E., and Wang X. (2014) South Pacific Split Jet, ITCZ shifts, and atmospheric North–South linkages during abrupt climate changes of the last glacial period: *Earth and Planetary Science Letters* **406** 233-246.

Clark D., Gillespie A. R., Clark M., and Burke R. (2003) Mountain glaciation of the Sierra Nevada, In *Quaternary Geology of the United States: INQUA 2003 Field Guide Volume* (D. J. Easterbrook; ed.), Desert Research Institute, Reno, Nevada, pp. 287-312.

Clark D. H. and Clark M. M. (1995) New evidence of late-Wisconsin deglaciation in the Sierra Nevada, California, refutes the Hilgard Glaciation: *Geological Society of America Abstracts with Programs* **27**(5) 10.

Clark D. H. and Gillespie A. R. (1997) Timing and significance of late-glacial and Holocene cirque glaciation in the Sierra Nevada, California: *Quaternary International* **38/39** 21-38.

Clark M. M. (1976) Evidence for rapid destruction of latest Pleistocene glaciers of the Sierra Nevada, California: *Geological Society of America Abstracts with Programs* **8** 361-362.

Fullerton D. S. (1986) Chronology and correlation of glacial deposits in the Sierra Nevada, California, In *Quaternary Glaciations in the Northern Hemisphere: Report of the International Geological Correlation Programme Project 24* (V. Sibrava, D. Q. Bowen, and G. M. Richmond; eds.), Pergamon Press, Oxford, pp. 161-169.

Gillespie A. R., Clark M. M., and Burke R. M. (1999) Eliot Blackwelder and the alpine glaciations of the Sierra Nevada, Vol. Special Paper 338, In *Classic Cordilleran concepts: A View from California* (E. M. Moores, D. Sloan, and D. L. Stout; eds.), Geological Society of America Special Paper 338, Boulder, pp. 443-452.

Hendy I., Kennett J. P., Roark E. B., and Ingram B. L. (2002) Apparent synchroneity of submillennial scale climate events between Greenland and Santa Barbara Basin, California from 30-10 ka: *Quaternary Science Reviews* **21** 1167-1184.

Izett G. A. and Obradovich J. D. (1991) Dating of the Matuyama-Bruhnes boundary based on $^{40}Ar/^{39}Ar$ ages of the Bishop Tuff and Cerro San Luis rhyolite:: *Geological Society of America Abstracts with Programs* **23**(5) A106.

Kennett D. J., Kennett J. P., West G. J., Erlandson J. M., Johnson J. R., Hendy I. L., West A., Culleton B. J., Jones T. L., and Stafford Jr T. W. (2008) Wildfire and abrupt ecosystem disruption on California's Northern Channel Islands at the Ållerød–Younger Dryas boundary (13.0–12.9 ka): *Quaternary Science Reviews* **27** 2530-2545.

Knopf A. (1918) A geologic reconnaissance of the Inyo Range and the eastern slope of the Sierra Nevada, California, with a section on the stratigraphy of the Inyo Range by Edwin Kirk: U. S. Geological Survey Professional Paper 110, 130 pp.

Marrero S. M., Phillips F. M., Caffee M. W., and Gosse J. C. (2016) CRONUS-Earth cosmogenic ^{36}Cl calibration: *Quaternary Geochronology* **31** 199-219.

Osborn G. and Bevis K. (2001) Glaciation in the Great Basin of the Western United States: *Quaternary Science Reviews* **20**(13) 1377-1410.

Phillips F. (2017) Glacial chronology of the Sierra Nevada, California, from the Last Glacial Maximum to the Holocene: *Cuadernos de Investigación Geográphica* **43** 527-552, doi:10.18172/cig.3233.

Phillips F. M. (2016) Constraints on cosmogenic nuclide production rates by samples from the Sierra Nevada, California: I. Late Pleistocene glacial chronology: *Quaternary Geochronology* **35** 119-129.

Phillips F. M., Stone W. D., and Fabryka-Martin J. T. (2001) An improved approach to calculating low-energy cosmic-ray neutron fluxes near the land/atmosphere interface: *Chemical Geology* **175** 689-701.

Phillips F. M., Zreda M., Plummer M. A., Elmore D., and Clark D. H. (2009) Glacial geology and chronology of Bishop Creek and vicinity, eastern Sierra Nevada, California: *Geological Society of America Bulletin* **121** 1013-1033.

Plummer M. A. and Phillips F. M. (2003) A 2-D numerical model of snow/ice energy balance and ice flow for paleoclimatic interpretation of glacial geomorphic features: *Quaternary Science Reviews* **22** 1389-1406.

Porter S. C., Pierce K. L., and Hamilton T. D. (1983) Late Wisconsin mountain glaciation in the western United States, In *Late Quaternary Environments of the United States* (H. E. Wright, Jr.; ed.), University of Minnesota Press, Minneapolis, pp. 71-111.

Reheis M. C., Adams K. D., Oviatt C. G., and Bacon S. N. (2014) Pluvial lakes in the western United States - A view from the outcrop: *Quaternary Science Reviews* **97** 33-57.

Sarna-Wojcicki A., Pringle M. S., and Wijbrans J. (2000) New ^{40}Ar/^{39}Ar age of the Bishop Tuff from multiple sites and sediment rate calibration for the Matuyama-Brunhes boundary: *Journal of Geophysical Research-Solid Earth* **105** 21431-21443.

Sharp R. P. (1968) Sherwin Till-Bishop Tuff geological relationships, Sierra Nevada, California: *Geological Society of America Bulletin* **79** 351-364.

Sharp R. P. and Birman J. H. (1963) Additions to classical sequence of Pleistocene glaciations, Sierra Nevada, California: *Geological Society of America Bulletin* **74** 1079-1086.

Warhaftig C. and Birman J. H. (1965) The Quaternary of the Pacific mountain system in California, In *The Quaternary of the United States* (H. E. Wright, Jr. and D. G. Frey; eds.), Princeton University Press, Princeton, New Jersey, pp. 299-340.

Zreda M. G., Phillips F. M., and Elmore D. (1994) Cosmogenic ^{36}Cl accumulation in unstable landforms, 2. Simulations and measurements on eroding moraines: *Water Resources Research* **30** 3127-3136.

Road Log

37.6 Exit the old Entrance Station drive on to the Bishop Creek Road, turning left (E). WATCH FOR HIGH-SPEED TRAFFIC IN BOTH DIRECTIONS. Drive down the Bishop Creek Road, back toward Bishop.

43.9 Oteys Road. Turn left (N). WATCH FOR ONCOMING HIGH-SPEED TRAFFIC.

44.1 Red Hill Road. Turn left (W). The road cuts through the base of the Red Hill cinder cone, exposing the soil underlying the cinders. Note the prominent columnar soil peds with calcite-lined fractures and strong rubification.

45.1 Ed Powers Road. Turn right (N).

46.5 Highway 395. Turn left (W). WATCH CAREFULLY FOR HIGH-SPEED TRAFFIC IN BOTH DIRECTIONS.

51.1 Highway 395 curves northward and begins to skirt the edge of the Volcanic Tableland (the margin of the welded Bishop Tuff). To the south we have been driving on the Bishop Tuff surface, in most places somewhat eroded and covered by a veneer of Pleistocene Owens River gravels. Here, as the margin direction shifts northward, the edge of the tuff sheet is formed by a gentle down-warping to the west. This is an expression of the anticlinal rollover of the hanging wall of the Round Valley fault, which is visible at the foot of Wheeler Crest to the west. The accommodation space created by this rollover is filled with sediment from Pine Creek and Rock Creek, forming the green floor of Round Valley. The dip of the Round Valley fault increases from about 30° where it crosses the Pine Creek moraines to >70° near the north end of Wheeler Crest. As it does so, the amount of rollover on the Bishop Tuff decreases northward.

54.5 The highway ascends onto the surface of the Bishop Tuff. Occasional conical mounds on the tuff surface appear to be the remnants of pervasive fumaroles that vented from the tuff sheet immediately after its emplacement (cf. the "Valley of Ten Thousand Smokes"). Geothermal processes hardened the area around the fumarole conduits, making them more resistant to erosion than the rest of the tuff sheet (Sheridan, 1970).

61.3 Highway 395 begins to curve toward the north, revealing good views of the base of Wheeler Crest. If the light is favorable, the trace of the Round Valley fault can clearly be seen at the base. The small community on the west side of Rock Creek Gorge is Swall Meadows. If you look closely at the fault just west and north of Swall Meadows you can see evidence of dextral offset on the fault, in the form of offset debris fans and stream channels (Phillips and Majkowski, 2011).

62.6 The large, rounded hill to the right (E) of the highway is formed of Sherwin Till. Based on field relations in this area, Blackwelder (1931) mistakenly thought that the Sherwin Till was superposed on the Bishop Tuff. Can you tell the difference?

63.5 Highway 395 begins to turn westward. Turn right here onto an unmarked gravel road. Keep right on the gravel road, basically 180° from the direction you were going on 395. Keep going straight on the main road and ignore several small side roads. In 0.9 mile the road makes an ‘S’ bend with several roads coming in from the left making ‘Y’ junctions. Keep on the main road.

64.5 A smaller road coming in from the left (N) makes another ‘Y’ junction. Take this road. Numerous small roads join, but stay on main road going straight north. At 69.7 the road begins to curve east.

64.8 ‘Y’ junction, keep right. Take care to avoid rocks and bushes along and in roadway.

65.0 Park on road. Stop 2.2. Walk ~100 m northeast to the edge of the Owens River Gorge. BRING YOUR LUNCH!

Stop 2.2: (Re)incision of Owens River Gorge (Hildreth).

Stop 2.2: The (Re)incision of Owens River Gorge

Wes Hildreth and Judy Fierstein

US Geological Survey

(This passage is quoted from Hildreth and Fierstein, 2017, p. 35 and 41, with minor editing to make it consistent with this guidebook)

Across the gorge, which is here ~250 m deep, a wall of Triassic granodiorite is 180 m high and is draped by a Pliocene stack of ~15 basaltic lava flows that dip ~20º WSW., all the way to the modern gorge floor (fig. 1). Just up-canyon, the basalt is as thick as 190 m and is overlain by 60–100 m of Bishop Tuff, which extends to the rim on both sides. Both basalt and ignimbrite thin markedly where they drape over the granodiorite high, but both thicken again farther downstream. Between the 3.3-Ma basalt and the 767-ka Bishop Tuff, exposures of white granitic boulders on both walls represent deposits of Sherwin Till ~25 m thick, which were deposited by a Sierran glacier during MIS 22 (900–866 ka) and (or) 20 (814–790 ka) (Lisiecki and Raymo, 2005). Because most of 30-km-long Owens River Gorge is walled only by Bishop Tuff, it has not been widely appreciated that the gorge dates from the Miocene (Hildreth and Fierstein, 2016). The Owens River had crossed the later site of the caldera from sources farther north and had cut the deep granodiorite gorge before the 3.3-Ma basalt filled it from floor to rim. Because the Sherwin glacier crossed this reach of the gorge and because the Bishop Tuff is nowhere inset against either the granodiorite or the rubbly basalt, it is clear that the 5-km-long basalt-blocked reach of the gorge was not re-excavated until after emplacement of the Bishop Tuff. Between 3.3 Ma and 767 ka, the Owens River was diverted to nearby Rock Creek along a channel later buried by the Bishop Tuff. The earliest ignimbrite, distinctive subpackage Ig1Ea, as thick as 80 m, was completely blocked by the basement high, confirming that the basalt-filled reach had not, by then, been re-excavated. Several thin fall beds are intercalated within Ig1Ea, which overlies only ~44 cm of fall deposits (F1 and lower F2), showing that pyroclastic flows began very soon after onset of the eruption (Wilson and Hildreth, 1997). After the caldera collapse, the upper Owens River terminated in an intracaldera lake that slowly filled a profound depression initially more than 700 m deep. Only after the lake filled with 700 m of sediment, reaching its spillpoint ~150 ka, was the gorge reincised through the ignimbrite and the basalt (Hildreth and Fierstein, 2016).

(The following passage is for a site on Rock Creek, but is relevant here because ~2 km down the Owens River Gorge the Sherwin Till is exposed on both sides of the Gorge, intercalated between the Pliocene basaltic lava flows and the Bishop Tuff.)

Glacial erosion in the Sierra Nevada is likely to have been most profound during the Sherwin glaciation. Not only was the Sherwin advance greater than any subsequent glacial advance in the Sierra, but MIS 22 was the first of five great global episodes of ice accumulation (along with MIS 16, 12, 6 and 2) that followed the “Mid-Pleistocene Revolution” (Berger and others, 1993; Muttoni and others, 2003), which was the transition from higher-frequency lower-amplitude climatic oscillations to lower-frequency higher-amplitude glacio-eustatic fluctuations. In the Sierra Nevada, glacial deposits of MIS 6 (regionally called the Tahoe glaciation) and 2 (Tioga glaciation) are well preserved, those of MIS 22 scattered and erosively subdued, and those of MIS 16 (~630 ka) and 12 (~410 ka) glaciations unreported and presumed obliterated during MIS 6.

Sherwin Till is as thick as 200 m and derived almost entirely from granitic rocks. The glacier that carried it emerged from the canyon of Rock Creek only 4 km southwest of here. From the canyon's narrow mouth, the ice spread out 5–8 km eastward into a piedmont lobe at least 7 km wide. Locally it crossed Owens River Gorge, a 5-km reach of which had been completely filled by Pliocene basalt, thus depositing till on both rims. After the Sherwin episode, normal and dextral displacement on the Round Valley range-front fault promoted redirection of Rock Creek, which cut a northeast-trending canyon through a downdropped granitic buttress. Dextral offset of the apex of Sherwin deposits near the canyon mouth is at least 500 m, giving an average strike-slip rate of >0.6 mm/yr since MIS 22. The piedmont lobe of Sherwin Till was thus displaced and bypassed, whereas emplacement of Tahoe and Tioga (MIS 6 and 2) glacial deposits was controlled by the new northeast drainage toward Toms Place. A long history of erosion has destroyed primary morainal landforms and reduced the Sherwin deposit to a rolling hill-and-gully terrain.

Stones in the till are ~98 percent granitic and range from pebbles to boulders as large as 2.5 m, many of them grussy. Many of the subordinate metamorphic clasts (10–50 cm) are blocky and angular. The till matrix is rich in crystal sand, not unexpected for so proximal a granite-derived glacial deposit. We sieved 2-kg samples of till matrix (excluding clasts larger than 8 mm, which make up at least half by weight of the bouldery till) from two roadcut exposures of the type Sherwin Till along Rock Creek. Both matrix samples are dominated by sand and granules (median diameter 1.5 and 1.7 mm, respectively), and both are poor in fines (0.5 and 1.7 weight percent finer than 1/16th mm). Eroded scarps of Bishop Tuff overlie Sherwin Till deposits north and east of here.

F

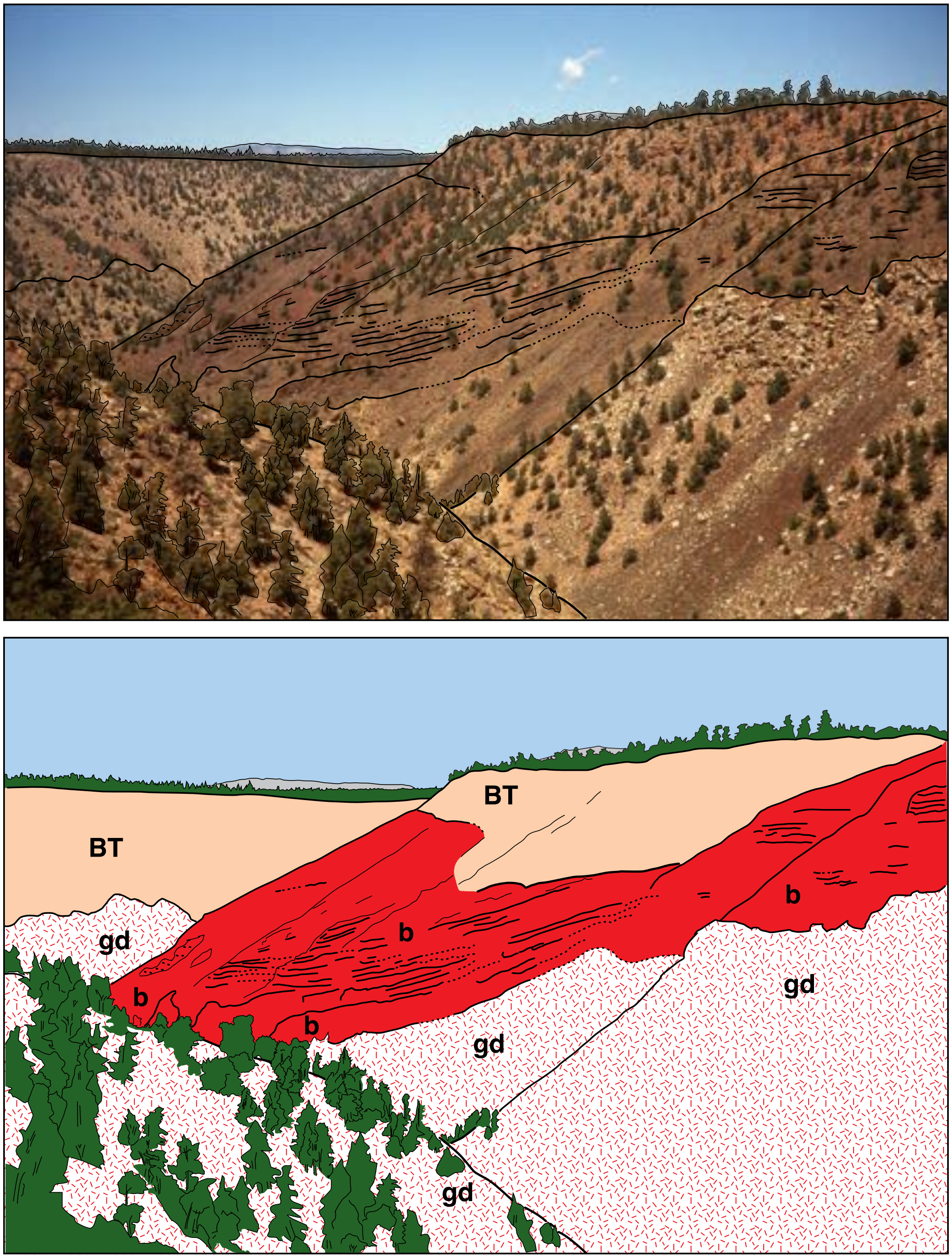

Figure 1. View upstream from right-bank rim of Owens River Gorge near Stop 19. Gorge depth here is ~250 m. On opposite (left-bank) side, granodiorite wall in right foreground is 180 m high and is draped by stack of ~15 basaltic lava flows that dip ~20o WSW, all the way to gorge floor. Canyon-filling basalt is as thick as 190 m at left center and overlain by 60–100 m of Bishop Tuff, which extends to rim on both sides. Basalt (b)

and Bishop Tuff (BT) thin markedly to right where they drape over the granodiorite (gd) high, but both thicken again farther downstream. From Hildreth and Fierstein (2016).

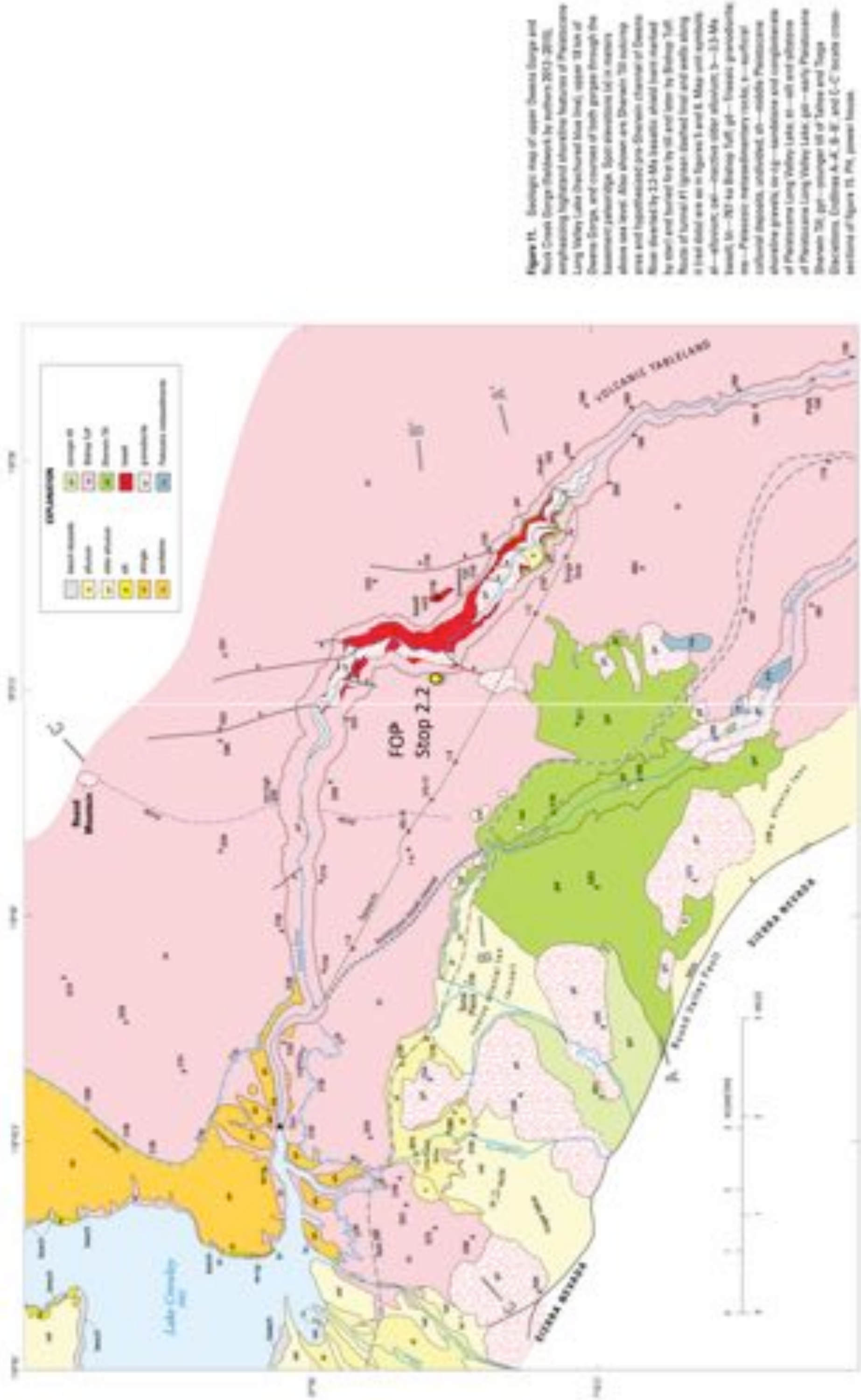

Figure 2. Geologic map of upper Owens Gorge and Rock Creek Gorge (fieldwork by authors 2012–2015), emphasizing highstand shoreline features of Pleistocene Long Valley Lake (hachured blue line), upper 18 km of Owens Gorge, and courses of both

gorges through the basement paleoridge. Spot elevations (x) in meters above sea level. Also shown are Sherwin Till outcrop area and hypothesized pre-Sherwin channel of Owens River diverted by 3.3-Ma basaltic shield (vent marked by star) and buried first by till and later by Bishop Tuff. Route of tunnel #1 (green dashed line) and wells along it (red dots) are as in figures 5 and 6. Map-unit symbols: al—alluvium; oal—inactive older alluvium; b—3.3-Ma basalt; bt—767-ka Bishop Tuff; gd—Triassic granodiorite; ms—Paleozoic metasedimentary rocks; s—surficial colluvial deposits, undivided; sh—middle Pleistocene shoreline gravels; ss-cg—sandstone and conglomerate of Pleistocene Long Valley Lake; st—silt and siltstone of Pleistocene Long Valley Lake; gst—early Pleistocene Sherwin Till; gyt—younger till of Tahoe and Tioga Glaciations. Endlines A–A’, B–B’, and C–C’ locate cross- sections of figure 15. PH, power house.

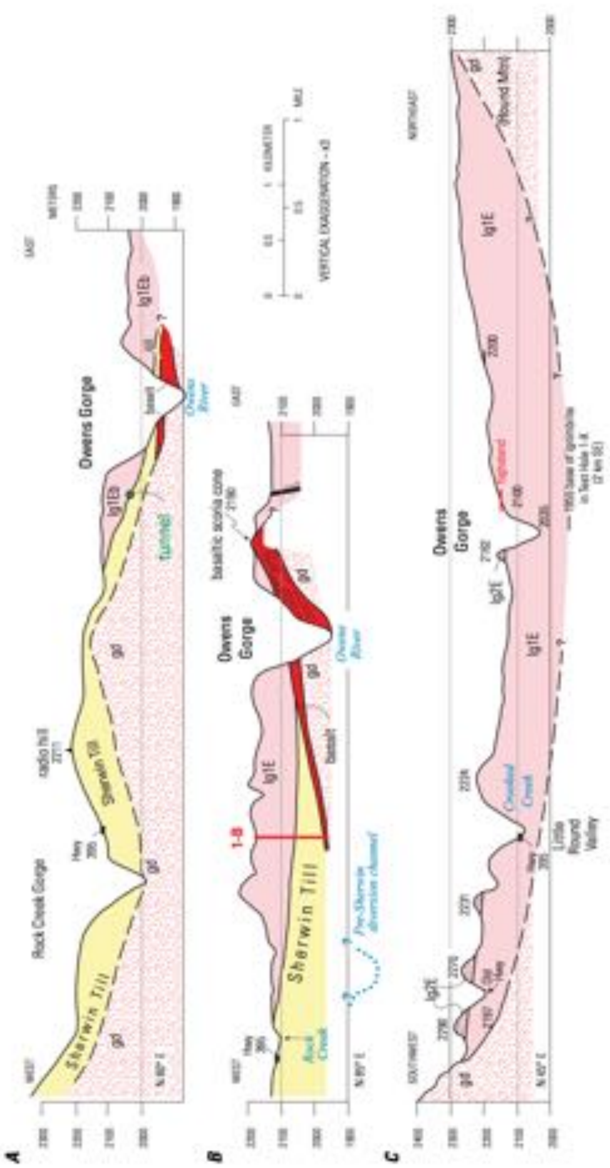

Figure 3. Schematic cross sections of Owens Gorge and vicinity. Vertical exaggeration ~3x. Elevations in meters above sea level. Profile orientations given at lower left of each panel and on figure 2. *A*, Along main lobe of Sherwin Till, from near Whisky Canyon across both gorges; profile trends N. 80^o E. Bishop Tuff here consists entirely of package Ig1Eb. It overlies Sherwin Till, which distally crosses Owens Gorge atop shelves of 3.3-Ma basalt. From vent shown in profile B, basalt flowed north and south along granodiorite gorge, which was already as deep as it is today. Granodiorite (gd) crops out in several windows through the till (fig. 2). Los Angeles Department of Water and Power (LADWP) tunnel #1 intersects contact between Sherwin Till and Bishop Tuff. *B*, From Rock Creek ~1 km east of Toms Place to vent cone of 3.3-Ma basalt atop basement high east of Owens Gorge; profile trends N. 85^o E. Basaltic lavas and agglutinate drape east wall of granodiorite paleo-gorge all the way to present-day riverbank (fig. 2). Covered by basalt in line of section, granodiorite (gd) crops out as high as 2,140 m on east wall ~800 m south of profile. Contact elevations in test hole 1–B are from Putnam's (1960) survey of LADWP tunnel #1. Hypothesized post-basalt pre-Sherwin channel of Owens River diverted by basalt toward Rock Creek, later covered by thick Sherwin Till, is sketched at elevation consistent with that of base of till (1,833 m) in test hole 1–X, 2 km upstream, northwest of profile. Till reaches Owens Gorge (as in profile A) only south of profile B. (C) From west wall of Little Round Valley to Round Mountain; profile trends N. 45^o E. Base of Bishop Tuff is exposed only at far ends of section but lies on Sherwin Till at ~1,955 m in test hole 1–X, which is 2 km south of central part of section. Lower nonwelded zone of ignimbrite is exposed at Crooked Creek. Remnants of late-erupted package Ig2E cap knolls near Owens Gorge and Little Round Valley (elevations in meters).

References

Berger, W.H., Bickert, T., Schmidt, H., and Wefer, G., 1993, Quaternary oxygen isotope record of pelagic foraminifers— Site 806, Ontong Java Plateau, *in* Berger, W.H., Kroenke, L.W., Mayer, L.A., eds., Proceedings of the Ocean Drilling Program, Scienti c results: v. 130, p. 381–395, College Sta- tion, Texas, Ocean Drilling Program.

Hildreth W. and Fierstein J. (2016) Long Valley caldera lake and reincision of Owens River Gorge: U.S. Geological Survey Scientific Investigations Report 2016-5120, 63 pp.

Hildreth, W., and Fierstein, J. (2017) Geologic field-trip guide to Long Valley Caldera, California: USGS Scientific Investigations Report 2016-5022-Y, 119 p.

Muttoni, G., Carcano, C., Garzanti, E., Ghielmi, M., Piccin, A., Pini, R., Rogledi, S., and Sciunnach, D., 2003, Onset of major Pleistocene glaciations in the Alps: Geology, v. 31, no.11, p. 989–992.

Putnam, W.C., 1960, Origin of Rock Creek and Owens River gorges, Mono County, California: University of California Publications in Geological Sciences, v. 34, p. 221–280.

Wilson, C.J.N., and Hildreth, W., 1997, The Bishop Tuff—New insights from eruptive stratigraphy: Journal of Geology, v. 105, p. 407–439.

Road Log

65.2 Keep right at fork in road.

65.3 Beware of large and potentially damaging rock in road!

66.0 Junction with Forest Service sign “5S110D”. Turn right.

66.2 Base of hill and junction with road we came in on. Turn left. Road almost immediately curves to the west. Reverse entrance route and return to 395.

67.4 Highway 395. Turn right (NW). WATCH FOR HIGH-SPEED TRAFFIC IN YOUR LANE.

68.4 On your right is the most famous road cut in the eastern Sierra: the “Big Pumice Cut”. Excavation of this road cut in the 1950’s during the construction of ‘new Sherwin Grade’ clearly demonstrated that the Bishop Tuff was superposed on the Sherwin Till and not visa versa as Blackwelder had concluded (Sharp, 1968). During trips up and down Highway 395, Bob Sharp used to make his family take off their hats as they passed the Big Pumice Cut.

68.5 Cross Rock Creek. To the left (S) are Tahoe-age moraines of Rock Creek.

71.0 Entering Little Round Valley. This small valley is surrounded by cliffs and steep slopes of Bishop Tuff on all sides but the south. Bailey (1989) speculated that this unusual topography might be attributed to emplacement of the Bishop Tuff ignimbrite flow atop an active glacier, but after reexamination, Hildreth and Fierstein (2016b) have concluded that “abundant evidence compels rejection of this suggestion.” They instead attribute the valley topography to fluvial incision, mainly by Crooked Creek.

72.1 Crowley South Landing exit. Exit to right, then turn left (W) and proceed over the overpass and through the small community of Crowley Lake. BE ALERT FOR TRAFFIC, PEDESTRIANS, AND PETS.

72.9 Crowley Lake Drive. Turn right (NW). The bouldery moraines of Hilton Creek loom over the community on the west. The Hilton Creek fault runs parallel to the range front here.

74.7 Turnoff to Crowley Lake Campground. Turn left (W), watching for oncoming traffic.

74.8 Intersection with unpaved road paralleling power line. Turn right (N).

75.3 Park along road. Stop 2.3 will be on the hillside above the road.

Stop 2.3: History and draining of the paleo-Long Valley lake (Hildreth).

Stop 2.3: Paleoshorelines, the Draining of Pleistocene Long Valley Lake, and Proximal Exposures of the Bishop Tuff

Wes Hildreth and Judy Fierstein

US Geological Survey

(This passage is quoted from Hildreth and Fierstein, 2017, p. 43-45, with minor editing to make it consistent with this guidebook)

On both sides of the outlet arm of Lake Crowley, gently sloping smooth terraces contrast with the raggedly eroded Bishop Tuff (fig. 1). The terraces were wave-planed during the late middle Pleistocene highstand of the caldera lake (originally described by Mayo, 1934), and they are mantled by sheets of well-rounded beach gravels, both loose shingle and carbonate-cemented sandy-pebbly beachrock. A wave-cut shoreline scarp of Bishop Tuff stands as high as 50 m above the terrace and extends several kilometers north of the outlet arm. Highstand lake gravels are continuous for 13 km, as far as Wilfred Canyon at the foot of Glass Mountain, beyond which the shoreline features are obliterated by younger alluvial fans. Near Wilfred Canyon the continuous highstand shoreline is ~185 m higher in elevation than at the outlet arm, showing that the shoreline has been tectonically tilted ~0.8º S. since the lake drained soon after 150 ka (Hildreth and Fierstein, 2016). The southward tilting is toward the Round Valley Fault, which farther south trends north-south and has 2,000 m of steep range-front relief (fig. 2). Here, the fault wraps around to trend N.65º W., exhibits both normal and dextral displacement, and dips less steeply. Fig. 3 shows the shoreline deposits of Pleistocene Long Valley Lake.

To the right, a chain of ignimbrite knolls consists mostly of Bishop Tuff package Ig1E but is capped by thin remnants of Ig2E. Much of Ig2E shingled off downslope over the smooth, hot, gassy surface of Ig1E, thickening southward to as much as 115 m at Pleasant Valley. Stripping of nearly all of Ig2E and part of Ig1Eb from the proximal region suggests at least 50 m of erosive reduction of the primary ignimbrite surface on the caldera-facing slope. The chain of knolls also suggests an ignimbrite slope of ~2º NNE. toward the head of Owens River Gorge, opposing the southward slope of the tilted highstand north of the gorge. The slope suggested by the knolls could reflect primary run-up of the ignimbrite against the granitic range front or, alternatively or additionally, differential compaction of thicker ignimbrite that filled the precaldera drainage axis.

Figure 1. Photo of outlet arm of Lake Crowley reservoir. View northward from knoll 2224 at north rim of Little Round Valley. Outlet arm trends east toward dam at head of Owens River Gorge, along the very same channel that drained Long Valley's Pleistocene caldera lake ~150 ka. Raggedly eroded Bishop Tuff in right foreground contrasts with smooth wave-planed terraces that were submerged by the caldera lake on both sides of the outlet arm. White exposures beyond reservoir in Long Valley lowland are lake-silt deposits of the Pleistocene caldera lake, more than 700 m thick in the subsurface. At lower left, the lower end of the Crooked Creek tributary is drowned by the reservoir (as it also had been by the Pleistocene lake). Bald Mountain and Glass Mountain rise above the north-to- northeast wall of the caldera. From Hildreth and Fierstein (2017).

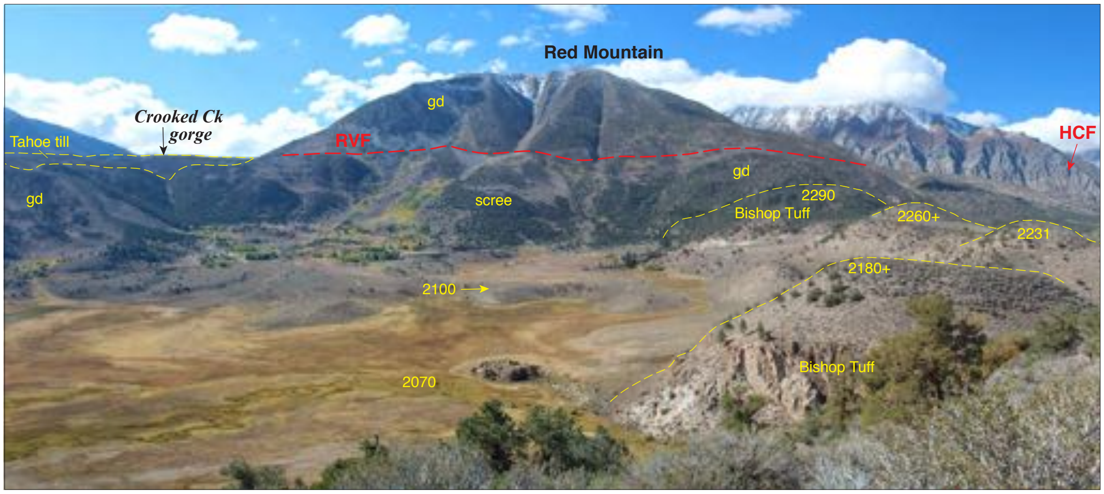

Figure 2. Little Round Valley viewed southward from crest of knoll 2224. Bishop Tuff fringes most of valley floor as low as 2,070m above sea level, but at right it also forms four eroded knolls (outlined) that rise southward from ~2,180 m to 2,290 m, showing that more than 200 m of ignimbrite was eroded away in excavating Little Round Valley. Removal of as much as 1 km3 of ignimbrite was accomplished principally by Crooked Creek, which cut a granodiorite gorge at upper left and was a major distributary of Rock Creek until its permanent blockage by a Tahoe moraine during Marine Isotope Stage 6. At its highstand (but not before), Pleistocene Long Valley Lake then shallowly inundated Little Round Valley, producing a wave-planed terrace at ~2,100 m, atop nonwelded Bishop Tuff, that has subsequently been veneered by alluvium and colluvium. Before and after the lake's highstand, Crooked Creek drained from Little Round Valley to Long Valley via a gorge just below lower right edge of the image. Red Mountain and valley wall at left consist of Triassic Wheeler Crest Granodiorite of Scheelite Intrusive Suite (labelled gd; Bateman, 1992). In upper-right distance, triangular facets on Paleozoic metasedimentary rocks mark the north-striking Hilton Creek (normal) Fault (HCF). Three major ravines that descend face of Red Mountain have together deposited an enormous apron of granodioritic scree, and all three have been displaced dextrally ~150 m by the oblique-slip Round Valley Fault (RVF). Little Round Valley was never glaciated. From Hildreth and Fierstein (2017); photo by Fierstein in October 2015.

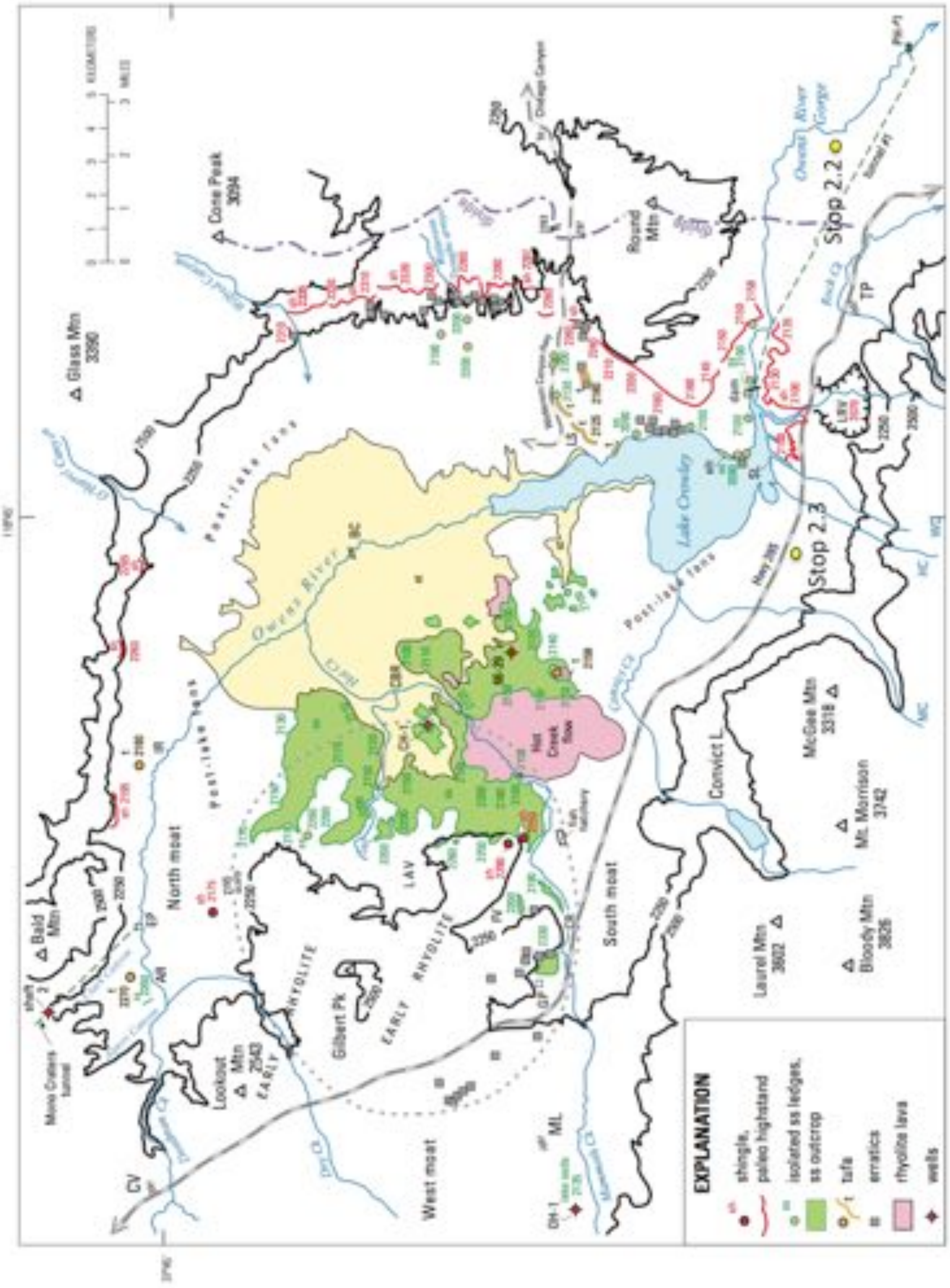

Figure 3. Map showing shoreline features and deposits of Pleistocene Long Valley Lake. Elevation 2,250 and 2,500 m contours indicate lower part of caldera wall, delimiting caldera floor. Area underlain by siltstone facies (st, central part of ancient lake), shown in yellowish tan, is actually exposed discontinuously, widely veneered by post-lake

alluvium. Shown in green is present-day outcrop of littoral facies (ss)—pebble conglomerate and sandstone. Both facies are in some places overlain by alluvial fans that have encroached from north, east, and southwest since draining of the lake. Lake Crowley reservoir, dammed in 1941, is unrelated to the Pleistocene lake but shares its outlet. Red line segments with elevations are mapped remnants of highstand shoreline (sh), mostly wave-rounded pebbles and shingle. Dotted circle 10 km in diameter encloses postcaldera resurgent uplift, which lifted intracaldera early rhyolites >400 m and mildly tilted sandstones deposited against its eastern slope; elevations (in meters above sea level) of sandstone contacts are indicated. Hot Creek flow is rhyolite coulee that flowed north into lake at 333 ka. Three smaller rhyolite lavas east of Hot Creek flow, all sediment-mantled, are likewise colored pink. Isolated patches of indurated sandstone (ss), loose shoreline gravel (sh), and tufa (t) are indicated by dots colored as in map explanation. Gray dots mark clusters of erratics (many larger than 1 m) ice-rafted across the Pleistocene lake from Sierran glaciers. Well OH-1 in town of Mammoth Lakes penetrated lake sediments at elevations 2,078–2,135 m above sea level. Wells CH–1 and 66–29, near center of diagram, penetrate ash-rich lake sediments 305 m and 700 m thick, respectively. Dash–dot gray line traces eastern drainage divide separating Long Valley from Owens Valley that was breached when Long Valley Lake overflowed its threshold and cut modern Owens River Gorge. Saddles 2293 and 2297 on the divide remained slightly higher than highstand of lake, which never overflowed eastward toward Chidago Canyon. Abbreviations: AR, Arcularius Ranch; BC, Benton Crossing bridge; CBR, Cashbaugh Ranch; CR, Chance Ranch; CV, Crestview; EP, East Portal of Mono Craters tunnel; FV, Fumarole Valley; GP, geothermal plant at site of former Casa Diablo Hot Springs; HC, Hilton Creek; IR, Inaja Ranch; LAV, Little Antelope Valley; LHC, Little Hot Creek; LRV, Little Round Valley; hachures outline bowl eroded in Bishop Tuff; LS, Layton Springs; MC, McGee Creek; ML, downtown Mammoth Lakes; PH-1, power house #1; SL, South Landing; TP, Toms Place; WC, Whisky Creek. For shaft 2, see figure 2. Tunnel #1 brings reservoir water to power house #1 of Los Angeles Department of Water and Power. From Hildreth and Fierstein (2017).

References

Hildreth W. and Fierstein J. (2016) Long Valley caldera lake and reincision of Owens River Gorge: U.S. Geological Survey Scientific Investigations Report 2016-5120, 63 pp.

Hildreth, W., and Fierstein, J. (2017) Geologic field-trip guide to Long Valley Caldera, California: USGS Scientific Investigations Report 2016-5022-Y, 119 p.

Mayo, E.B., 1934, The Pleistocene Long Valley Lake in eastern California: Science, v. 80, p. 95–96.

Road Log

75.3 Drive straight ahead on dirt power-line road.

75.6 Gregory Lane (paved). Turn right (E).

75.7 Crowley Lake Drive. Turn right (S), watching for oncoming traffic. Reverse course, heading back to the South Landing Road.

78.4 South Landing Road. Turn left (E), watching for oncoming traffic.

79.2 Highway 395. Go over the overpass and turn left (N) and merge carefully onto northbound traffic on 395.

81.8 Crossing McGee Creek. To the west are the moraines of McGee Creek. Relatively little work has been done on these moraines. Rinehart and Ross (1964) mapped the moraines closer to Highway 395 as pre-Tahoe and those closer to the mountain front as both Tahoe and Tioga. Berry (1994) mapped those closer to the highway as Tahoe and those inboard as Tioga. Given that Rinehart and Ross (1964) mapped the Convict Creek moraines in an analogous fashion and recent cosmogenic dating there has demonstrated that their combined Tioga/Tahoe moraines are entirely Tioga age (Stop 2.4), it seems likely that the mapping of Berry (1994) is correct.

The Tioga moraine at McGee Creek is prominently offset by the Hilton Creek fault at the canyon mouth. The maximum offset is about 26 m (Berry, 1997). The offset is only in the down-dip direction. Following the 25 May 1980 M6.0/6.3 'Mammoth' earthquakes, east-side-down ground rupture ranging from 10 to 25 cm was observed where the McGee Creek road crosses the Hilton Creek fault and elsewhere along the trace of the fault (McJunkin and Bedrossian, 1980). However, the main shock of this event and associated events was on a fault about 5 km to the west of the Hilton Creek fault and no aftershocks were recorded on the Hilton Creek fault, thus the surface rupture was most likely due to differential compaction in response to the vibrations.

Highway 395 parallels the Hilton Creek fault for the next two miles and the scarp can in many places easily be distinguished at the base of the McGee Mountain to the west. McGee Mountain is the type site for Blackwelder's McGee glaciation. The designation is based on a deposit of very large granitic boulders (up to 10 m length) atop Paleozoic slate on the top of the mountain. The closest source for the granite is at the headwaters of McGee Creek, 5.5 km south and separated from the boulder deposit by the deep canyon of McGee Creek. Presuming that the boulders are remnants of a till (which Blackwelder said is likely but not proven), the age of deposition must predate substantial movement on the Hilton Creek fault, probably several million years.

83.8 There is a small residential community to the west of 395. This is the northern limit of McGee Mountain, but the Hilton Creek fault extends into Long Valley to the north, with a glacial outwash plain forming a flat top to the riser formed by the scarp. There is a highway maintenance station on the right, and just past it on the west side of the highway is a small valley incised through the scarp. This was the outflow channel for meltwater from the Tahoe-age glacier of Convict Creek. Since the withdrawal of Tioga ice the channel has moved one mile to the north.

84.7 The gentle sagebrush-covered ridge to the left (S) is the left-lateral Tahoe moraine from Convict Creek. The hummocky mound to the north is the Rhyolite of Hot Creek flow, dated by Ar/Ar to 333±2 ka (Hildreth and Fierstein, 2016a). It is mantled by Long Valley lake deposits on its northern portion.

85.9 Convict Creek Road. Do you remember the historical incident from the road log for Day 1 in which two convicts who had escaped from the Territorial Prison at Carson City were hung in the Owens Valley near Bishop? Convict Lake was named for these same characters. On September 23, 1871 a posse from Benton, California, encountered some of a large gang of convicts who had escaped from the prison. A member of the posse who was a merchant in Benton, Robert Morrison, and a local Paiute Indian, Mono Jim, were killed in the gunfight and the convicts escaped. The precipitous mountain dominating the lake was named Mt. Morrison and a smaller one nearby Mono Jim Peak. The convicts continued traveling south, but a week later were surrounded near Bishop and hung.

87.3 Mammoth-Yosemite Airport/Fish Hatchery access road. Turn right.

87.8 Turnoff to Fish Hatchery to left, keep right.

89.1 Park alongside road. Stop 2.4.

Stop 2.4: Lava flows of the Long Valley caldera (Hildreth), Chronology of the Tioga moraines at Convict Creek (Putnam).

Stop 2.4: A Detailed Cosmogenic Chronology for Tioga Glacial Deposits at Convict Lake, Mono County, California

Aaron Putnam[1] and Ben Hatchett[2]

[1]University of Maine, Orono
[2]Desert Research Institute, University of Nevada, Reno

Identifying the climatic mechanisms for Late Quaternary glacial cycles remain a major objective of paleoclimatology. Establishing robust chronologies of mountain glaciation at many different latitudes in both hemispheres can aid discrimination among different hypotheses for Quaternary ice-age climate dynamics. In addition, accurate glacier reconstructions, together with glaciological and hydrological modeling, can help to improve our understanding of the sensitivity of mountain snow and ice in dryland regions to the effects of atmospheric warming, and consequent impacts on regional water availability (Birkel et al., 2012; Broecker and Putnam, 2013; Hatchett et al., 2015; Putnam, 2015; Barth et al., 2016; Hatchett et al., 2016; Putnam and Broecker, 2017). This is particularly important for communities dependent upon snowmelt for consumptive use in the Sierra Nevada watershed (Stine, 1994) and in many other midlatitude regions worldwide ().

Glaciers of the Sierra Nevada monitored regional climate during the peak of the last ice age and its subsequent termination (Phillips et al., 2009; Rood et al., 2010; Phillips, 2016; Phillips et al., 2016). Multiple Pleistocene glacial advances carved deep troughs and constructed prominent moraines on the Sierran forelands. These glacial 'footprints' constitute a spectacular archive of past climate imprinted on the landscape, and are suitable targets for geomorphologic mapping, snowline reconstruction, and surface-exposure dating techniques. The generation of accurate and precise glacial chronologies provide targets for numerical modeling efforts aimed at constraining past climate conditions (e.g., Birkel et al., 2012; Barth et al., 2016). When constraints developed independently from separate systems, such as terminal lakes and alpine glaciers, are in agreement (e.g., Barth et al. 2016; Figure 1), increased confidence is afforded to paleoclimate reconstructions.

Convict Lake - Sierra Nevada, California, USA. Convict Lake is a moraine-dammed lake at the foot of the eastern Sierra Nevada in east-central California (Figure 2). The lake is about three kilometers southwest of U.S. Highway 395. Convict Lake is set within the north-south-trending Convict Canyon and lies beneath the faulted metasedimentary complexes forming Laurel Mountain and Mt. Morrison. The lake is impounded by a complex of exceptionally well-preserved moraine ridges that were constructed by the north-flowing Convict glacier at the peak of the last ice age. Studies by Kesseli (1941), Putnam (1962), Rhinehart and Ross (1964), and Sharp (1969) attempted to map and subdivide the Convict Lake moraine sequence into different glacial stages. Sharp (1969) summarized the discussion nicely. To the east of Convict Lake are a series of right-lateral moraine ridges deposited by a distributary lobe of the Convict glacier. The most extensive of these lateral ridges have been attributed to the penultimate glacial period (i.e., 'Tahoe' stage; MIS 6), and the innermost lobate moraines of this complex at Tobacco Flat (Figure 2) have been assigned to the last glacial maximum (i.e., 'Tioga' stage; MIS 2; Sharp, 1969). North of Convict Lake is a belt of at least 19 exceptionally well-preserved terminal moraine ridges. There have been at least three different interpretations of how many glaciations the Convict Lake terminal moraine sequence represents. Rhinehart and Ross (1964) suggested that the moraine sequence comprises moraines constructed over the course of three separate glaciations. Putnam (1962) subdivided the sequence into two glacial stages. Sharp (1969) concluded that the terminal moraine belt was constructed during the Tioga glacial stage.

In 2010, Putnam mounted a field campaign aimed developing a glacial geomorphologic map and ^{10}Be surface-exposure chronology of the Convict Lake terminal moraine sequence. The results of this effort are shown in Figure 3. ^{10}Be ages were determined primarily from granodiorite boulders either rooted in or resting in stable positions on moraine ridge crests. As also observed by Sharp (1969), many of the boulders retain glacial polish, implying minimal erosion and spalling of boulder surfaces. Samples were processed at the Lamont-Doherty Earth Observatory Cosmogenic Nuclide Laboratory and analyzed at the Lawrence-Livermore National Laboratory Center for Accelerator Mass Spectrometry. Ages were calculated using a sea-level/high-latitude ^{10}Be (neutron spallation) production rate of 3.84 at g^{-1} yr^{-1} together with the time-dependent 'Lm' scaling protocol (using a modified version of the UW online calculator and version 2.2 of the wrapper script). We chose this calculation scheme because it (1) reconciles ^{10}Be surface-exposure ages and minimum-limiting ^{14}C dates from the Baboon Lakes region (Phillips et al., 2016; Putnam et al., in prep) and (2) is compatible with several precise SLHL production-rate values determined from well-dated geological calibration sites (i.e., where independent radiometric dates directly constrain the target landform).

Although the primary aim was to permit broad-scale comparisons among glacial reconstructions from both hemispheres, an important outcome of the study was that the ^{10}Be chronology supports the conclusion of Sharp (1969). The oldest moraine ridges of the terminal 'lobate' complex are ~26 kyrs old. These outermost moraine-ridge fragments project outboard from overlying composite ~22-kyr old terminal moraine complex. Surface-exposure ages from the youngest ridges, including the bouldery ice-contact slope that dams Convict Lake, afford ages averaging ~16 kyrs old. These ~16-kyr old moraine ridges mark the innermost constructional landforms of the Convict Lake terminal moraine complex. Landforms inboard of the terminal moraine complex indicate unhalted glacier recession well into the mountains (i.e., toward the 'Recess Peak' type moraines, which represent a snowline only moderately lower than the Little Ice Age). The Convict Lake trough, ice-molded bedrock, and the general lack of constructional ice-marginal landforms are examples of this major recession that commenced beginning with the exposure of the 16-kyr ice-contact slope at the north end of Convict Lake.

We have conducted preliminary glaciological modeling experiments of the Convict Lake system following the approach of Birkel et al. (2012). The purpose is twofold. First, we hope to determine the climatic conditions that favored the full-glacial LGM extent of the Convict glacier. Second, in collaboration with Doug Boyle and his team at University of Nevada, Reno, we hope to combine the information gleaned from the Convict Lake glaciological model, targeting dated LGM moraine ridges, with paleo-hydrological modeling results for Mono Lake, targeting LGM lake shorelines dated by Xianfeng Wang (Earth Observatory of Singapore) and Guleed Ali (Columbia University). This effort will derive unique solutions for temperature and precipitation during specific periods of coeval moraine building and shoreline construction. This is a work in progress. However, a preliminary visualization of the Convict Lake model is shown in Figure 4. Early results indicate that construction of the ~16-kyr moraine ridges and ~16-kyr Mono Lake shorelines occurred under a climate ~7.5°C colder than today and precipitation amounts double that of today. These values are consistent with estimates derived for the LGM ice extent in the Wind River Range, Wyoming, by Birkel et al. (2012) and the ~16-kyr highstand of Jakes Lake, Nevada, by Barth et al. (2016). We are currently working on obtaining solutions for each pair of dated moraines and shorelines going back to ~22 kyrs ago.

Stop 1. Convict Lake/Canyon, ~16-kyr old ice-contact slope, stratigraphic section.

Follow Convict Lake Rd. from U.S. Highway 395 across the LGM outwash fan toward the terminal moraine belt. The road winds through a meltwater channel formed during the latter stages of moraine development in the terminal moraine complex. Take the road to Convict Lake and park in the lot to the northwest. There are three points of interest here:

1) A view toward the southwest reveals Convict Lake, set within Convict Canyon. Toward the head of the lake are some large ice-molded bedrock hills mantled with a thin veneer of glacial erratic boulders. The lake trough, ice-molded bedrock terrain, and moraine-free topography indicate unhalted ice-recession to deep within the mountains following the construction of the innermost terminal moraines.
2) At the northernmost end of the parking area there is an anastomosing mule trail that will take you into the bouldery terrain of the ice-contact slope that marks the onset of deglaciation at 16-kyr ago. Note the contrast between the large granodiorite boulders on the moraine and the metasedimentary hornfels that constitute the local bedrock cliffs.
3) The northern perimeter of the parking area features an exposure into the ice-contact slope of the innermost ~16-kyr moraine ridge. Note that the moraine is cored with contorted silt and sand. The sequence is capped by a thin diamicton containing large boulders. We interpret this section to indicate that the final advance of Convict Glacier was through a shallow glaciolacustrine environment. The bouldery till armors the very uppermost portion of the morainal stratigraphy. Moraine degradation models typically rely on the assumption that glacial boulders are distributed randomly throughout a moraine matrix, and that they ‘pop out’ as the moraine deflates. The moraine stratigraphy near the mouth of Convict Lake suggests that this underlying assumption may not always be correct.

Stop 2. 22-kyr moraine ridge (Near point 2 in Figure 2).

Points of Interest:

1) Looking north from this point affords views of the well-preserved lateral Tahoe (MIS6; penultimate glacial maximum) and Tioga (MIS2; LGM) moraines.
2) Walking along the moraine ridge crest will allow us to find and examine several boulders deposited during peak LGM conditions resting along the ice contact slope or embedded in the moraine crest. Samples from several of these boulders correspond to surface-exposure ages plotted in Figure 3.

Stop 3. Drive to northern base of outermost moraine and hike up to lookout

Points of Interest:

1) This outermost LGM/Tioga moraine ridge is offset by a well-preserved fault scarp that traces along the mountain front very close to the lookout landing (point F in Figure 2).
2) This vantage provides a clear view of the lower recessional moraine ridge sequences that lie inboard of the terminal 22-kyr moraine ridge (Figures 3 and 4). These moraines record millennial pulses of a healthy Convict Lake glacial system, prior to the rapid recession that led to the abandonment of the innermost ice-contact slope visited on Stop 1. Figure 4 provides an example of how one of these inner moraine ridges can be used as a target for alpine ice glacier modeling following the methods of Birkel et al. (2012). These model results will be compared against results of an independent hydrologic model seeking to replicate conditions allowing the formation of nearby closed-basin lakes (Figure 1; Barth et al. 2016).
3) Having examined a variety of well-preserved geomorphic indicators of past glaciation, we will pause for a discussion about climate mechanisms driving the abrupt nature of glacial terminations, how these climate changes are recorded in various landscapes, and the physical processes producing the changes.

Stop 4. Beers and continued discussion at Convict Lake Resort

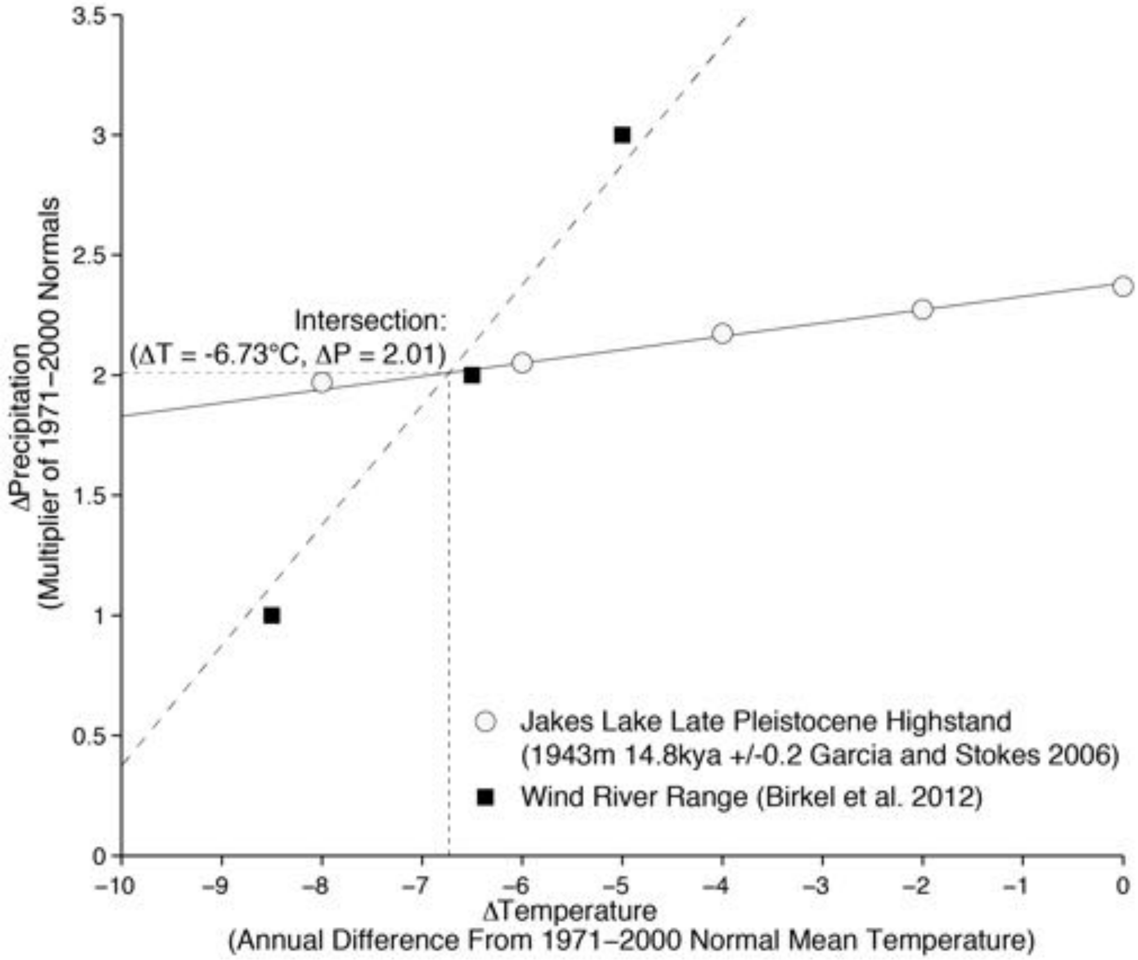

Figure 1. Changes in annual temperature and precipitation relative to 1971-2000 normals required to simulate Late Pleistocene conditions at a pluvial lake in Jakes Valley, Nevada (white circles) and the LGM ice extent in the Wind River Range of Wyoming (black squares) using a semi-distributed hydrologic model and alpine ice sheet model, respectively. The intersection of the lines provides an estimate of the mean climate conditions during the Late Pleistocene. Figure from Barth et al. 2016.

Figure 2. Vertical air photo of Convict Lake and nearby moraine ridges, Sierra Nevada, California, U.S.A. Numbers correspond to individual constructional moraine ridges identified and studied by Sharp (1969). Sharp analyzed surface-boulder frequency and weathering characteristics, grain-size relationships, and soil pH and color properties to infer relative ages of the Convict Lake moraines. CCL = Convict Creel Lateral. CL = Convict lateral. F = fault. OLL = "old looking" laterals; TFL = Tobacco Flat laterals. Reproduced from Plate 2 of Sharp (1969).

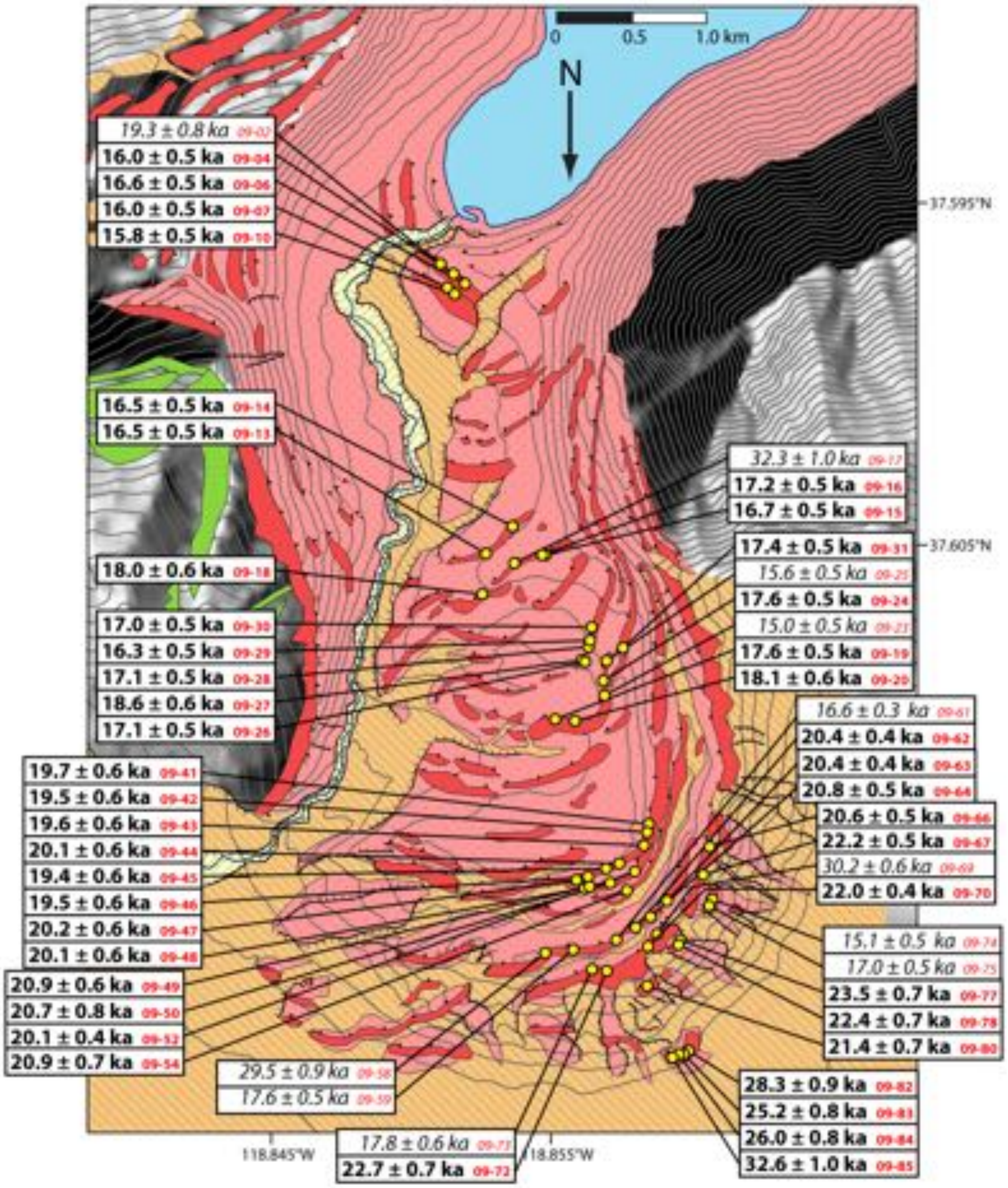

Figure 3. Preliminary glacial geomorphologic map of the Convict Lake region, Sierra Nevada, California, U.S.A. Red units are moraines deposited during the LGM, green units are moraines deposited earlier than the LGM, and tan represents outwash (note that not all 'Tahoe'-ages landforms have yet been mapped). Ages are in white boxes, and yellow dots give sample locations. Ages are calculated using a sea-level/high-latitude ^{10}Be production rate of 3.74 at g^{-1} yr^{-1} and the Lm scaling. We chose this rate because it produces ^{10}Be ages compatible with independent ^{14}C dating in the Baboon Lakes region of the Sierra, and is consistent with production rates developed from other well-dated calibration sites throughout the world.

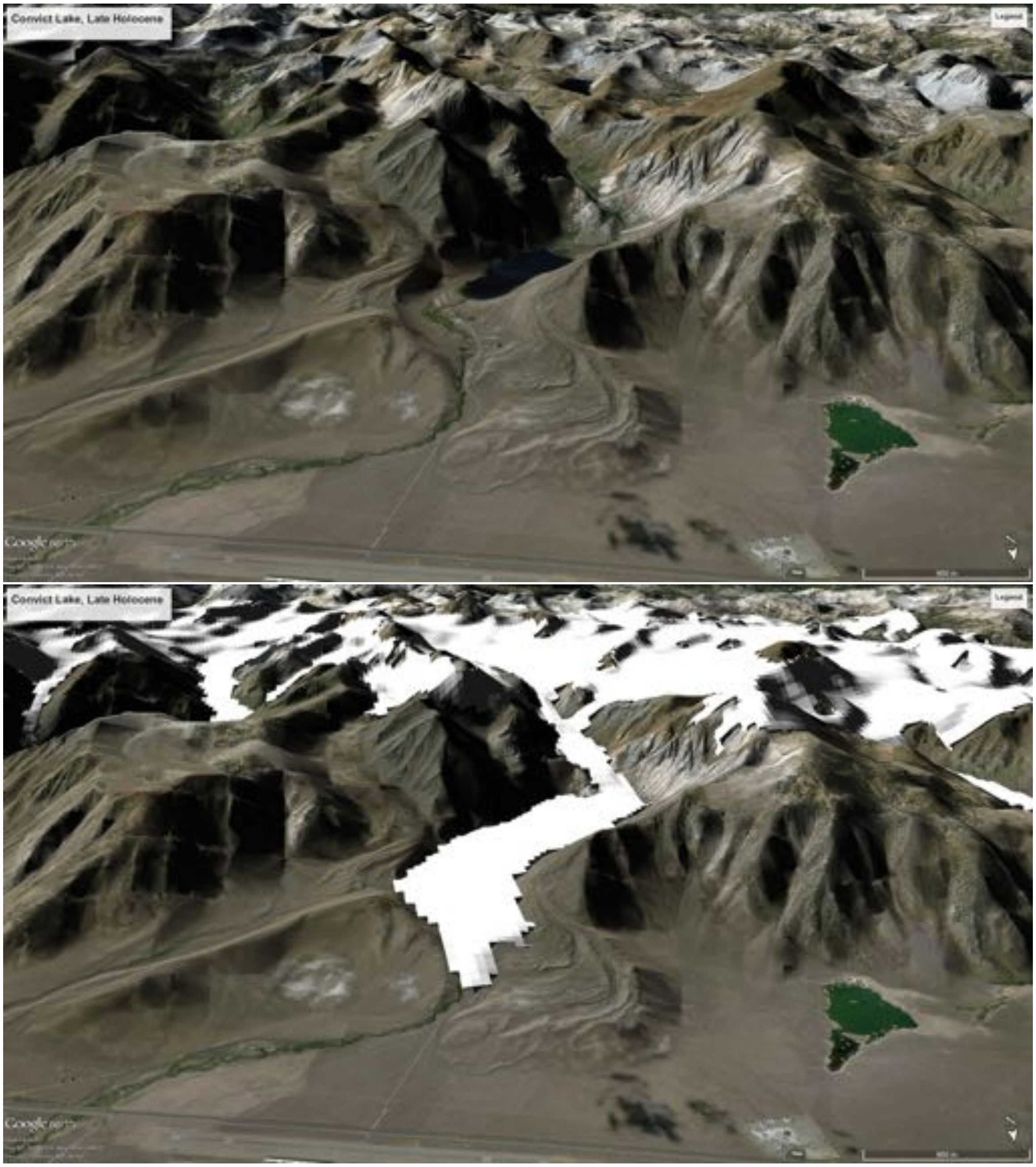

Figure 4. Top: Oblique view to the south of Convict Canyon and Sierran crest. **Bottom:** The same view superimposed with output from a glaciological model of the Convict Creek glacier extending to moraine ridges constructed ~16 kyrs ago. This glacier configuration was achieved under conditions 7.5 °C cooler than today, and precipitation 200% higher than today. This particular ΔT and ΔP combination achieves the best fit with preliminary results from hydrological modeling of the coeval 16-kyr highstand of Mono Lake. Preliminary modeling results for the full glacial configuration (not shown) indicate that conditions were likely ~9°C colder than today, with precipitation levels similar to those of today, at about 22-kyrs ago. We employed the University of Maine Ice Sheet Model (UMISM), following the approach of Birkel et al. (2012), to develop these reconstructions.

References

Barth, C., Boyle, D.P., Hatchett, B.J., Bassett, S.D., Garner, C.B. and Adams, K.D., 2016. Late Pleistocene climate inferences from a water balance model of Jakes Valley, Nevada (USA). Journal of Paleolimnology 56(2), 109-122.

Birkel, S.D., Putnam, A.E., Denton, G.H., Koons, P.O., Fastook, J.L., Putnam, D.E. and Maasch, K.A., 2012. Climate Inferences from a Glaciological Reconstruction of the Late Pleistocene Wind River Ice Cap, Wind River Range, Wyoming. Arctic, Antarctic, and Alpine Research 44(3), 265-276.

Broecker, W.S. and Putnam, A.E., 2013. Hydrologic impacts of past shifts of Earth's thermal equator offer insight into those to be produced by fossil fuel CO2. Proceedings of the National Academy of Sciences 110(42), 16710-16715.

Hatchett, B.J., Boyle, D.P., Garner, C.B., Kaplan, M.L., Putnam, A.E. and Bassett, S.D., 2016. Magnitude and frequency of wet years under a megadrought climate in the western Great Basin, USA. Quaternary Science Reviews 152, 197-202.

Hatchett, B.J., Boyle, D.P., Putnam, A.E. and Bassett, S.D., 2015. Placing the 2012-2015 California-Nevada drought into a paleoclimatic context: Insights from Walker Lake, California-Nevada, USA. Geophysical Research Letters 42, doi:10.1002/2015GL065841.

Kesseli, J.E., 1941. Studies in the Pleistocene glaciation of the Sierra Nevada, California. University of California Publications in Geography, 6, 315-362.

Phillips, F.M., 2016. Cosmogenic nuclide data sets from the Sierra Nevada, California, for assessment of nuclide production models: I. Late Pleistocene glacial chronology. Quaternary Geochronology 35, 119-129.

Phillips, F.M., Hinz, M., Marrero, S.M. and Nishiizumi, K., 2016. Cosmogenic nuclide data sets from the Sierra Nevada, California, for assessment of nuclide production models: II. Sample sites and evaluation. Quaternary Geochronology 35, 101-118.

Phillips, F.M., Zreda, M., Plummer, M.A., Elmore, D. and Clark, D.H., 2009. Glacial geology and chronology of Bishop Creek and vicinity, eastern Sierra Nevada, California. Geological Society of America Bulletin 121(7/8), 1013-1033.

Putnam, W.C., 1962. Late Cenozoic geology of McGee Mountain, Mono County, California. University of California Publications in Geological Sciences, 40, 181-218.

Putnam, A.E., 2015. A glacial zephyr. Nature Geoscience 8, 175-176.

Putnam, A.E. and Broecker, W.S., 2017. Human-induced changes in the distribution of rainfall. Science Advances 3(5).

Rinehart, C.D., and Ross, D.C., 1964. Geology and mineral resources of the Mount Morrison quadrangle, Sierra Nevada, California. U.S. Geological Survey Professional Paper 385, 106 p.

Rood, D.H., Burbank, D.W. and Finkel, R.C., 2010. Chronology of glaciations in the Sierra Nevada, California, from ^{10}Be surface-exposure dating. Quaternary Science Reviews 30(5-6), 646-661.

Sharp, R.P., 1969. Semiquantitative Differentiation of Glacial Moraines near Convict Lake, Sierra Nevada, California. The Journal of Geology 77(1), 68-91.

Stine, S., 1994. Extreme and Persistent Drought in California and Patagonia During Medieval Time. Nature 369(6481), 546-549.

94.6   This is the end of Day 2. You can exit this stop by driving almost due south on the road that heads toward the Mammoth-Yosemite Airport, then turning right (NW) on the airport access road and returning to Highway 395. The Convict Creek exit is 1.4 miles south on 395, if you wish to view the moraines close up.

Day 3

Cedar Flat to Tinemaha Creek: Nature and Kinematics of Contemporary Faulting in the Central Owens Valley

The field trip will depart from Cedar Flat Group Camp at 8:00 AM, Monday, October 9.

NOTE: This day's trip requires high-clearance vehicles! If you are driving a standard passenger car, car-pool with someone in a 4WD or high-clearance 2WD.

Summary: The portion of the Owens Valley immediately north of Big Pine constitutes an accommodation zone for the Owens Valley rift. South of Big Pine the Inyo Mountain fault is largely inactive. Transtensional displacement is partitioned between dextral strike slip on the Owens Valley fault and vertical displacement on the Sierra Nevada frontal fault. But the Owens Valley fault dies out just north of Big Pine and the locus of normal faulting shifts to the east side of the valley. North of Black Canyon it is taken up by oblique slip on the White Mountain fault. North of the Coyote Warp, dip slip on the Round Valley fault also comes into play. But between Big Pine and Black Canyon there are no obvious structures to accommodate NE-directed transtension.

Today's questions focus on the mechanics in and near this zone. What kind of structures take up the regional strain? How is the switch in normal-faulting polarity accomplished? Can we resolve the strain budget across the valley?

Mileage   **Description**

0.0   Start point is the intersection of the exit road from the Cedar Flats Group Campground to state highway 168, the Westgard Pass road. Set your odometer as you reach the intersection, and turn right (west). Our route follows that of Day 1 down to the Big Pine/Death Valley Road intersection. Remember to give way to uphill traffic on the one-lane road through The Narrows.

10.3   Big Pine/Death Valley Road intersection. Continue straight ahead (W) toward Big Pine.

12.5   Highway 395. Go straight across the highway, WATCHING FOR TRAFFIC FROM BOTH DIRECTIONS. Continue westward on County Road.

13.5   Baker Creek Campground Road. Turn left (S).

13.7 Baker Creek Campground main entrance. Continue southward. The rocky hillside to the northwest is the westernmost tip of Warren Bench, our first destination today. It is comprised of three small fault blocks bounded on the east by the northern tip of the Owens Valley fault that have been rotated clockwise from a presumably original north-south orientation in the shear between the fault and the Sierra Nevada to the west.

13.9 Road makes a right-angle turn to the west.

14.3 Unmarked road junction, turn left (S). For the next 0.3 miles the road first approaches, then parallels on the west side the scarp of a mountain-down fault. It is one of many that cut this alluvial fan.

14.9 Glacier Lodge Road. Turn right (W), WATCHING FOR TRAFFIC FROM THE RIGHT.

15.3 Sugerloaf Road. Turn right. (N)

15.9 Arc Road 'Y' junction. Keep right.

16.4 Road goes over or past three mountain-down scarps. The road ahead goes over boulders and should not be attempted by low-clearance vehicles.

17.2 Park on loop road. Stop 3.1.

Stop 3.1: Antithetic (mountain-down) faulting of Warren Bench and the Big Pine accommodation zone (Phillips).

Stop 3.1: The Coyote warp – why did it warp?

Fred M. Phillips

Earth & Environmental Science Department, New Mexico Tech, Socorro NM 87801

Introduction

The Coyote warp is a structurally anomalous interval along the eastern margin of the Sierra Nevada, facing the Owens Valley. The interval is anomalous because for the entire rest of the Owens Valley, stretching from Owens Lake in the south to the northern end of Wheeler Crest in the north, the physiography of the mountain face is clearly defined by one or more large-displacement normal faults, producing a very steep and relatively planar mountain face (Stevens et al., 2013). In contrast, in the section between Big Pine and Bishop there is no obvious large-displacement valley-down normal fault and the topographic transition from mountain crest to valley floor is accomplished by a relatively gradual downward arching. Bateman (1965) stated: "The Coyote warp has little in common either physiographically or structurally with the precipitous fault scarp that is ordinarily envisaged." Although numerous geologists have commented on this pronounced difference, there has been no clear explanation for the reason that displacement should differ here from elsewhere along the range front, and for the mechanism of deformation.

Knopf (1918) noted the physiographic contrast. He attributed the difference to distributed valley-down faulting of the Coyote warp, contrasted to offset on a single major fault to the south and north. Taylor (1933) commented extensively on the Coyote warp, which he termed the "Bishop offset". In a prescient insight he correctly interpreted the ramp descending the north face of Coyote Ridge to the Tungsten Hills as a relay ramp, which he referred to as a "scarpramp". However, like Knopf (1918) he misinterpreted most of the faults along the eastern base of the Coyote warp as valley-down normal faults rather than mountain-down normal faults. He therefore incorrectly inferred that the physiographic difference between the Warp and the rest of the Sierra front was mainly attributable to an older age of faulting rather than to a fundamental structural difference.

The definitive field work on the Coyote warp was performed by Paul Bateman (1965), who mapped the area with great care and who named it the 'Coyote warp'. He corrected Taylor's error (although without citing him) and pointed out that nearly all of the faults on the east side of the warp were mountain down. He identified the graben that forms Coyote Flat. However, the closest he came to explaining the cause of the warping was to write: "Similar relations between faults and warps or broad folds very likely exist elsewhere in the Great Basin, and mapping of the warps should lead to a better understanding of the nature of Basin and Range structure than we now have."

Jayko (2009) and Phillips and Majkowski (2011) both treated the Coyote warp very briefly in their regional-scale studies. Both asserted that the Coyote warp was the surface expression of an anticlinal rollover in the hanging wall of the White Mountain fault zone, but offered very limited evidence to support this hypothesis. The objective of this short paper is to provide some basic information on the deformation of the Coyote warp and a simple model to support a mechanical explanation for its features.

Features of the Coyote warp

One important aspect of the setting of the Coyote warp is that it is located in an accommodation zone. South of the Big Pine, vertical tectonic displacement is focused on the Tinemaha fault at the base of the Sierra Nevada front. North of Big Pine it is focused on the White Mountain fault zone, on the east side of the Owens Valley. As noted originally by Taylor (1933), the tips of the two faults fan out into a zone of overlapping distributed deformation on both sides of the Valley. North of Bishop Creek, displacement resumes on the west side of the Valley on the Round Valley fault, but between Big Pine and the northern end of the Coyote Warp the regional transtension is taken up largely by the White Mountain fault zone, the only place in the Owens Valley that this is the case.

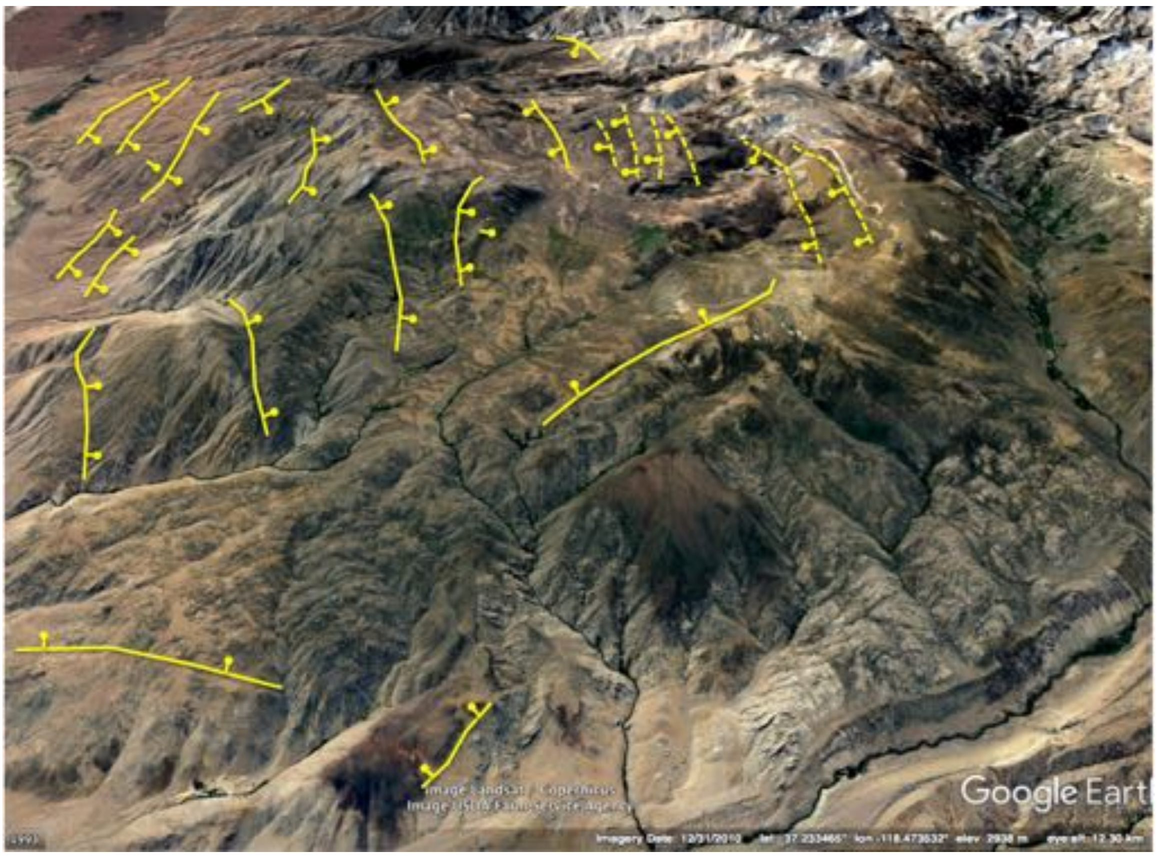

Figure 1. Overview of the Coyote warp, from the north. Bishop Creek is in the right foreground, Big Pine in the upper left corner. Fault mapping is from Bateman (1965). All mapped faults are not shown. North-south-oriented faults are strongly foreshortened by the perspective.

Fig. 1 illustrates the distribution of faults across the Coyote warp. The main features to note are the large number of mountain-down faults on the eastern side of the warp and the shallow graben forming Coyote Flat, in the middle of the image. Interestingly, the faults on the west side of the graben are valley down. These features have been commonly observed in marine seismic-reflection profiles taken for petroleum prospecting. A typical example is shown in Fig. 2, from Ren et al. (2014). Note the numerous high-side-down faults above the label ‘Lingshui Sag’ in the center of the interpretation and the graben structure (opposing dips on either side) above label ‘Lingnan High’. These are shown as being in the hanging wall of a major listric fault.

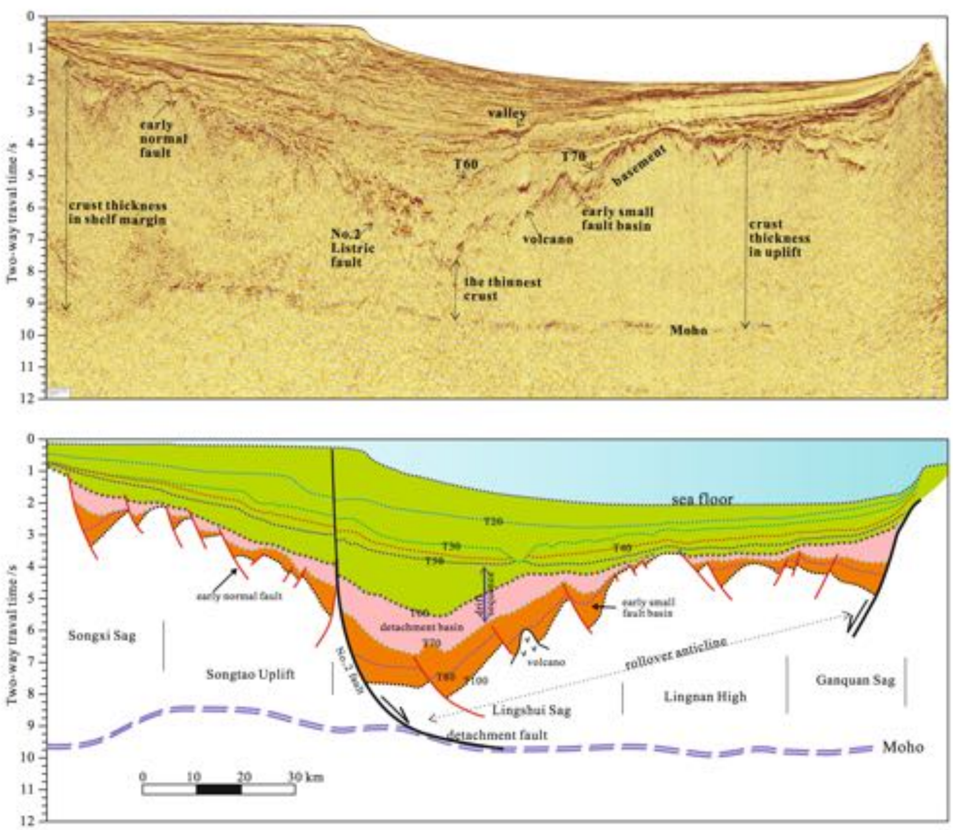

Fig.3. Structure-stratigraphic framework interpretation section across the eastern Lingshui sag in the Qiongdongnan Basin (profile position see as Fig. 1).

Figure 2. Seismic reflection profile and interpretation from the Qiongdongnan Basin of South China Sea. Figure is reproduced from Ren et al. (2014).

Similar structures are also observed in the Great Basin. Fig. 3 shows a structural interpretation of faulting observed in the Highland Range, south of Las Vegas, Nevada. Like the Coyote warp, the Highland Range is in an accommodation zone, as can be seen from the illustration. Like the South China Sea interpretation, the high-side-down faults are in the hanging wall of a listric fault. The formation of the crestal graben shown in Fig. 3 is a geometric result of the rotation of the blocks close to the outcrop of the listric fault, as the hanging wall slides down the curved surface.

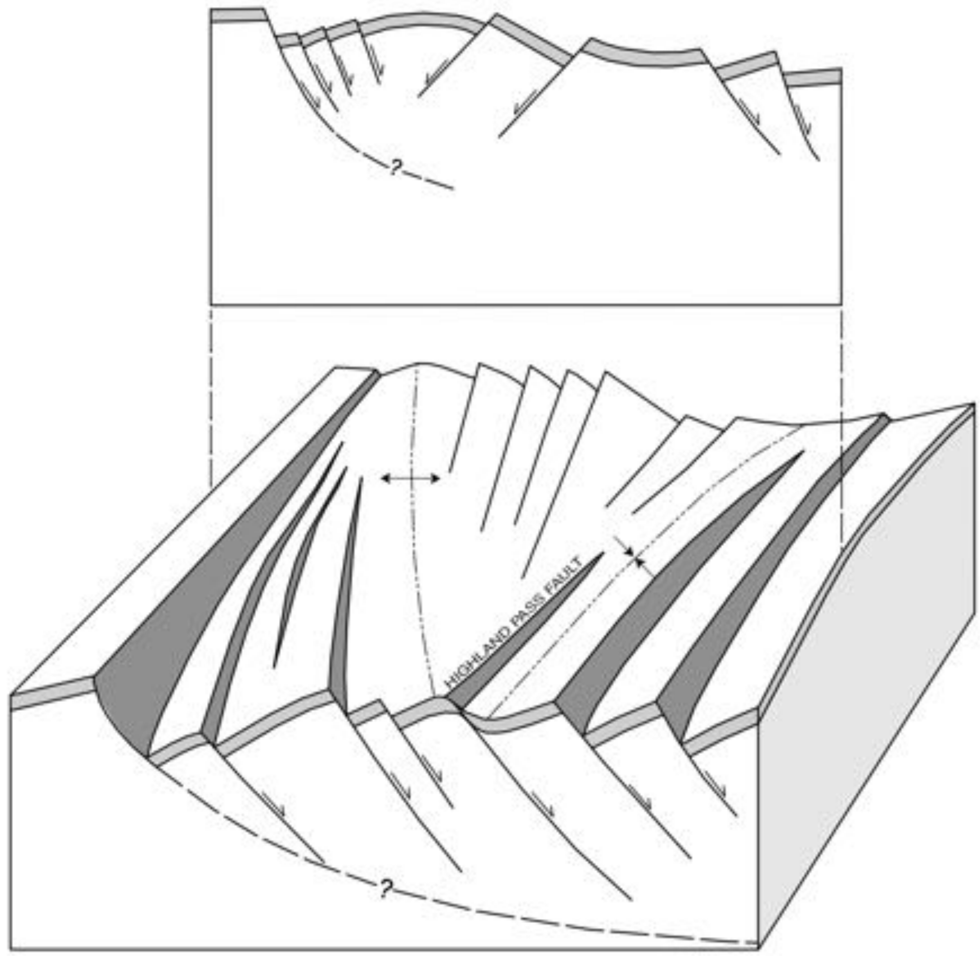

Figure 3. Block diagram illustrating faulting in the Highland Range south of Las Vegas, from Faulds et al. (2002). Note in the upper panel the mountain-down faults on the left side and the crestal graben in the anticline to the right of the listric fault.

Structural model of the Coyote warp

I propose that the main features of the Coyote warp (arched surface down toward the White Mountain fault, predominant mountain-down faulting, and formation of a graben on the top of the arch) are explained by the warp constituting the hanging wall block of a listric fault (the White Mountain fault). In Fig. 4 I construct a simple model of the White Mountain fault and deformation during displacement of the hanging wall.

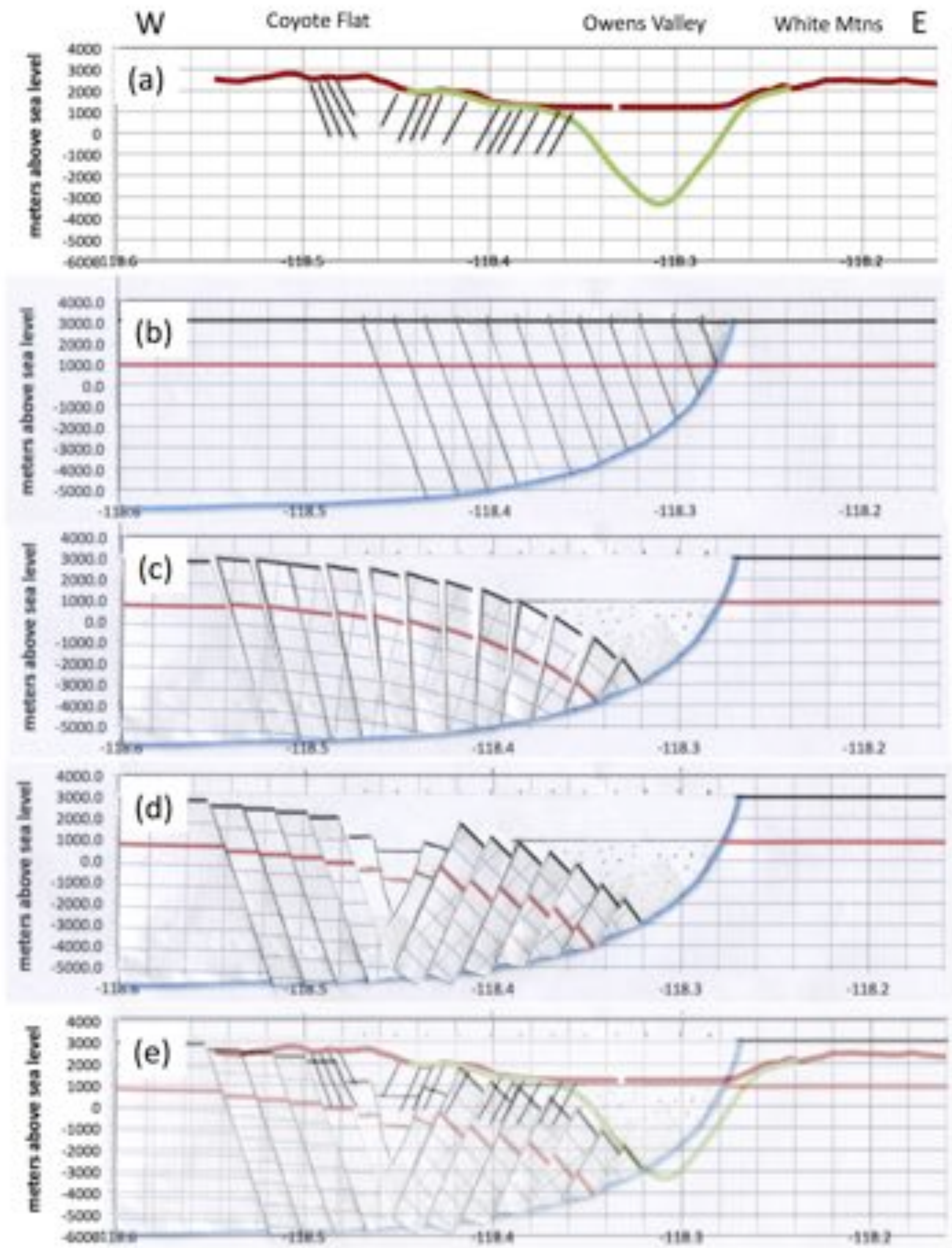

Figure 4. Geometric cross-sectional model for the formation of the Coyote warp. (a) Topographic profile along latitude 37.30°, basin depth from gravity inversion by Saltus and Jachens (1995), and faults from Bateman (1965). (b) Hypothesized listric fault and internal faults in the hanging wall. Red line is for reference only. (c) Deformation resulting from translating hanging wall. Note wedge-shaped spaces between fault blocks. (d) Additional deformation from block rotation to fill spaces. (e) Fig. 4(a) superposed on 4(d).

Fig. 4(a) illustrates cross-sectional data across the Owens Valley at the Coyote Warp. The location of the graben on the summit of the Coyote Plateau is clear from the faulting data. Fig. 4(b) represents the White Mountain fault as a very simple listric fault. In Fig. 4(c) the hanging wall has been displaced 14 km west on the White Mountain fault, measured from the crest of the White Mountains westward to the position of the maximum basin depth from the gravity inversion. This is very close to the 13.7 km of displacement calculated using the contemporary geodetic east-west velocity differential between the Westgard GPS station and the Sierra Nevada block (3.7 mm/yr to the west) and a time interval of 3.7 Ma since initiation of active transtension (Stockli et al., 2003; Lee et al., 2009; Phillips et al., 2011). The internal fault blocks have been rotated to keep their bases parallel to the angle of the detachment fault. Since arching of the top of the anticlinal rollover is necessarily extensional, this has resulted in wedge-shaped gaps between the blocks. In Fig. 4(d) the fault blocks have been tilted to close the gaps. In Fig. 4(e) the geologic data from Fig. 4(a) have been superposed on the structural diagram in Fig. 4(d).

Discussion and Conclusions

Fig. 4(e) shows that the modeled topography and faulting compare favorably with the field data. The position of the topographic surface and the gravity-derived basement/alluvial-fill contact is similar to that produced by the model, with the exception of the area under the crestal graben, which is much deeper in the model than the data would indicate. This may be because the rigid-block model precludes internal deformation of the blocks, which would tend to redistribute mass so as to minimize the graben depth. The model does reasonably well reproduce the location of the graben and the dips of the faults surrounding it. In particular, it produces valley-down faults on the east side of the graben and mountain-down ones on the west, just as is observed on Coyote Flat.

The success of this very simplistic model in reproducing a number of the key features of the Coyote warp indicates that anticlinal rollover on a very large listric detachment fault is a plausible explanation for the formation of the warp. The conceptual model is attractive in that a single, simple scenario can explain most of the salient features of the warp, including several that are otherwise rather anomalous.

References

Bateman P. C. (1965) Geology and tungsten mineralization of the Bishop District, California: U.S. Geological Survey Professional Paper 470, Professional Paper 470, 208 p. pp.

Faulds J. E., Olson E. L., Harlan S. S., and McIntosh W. C. (2002) Miocene extension and fault-related folding in the Highland Range, southern Nevada: a three-dimensional perspective: *Journal of Structural Geology* **24**(4) 861-886.

Jayko A. S. (2009) Deformation of the late Miocene to Pliocene Inyo Surface, eastern Sierra region, California, In *Late Cenozoic Stucture and Evolution of the Great Basin-Sierra Nevada Transition* (J. S. Oldow and P. H. Cashman; eds.),

Geological Society of America Special Paper 447, Boulder, Colorado, pp. 313-350.
Knopf A. (1918) A geologic reconnaissance of the Inyo Range and the eastern slope of the Sierra Nevada, California, with a section on the stratigraphy of the Inyo Range by Edwin Kirk: U. S. Geological Survey Professional Paper 110, 130 pp.
Lee J., Stockli D. F., Owen L. A., Finkel R. C., and Kislitsyn R. (2009) Exhumation of the Inyo Mountains, California: Implications for the timing of extension along the western boundary of the Basin and Range Province and distribution of dextral fault slip rates across the eastern California shear zone: *Tectonics* **28** TC1001, doi:10.1029/2008TC002295.
Phillips F. M. and Majkowski L. (2011) The role of low-angle normal faulting in active tectonics of the northern Owens Valley, California: *Lithosphere* **3**(1) 22-36.
Phillips F. M., McIntosh W. C., and Dunbar N. W. (2011) The chronology of late Cenozoic volcanic eruptions on relict surfaces in the south-central Sierra Nevada, California: *Geological Society of America Bulletin* **123** 890-910.
Ren J., Zhang D., Tong D., Huang A., Wang Y., Lei C., Zuo Q., Zhao Y., He W., and Yang L. (2014) Characterising the nature, evolution and origin of detachment fault in central depression belt, Qiongdongnan Basin of South China Sea: evidence from seismic reflection data: *Acta Oceanologica Sinica* **33**(12) 118-126.
Saltus R. W. and Jachens R. C. (1995) Gravity and basin-depth maps of the Basin and Range Province, western United States: U.S. Geological Survey, Geophysical Investigation Map GP-1012, Scale??
Stevens C. H., Stone P., and Blakely R. J. (2013) Structural evolution of the East Sierra Valley System (Owens Valley and vicinity), California: A geologic and geophysical synthesis: *Geosciences* **3** 176-215.
Stockli D. F., Dumitru T. A., McWilliams M. O., and Farley K. A. (2003) Cenozoic tectonic evolution of the White Mountains, California and Nevada: *Geological Society of America Bulletin* **115** 788-816.
Taylor G. F. (1933) Quaternary fault structure of the Bishop region, east-central California: unpublished Ph.D. dissertation, California Instutite of Technology, Pasadena, 161 pp.

Road Log

17.2 Going around the loop road, reverse course and return to Glacier Lodge Road.

18.9 Glacier Lodge Road. Turn left (E) WATCHING FOR HIGH-SPEED DOWNHILL TRAFFIC.

19.3 Unmarked unpaved road under high-tension electrical transmission line. Turn right (S). This road has several deep stream crossings and should not be attempted by low-clearance vehicles. Stop 3.2 can also be accessed by continuing east on the Glacier Lodge Road to the center of Big Pine and turning right on Highway 395.

20.7 Old Big Pine dump site. Park alongside the dirt road. Stop 3.2

Stop 3.2: Kinematics of the northern portion of the Owens Valley fault (Haddon, Kirby).

Surface slip during large Owens Valley earthquakes

Elizabeth Haddon, U.S. Geological Survey
Colin Amos, Western Washington University
Olaf Zielke, King Abdullah University of Science and Technology
Angela Jayko, U.S. Geological Survey
Roland Burgmann, University of California, Berkeley

Summary

The Owens Valley Fault (OVF) (Figure 1) represents one structure in a network of distributed strike-slip and normal faults forming the eastern boundary of the Sierra Nevada–Great Valley microplate [Unruh et al., 2003] collectively termed the eastern California shear zone (ECSZ) or Walker Lane (WL) [e.g., Stewart, 1988; Wesnousky, 2005]. Geodetic measurements spanning this region indicate present-day dextral shear at 10.6 ± 0.5 mm/yr [Lifton et al., 2013], upward of 20% of the relative Pacific–North American plate motion [e.g., Dokka and Travis, 1990]. Contemporary background seismicity demonstrates that northwestward translation of the Sierra Nevada–Great Valley microplate drives deformation across this region [Unruh et al., 2003]. Because the OVF strikes generally clockwise (~340°) of local plate boundary motion (~323°) [Lifton et al., 2013], the structure accommodates strike-slip motion with an overall releasing geometry (Figure 1) [e.g., Unruh et al., 2014].

The OVF experiences large but relatively infrequent earthquakes (~10^{-3} to 10^{-4} year) involving predominantly right-lateral slip [e.g., Beanland and Clark, 1994; Lee et al., 2001a; Bacon and Pezzopane, 2007]. The March 26, 1872 Owens Valley earthquake is the third largest known historical earthquake in California with shaking intensities comparable to the 1906 and 1857 San Andreas earthquakes (Hough and Hutton, 2008). The complex surface rupture trace spanned multiple geometric fault segments, similar to the 1992 Mw 7.3 Landers and 1999 Mw 7.1 Hector Mine earthquakes [Sieh et al., 1993; Treiman et al., 2002]. Early investigation of the 1872 earthquake surface slip distribution noted high average and maximum lateral surface displacements (~4–6 and 7–11 m, respectively) [Lubetkin and Clark, 1988; Vittori et al., 1993; Beanland and Clark, 1994; McCalpin and Slemmons, 1998] with respect to the ~113–120 km rupture trace [Slemmons et al., 2008; Amos et al., 2013a], suggesting the 1872 Owens Valley earthquake was a high stress drop event [e.g., Hanks and Bakun, 2002]. Relatively sparse field data and a complex rupture trace, however, inhibited attempts to fully resolve the slip distribution and reconcile the total moment release. Apparent discrepancies between estimates of 1872 magnitude from geologic observations (Mw 7.5–7.7) [e.g., Beanland and Clark, 1994; Stein and Hanks, 1998] and interpretations of macroseismic accounts by Bakun [2006] (Mw 7.4–7.5) and Hough and Hutton [2008] (Mw 7.8–7.9) emphasize the importance of resolving fundamental rupture parameters, such as rupture length and average slip during OVF earthquakes.

Recent advances in the ability to image and analyze active faults using high-resolution lidar topography and imagery provide an opportunity to map past earthquake surface ruptures with unprecedented detail and improve upon existing field catalogs of geomorphic offset [e.g., Zielke et al., 2015]. We present a new, comprehensive record of surface slip based on lidar and field investigation, documenting 162 new measurements of laterally and vertically displaced landforms for 1872 and prehistoric Owens Valley

earthquakes. Our lidar analysis uses a newly developed analytical tool to measure fault slip based on cross-correlation of sublinear topographic features and to produce a uniquely shaped probability density function (PDF) for each measurement. Stacking these PDFs along strike to form cumulative offset probability distribution plots (COPDs) highlights common values corresponding to single and multiple-event displacements. Lateral offsets for 1872 vary systematically from ~1.0 to 6.0 m and average 3.3 ± 1.1 m (2σ). Vertical offsets are predominantly east-down between ~0.1 and 2.4 m, with a mean of 0.8 ± 0.5 m. The average lateral-to-vertical ratio compiled at specific sites is ~6:1. Summing displacements across subparallel, overlapping rupture traces implies a maximum of 7–11 m and net average of 4.4 ± 1.5 m, corresponding to a geologic Mw ~7.5 for the 1872 event. We attribute progressively higher-offset lateral COPD peaks at ~7.1 ± 2.0 m, 12.8 ± 1.5 m, and 16.6 ± 1.4 m to three earlier large surface ruptures. Evaluating cumulative displacements in context with previously dated landforms in Owens Valley suggests relatively modest rates of fault slip, averaging between ~0.6 and 1.6 mm/yr (1σ) over the late Quaternary.

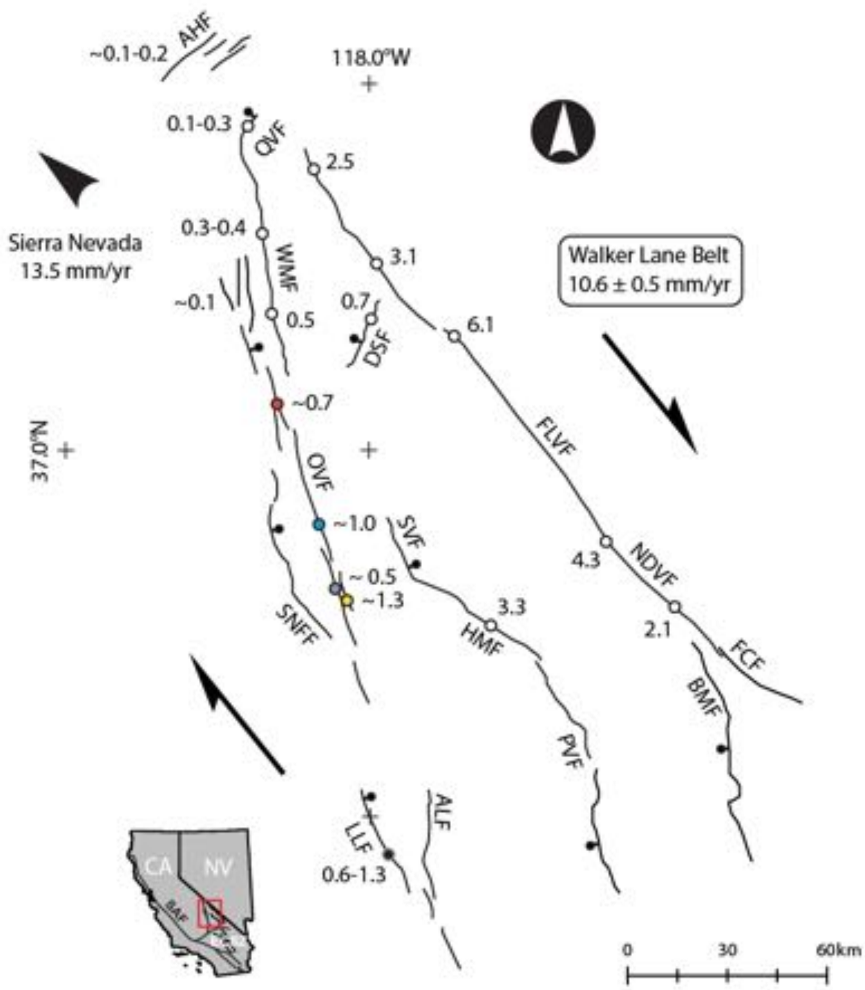

Figure 1. (Previous page) Compilation of reported slip rates in mm/yr on active faults in the southern Walker Lane (modified from Foy et al. [2012]) with respect to the geodetic rate across the zone derived from the global positioning system and the relative motion of the Sierra Nevada– Great Valley microplate [Lifton et al., 2013]. Geologic slip rate studies, from south to north: Amos et al. [2013b], (this study), Oswald and Wesnousky [2002], Frankel et al. [2007a,b], Lubetkin and Clark [1988], Reheis and Sawyer [1997], Lee et al. [2001b], Ganev et al. [2010], Kirby et al. [2006], and Nagorsen-Rinke et al. [2013]. Faults listed alphabetically: AHF, Adobe Hills fault; ALF, Airport Lake fault; BMF, Black Mountain fault; DSF, Deep Springs fault; FCF, Furnace Creek fault; FLVF, Fish Lake Valley fault; HMF, Hunter Mountain fault; LLF, Little Lake fault; OVF, Owens Valley fault; NDVF, Northern

Death Valley fault; PVF, Panamint Valley fault; QVF, Queen Valley fault; SAF, San Andreas fault; SNFF, Sierra Nevada frontal fault; SVF, Saline Valley fault; WMF, White Mountain fault

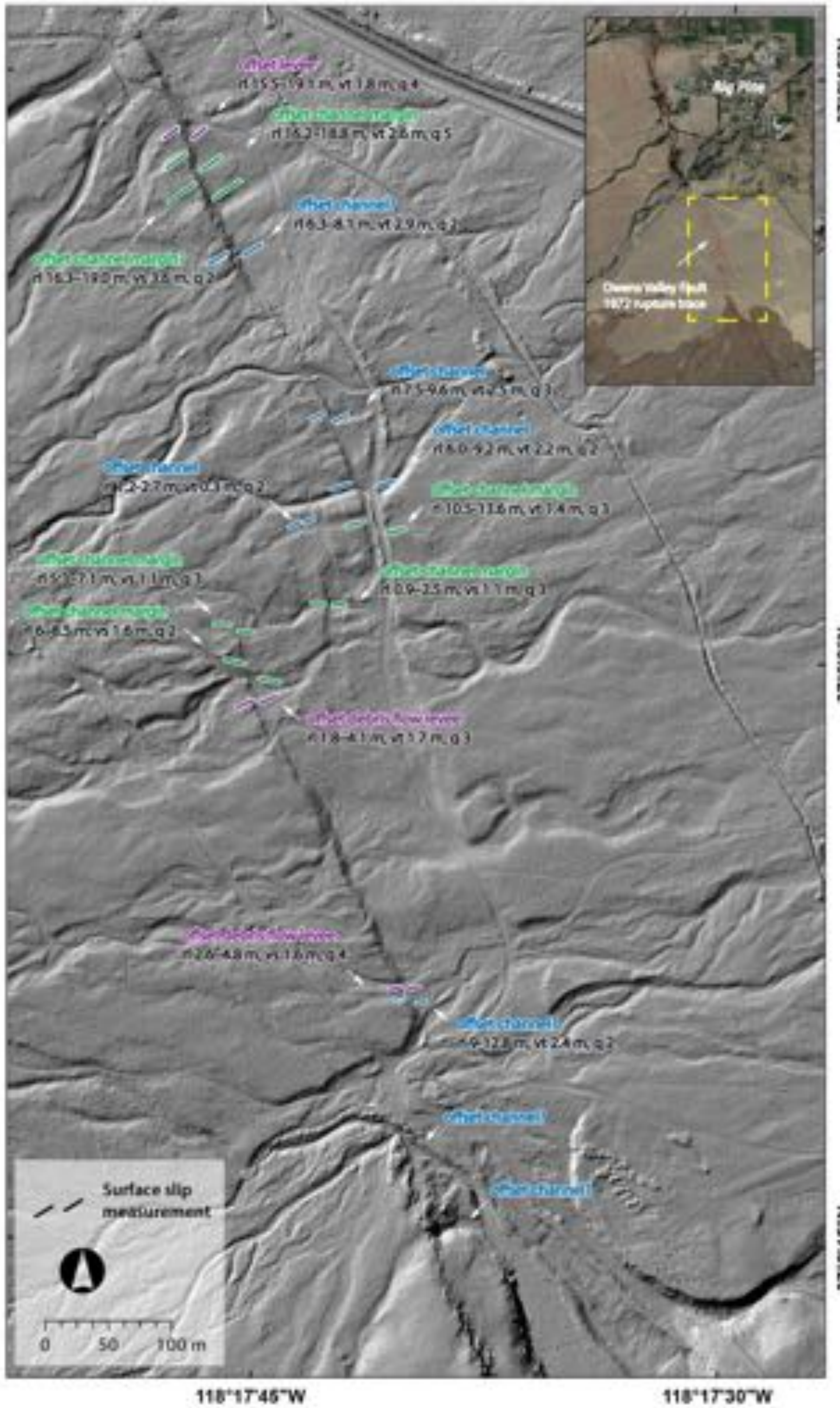

Figure 2. (Previous page) Lidar hillshade image shows the Owens Valley fault intersecting the Big Pine Creek alluvial fan south of Big Pine. We revisit the surface rupture using high spatial resolution (25-cm) lidar topography and complementary field study. Our mapping and field investigations highlight previously unrecognized faulted landforms useful for reconstructions of surface slip along strike. We adopt a newly developed analysis tool based on cross-correlation to measure discrete lateral and vertical offset of sublinear geomorphic features from lidar. Offset values (yellow triangles) indicate optimum right-lateral slip determined from EarthScope lidar using LaDiCaoz_v2 and field study.

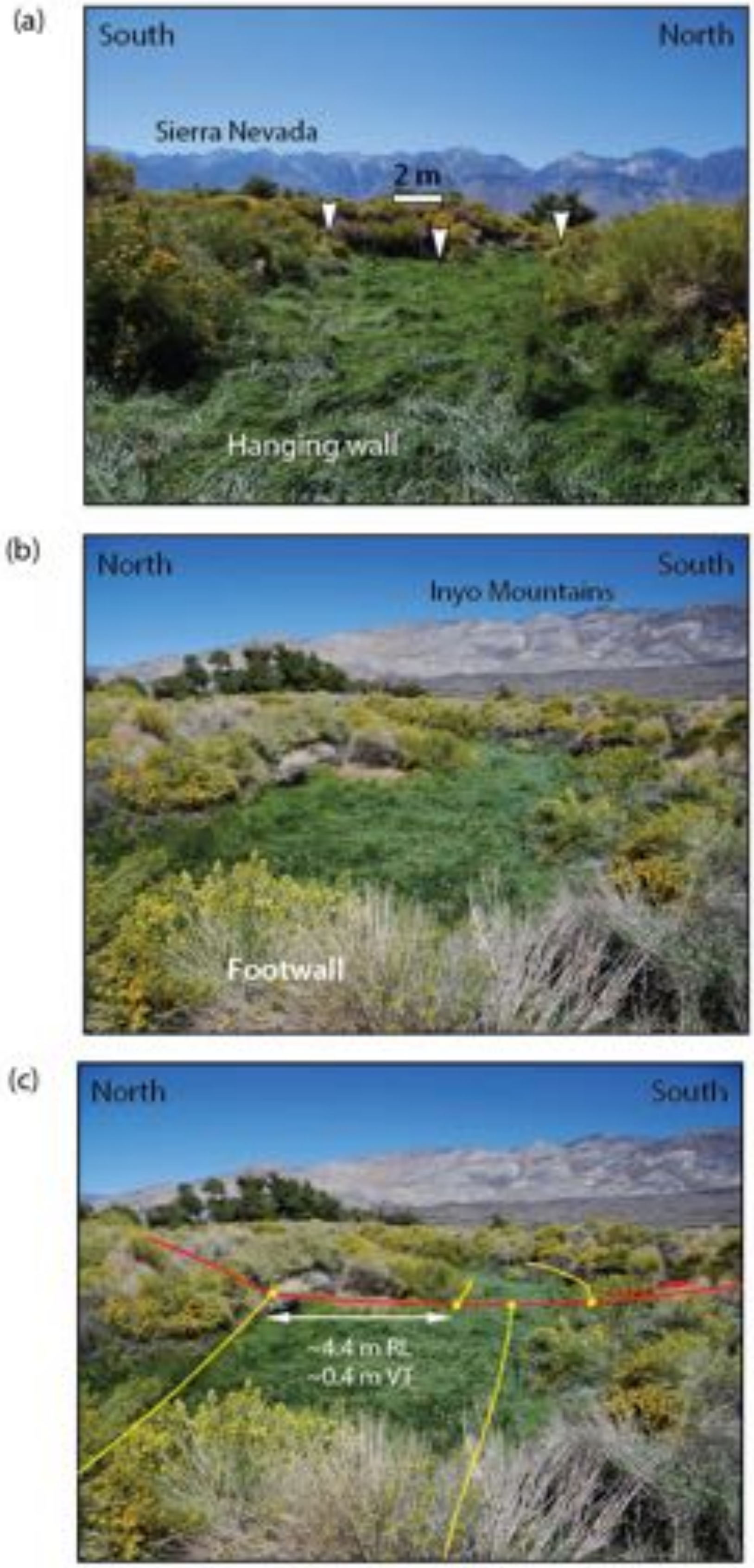

Figure 3. Example of a high confidence geomorphic offset documented in the field. (a) View from the hanging wall to the west down-channel and normal to the OVF. White arrows mark the intersection of the OVF with the thalweg and channel margins. (b) Uninterpreted view from the footwall up-channel and to the east toward the hanging wall. (c) Offset values (~4.4 m right-lateral, 0.4 m east- down vertical) rely on field measurement of channel margins (traced in yellow) and bounding tread surface to the north. The Tinemaha section of the OVF is mapped in red. RL, right-lateral; VT, vertical throw.

Figure 4. (Next Page) (a) Schematic illustration of summing approach for features offset across multiple discrete faults. (b) Individual offset measurements represent partial slip with uncertainty ranges provided by back-slipping. Multiple partial slip measurements contribute to an offset sum with associated uncertainties determined using a Monte Carlo routine. The lower distributions in the binned COPD plot reflect stacked values of partial offset, whereas the uppermost distribution is the sum of the partial offset distribution. The sum is equal to the estimated net offset and contributes to COPD plots binned along strike.

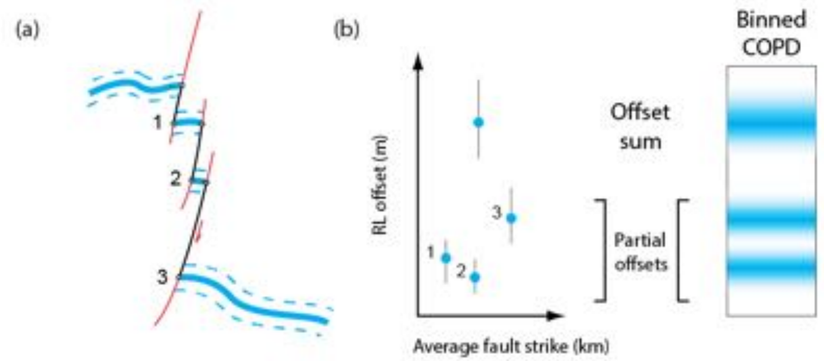

Figure 5. (Below) Our new and comprehensive database of 238 surface slip measurements includes 162 new measurements, 21 remeasured landforms, and 55 previously published field measurements. This compilation shows small geomorphic offsets along average OVF strike (340°) including measurements with confidence ratings of low-moderate to high. Gray error bars show uncertainty limits determined visually from back-slipping. (a) The spatial distribution of OVF scarps (red lines) mapped from EarthScope lidar and classified by Owens Valley fault section (orange and black points), following previous mapping by Beanland and Clark [1994], Bryant [1984a, 1984b], and Slemmons et al. [2008]. Nearby faults are taken from the U.S. Geological Survey Quaternary fault and fold database. From south to north: DS, Dirty Socks; OL, Owens Lake; LP, Lone Pine fault; DL, Diaz Lake; IS, southern Independence; MF, Manzanar fault; I, Independence; T, Tinemaha; TW, western Tinemaha; FS, Fish Springs; BP, Big Pine; K, Keough section of Sierra Nevada frontal fault (SNNF), KLF, Klondike Lake fault; KSF, Klondike Springs fault; WMF, White Mountain fault. (b) Right-lateral offset measurements symbolized by fault section include previously reported values (orange diamonds) from Bateman [1961], Lubetkin and Clark [1988], Beanland and Clark [1994], Lee et al. [2001a], Zehfuss et al. [2001], and Slemmons et al. [2008]. (c) Along-strike compilation of measured vertical throw. Throw is predominantly east-down, with negative values indicative of downward motion to the west.

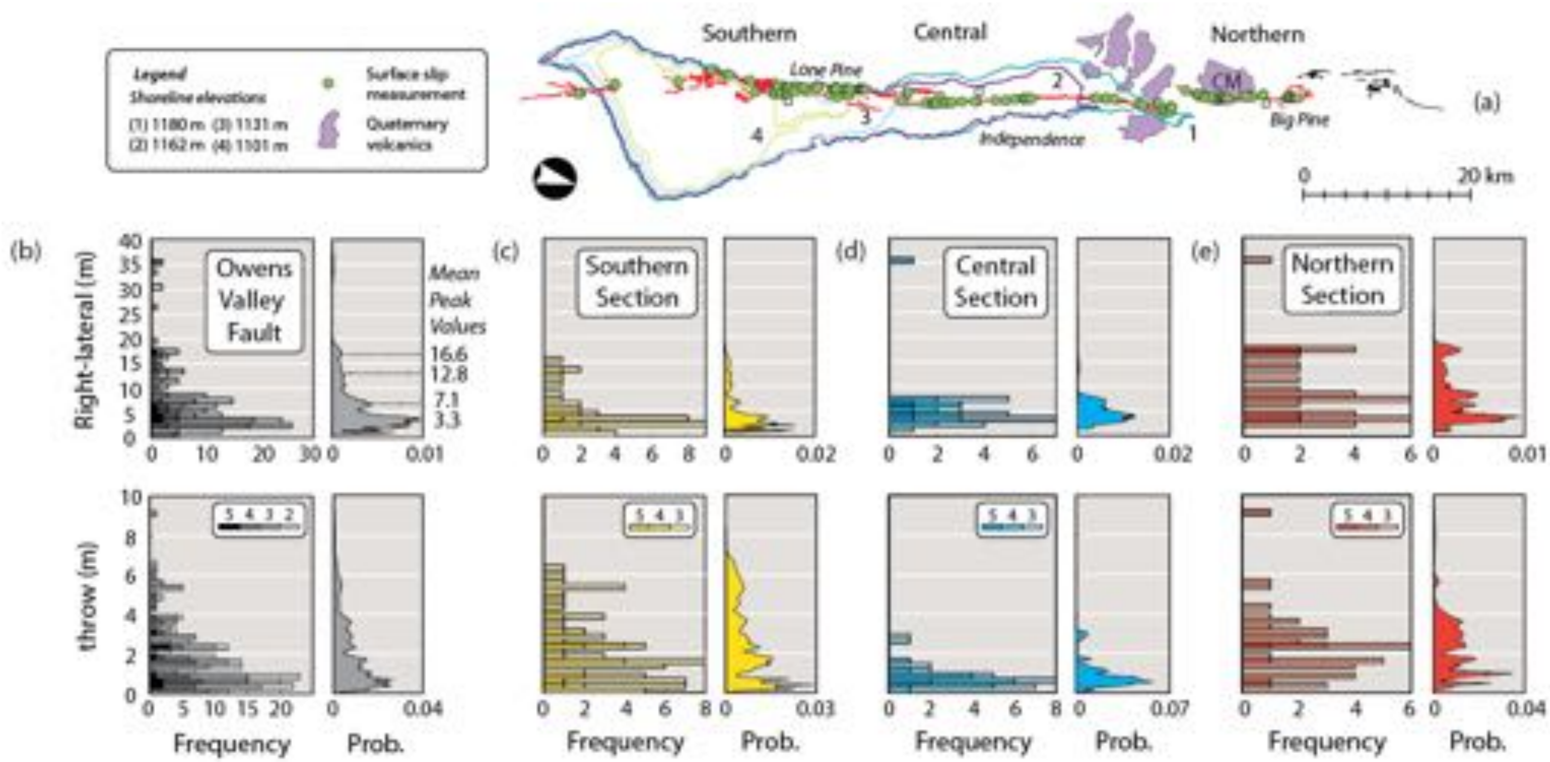

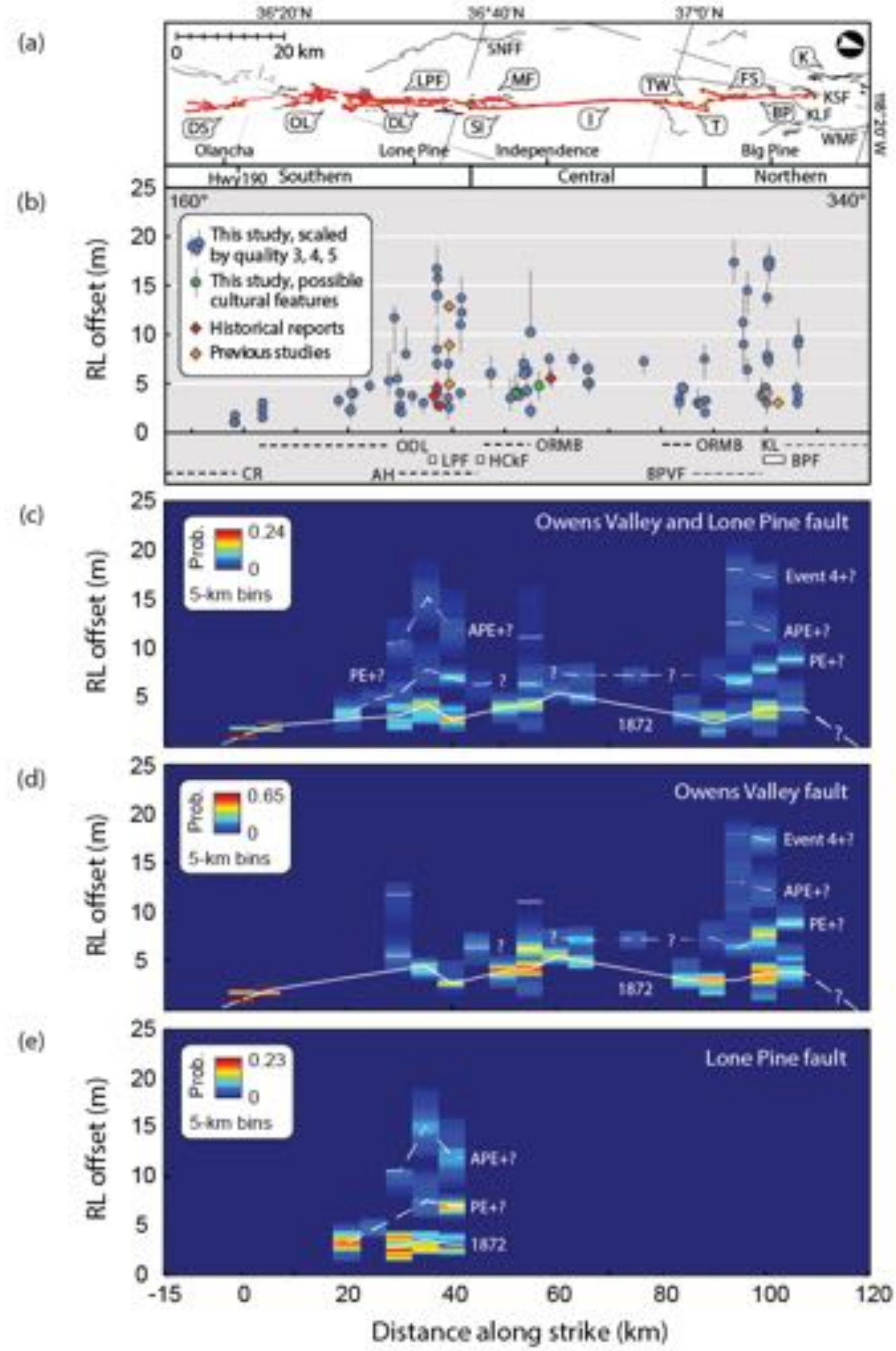

Figure 6. Possible surface slip reconstructions for past large Owens Valley fault earthquakes derived from binned COPD plots. PE, penultimate event; APE, antepenultimate event. (a) Scarps mapped from EarthScope lidar with fault section abbreviations similar to Figure 5a. (b) Right-lateral offset measurements scaled by confidence rating, including historic measurements (red points) summarized in Bateman [1961], possible cultural features (green points), and previously reported values (orange diamonds) [Lee et al., 2001a]. Grey bars reflect the range of uncertainty previously reported or provided by back-slipping. Lower scale bar describes the along-strike spatial extent of key geologic and geomorphic features. From south to north: CR, Coso Range; ODL, Owens dry lake; AH, Alabama Hills; LPF, Lone Pine fan; HCkF, Hogback Creek fan; BPVF, Big Pine volcanic field; ORMB, Owens River meander belt; KL, Klondike Lake; BPF, Big Pine fan. (c) 5-km binned COPD plot calculated along strike for data ranked moderate and higher in confidence. Warmer values correspond to

peaks in distributed offset probability. (d-e) Additional binned COPDs depict the distribution of surface slip measurements compiled along main traces of the OVF and the Lone Pine fault in southern Owens Valley.

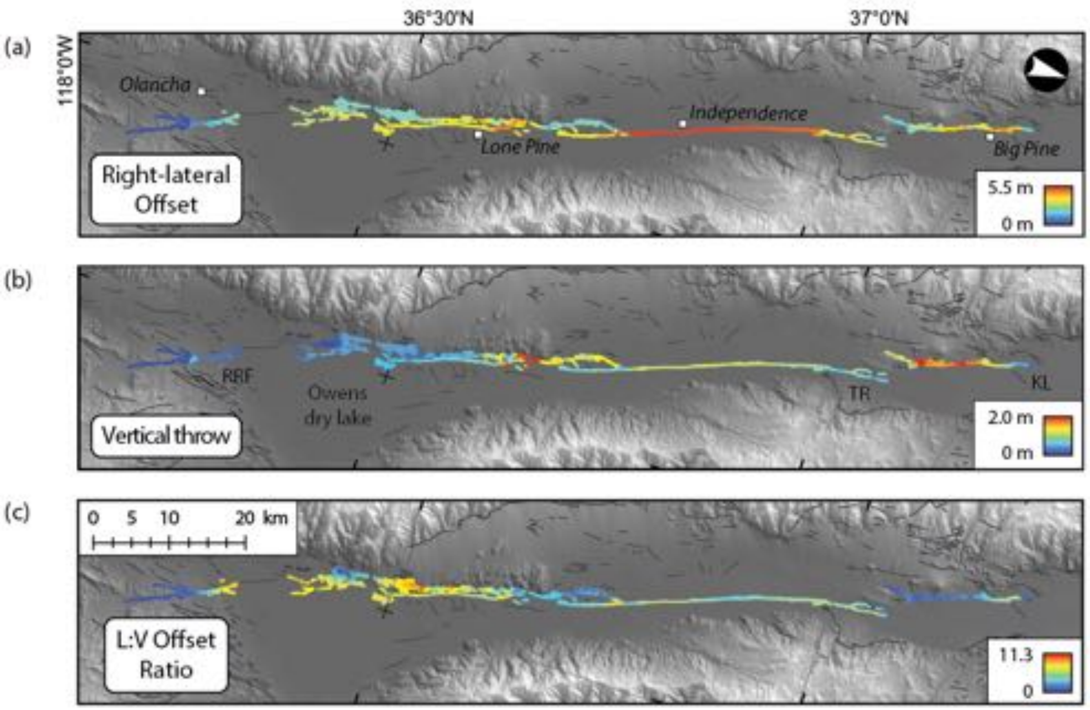

Figure 7. (Above) Slip distributions for the 1872 Owens Valley surface rupture interpolated from offset measurements compiled along strike (e.g., Figure 4). (a) Right-lateral measurements and summed offset values show the distribution of lateral slip without uncertainties. (b) Distribution of vertical throw following the same approach. (c) Lateral-to-vertical (L:V) offset ratios calculated at sites where both measurements rank moderate in confidence or higher. Active faults from the U.S. Geological Survey Quaternary fault and fold database appear gray and drape a hillshade image combined with 10-m National Elevation Data from the U.S. Geological Survey. Features abbreviated, from south to north: RRF, Red Ridge fault; TR, Tinemaha Reservoir; KL, Klondike Lake.

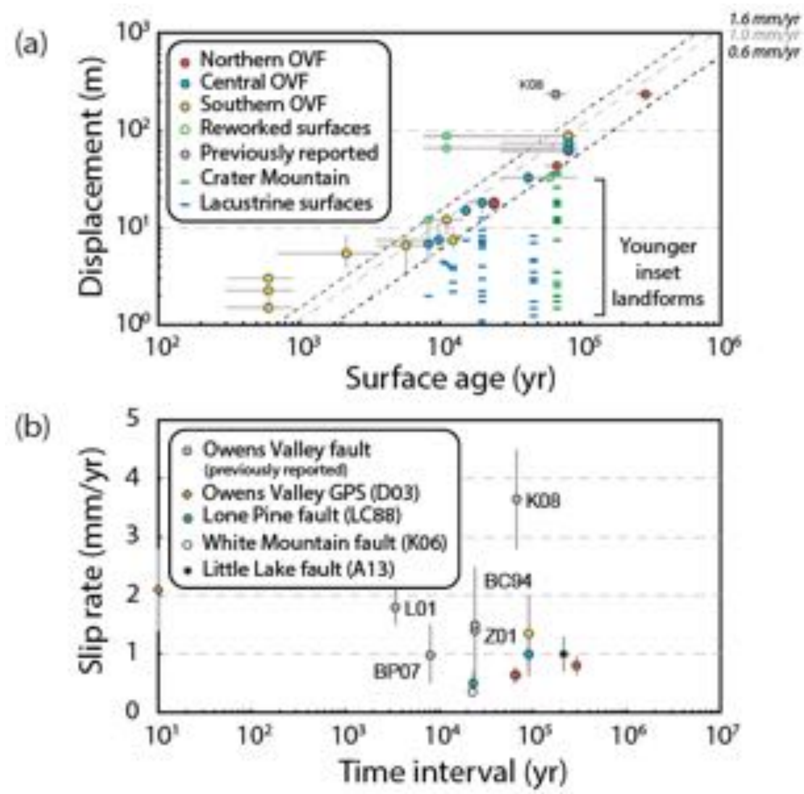

Figure 8. OVF slip rates estimated from cumulative surface slip measurements combined with previously published ages for geologic features and geomorphic surfaces in Owens Valley. Ages, elevations, and references for these dates are provided in supporting information. (a) Linear regressions indicate the suggested range of average lateral-oblique slip rates between ~0.6 and 1.6 mm/yr for the northern (red, ~0.7 mm/ yr), central (blue, ~1.0 mm/yr), and southern (yellow, ~1.3 mm/yr) fault sections. Displacements reflect optimum values and associated uncertainties derived from the lateral and vertical offset and average fault dip (80°). Points also represent optimum ages or preferred values for surfaces formed over a single MIS interval. Horizontal gray bars reflect the breadth of the MIS interval or range of reported uncertainties. For large offsets occupying apparently young surfaces (hollow points), uncertainties also incorporate the likely surface age prior to the last pluvial highstand. Smaller offsets (dashes) represent features formed on lacustrine surfaces (blue) or Crater Mountain basalts (green). (b) Compilation of fault slip rates for the southwestern Walker Lane plotted against age, including the OVF, Lone Pine fault (LPF), and adjoining normal-oblique White Mountain fault and dextral Little Lake fault. We derive an additional rate for the northern OVF (~0.8 mm/yr) based on dextral offset from Kirby et al. [2008] (235 ± 15 m) and age from Turrin

and Gillespie [1986] (290 ± 40 ka). A13, Amos et al. [2013b]; BC94, Beanland and Clark [1994]; BP07, Bacon and Pezzopane [2007]; D03, Dixon et al. [2003]; K06, Kirby et al. [2006]; K08, Kirby et al. [2008]; L01, Lee et al. [2001a]; LC88, Lubetkin and Clark [1988]; Z01, Zehfuss et al. [2001].

References

Amos, C. B., A. T. Lutz, A. S. Jayko, S. A. Mahan, G. B. Fisher, and J. R. Unruh (2013a), Refining the southern extent of the 1872 Owens Valley Earthquake Rupture through paleoseismic investigations in the Haiwee area, Southeastern California, Bull. Seismol. Soc. Am., 103(2A), 1022–1037, doi:10.1785/0120120024.

Amos, C. B., S. J. Brownlee, D. H. Rood, G. B. Fisher, R. Bu€rgmann, P. R. Renne, and A. S. Jayko (2013b), Chronology of tectonic, geomorphic, and volcanic interactions and the tempo of fault slip near Little Lake, California, Geol. Soc. Am. Bull., 125(7–8), 1187–1202, doi:10.1130/B30803.1.

Bacon, S. N., S. K. Pezzopane, and R. M. Burke (2003), Paleoseismology on the Owens Valley fault and latest Quaternary stratigraphy in Owens Valley near Lone Pine, eastern California, US Geological Survey, National Earthquake Hazards Reduction Program (NEHRP) Final Technical Report, 42 pp. [Available at http://erp-web.er.usgs.gov/reports/abstract/2002/ni/02hqgr0003.pdf.]

Bakun, W. H. (2006), MMI attenuation and historical earthquakes in the basin and range province of western North America, Bull. Seismol. Soc. Am., 96, 2206–2220, doi:10.1785/0120060045.

Bateman, P. C. (1961), Willard D. Johnson and the strike-slip component of fault movement in the Owens Valley, California, Bull. Seismol. Soc. Am., 51, 483–493.

Beanland, S., and M. M. Clark (1994), The Owens Valley fault zone, eastern California, and surface rupture associated with the 1872 earth- quake, U.S. Geol. Surv. Bull., 1982, 29 pp.

Bryant, W. A. (1984a), Northern Owens Valley, Fish Slough, and White Mountains frontal faults, Inyo and Mono counties, California, in California Division of Mines and Geology Fault Evaluation Reports, FER-153, scale 1:24,000, 19 pp., Calif. Geol. Surv. [Available at http://www.quake.ca.gov/gmaps/WH/regulatorymaps.htm.]

Bryant, W. A. (1984b), Owens Valley and White Mountains frontal fault zones, Big Pine area, Inyo County, California, in California Division of Mines and Geology Fault Evaluation Reports, FER-159, scale 1:24,000, 19 pp., Calif. Geol. Surv. [Available at http://www.quake.ca.gov/gmaps/WH/regulatorymaps.htm.]

Dixon, T. H., E. Norabuena, and L. Hotaling (2003), Paleoseismology and global positioning system: Earthquake-cycle effects and geodetic versus geologic fault slip rates in the eastern California shear zone, Geology, 31, 55–58, doi:10.1130/0091-7613(2003)031 < 0055:PAG-PSE>2.0.CO;2.

Dokka, R. K., and C. J. Travis (1990), Role of the eastern California shear zone in accommodating Pacific–North American Plate motion, Geophys. Res. Lett., 17(9), 1323–1326, doi:10.1029/GL017i009p01323.

Foy, T. A., K. L. Frankel, Z. M. Lifton, C. W. Johnson, and M. W. Caffee (2012), Distributed extensional deformation in a zone of right-lateral shear: Implications for geodetic versus geologic rates of deformation in the eastern California shear zone-Walker Lane, Tectonics, 31, TC4008, doi:10.1029/2011TC002930.

Frankel, K. L., J. F. Dolan, R. C. Finkel, L. A. Owen, and J. S. Hoeft (2007a), Spatial variations in slip rate along the Death Valley–Fish Lake Valley fault system determined from LiDAR topographic data and cosmogenic 10Be geochronology, Geophys. Res. Lett., 34, L18303, doi:10.1029/2007GL030549.

Frankel, K. L., et al. (2007b), Cosmogenic 10Be and 36Cl geochronology of offset alluvial fans along the northern Death Valley fault zone: Implications for transient strain in the eastern California shear zone, J. Geophys. Res., 112, B06407, doi:10.1029/2006JB004350.

Ganev, P. N., J. F. Dolan, K. L. Frankel, and R. C. Finkel (2010), Rates of extension along the Fish Lake Valley fault and transtensional deformation in the eastern California shear zone–Walker Lane belt, Lithosphere, 2(1), 33–49, doi:10.1130/L51.1.

Hanks, T. C., and W. H. Bakun (2002), A bilinear source-scaling model for M-log a observations of continental earthquakes, Bull. Seismol. Soc. Am., 92, 1841–1846, doi:10.1785/0120010148.

Hough, S. E., and K. Hutton (2008), Revisiting the 1872 Owens Valley California earthquake, Bull. Seismol. Soc. Am., 98(2), 931–949, doi:10.1785/0120070186.

Kirby, E., D. W. Burbank, M. Reheis, and F. Phillips (2006), Temporal variations in slip rate of the White Mountain fault zone, eastern California, Earth Planet. Sci. Lett., 248, 168–185, doi:10.1016/j.epsl.2006.05.026.

Kirby, E., S. Anandakrishnan, F. Phillips, and S. Marrero (2008), Late Pleistocene slip rate along the Owens Valley fault, eastern California, Geophys. Res. Lett., 35, L01304, doi:10.1029/2007GL031970.

Lee, J., J. Spencer, and L. Owen (2001a), Holocene slip rates along the Owens Valley fault, California: Implications for the recent evolution of the eastern California shear zone, Geology, 29(9), 819–822, doi:10.1130/00917613(2001)029 < 0819:HSRATO>2.0.CO;2.

Lee, J., C. M. Rubin, and A. Calvert (2001b), Quaternary faulting history along the Deep Springs fault, California, Geol. Soc. Am. Bull., 113(7), 855–869, doi:10.1130/0016-7606(2001)113 < 0855:QFHATD>2.0.CO;2.

Lifton, Z. M., A. V. Newman, K. L. Frankel, C. W. Johnson, and T. H. Dixon (2013), Insights into distributed plate rates across the Walker Lane from GPS geodesy, Geophys. Res. Lett., 40, 4620–4624, doi:10.1002/grl.50804.

Lubetkin, L. K. C., and M. M. Clark (1988), Late Quaternary activity along the Lone Pine fault, eastern California, Geol. Soc. Am. Bull., 100(5), 755–766, doi:10.1130/0016-7606(1988)100 < 0755:LQAATL>2.3.CO;2.

McCalpin, J. P., and D. B. Slemmons (1998), Statistics of paleoseismic data, final technical report, U.S. Geological Survey National Earthquake Hazards Reduction Program, Final Technical Report, Contract 1434-HQ-96-GR-02752, 62 pp. [Available at http://works.bepress.com/james_mccalpin/12/.]

Nagorsen-Rinke, S., J. Lee, and A. Calvert (2013), Pliocene sinistral slip across the Adobe Hills, eastern California–western Nevada: Kinematics of fault slip transfer across the Mina deflection, Geosphere, 9, 37–53, doi:10.1130/GES00825.1.

Oswald, J. A., and S. G. Wesnousky (2002), Neotectonics and Quaternary geology of the Hunter Mountain fault zone and Saline Valley region, southeastern California, Geomorphology, 42(3), 255–278, doi:10.1016/s0169-555x(01)00089-7.

Reheis, M. C., and T. L. Sawyer (1997), Late Cenozoic history and slip rates of the Fish Lake Valley, Emigrant Peak, and Deep Springs fault zones, Nevada and California, Geol. Soc. Am. Bull., 109(3), 280–299, doi:10.1130/0016-7606(1997)109 < 0280:LCHASR>2.3.CO;2.

Sieh, K., et al. (1993), Near-field investigations of the Landers earthquake sequence, April to July 1992, Science, 260(5105), 171–176, doi:10.1126/science.260.5105.171.

Slemmons, D. B., E. Vittori, A. S. Jayko, G. A. Carver, and S. N. Bacon (2008), Quaternary fault and lineament map of Owens Valley, Inyo County, eastern California, Map Chart 96, 25 pp., Geol. Soc. of Am., doi:10.1130/2008.MCH096.

Stein, R. S., and T. C. Hanks (1998), Mw6 earthquakes in southern California during the twentieth century: No evidence for a seismicity or moment deficit, Bull. Seismol. Soc. Am., 88, 635–652.

Stewart, J. H. (1988), Tectonics of the Walker Lane belt, western Great Basin Mesozoic and Cenozoic deformation in a zone of shear, in Metamorphism and Crustal Evolution of the Western US, vol. VII, edited by W. G. Ernst, pp. 685–713, Prentice Hall, Englewood Cliffs, N. J.

Treiman, J. A., K. J. Kendrick, W. A. Bryant, T. K. Rockwell, and S. F. McGill (2002), Primary surface rupture associated with the Mw 7.1 16 October 1999 Hector Mine earthquake, San Bernardino County, California, Bull. Seismol. Soc. Am., 92(4), 1171–1191, doi:10.1785/ 0120000923.

Turrin, B., and A. R. Gillespie (1986), K/Ar ages of basaltic volcanism of the big pine volcanic field, California: Implications for glacial stratigraphy and neotectonics of the Sierra Nevada, Geol. Soc. Am. Abstr. Programs, 18(6), 777.

Unruh, J., J. Humphrey, and A. Barron (2003), Transtensional model of Sierra Nevada frontal fault system, eastern California, Geology, 31, 327–330, doi:10.1130/00917613(2003)031 <0327:TMFTSN>2.0.CO;2.

Unruh, J., E. Hauksson, and C. H. Jones (2014), Internal deformation of the southern Sierra Nevada microplate associated with foundering lower lithosphere, California, Geosphere, 10(1), 107–128, doi:10.1130/GES00936.1.
Vittori, E., A. M. Michetti, D. B. Slemmons, and G. Carver (1993), Style of recent surface deformation at the south end of the Owens Valley fault zone, eastern California, Geol. Soc. Am. Abstr. Programs, 25(5), 159.
Wesnousky, S. G. (2005), Active faulting in the Walker Lane, Tectonics, 24, TC3009, doi:10.1029/2004TC001645.
Zielke, O., Y. Klinger, and J. R. Arrowsmith (2015), Fault slip and earthquake recurrence along strike-slip faults—Contributions of high- resolution geomorphic data, Tectonophysics, 638, 43–62, doi:10.1016/j.tecto.2014.11.004.
Zehfuss, P. H., P. R. Bierman, A. R. Gillespie, R. M. Burke, and M. W. Caffee (2001), Slip rates on the Fish Springs fault, Owens Valley, California, deduced from cosmogenic 10Be and 26Al and soil development on fan surfaces, Geol. Soc. Am. Bull., 113(2), 241–255, doi:10.1130/0016-7606(2001)113 < 0241:SROTFS>2.0.CO;2.

Stop 3.2: Pleistocene slip rate along the Owens Valley fault

Eric Kirby - Oregon State University and **Fred M Phillips** – New Mexico Tech

It has long been recognized that geodetic strain rates across the Owens Valley are relatively high (Savage and Lisowski, 1980; 1995), and models of elastic strain accumulation anywhere from ~4 – 7 mm/yr of shear at depth to explain these observations (e.g., Gan et al., 2000). These results exceed paleoseismic estimates of Late Pleistocene - Holocene slip along the Owens Valley fault zone of 1 – 3 mm/yr (Haddon et al., 2016; Bacon and Pezzopane, 2007; Beanland and Clark, 1994; Bierman et al., 1995; Lee et al., 2001; Lubetkin and Clark, 1988). Some workers argue that this discrepancy reflects elevated post-seismic surface deformation following the 1872 Owens Valley earthquake (Dixon et al., 2003; Malservisi et al., 2001), but such a protracted transient signal is rather unusual, even for a large event.

At this stop, we will discuss the Late Pleistocene slip rate along the primary strand of the northern Owens Valley fault where displaced lava flows along the eastern flank of the Crater Mountain volcanic complex provide constraints on displacement over the past 60-80 ka (Kirby et al., 2008).

Driving Question:
What is the long-term slip rate of the Owens Valley fault?

Figure 3.2a: Oblique areal perspective view of Crater Mountain and the Owens Valley fault. Generated in Google Earth. Stop 3.2 is located at the northeastern flank of the flow complex, where the Owens Valley fault intersects the flow margins.

Displacement of the Crater Mountain flow complex

Along most of its length, the trace of the 1872 rupture along the Owens Valley fault runs near or within the floodplain of the Owens River, and long-term markers of fault displacement are relatively rare (Beanland and Clark, 1994; Haddon et al., 2016). South of the town of Big Pine (Figure 3.2a), the fault displaces basaltic lava flows along the eastern flank of Crater Mountain. Although correlation of individual flow margins across the fault is difficult, apparent right-lateral separation of the contact between the flow complex and alluvial fans is observed at the northeastern corner of the cone (Figure 3.2a). The fault geometry at this site is consistent with a small releasing step.

Dextral separation of the flow margin observed at the surface is approximately 235 ± 15 m (Figure 3.2b). Kirby et al. (2008) used ground-penetrating radar surveys to try and determine the subsurface geometry of basalt surfaces. Key observations are as follows:

West of the fault, the flow margin is shallowly buried beneath a relatively young alluvial fan deposit.

East of the pull-apart basin, the margin of the flow does not appear to be buried, and that the surface exposure is interpreted to reflect the former terminus of the flow.

Surveys do not reveal strong reflectors within that pull-apart basin that might be associated with buried flows.

These observations lead us to conclude that the surface exposures of the flow termini provide a reasonable marker with which to evaluate fault slip.

The age of the flow surface was estimated using the concentrations of cosmogenic ^{36}Cl in samples taken from well-preserved remnants of the flow surface. Samples were selected to minimize the chance of burial by eolian or alluvial material and were collected from outcrops that exhibited glassy surfaces and ropy flow textures whose preservation suggests minimal surface lowering since flow emplacement. Three samples were collected at this site, west of the fault (Figure 2), and three additional samples were collected from flows on the southwestern side of the vent complex, near the Red Mountain fault. For this FOP trip, we have updated the ages using the most recent calibrations of ^{36}Cl production incorporated into the CRONUS web calculator (Marrero et al., 2016a; 2016b; Borchers et al., 2016; Phillips et al., 2016). The six ages from both sample localities overlap within 2 sigma uncertainties, and indicate that the flow is 73 ± 9 ka, similar to the age determined by Kirby et al. (2008) of 70 ± 14 ka. Note that these ages are significantly younger than a K/Ar age of 290 ± 40 ka determined by Turrin and Gillespie (1986), but are similar to unpublished ^{3}He exposure ages obtained by J. Stone and A. Gillespie of 35-115 ka (A. Gillespie, personal communication 2004). Notably, flows west of the Fish Springs Hills, on the SW flank of Crater Mountain, bury Late Pleistocene alluvial fans that are dated to 120-150 ka (Zehfuss et al., 2001), and must therefore be younger than these deposits (see stop 3.3).

These results imply that the *minimum* slip rates on the Owens Valley fault during this time period have been ~2.7 mm/yr. Our data permit slip rates as high as ~3.9 mm/yr. Notably, even the lowest slip rate permitted by our ages is higher than recent estimates of Holocene – Late Pleistocene slip rates (Haddon et al., 2016; Bacon and Pezzopane, 2007). The rate is consistent, however, with the high end of some previous estimates (Beanland and Clark, 1994; Lee et al., 2001). Whether the difference between the well-determined Holocene rates of 0.6 – 1.6 mm/yr (e.g, Haddon et al., 2016) and these rates represent a period of rapid slip prior to ~20 - 25 ka remains uncertain (Kirby et al., 2008).

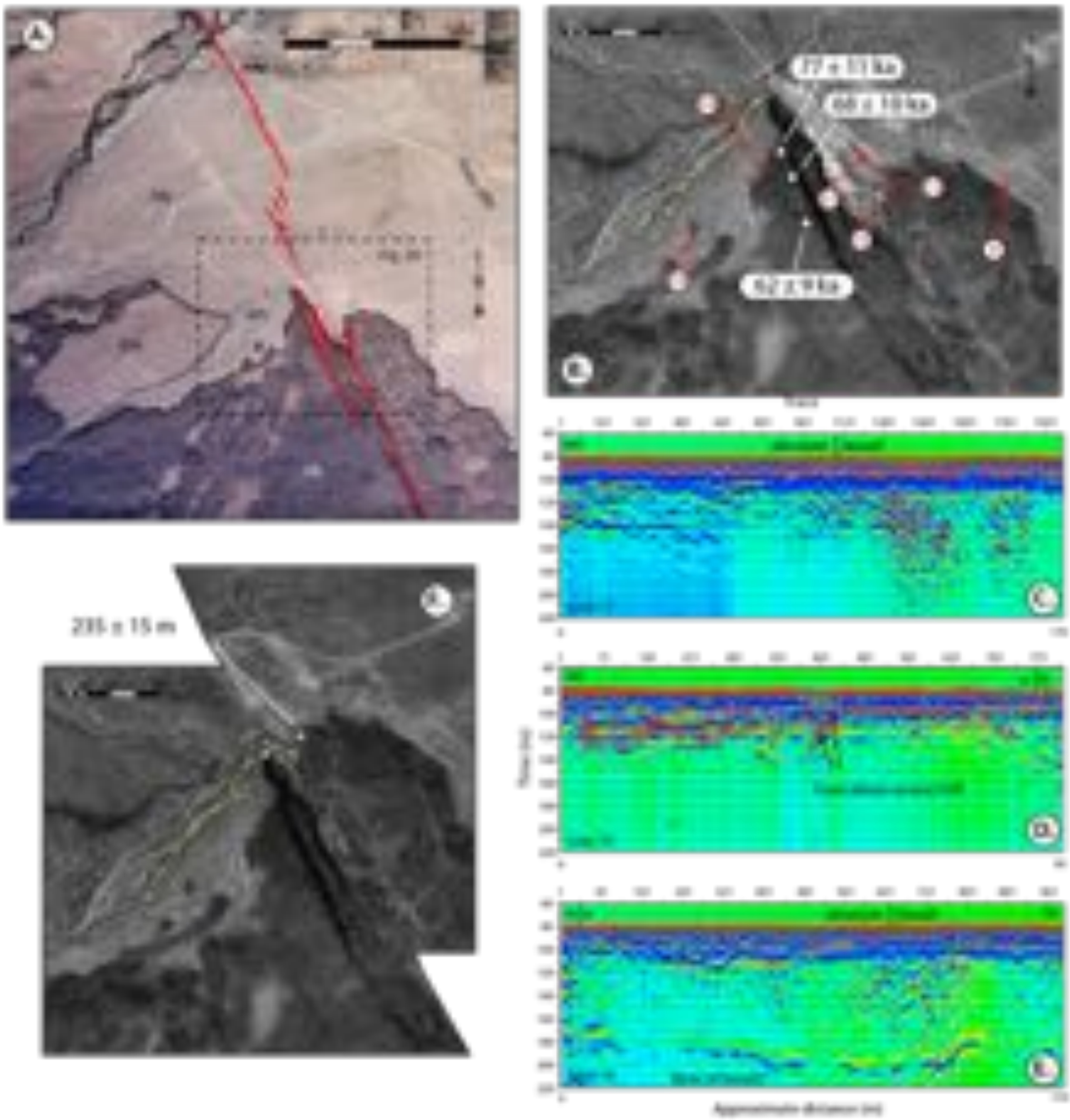

Figure 3.2b: A. Surficial geology of the northeastern flank of Crater Mountain. Note that basalt flows (Qb) overlie older alluvial fans (Qfo) west of the study area, and appear to be buried by younger alluvium (Qfy) west of the trace of the Owens Valley fault (red). Hachures represent the facing direction of the fault scarps. B. Close up of the offset flow margin. Background is a USGS digital orthophoto quadrangle (DOQ). Red lines represent GPR surveys conducted across the flow margin, and white circles represent sampling localities for cosmogenic isotope exposure ages. Ages shown are updated from Kirby et al. (2008) using the CRONUS web calculator. Yellow dashed line represents the inferred position of the buried flow margin west of the Owens Valley fault. C – E. GPR results from lines 11, 15, and 16 respectively. F. Reconstruction of slip along the Owens Valley fault restores inferred former positions of the flow margin. Dashed line represents inferred position of the buried flow margin. Figure modified after Kirby et al. (2008)

References

Bacon, S.N. and Pezzopane, S.K., 2007, A 25,000 year record of earthquakes on the Owens Valley fault near Lone Pine, California: Implications for recurrence intervals, slip rates and segmentation models: *Geological Society of America Bulletin*, v. 119, p. 823-847.

Beanland, S., and Clark, M. M., 1994, The Owens Valley fault zone, eastern California, and surface rupture associated with the 1872 earthquake, U.S. Geologic Survey Bulletin, p. 29.

Bellier, O., and Zoback, M. L., 1995, Recent state of stress change in the Walker Lane zone, western Basin and Range province, United States: *Tectonics*, v. 14, no. 3, p. 564-593.

Bierman, P. R., Gillespie, A. R., and Caffee, M. W., 1995, Cosmogenic ages for earthquake recurrence intervals and debris flow fan deposition, Owens Valley, California: *Science*, v. 270, p. 447-449.

Borchers, B., Marrero, S., Balco, G., Caffee, M., Goehring, B., Lifton, N., Nishiizumi, K., Phillips, F., Schaefer, J., and Stone, J., 2016, Geological calibration of spallation production rates in the CRONUS-Earth project: *Quaternary Geochronology,* v. 31, p. 188-198.

Dixon, T. H., Miller, M., Farina, F., Wang, H., and Johnson, D., 2000, Present-day motion of the Sierra Nevada block and some tectonic implications for the Basin and Range province, North American Cordillera: *Tectonics*, v. 19, no. 1, p. 1-24.

Dixon, T. H., Norabuena, E., and Hotaling, L., 2003, Paleoseismology and Global Positioning System: Earthquake-cycle effects and geodetic versus geologic fault slip rates in the Eastern California shear zone: *Geology*, v. 31, no. 1, p. 55-58.

Gan, W., Svarc, J. L., Savage, J. C., and Prescott, W. H., 2000, Strain accumulation across the Eastern California Shear Zone at latitude 36°30'N: *Journal of Geophysical Research*, v. 105, p. 16,229-16,236.

Gillespie, A. R., 1991, Quaternary subsidence of Owens Valley, California, *in* Hall, C. A., ed., Natural History of eastern California and high-altitude research: Los Angeles, White Mountain Research Station Proceedings, p. 356-382.

Haddon, E.K., Amos, C.B., Zielke, O., Jayko, A.S., and Burgmann, R., 2016, Surface slip during large Owens Valley earthquakes: *Geochemistry, Geophysics, Geosystems*, v. 17, p. 2239-2269.

Kirby, E., Anadakrishnan, S., Phillips, F., Marrero, S., 2008, Late Pleistocene slip rate along the Owens Valley fault, eastern California: *Geophysical Research Letters*, v. 35, L01304, doi: 10.1029/2007GL031970.

Lee, J., Spencer, J., and Owen, L., 2001, Holocene slip rates along the Owens Valley fault, California: Implications for the recent evolution of the Eastern California Shear Zone: *Geology*, v. 29, no. 9, p. 819-822.

Lubetkin, L. K. C., and Clark, M. M., 1988, Late Quaternary activity along the Lone Pine fault, eastern California: *Geologic Society of America Bulletin*, v. 100, p. 755-766.

Malservisi, R., Furlong, K. P., and Dixon, T. H., 2001, Influence of the earthquake cycle and lithospheric rheology on the dynamics of the Eastern California shear zone: *Geophysical Research Letters*, v. 28, p. 2731-2734.

Marrero, S.M., Phillips, F.M., Borchers, B., Lifton, N., Aumer, R., and Balco, G., 2016a, Cosmogenic nuclide systematics and the CRONUScalc program: *Quaternary Geochronology,* v. 31, p. 160-187.

Marrero, S.M., Phillips, F.M., Caffee, M.W., and Gosse, J.C., CRONUS-Earth cosmogenic ^{36}Cl calibration: *Quaternary Geochronology,* v. 31, p. 199-219.

Phillips, F.M., Argento, D.C., Balco, G., Caffee, M.W., Clem, J., Dunai, T.J., Finkel, R., Goehring, B., Gosse, J.C., Hudson, A.M., Jull, A.J.T., Kelly, M.A., Kurz, M., Lal, D., Lifton, N., Marrero, S.M., Nishiizumi, K., Reedy, R.C., Schaefer, J., Sotne, J.O.H., Swanson, T., and Zreda, M.G., 2016, The CRONUS-Earth Project: A Synthesis: *Quaternary Geochronology,* v. 31, p. 119-154.

Savage, J. C., and Lisowski, M., 1980, Deformation in Owens Valley, California: *Bulletin of the Seismological Society of America*, v. 70, no. 4, p. 1225-1232.

Savage, J.C. and Lisowski, M., 1995, Strain accumulation in Owens Valley, California, 1974 to 1988: *Bulletin of the Seismological Society of America*, v. 85, no. 1, p. 151-158.

Turrin, B. and Gillespie, A., 1986, K/Ar ages of basaltic volcanism of the Big Pine Volcanic Field, California: Implications for glacial stratigraphy and neotectonics of the Sierra Nevada: *Geological Society of America Abstracts with Programs*, v. 18, p. 414.

Road Log

20.7 Continue southeast on dirt road. It curves due east and becomes paved.

21.3 Highway 395. Turn right (S), WATCHING FOR HIGH-SPEED TRAFFIC FROM THE LEFT. The highway skirts the basalt-covered flank of Crater Mountain to the west, providing excellent views of the Owens Valley fault on its side.

24.7 Fish Springs Road. Turn right (W). The Owens Valley fault continues to parallel the road. Ahead we approach the small red Fish Springs cinder cone. The west flank of this cone is vertically offset across the fault. This locality was the subject of a cosmogenic dating study by Zehfuss et al. (2001) that established a vertical displacement rate of 0.24 m/kyr based on dated alluvial surfaces. The Poverty Hills are ahead.

26.9 'Y' road junction. Keep right (straight).

27.3 Tinemaha Creek Road. Turn right (W). The Poverty Hills loom to the south. They have alternatively been proposed to be a compressional flower structure at a restraining bend in the Owens Valley fault (Taylor, 2002) or a mega-landslide deposit, sourced from the Inyo Mountains to the southeast (Bishop and Clements, 2006). Note steeply tilted basalt flows on the slopes a short distance ahead. Also note in roadcuts the extremely shattered and deformed character of the rock.

27.7 Intersection with unmarked, unpaved road on the west. Turn right (W). Keep speed slow while driving through small residential area.

[*Alternative route:* To avoid BLM land, continue 1.1 miles south to the Tinemaha Creek Campground. Turn right into campground, drive through, and park on west side.]

29.6 Unmarked road junction. Take road coming in on the left (SW).

29.9 Unmarked junction with road coming in from the right (S). Park as directed. Stop 3.3.

Stop 3.3: Kinematics of extensional faults in the central Owens Valley (Kirby).

Stop 3.3: Quantifying distributed extension across Owens Valley

Eric Kirby - Oregon State University and **Fred Phillips** - New Mexico Tech

A persistent question concerning the pace and tempo of active deformation throughout the ECSZ/Walker Lane region is how one interprets differences between modern strain fields, typically measured with space geodesy (e.g., Bormann et al., 2016), and fault slip rates measured over millennia (e.g., Oskin et al., 2008). Recent efforts to characterize the role of distributed deformation have focused on the role of off-fault deformation associated with fault terminations and damage zones (e.g. Herbert et al., 2014).

In the northern Owens Valley, the active fault network exhibits significant complexity in the vicinity of the Big Pine Volcanic Field and the Coyote Warp. Not only does the Owens Valley fault take a left step through the restraining bend of the Poverty Hills, but the region between the Sierra Nevada crest and the Owens Valley is characterized by numerous normal faults, many of which displace Pleistocene alluvial deposits (Figure 3.3a). Perhaps the best-studied of these is the Fish Springs fault, which forms an striking, east-facing fault scarp just west of where it splays from the Owens Valley fault. Displacement of the flank of the Fish Springs cinder cone (314 ± 36 ka, Martel et al., 1987) and of Late Pleistocene alluvial fans (130-140 ka and 13-15 ka, Zehfuss et al., 2001) suggests relative steady throw at rates of 0.2 -0.3 m/kyr over the past ca. 300 kyr (Martel et al., 1987; Zehfuss et al., 2001). This rate is similar to that observed along the primary range-front fault of Sierra Nevada farther south (throw rates of 0.2 – 0.3 mm/yr, averaged over the past ~120 kyr; Le et al., 2007).

Figure 3.3a: Simplified geologic map of distributed normal faults and Pleistocene alluvial and volcanic deposits between Crater Mountain and Red Mountain. Letters refer to survey profiles across fault scarps shown in Figure 3.3d.

At this stop, we will discuss new constraints on slip rates along three other fault systems that lie west of the Fish Springs fault, between the Owens Valley and the Sierra Nevada range crest. Most of the work we will discuss is unpublished, except in field guide form (Frankel et al., 2008), and derives from the M.S. research of Dave Greene and the B.S. research of Aaron Bini at Penn State University.

Driving Question:

What contribution does distributed faulting play in the extension rate across Owens Valley?

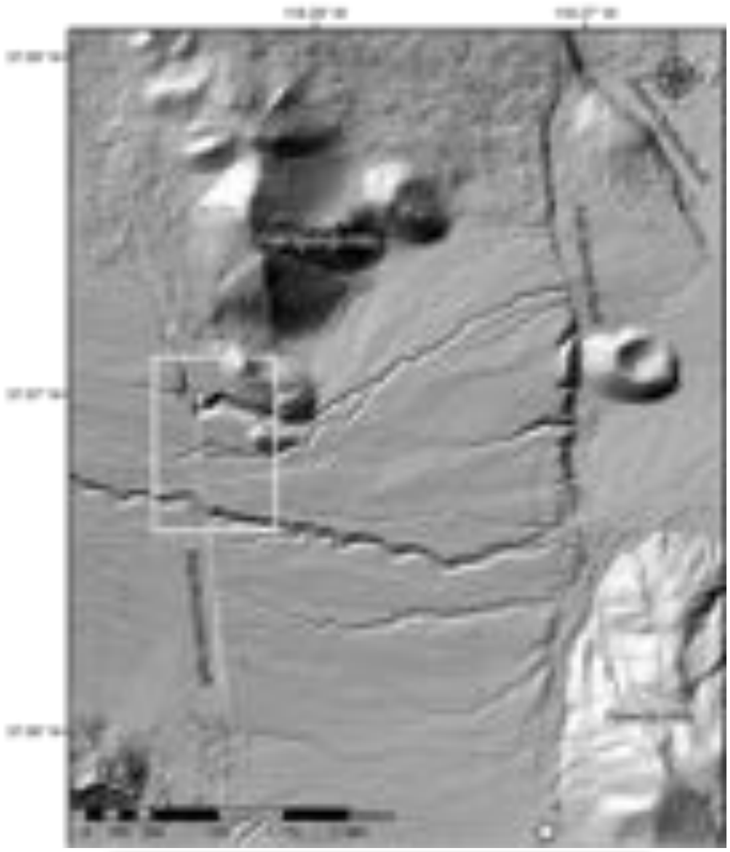

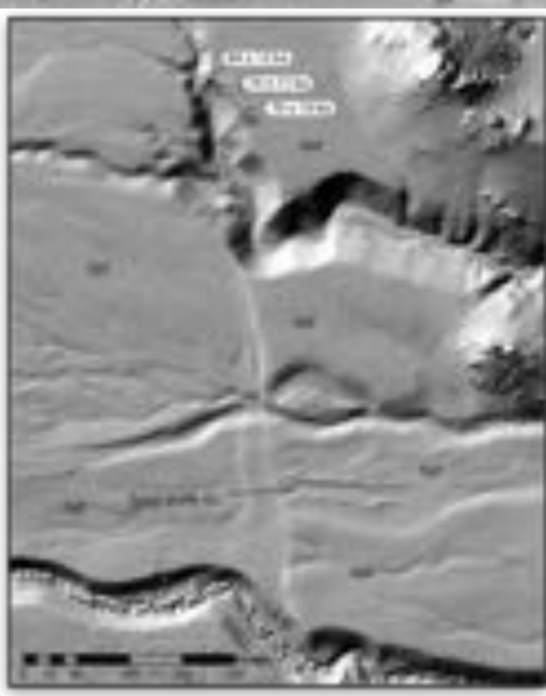

Figure 3.3b: Top. LiDAR-derived shaded relief image (illumination from the SW) of the Fish Springs and Red Mountain faults. Our location in the Tinemaha Campground is noted

by the white star at the bottom of the image. LiDAR collected by Chris Larsen of the University of Alaska, Fairbanks and shared courtesy of Anne Egger of Central Washington University. White box shows the location of inset at right. **Bottom**. Close-up of Red Mountain fault showing west-facing scarp displacing young (Qyf) and older (Qof) alluvial fans associated with drainage of Birch Creek. Cosmogenic ^{36}Cl ages shown are updated from Kirby et al. (2008) using the CRONUS web calculator.

Slip rate along the Red Mountain fault

The Red Mountain fault is a 10 km-long normal fault that extends south from the southwestern flank of Crater Mountain, subparallel to and approximately 2 km west of the Fish Springs fault (Figure 3.3a, b). It is marked along much of its trace by west-facing scarps that pond young alluvium in the hanging wall block. Despite its length and proximity to the Fish Springs fault, the Red Mountain structure has received considerably less attention, and the role of this fault in the extension budget across northern Owens Valley is essentially unknown.

Figure 3.3c: Top. Field photograph looking north along the Red Mountain fault. Basalt flow from Crater Mountain caps older alluvial fan deposits on eastern side of the fault. Displaced flow surface west of fault is buried by younger alluvial fans in the downthrown block (left of gully). **Bottom.** Close up of the flow base, showing oxidized, relict soil profile beneath 1-2 m thick flow. Flow thickens across scarp at left, suggesting that flow filled paleotopography along Red Mountain fault.

northern end of the fault, lava flows from Crater Mountain are displaced in a west-side-down sense, and have been subsequently buried by young alluvial fans emanating from Birch Creek. The flow itself buries an older alluvial fan surface with a moderately well-developed soil profile; surface and soil characteristics of this fan suggest that it is likely equivalent to surfaces dated 2 km to the east at ~137 ± 17 ka (Zehfuss et al., 2001), whereas the younger fan appears continuous with surfaces dated at 12 – 14 ka (Zehfuss et al., 2001). As discussed above, ^{36}Cl samples from the footwall exposures of the flow cluster at 73 ± 9 ka (revised from 70 ± 14 in Kirby et al., 2008), and are stratigraphically consistent with the chronology of Zehfuss et al. (2001). The flow surface has been offset vertically by 14.5 ± 1.5 m (Figure 3.3c), and two small scarps are present in the youngest Late Pleistocene surface that exhibit a combined throw of 2.5 ± 0.2 meters (Figure 3.3d). Both of these displacements are consistent with relatively steady, long-term throw rates along the Red Mountain fault of 0.2 – 0.3 m/kyr (Frankel et al., 2008). Thus, the Red Mountain fault accommodates as much displacement in the regional deformation budget as does the Fish Springs fault.

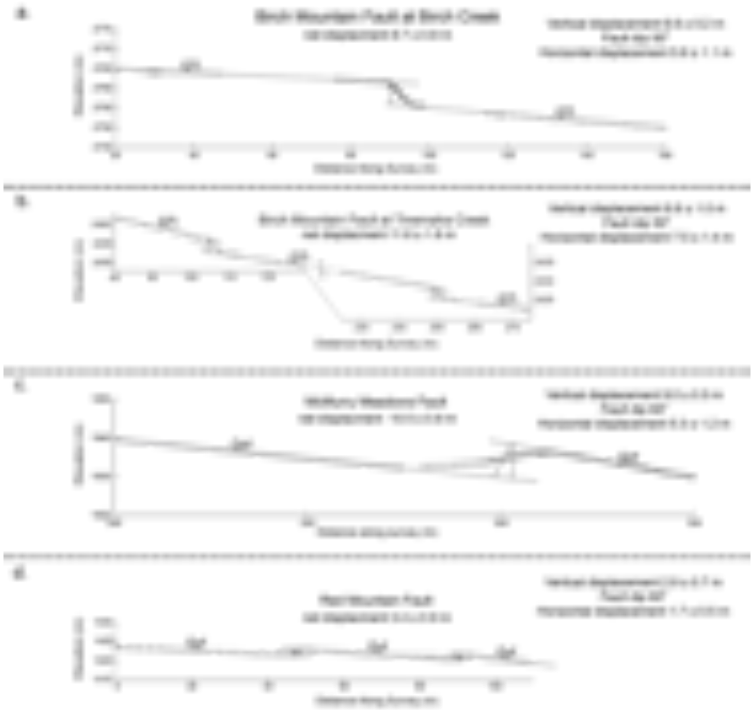

Figure 3.3d: Scarp profiles surveyed with differential GPS across faults in the study area. A. and B. Profiles across the Birch Mountain fault where it displaces glacial moraines in Birch Creek and Tinemaha Creek, respectively. C. Profile across the McMurry Meadows fault where it displaces alluvial deposits inferred to date to ~120-150 ka. D. Profile across the Red Mountain fault where it

Slip rate along the Birch Mountain fault

Significant slip is also present along the Sierra Nevada frontal fault at this latitude, as indicated by prominent scarps high on the range front along the eastern flanks of Mt. Tinemaha and Birch Mountain (Figure 3.3e). The fault displaces sharp, triangular moraine crests in both the Tinemaha and Birch Creek drainages; moraines appear fresh, with minimal soil development and little to no weathering of boulder surfaces. Fault throw estimates derived from scarp profiles is consistent in both drainages and ranges from 7 to 9 meters (Figure 3.3d). Exposure ages derived from cosmogenic ^{36}Cl concentrations in 6 samples taken from boulders atop the left-lateral moraine in Tinemaha Creek yielded ages averaging 15.2±0.9 ka, consistent with a Tioga 4 age assignment. Three samples from outboard moraines gave Tioga 3 (~18 ka) and Tioga 1 (~30 ka) ages. Thus, vertical displacement rates on this segment of the Sierra Nevada frontal fault system are 0.5 – 0.7 m/kyr. These rates are significantly higher than those determined for the range front farther south (0.2 – 0.3 mm/yr; Le et al., 2007), and we speculate that these rates may reflect relatively recent breaching of the relay between the northern tip of the southern Sierra Nevada frontal fault system and the southern tip of the Round Valley fault.

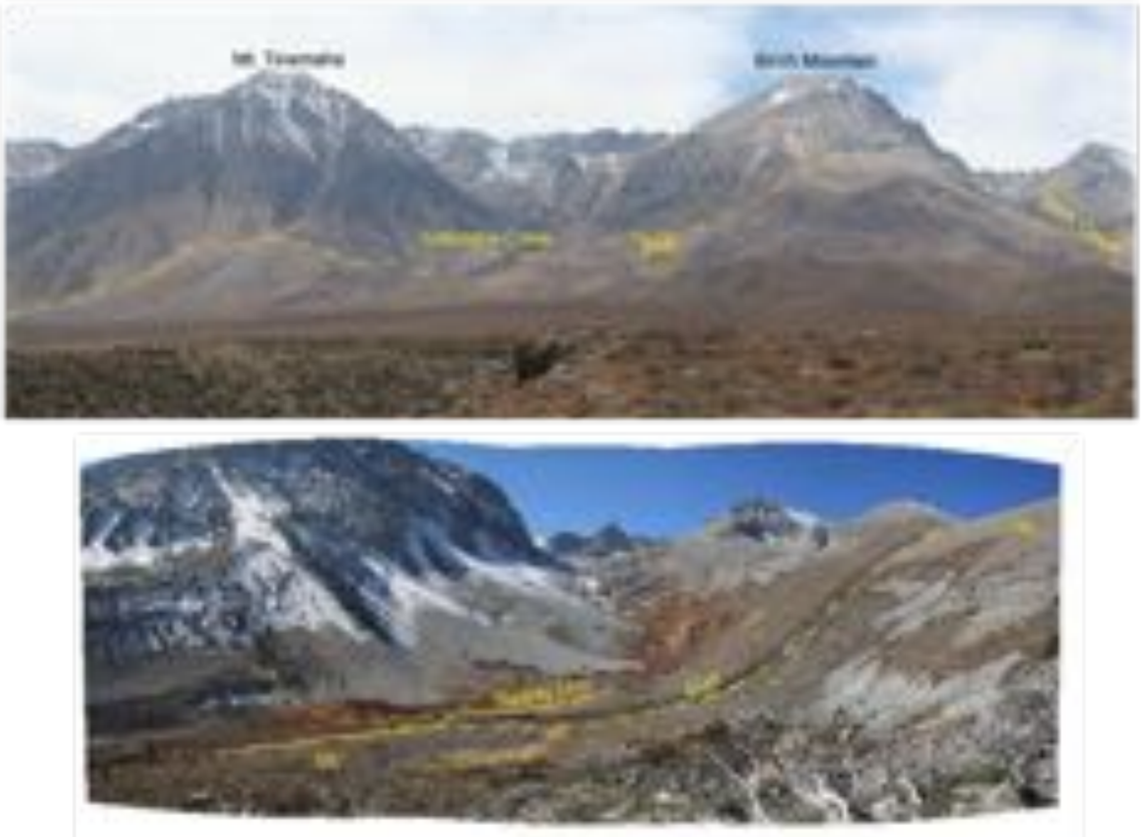

Figure 3.3e: Top. Panoramic photo looking west at the Sierra Nevada, with Birch Mountain fault (BMF) scarp marked with dashed yellow line. **Bottom.** Photo looking west at BMF scarp expressed in Birch Creek, clearly offseting Tioga moraines (Qti). Location of GPS survey, along Birch Creek, marked with solid yellow line.

Comparison to geodetic measurements of deformation across Owens Valley

Our results suggest that the rate of extension across Owens Valley at the latitude of Big Pine approaches ~1 mm/yr. To estimate the extension across fault systems, we assume that faults dip ~60°, consistent with field observations, except for the Birch Mountain fault where the fault trace across high-relief topography at the range front requires a somewhat shallower dip of ~50°. Extension rates on the Birch Mountain fault range from 0.4 - 0.6 mm/yr, while rates on the Red Mountain and Fish Springs faults are ~0.1 mm/yr on each structure. Finally, although we do not have direct dating on the McMurray Meadows fault (Figure 3.3a), the similarity of soil and surface characteristics of the displaced old alluvial fans (Qof) suggests correlation with dated deposits ca. 120-150 ka (Zehfuss et al., 2001). This suggests an extension rate of ~0.1 mm/yr for this fault as well. A simple sum of these rates across the transect suggests extension rates of 0.7 - 0.9 mm/yr across the Owens Valley west of the Owens Valley fault. When one accounts for the fact that some extension is accommodated along the eastern side of the valley (Waucobi embayment and White Mountain fault), it seems possible that Late Pleistocene extension rates are similar to the geodetically determined modern velocities (Figure 3.3f).

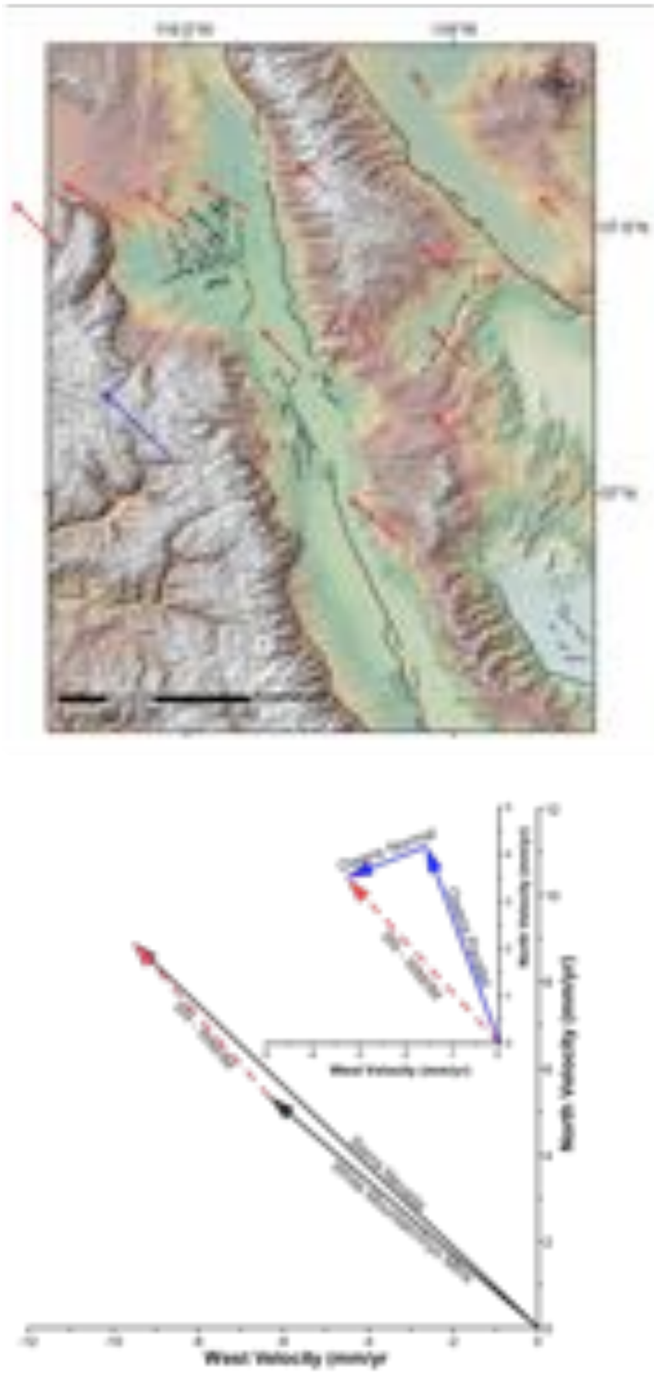

Figure 3.3f: Left. Geodetic velocity field in the central and northern Owens Valley. Data from UNAVCO, courtesy of P. LaFemina. **Right.** Velocity difference between stations on the White Mountains from the Sierra Nevada (dashed red line). **Right, inset.** Vector decomposition of Sierra Nevada - White Mountain velocity into directions parallel to, and orthogonal to, the strike of the Owens Valley fault. Fault orthogonal velocities are ~1.5 mm/yr.

As a final observation, the relatively high extension rates documented here appear to continue northward along the Owens Valley, where slip along the Round Valley fault system is inferred to be in the range of 0.5 - 1 mm/yr (Berry, 1997) and where distributed extension occurs across the Volcanic Tableland between the White Mountains and Sierra Nevada

(Dawers et al., 1993; Pinter et al., 1994).

References

Berry, M.E., 1997, Geomorphic analysis of late Quaternary faulting on Hilton Creek, Round Valley and Coyote warp faults, east-central Sierra Nevada, California, USA: *Geomorphology*, v. 20, p. 177-195.

Bormann, J.M., Hammond, W.C., Kreemer, C., and Blewitt, G., 2016, Accommodation of missing shear strain in the Central Walker Lane, western North America: Constraints from dense GPS measurements: *Earth and Planetary Science Letters*, v. 440, p. 169-177.

Dawers, N.H., Anders, M.H., and Scholz, C.H., 1993, Growth of normal faults: Displacement-length scaling: *Geology*, v. 21, p. 1107-1110.

Frankel, K.L., Glazner, A.F., Kirby, E., Monastero, F.C., Strane, M.D., Oskin, M.E., Unruh, J.R., Walker, J.D., Anandakrishnan, S., Bartley, J.M., Coleman, D.S., Dolan, J.F., Finkel, R.C., Greene, D., Kylander-Clark, A., Marrero, S., Owen, L.A., and Phillips, F., 2008, Active tectonics of the eastern California shear zone, *in* Duebendorfer, E.M., and Smith, E.I., eds., Field Guide to Plutons, Volcanoes, Faults, Reefs, Dinosaurs, and Possible Glaciation in Selected Areas of Arizona, California, and Nevada: Geological Society of America Field Guide 11, p. 43–81, doi: 10.1130/2008.fl d011(03).

Gillespie, A. R., 1991, Quaternary subsidence of Owens Valley, California, *in* Hall, C. A., ed., Natural History of eastern California and high-altitude research: Los Angeles, White Mountain Research Station Proceedings, p. 356-382.

Greene, D., Kirby, E., Dawers, N., Phillips, F., McGee, S., and Burbank, D., 2007, Quantifying accommodation of active strain along distributed fault arrays in Owens Valley, California: *Geologic Society of America Abstracts with Programs*, v. 39, no. 6, p. 441.

Herbert, J.W., Cooke, M.L., Oskin, M., and Difo, O., 2014, How much can off-fault deformation contribute to the slip rate discrepancy within the eastern California shear zone?: *Geology*, v. 42, p. 71-74, doi:10.1130/G34738.1

Kirby, E., Anadakrishnan, S., Phillips, F., Marrero, S., 2008, Late Pleistocene slip rate along the Owens Valley fault, eastern California: *Geophysical Research Letters*, v. 35, L01304, doi: 10.1029/2007GL031970.

Le, K., Lee, J., Owen, L. A., and Finkel, R., 2007, Late Quaternary slip rates along the Sierra Nevada frontal fault zone, California: Slip partitioning across the western margin of the Eastern California Shear Zone-Basin and Range Province: *Geologic Society of America Bulletin*, v. 119, p. 240-256.

Martel, S. J., Harrison, T. M., and Gillespie, A. R., 1987, Late Quaternary vertical displacement across the Fish Springs fault, Owens Valley fault zone, California: *Quaternary Research*, v. 27, p. 113-129.

Pinter, N., Keller, E.A., and West, R.B., 1994, Relative dating of terraces of the Owens River, northern Owens Valley, California, and correlation with moraines of the Sierra Nevada: *Quaternary Research*, v. 42, p. 266-276.

Oskin, M., Perg, L., Shelef, E., Strane, M., Gurney, E., Singer, B., and Zhang, X., 2008, Elevated shear zone loading rate during an earthquake cluster in eastern California: *Geology*, v. 36, p. 507–510, doi:10.1130/G24814A.1.

Zehfuss, P. H., Bierman, P. R., Gillespie, A. R., Burke, R. M., and Caffee, M. W., 2001, Slip rates on the Fish Springs Fault, Owens Valley, California, deduced from cosmogenic ^{10}Be and ^{26}Al and soil development on fan surfaces: *Geological Society of America Bulletin*, v. 113, no. 2, p. 241-255.

References for Road Log

Bach A. J. (1995) Aeolian modifications of glacial moraines at Bishop Creek, Eastern California, In *Desert Aeolian Processes* (V. P. Tchakerian; ed.), Chapman & Hall, London, pp. 179-197.

Bach A. J. and Elliott-Fisk D. L. (1996) Soil development on late Pleistocene moraines at Pine Creek, east-central Sierra Nevada, California: *Physical Geography* **17** 1-28.

Bailey R. A. (1989) Geologic map of the Long Valley caldera, Mono-Inyo Craters volcanic chain, and vicinity eastern California: U.S. Geological Survey, Map I-1933, Scale 1:62,500.

Bateman P. C. (1965) Geology and tungsten mineralization of the Bishop District, California: U.S. Geological Survey Professional Paper 470, Professional Paper 470, 208 p. pp.

Berry M. E. (1994) Soil-geomorphic analysis of late-Pleistocene glacial sequences in the McGee, Pine, and Bishop Creek drainages, east-central Sierra Nevada, California: *Quaternary Research* **41** 160-175.

Berry M. E. (1997) Geomorphic analysis of late Quaternary faulting on Hilton Creek, Round Valley and Coyote warp faults, east-central Sierra Nevada, California, USA: *Geomorphology* **20** 177-195.

Bishop K. M. and Clements S. (2006) The Poverty Hills, Owens Valley, California- Transpressional uplift or ancient landslide deposit?: *Environmental & Engineering Geoscience* **12** 301-314.

Blackwelder E. (1931) Pleistocene glaciation in the Sierra Nevada and Basin ranges: *Bulletin of the Geological Society of America* **42** 865-922.

Chamberlain K. J., Wilson C. J. N., Wooden J. L., Charlier B. L. A., and Ireland T. R. (2014) New perspectives on the Bishop Tuff from zircon textures, ages and trace elements: *Journal of Petrology* **55** 395-426.

Henry C. D., Hinz N. H., Faulds J. E., Colgan J. P., John D. A., Brooks E. R., Cassel E. J., Garside L. J., Davis D. A., and Castor S. B. (2012) Eocene-Early Miocene paleotopography of the Sierra Nevada-Great Basin-Nevadaplano based on widespread ash-flow tuffs and paleovalleys: *Geosphere* **8**(1) 1-27.

Hildreth W. and Fierstein J. (2016a) *Eruptive history of Mammoth Mountain and its mafic periphery, California*: U.S. Geological Survey Professional Paper 1812128 pp.

Hildreth W. and Fierstein J. (2016b) Long Valley caldera lake and reincision of Owens River Gorge: U.S. Geological Survey Scientific Investigations Report 2016-5120, 63 pp.

Jager J. M. (2002) Patterns of Quaternary deformation in the Waucobi embayment, Owens Valley, California: M.S. thesis, University of California, Santa Barbara, 53 pp.

Jayko A. S. (2009) Deformation of the late Miocene to Pliocene Inyo Surface, eastern Sierra region, California, In *Late Cenozoic Stucture and Evolution of the Great Basin-Sierra Nevada Transition* (J. S. Oldow and P. H. Cashman; eds.), Geological Society of America Special Paper 447, Boulder, Colorado, pp. 313-350.

Jones C. H., Farmer G. L., and Unruh J. (2004) Tectonics of Pliocene removal of lithosphere of the Sierra Nevada, California: *Geological Society of America Bulletin* **116** 1408-1422.

King C. (1878) Report of the geological exploration of the Fortieth Parallel: *Systematic Geology* **1** 459-529.

Kirby E., Burbank D. W., Reheis M., and Phillips F. M. (2006) Temporal variations in slip rate of the White Mountain Fault Zone, eastern California: *Earth and Planetary Science Letters* **248** 168-185.

Knopf A. (1918) A geologic reconnaissance of the Inyo Range and the eastern slope of the Sierra Nevada, California, with a section on the stratigraphy of the Inyo Range by Edwin Kirk: U. S. Geological Survey Professional Paper 110, 130 pp.

Lee J., Stockli D. F., Owen L. A., Finkel R. C., and Kislitsyn R. (2009) Exhumation of the Inyo Mountains, California: Implications for the timing of extension along the western boundary of the Basin and Range Province and distribution of dextral fault slip rates across the eastern California shear zone: *Tectonics* **28** TC1001, doi:10.1029/2008TC002295.

Lueddecke S. B., Pinter N., and Gans P. (1998) Plio-Pleistocene ash falls, sedimentation, and range-front faulting along the White-Inyo Mountains, California: *Journal of Geology* **106** 511-522.

Matthes F. E. (1929) Multiple glaciation in the Sierra Nevada: *Science* **70** 75-76.

Matthes F. E. (1930) Geologic history of the Yosemite Valley: U.S. Geological Survey, Professional Paper 160, 137 pp.

McJunkin R. D. and Bedrossian T. L. (1980) Mammoth Lakes earthquakes, May 25-27 1980, Mono County California: *California Geology* **33**(9) 194-201.

McQuarrie N. and Wernicke B. P. (2005) An animated tectonic reconstruction of southwestern North America since 36 Ma: *Geosphere* **1**(3) 147-172, doi: 110.1130/GES00016.00011.

Nelson C. A. (1966a) Geologic map of the Blanco Mountain quadrangle, Inyo and Mono Counties, California: U.S. Geological Survey Geologic Quadrangle Map GQ-529, Scale 1:62500.

Nelson C. A. (1966b) Geologic map of the Waucoba Mountain Quadrangle, Inyo County, California: U.S. Geological Survey Map GQ-0528, U.S. Geological Survey Map GQ-0528, Scale 1:62,500.

Phillips F. (2017) Glacial chronology of the Sierra Nevada, California, from the Last Glacial Maximum to the Holocene: *Cuadernos de Investigación Geográphica* **43** preprint, doi:10.18172/cig.3233.

Phillips F. M. (2008) Geological and hydrological history of the paleo-Owens River drainage since the late Miocene, Vol. Special Paper 439, In *Late Cenozoic Drainage History of the Southwestern Great Basin and Lower Colorado River Region: Geologic and Biotic Perspectives* (M. C. Reheis, R. Hershler, and D. M. Miller; eds.), Geological Society of America, Boulder, Colorado, pp. 115-150.

Phillips F. M. and Majkowski L. (2011) The role of low-angle normal faulting in active tectonics of the northern Owens Valley, California: *Lithosphere* **3**(1) 22-36.

Phillips F. M., McIntosh W. C., and Dunbar N. W. (2011) The chronology of late Cenozoic volcanic eruptions on relict surfaces in the south-central Sierra Nevada, California: *Geological Society of America Bulletin* **123** 890-910.

Plummer M. A. (2002) Paleoclimatic conditions during the last deglaciation inferred from combined analysis of pluvial and glacial records: Ph.D., New Mexico Institute of Mining & Technology, Socorro, 308 pp.
Rinehart C. D. and Ross D. C. (1964) Geology and mineral deposits of the Mount Morrison quadrangle, Sierra Nevada, California: U.S. Geological Survey Professional Paper 385, 106 pp.
Sharp R. P. (1968) Sherwin Till-Bishop Tuff geological relationships, Sierra Nevada, California: *Geological Society of America Bulletin* **79** 351-364.
Sheridan M. F. (1970) Fumarolic mounds and ridges of the Bishop Tuff, California: *Geological Society of America Bulletin* **81** 851-868.
Stockli D. F., Dumitru T. A., McWilliams M. O., and Farley K. A. (2003) Cenozoic tectonic evolution of the White Mountains, California and Nevada: *Geological Society of America Bulletin* **115** 788-816.
Taylor T. R. (2002) Origin and structure of the Poverty Hills, Owens Valley Fault Zone, Owens Valley, California: M.S., Miami University, Miami, Ohio, 102 pp.
Turner H. W. (1900) The Pleistocene geology of the south-central Sierra Nevada with especial reference to the orign of Yosemite Valley: *California Academy of Sciences Proceedings, Geology* **3** 261-321.
Zehfuss P. H., Bierman P. R., Gillespie A. R., Burke R. M., and Caffee M. W. (2001) Slip rates on the Fish Springs fault, Owens Valley, California, deduced from cosmogenic ^{10}Be and ^{26}Al and soil development on fan surfaces: *Geological Society of America Bulletin* **113** 241-255.